STUDIA UNIVERSITATIS
BABEŞ-BOLYAI

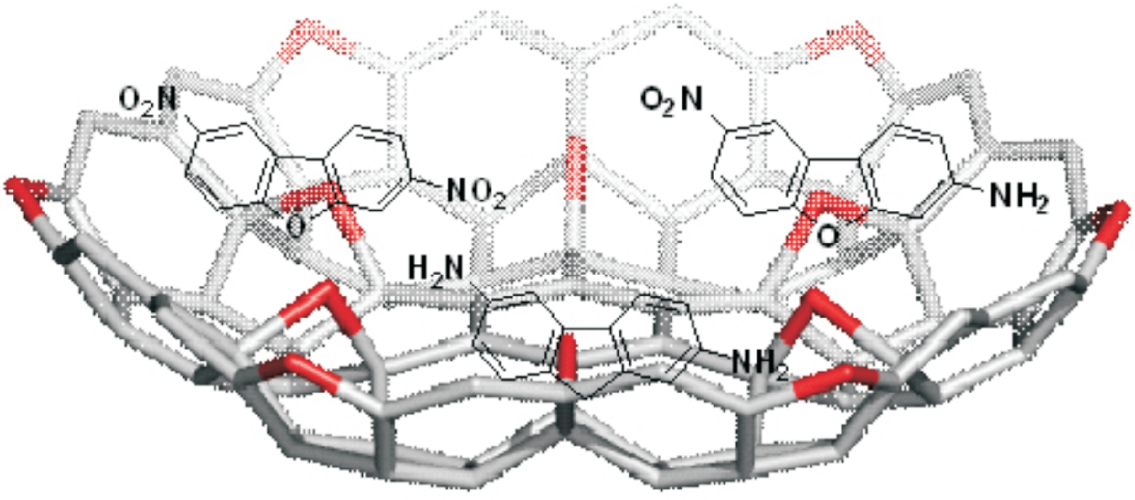

CHEMIA

4/2009
tom I

ANUL LIV **2009**

S T U D I A

UNIVERSITATIS BABEŞ-BOLYAI

CHEMIA

4

tom I

Desktop Editing Office: 51ST B.P. Hasdeu Street, Cluj-Napoca, Romania, Phone + 40 264-405352

CUPRINS – CONTENT – SOMMAIRE – INHALT

Studia Universitatis Babes-Bolyai Chemia has been selected for coverage in Thomson Reuters products and custom information services. Beginning with V. 53 (1) 2008, this publication is indexed and abstracted in the following:

- Science Citation Index Expanded (also known as SciSearch®)
- Chemistry Citation Index®
- Journal Citation Reports/Science Edition

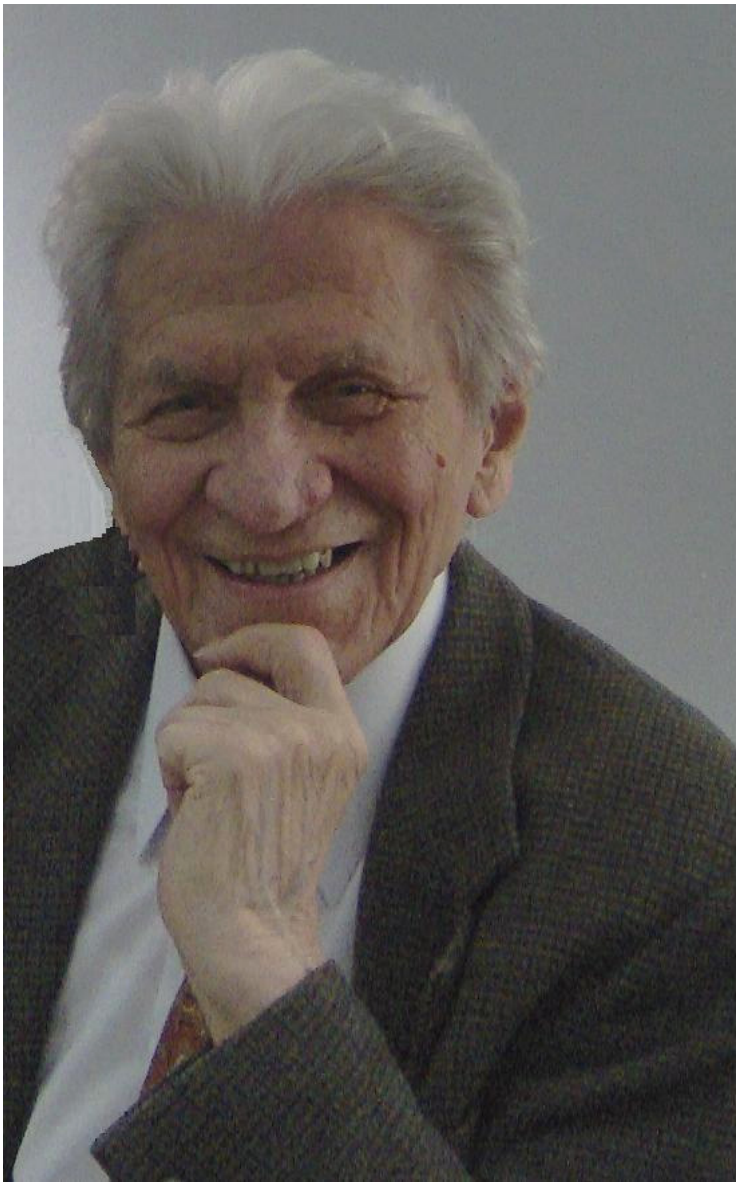

Professor Valer Fărcăşan at his 90th anniversary
October the 3rd 2009

STUDIA UNIVERSITATIS BABEŞ-BOLYAI, CHEMIA, LIV, 4, 2009

NEW WAYS FOR OLD STRUCTURES

FLORIN DAN IRIMIE[a], CSABA PAIZS[a], MONICA TOSA[a], PAULA PODEA[a]

ABSTRACT. Classical heterocyclic structures of furan, benzofuran, dibenzofuran, phenothiazine and benzothiazole type, previously synthesized and studied by Professor Fărcăşan, were derivatized using cell- or enzyme-assisted regio-, chemo- and stereoselective techniques, providing compounds extremely difficult or even impossible to produce by traditional chemical methods. The present report underlines the high potential of biocatalysis to perform selective enantiomer- and enantiotope-transformations with remarkable conversion rates and purities.

Keywords: heterocycles, bezofuran, (furyl)benzothiazole, regioselectivity, chemoselectivity, enantiomer-selectivity, enantiotop-selectivity

INTRODUCTION

Heterocyclic systems of type benzofuran, benzothiazole, (furyl)benzothiazole, dibenzofuran are found as building-blocks for compounds with specific biological activities, as antimicrobial and antifungal agents [1 - 2] cytotoxic compounds [3], antidiabetics [4 - 5] etc.

These basic five membered heterocycles were prepared and functionalised thanks to the pioneering works of Professor Farcasanu research group in the period of 1950 – 1980' [6-14]. Thus, during the initial heterosynthesis state of art, really nice achievements had been accomplished using traditional means of synthesis and analysis.

Over the years, the above heterocyclic structures were much developed, as a need for diversifying their applicability area, for example by increasing the selectivity of biological impact of the products.

Nowadays, the insertion of the initial heterocyclic systems in new compounds with high structural complexity became possible, by means of highly selective techniques, with increased efficiency and compatibility with the environment. Among these techniques, enzymatic and cellular biocatalysis detaches through their advantages concerning activity and selectivity, which impose biocatalysis as a powerful tool with a reliable future.

[a] *"Babes-Bolyai" University, Department of Biochemistry and Biochemical Engineering, 11 Arany Jànos st., 400 028 Cluj-Napoca, ROMANIA, irimie@chem.ubbcluj.ro*

The present dedicated mini-review is intended to highlight these recent advances in highly functionalised five membered heterocyclic chemistry, in a biochemical approach.

1. Regioselective processes

Regioselectivity is an undeniable advantage of enzymatic activity, making possible the discrimination and modification of chemically identical structures, located in different environments. For example, hydrolases express most evidently this property, being used for manipulation of polyfunctional bio compounds as carbohydrates [15], nucleosides [16], steroids [17]. Thus, Michael additions [18], hydroxylations [19 - 20] and several reduction reactions [21 - 22] are good examples of enzymatic regioselective processes.

In context, dibenzofuran was used as a substrate in the research group of Professor Fărcăşan. Thus, by nitration, 3-nitro-, and 3,8-dinitrobenzofuran were obtained. Reduction of 3-nitrodibenzofuran to 3-aminodibenzofuran and that of 3,8-dinitrobenzofuran to 3-amino-8-nitrodibenzofuran, in the presence of baker's yeast was accomplished by our group in 1997 (Scheme 1) [23].

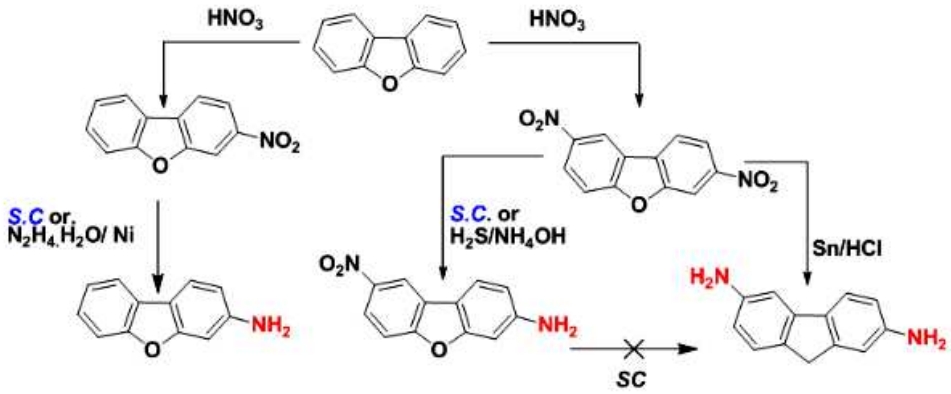

Scheme 1

The chemoselective processes involve the selective transformation of just one functional group from two or more functionally related groups which may be present i) on different substrates (substrate chemoselectivity - chemospecificity) or ii) on the same substrate (product chemoselectivity or merely chemoselectivity) [24].

For example, Baker's yeast can selectively reduce the aldehyde group attached to a heterocyclic skeleton, such as (phenyl)furan, which has functional groups potentially vulnerable to the enzymatic equipment of yeast, nitro for reduction and ethoxycarbonyl for hydrolysis [23, 24] (Scheme 2).

2. Stereoselective processes

Stereoselectivity may be one of the major advantages of biocatalysis.

Through processes assisted by stereoselective biocatalysts, compounds with high enantiopurity can be produced. Enantiopurity is a necessary condition for bioactive compouds, because their two stereoisomers have different biological properties. At the same time, the impure nature of the unwanted enantiomer affects the economy of the synthesis. The preference of biocatalyst for a certain surface or enantiotope group in the substrate's structure conducts to the preferential forming of a certain enantiomeric product. This kind of preference defines *an enantiotope-selective process* and creates, from a symmetrical structure, a chiral one [24]. Through the preference of the biocatalyst for one of the two enantiomers of a racemic mixture, a converted enantiomer is obtained, while the other one, the unmodified enantiomer, remains in the medium. This process we entitled as *enantiomer-selective*.

Several illustrative examples of us will be discusssed hereafter.

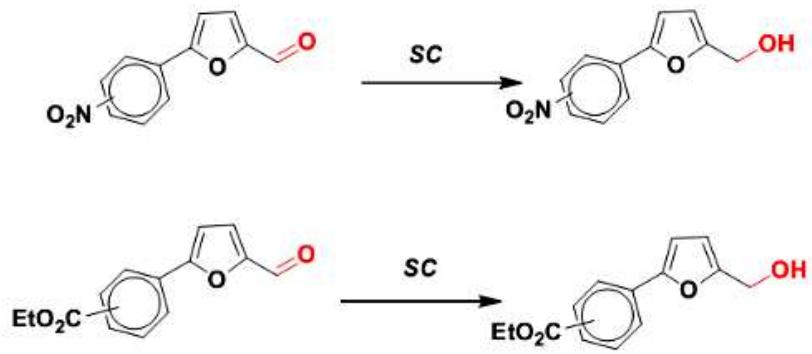

Scheme 2

2.1. Enantiotope selective-processes

These processes allow desymmetrization of prochiral substrates, which posess either enantiotope faces or enantiotope groups, resulting in enantiopure compounds according to the selectivity of the biocatalyst.

Our group transformed 2-substituted (methyl, acetoxymethyl) benzothiazole keto-derivatives into the corresponding secondary alcohols by enantiotope-selective reduction of their prochiral carbonyl group. The biocatalyst used was Baker's yeast (*Saccharomyces Cerevisiae, SC*) which contains a complex dehydrogenase equipment, able to catalyze redox processes. Due to the presence of several dehydrogenases, some of them with opposite selectivity, the latter can be modulated by using certain additives, or by modifying the operating conditions, fermentative or non-fermentative, in order to optimise the working system.

There is a general rule, known as that of Prelog, which states that in the reduction of a prochiral ketone with a biocatalyst, a secondary alcohol with (*S*) configuration is formed. This rule can be explained by mean of the topology of the catalytic site of a dehydrogenase present in the yeast (Figure 1).

For example, reduction of (2-oxo-2-hetaryl)ethyl acetates **3a-d** and (2-hydroxy-1-hetaryl)ethanones **4a-d** (Scheme 3) was performed with opposite enantiotope preference affording, after optimization, excellent yields (92-94%) and good enantiomeric excesses (89-99%), for each enantiomer of the hetarylethane-1,2-diols **5a-d** [25]. One can note the fast hydrolysis of the intermediates (*R*)-(2-hydroxy-2-hetaryl)ethyl acetates, post slow reduction step, by the enzymatic equipment of Baker's yeast. Similar results we obtained in the case of 1-(benzofuran-2-yl)ethanols and ethane-1,2-diols [26]

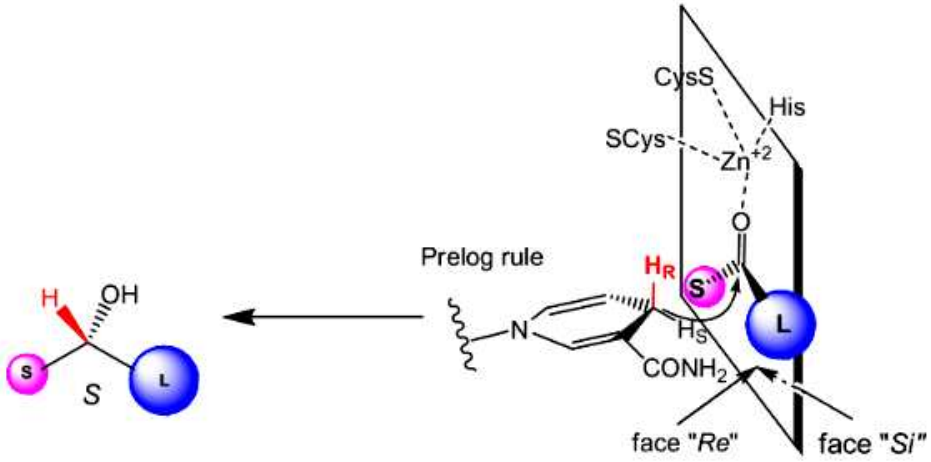

Figure 1. Topology of catalytic site of alcohol dehydrogenase from Baker`s yeast

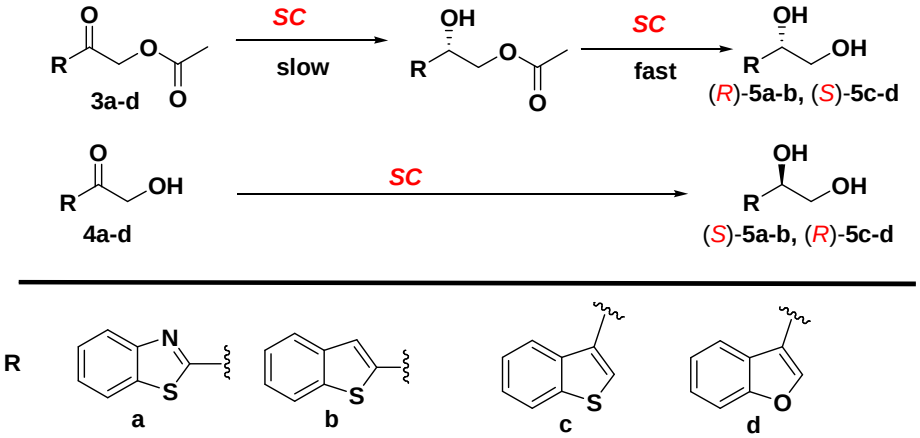

Scheme 3

2.2. Enantiomer selective processes

If biocatalysis assisted *enantiotope-selective processes* can be applied to prochiral substrates, *enantiomer-selective processes* are used to transform enantiomeric mixtures, most frequently racemic, in their nature. *Enantiomer-selectivity* implies that one enantiomer is converted faster than the other one. The reaction products will have different values of a certain separation property (solubility, melting point, etc.). So, the untransformed enantiomer can be easier separated from the reacted one. This system defines a kinetic resolution.

2.2.1. Kinetic resolution

An illustrative example of kinetic resolution is that of substituted 1-(benzofuran-2-yl)ethanols racemates (*rac*-**1a-d**, Scheme 4). They were synthesized upon unselective reduction of certain substituted 1-(benzofuran-2-yl)ethanones [27].

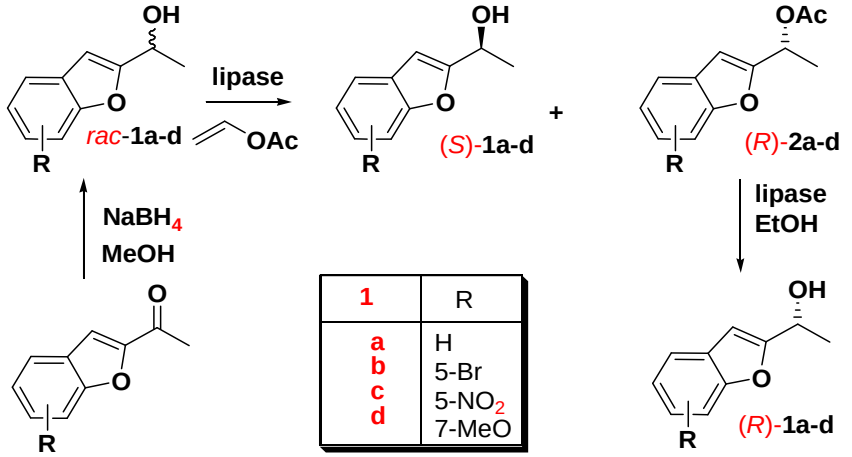

1	R
a	H
b	5-Br
c	5-NO_2
d	7-MeO

Scheme 4

The enantiopreference of enzyme for certain configuration can also be exploited for synthetic purposes [28].

Thus, starting from a racemic mixture, if enzyme is (*S*) selective, it will mediate only the acylation of a the (*S*) hetarylethanol, leaving the (*R*) alcohol unaffected (Scheme 5, the nature of heterocycles is the same as in Scheme 3). If the same enzyme will catalyze the hydrolysis of a racemic mixture of *O*-acylated hetarylethanols, such as *rac*-**2a-d**, the product will be the (*S*) alcohol, and the (*R*) ester remains untransformed. So, using racemates, *via* *O*-acylation, one can isolate the (*R*) alcohol, and by hydrolysis the (*S*) enantiomer becomes accessible. To conclude, by exploiting the conservation of enantiopreference of a lipase, one can obtain any of the two enantiomers, up to desire, from their racemic mixture, by mean a selective acylation or unselective acylation followed by a selective hydrolysis

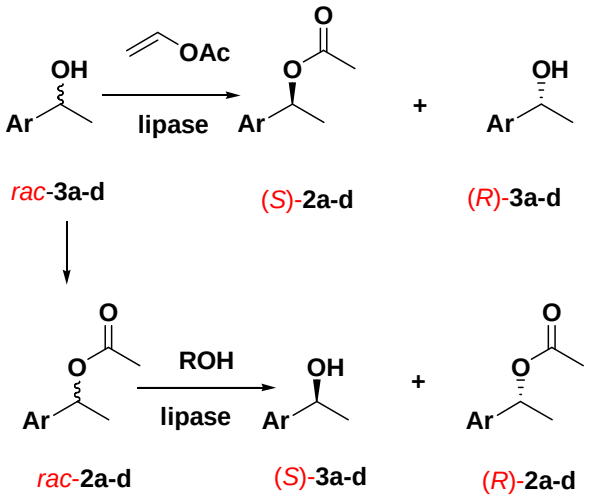

Scheme 5

However, the main drawback of kinetic resolution remains the maximum conversion as 50% calculated with respect to the racemic mixture.

2.2.2. Dynamic kinetic resolutions (DKR)

DKR are alternatives to kinetic resolutions, which eliminate the main disadvantage of kinetic resolutions: the limitation of conversion to 50%. Indeed the enatiopreference for one enantiomer leaves the other one unmodified, hence creating problems of i) separation (even if they are not as important as in the case of separation of enantiomers) and ii) in finding an applicability for the "non-preferred" enantiomer.

The DKR mechanism is simple and useful in systems for which one can find a reaction of racemization involving the starting enantiomers **A** and **B** (Scheme 6), [29 - 30].

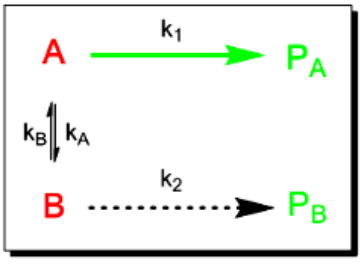

Scheme 6

If **A** is the preferred enantiomer by the biocatalyst, its concentration will be decreasing faster than that of **B**. Similarly, the concentration of product $\mathbf{P_A}$ will be increasing faster than the concentration of $\mathbf{P_B}$, these being the conditions for a successful kinetic resolution.

In contrast, if the system allows racemization of mixture of **A** and **B**, as **A** is consumed, a part of **B** is converted into **A**, to reestablish the equilibrium.

To setup an efficient DKR system as good selectivity, it is necessary that direct reaction(s), **A → P_A** and **B → P_B**, be irreversible. That is, the racemization rate should be greater than direct transformation rate, $k_{rac} > max(k_1,k_2)$. Side reactions and product racemization should be avoided and generally, the **DKR** methodology is limited, so far, to compounds having a single stereocenter.

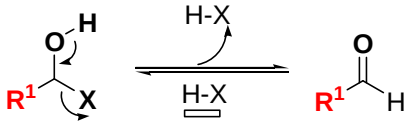

Scheme 7

The key feature of a DKR system is the racemization system. One of the most valuable systems are those in which, by sequence elimination – addition, such the one described in Scheme 7, the stereogenic center is firstly suppressed then recreated in a totally unselective manner. Another strategy can be used when, at the stereogenic center, one can find a "mobile proton" activated by an electron withdrawing group.

For instance, by applying the DKR mthodology, we were able to obtain α-(hetaryl)cyanomethyl acylates from the corresponding cyanohydrins (Scheme 8) in high enatiopure forms [31-33] with good conversions.

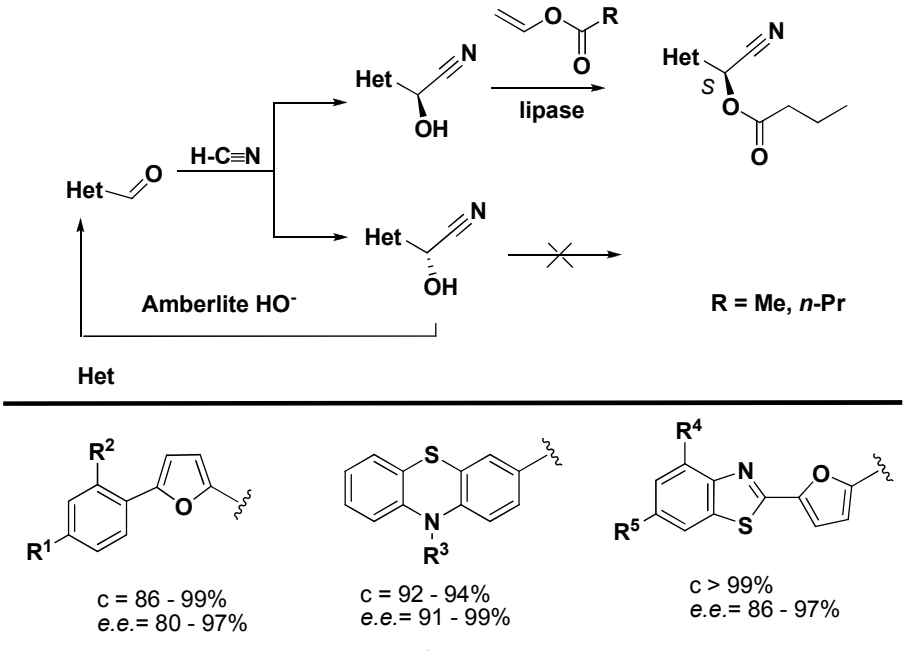

Scheme 8

The racemization step consisted of elimination – addition of hydrogen cyanide in the presence of a basic resin, Amberlite IRA-904.

The DKR we also used for the preparation of some hetaryl L-alanines of high enantiopurity [34] in a chemical and enzymatic sequence (Scheme 9). The racemization step in this DKR system had 4-(hetaryl)methyl-2-methyloxazol-5(4*H*)-ones, *rac*-**11a-d**, as a substrates [34]. We demonstrated that, due to the low pKa of their C-4 proton combined with a high reactivity against different nucleophiles, 2-substituted oxazol-5(4*H*)-ones are excellent substrates to undergo enzymatic dynamic kinetic resolution [35].

The oxazolone ring opening was performed through lipase-mediated alcoholysis. The L-hetaryl aminoacid was released after the basic hydrolysis of the ester bond (**III**, Scheme 9) followed by the enzymatic hydrolysis of the amidic bond. Consequently, this last enzymatic *N*-deprotection made a second chiral selection, promoting a final enantiopurity almost absolute. The global conversion of chemoenzymatic synthesis of enantiopure L-benzofuranyl- and L-benzo[*b*]thiophenyl alanines ranged between 76-85%. It was by far greater than the maximal theoretical conversion of enzymatic kinetic resolution assisted by Acylase I (50%).

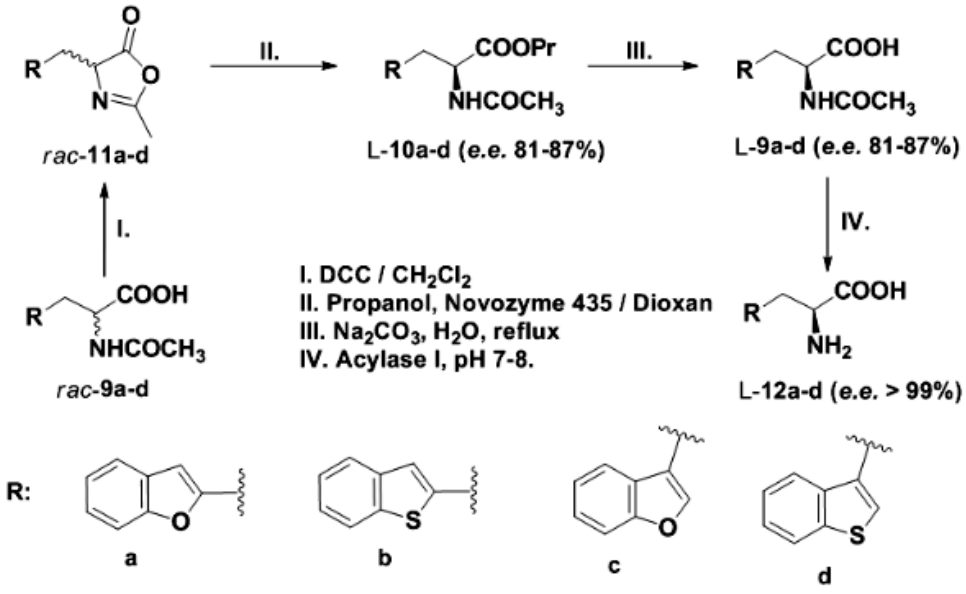

Scheme 9

3. Green processes

One of the most important features of a biocatalyst is its compatibility with the environment, face to the aggressivity of certain chemocatalysts and substrates. An illustrative example is provided by the cyclization of thiofuranilides assisted by *Saccharomyces Cerevisiae* (Scheme 10) [36].

The mechanism of cyclization involves the hydride ion transfer from thioenolic form to the NAD^+ cofactor. The chemical oxidant conventionally used is potassium dichromate. The conversions of the chemical *vs.* biochemical protocol are comparable [36].

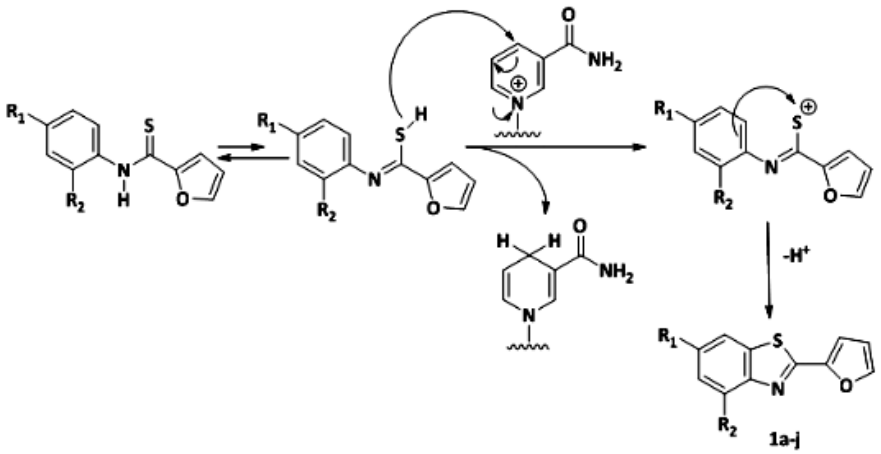

Scheme 10

CONCLUSIONS

Biotransformations are versatile, environmentally friendly, selective ways for synthesis of organic compounds, particularly chiral ones with high enantiopurity, being able to replace toxic and environmental aggressive catalysts or reagents.

ACKNOWLEDGMENTS

We kindly wish to express here our gratitude to Professor Valer Fărcăşan, for his helpful advices and discussions along the years.

REFERENCES

1. F. Messina, M. Botta, F. Corelli, A. Paladino. *Tetrahedron: Asymmetry,* **2000**, *11*: 4895.
2. B.F. Abdel-Wahab, H.A. Abdel-Aziz, E.M. Ahmed. *European Journal of Medicinal Chemistry,* **2009**, *44*: 2632.
3. K. Kaniwa, T. Ohtsuki, Y. Yamamoto, M. Ishibashi. *Tetrahedron Letters,* **2006**, *47*: 1505.
4. L. Di Nunno, C. Franchini, A. Scilimati, M.S. Sinicropi, P. Tortorella. *Tetrahedron: Asymmetry,* **2000**, *11*: 1571.
5. H. Moreno-Díaz, R. Villalobos-Molina, R. Ortiz-Andrade, D. Díaz-Coutiño, J.L. Medina-Franco, S.P. Webster, M. Binnie, S. Estrada-Soto, M. Ibarra-Barajas, I. León-Rivera, G. Navarrete-Vázquez. *Bioorganic & Medicinal Chemistry Letters,* **2008**, *18*: 2871.

6. C. Bodea, V. Farcasan, I. Oprean. *Studii si Cercetari de Chimie,* **1965**, *13*: 1157.
7. C. Bodea, V. Farcasan, I. Oprean. *Revue Roumaine de Chimie,* **1966**, *11*: 1117.
8. C. Bodea, V. Farcasan, T. Panea. *Revue Roumaine de Chimie,* **1966**, *11*: 239.
9. V. Farcasan, F. Paiu. *Studia Universitatis Babes-Bolyai, Chemia,* **1966**: 107.
10. V. Farcasan, I. Mester. *Studia Universitatis Babes-Bolyai, Chemia,* **1967**, *12*: 69.
11. C. Bodea, V. Farcasan, T. Panea. *Revue Roumaine de Chimie,* **1968**, *13*: 971.
12. V. Farcasan, I. Balazs. *Studia Universitatis Babes-Bolyai, Chemia,* **1968**, *13*: 123.
13. V. Farcasan, F. Paiu. *Studia Universitatis Babes-Bolyai, Chemia,* **1968**, *13*: 103.
14. V. Farcasan, S. Florea. *Journal fuer Praktische Chemie (Leipzig),* **1970**, *312*: 1007.
15. A. Xia, Q. Wu, B. Liu, X. Lin. *Enzyme and Microbial Technology,* **2008**, *42*: 414.
16. N. Li, M.-H. Zong, D. Ma. *Tetrahedron,* **2009**, *65*: 1063.
17. M.M. Cruz Silva, S. Riva, M.L. Sá e Melo. *Tetrahedron,* **2005**, *61*: 3065.
18. J.-L. Wang, J.-M. Xu, Q. Wu, D.-S. Lv, X.-F. Lin. *Tetrahedron,* **2009**, *65*: 2531.
19. M. Rahman, C. Hayes Sutter, G.L. Emmert, T.R. Sutter. *Toxicology and Applied Pharmacology,* **2006**, *216*: 469.
20. C. Roh, S.-H. Seo, K.-Y. Choi, M. Cha, B.P. Pandey, J.-H. Kim, J.-S. Park, D.H. Kim, I.S. Chang, B.-G. Kim. *Journal of Bioscience and Bioengineering,* **2009**, *108*: 41.
21. C.L. Davey, L.W. Powell, N.J. Turner, A. Wells. *Tetrahedron Letters,* **1994**, *35*: 7867.
22. K. Nakamura, S.-i. Kondo, Y. Kawai, K. Hida, K. Kitano, A. Ohno. *Tetrahedron: Asymmetry,* **1996**, *7*: 409.
23. F.-D. Irimie, C. Paizs, M.-I. Tosa, C. Afloroaei, V. Miclaus. *Heterocyclic Communications,* **1997**, *3*: 549.
24. F.D. Irimie, C. Paisz, M. Tosa. "Biotransformari in sinteza organica, aspecte fundamentale". Napoca Star, **2006**
25. P.V. Podea, C. Paizs, M.I. Tosa, F.D. Irimie. *Tetrahedron Asymmetry,* **2008**, *19*: 1959.
26. C. Paizs, M. Tosa, C. Majdik, P. Moldovan, L. Novak, P. Kolonits, A. Marcovici, F.-D. Irimie, L. Poppe. *Tetrahedron Asymmetry,* **2003**, *14*: 1495.
27. C. Paizs, M. Tosa, V. Bodai, G. Szakacs, I. Kmecz, B. Simandi, C. Majdik, L. Novak, F.-D. Irimie, L. Poppe. *Tetrahedron Asymmetry,* **2003**, *14*: 1943.
28. M. Tosa, S. Pilbak, P. Moldovan, C. Paizs, G. Szatzker, G. Szakacs, L. Novak, F.-D. Irimie, L. Poppe. *Tetrahedron Asymmetry,* **2008**, *19*: 1844.
29. H. Pellissier. *Tetrahedron,* **2008**, *64*: 1563.
30. A. Kamal, M.A. Azhar, T. Krishnaji, M.S. Malik, S. Azeeza. *Coordination Chemistry Reviews,* **2008**, *252*: 569.
31. C. Paizs, P. Taehtinen, M. Tosa, C. Majdik, F.-D. Irimie, L.T. Kanerva. *Tetrahedron,* **2004**, *60*: 10533.
32. C. Paizs, M. Tosa, C. Majdik, P. Tahtinen, F.D. Irimie, L.T. Kanerva. *Tetrahedron Asymmetry,* **2003**, *14*: 619.
33. C. Paizs, P. Tahtinen, K. Lundell, L. Poppe, F.-D. Irimie, L.T. Kanerva. *Tetrahedron Asymmetry,* **2003**, *14*: 1895.
34. P.V. Podea, M.I. Tosa, C. Paizs, F.D. Irimie. *Tetrahedron Asymmetry,* **2008**, *19*: 500.
35. S.A. Brown, M.-C. Parker, N.J. Turner. *Tetrahedron: Asymmetry,* **2000**, *11*: 1687.
36. C. Paisz, C. Majdik, M. Tosa, R. Misca, F.D. Irimie. *Romanian Biotechnological Letters,* **2001**, *6*: 325.

STUDIA UNIVERSITATIS BABEŞ-BOLYAI, CHEMIA, LIV, 4, 2009

SYNTHESIS AND FLUORESCENCE PROPERTIES OF NEW SCHIFF BASES CONTAINING PHENOTHIAZINE UNITS

EMESE GÁL[a], LUIZA GĂINĂ[a], TAMÁS LOVÁSZ[a], CASTELIA CRISTEA[a] AND LUMINIȚA SILAGHI-DUMITRESCU[a]

ABSTRACT. New heterocyclic Schiff bases exhibiting fluorescent properties were obtained in good yields by thermal condensation of (10-alkyl)-3-formyl-10*H*phenothiazine derivatives with aromatic amines. Structural characterization was based on high resolution NMR, UV-Vis and fluorescence spectroscopy. Emission maxima were situated in the range 524-588 nm showing large Stokes shifts.

Keywords: Schiff bases, formylphenothiazine, fluorescence spectroscopy.

INTRODUCTION

Schiff bases characterized by diverse structural properties can be obtained by relatively simple preparation procedures based on condensation reaction of aromatic amines and carbonyl derivatives [1] This synthetic flexibility enabled the design of molecular structures with tuneable properties and numerous representative derivatives found a wide variety of applications in many fields such as biology (due to similarities with natural biological compounds [2] analytical chemistry (optical, electrochemical, and chromatographic sensors) [3,4] and materials chemistry (*e.g.* due to electroluminescent properties required in *light emitting diodes* OLED, PLED)

Successful application of Schiff bases requires a careful study of their characteristics because many of these azomethines are chemically unstable and show a pronounced tendency to be involved in tautomeric equilibria, hydrolysis, or formation of ionized species [5]

Schiff bases containing phenothiazine units were obtained either by condensation of N-alkyl-3-aminophenothiazine derivatives with benzaldehyde derivatives [6,7], or by condensation of N-alkyl-3-formylphenothiazine derivatives with aromatic primary amines such as aniline [8], aminobenzoic acid derivatives [9] and 5-amino-1-phenyl-pyrazol derivatives [10]. Previous studies regarding the preparation of *bis*-Schiff bases containing phenothiazine units indicate also two alternative synthetic routes, the condensation of N-alkyl-3-formylphenothiazine derivatives with aliphatic or aromatic diamines [10,11] as well as condensation

[a] *Universitatea Babeş-Bolyai, Facultatea de Chimie şi Inginerie Chimică, Str. Kogălniceanu, Nr. 1, RO-400084 Cluj-Napoca, Romania, castelia@chem.ubbcluj.ro*

of N-alkyl-3,7-diformylphenothiazine with amines [12]. Polyazomethine-type conjugated polymers with alternating phenothiazine (PZ) and azomethine units (-C=N-), were synthesized and their electroluminescent properties were studied from the viewpoint of polymer structure vs. emission color and efficiency. Single- and double-layer ***p**olymer **l**ight-**e**mitting **d**iode* PLEDs were fabricated [13]. The conjugated copolymer, poly[N-(2-ethylhexyl)phenothiazine-alt-6-Ph phenanthridine] [poly(PZ-PTI)], with azomethine linkages, was also synthesized by a Schiff-base reaction. Single-layered and double-layered PLED made with poly(PZ-PTI) as an emitting layer were fabricated and exhibited EL (emission) at 572 nm [14].

The aim of this work is to add new data to our previous reports, by describing the synthesis and structural characterization of new Schiff bases containing phenothiazine units and to emphasize their electroluminescent properties by fluorescence spectroscopy.

RESULTS AND DISCUSSION

A series of new Schiff bases **3-4** were obtained by the condensation of 10-alkyl-3-formylphenothiazine **1** with aniline*/p*-aminobenzoic acid derivatives **2** as shown in scheme 1.

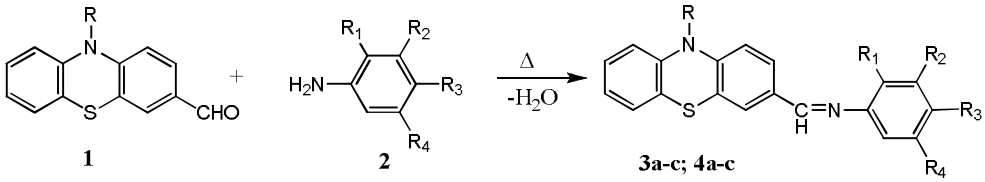

3.a.: R= -CH_2-CH_3; R_1= R_2=R_4= H; R_3 = -COOH
3.b.: R = -CH_2-CH_3; R_1 = Cl, R_2,=R_3= H; R_4 = -COOH
3.c.: R = -CH_2-CH_3; R_1=R_2=R_4= H; R_3 = -OCH_3
4.a.: R = -CH_3; R_1=R_2=R_4= H; R_3 = -COOH
4.b.: R= -CH_3; R_1 = Cl, R_2=R_3= H; R_4 = -COOH
4.c.: R = -CH_3; R_1=R_2=R_4 = H; R_3 = -Cl

Scheme 1

Similar conditions consisting of heating the reaction mixture to reflux in ethanol solution, were applied for the condensation of 10-alkyl-3,7-diformylphenothiazine with aniline*/p*-aminobenzoic acid derivatives leading to *bis*-Schiff bases **5a-c** (scheme 2).

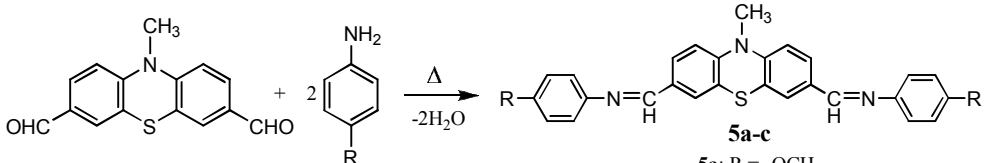

5a: R = -OCH_3
5b: R = -Br
5c: R = -COOH

Scheme 2

Bis-Schiff base **6** was obtained in good yields by the condensation of 3-formyl-10*H*-phenothiazine [15] with *p,p'*-diamino diphenylmethane (scheme 3). Due to unsubstituted NH group in the heterocycle unit, oxidation occurs easily in the presence of air.

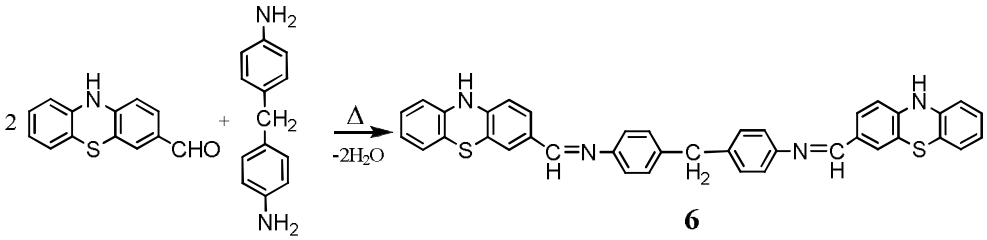

6

Scheme 3

The structure assignment of new Schiff bases **3-6** is supported by spectroscopic data. EI mass spectra revealed the corresponding molecular peaks. In particular, azomethine group can be clearly identified by the appearance of the characteristic proton and carbon resonances in NMR spectra, as a deshielded singlet signal situated at 8.3-8.5 ppm in the ^{1}H-NMR spectra and a signal situated at 153-160 ppm in the ^{13}C-NMR spectra.

The absorption of the *e.m*. radiation in the UV-Vis domain generated electronic spectra with characteristic maxima presented in table 1 for both starting materials (3-formyl-phenothiazine derivatives) and new Schiff bases. All Schiff bases **3-6** contain the same cromophor unit consisting of an extended π conjugated system containing phenothiazinyl and phenyl aromatic units linked by an azomethine group and thus, very similar absorption maxima were recorded in the UV spectra. However, a small bathochromic shift can be noticed for lowest energy absorption maxima of *bis*-Schiff bases **5** as compared to mono Schiff bases **3**-**4**.

As expected, substitution of the heterocyclic nitrogen atom does not exert great influence upon the position of the absorption maxima. Small shifts can be correlated with the nature of auxochrome groups attached in position *meta* or *para* of the phenyl units.

The emission spectra of Schiff bases **3-6** contain broad bands in the range 525-588 nm with large Stokes shifts (6000-8600 cm^{-1}) as shown in Table 1.

The Schiff bases **3a** and **4a** are characterized by lower energy emission maxima ($\lambda_{max,\ em}$ 588 nm and 583 nm respectively) as compared to *bis*-Schiff base **5c** ($\lambda_{max,\ em}$ 535 nm). Meanwhile, the smallest Stokes shifts were observed for *bis*-Schiff bases **5** (5800-6100 cm^{-1}), a fact in agreement with literature data stating that great Stokes shifts can be assigned to large geometrical changes upon excitation from nonplanar ground state to a essentially planarized excited state [16].

Table 1. Electronic properties of Schiff base determined by UV-Vis and LE spectroscopy in THF

Compound	Absorption $\lambda_{max, abs}$ [nm]	Emission $\lambda_{max, em}$ [nm]	Stokes shift (cm^{-1})
3.a.	243, 278, **392**	**588**	8500
3.b.	245, 279, **389**	572	8200
3.c.	236, 273, **379**	528	7400
4.a.	243, 275, **388**	**583**	8600
4.b.	244, 285, **381**	554	8200
4.c.	239, 275, **380**	545	8000
5.a.	234, 290, **401**	524	5800
5.b.	241, 298, **411**[a]	546	5900
5.c.	287, **404**	**535**	6100
6.	244, 294, **399**[a]	525	6000
10-Me-3-formyl-phenothiazine	286, **377**[a]	525	7500
10-Et-3-formyl-phenothiazine	294, **381**[a]	528	7300
10*H*-3-formyl-phenothiazine	292, **393**[a]	523	6300
10-Me-3,7-diformyl-phenothiazine	284, **394**[a]	521	6200

[a]-the UV-Vis, and Fluorescence spectra were recorded in ACN

CONCLUSIONS

Thermal condensation of (10-alkyl)-3-formyl-10*H*phenothiazine derivatives with aromatic amines generate heterocyclic Schiff bases characterized by green-yellow fluorescence. The exhibited emission maxima were situated in the range 524-588 nm showing large Stokes shifts (6000-8500 cm^{-1}), thus recommending these compounds for possible applications in nonlinear optical materials.

EXPERIMENTAL SECTION

FT-IR spectrometer Bruker Vector 22; 300 MHz NMR spectrometer Bruker; UV-Vis spectrometer Perkin Elmer Lambda 35; Luminescence Spectrometer Perkin Elmer LS 55; EI MS Shimadzu QP 2010; Merck reagents.

4-((10-ethyl-10*H*phenothiazin-3yl)-methylenamino)benzoic acid 3.a.
3-Formyl-10-ethyl-phenothiazine 0.5g (1.9mmol) and p-amino-benzoic acid 0.268g (1.9mmol) were refluxed in ethanol for 24 hours. After solvent evaporation an orange powder product with melting point 249℃ w as obtained in 80% yield.
MS (EI) m/z= 374 (63%) $M^{+\cdot}$
^{1}H NMR, 400 MHz, DMSO-d_6: -CH_2 δ= 3.98 ppm (q, ^3J=6.80 Hz, 2H) -CH_2; δ= 1.34 ppm (t, ^3J=6.8 Hz, 3H) -CH_3; δ= 7.13 ppm, (d, ^3J= 8.8 Hz, 1H) H_1; δ= 7.75 ppm, (d, ^3J= 8.8 Hz, 1H) H_2, δ=8.50 ppm, (s, 1H) CH=N; δ=7.67 ppm, (s, 1H) H_4; δ=7.07 ppm, (d, ^3J= 8 Hz, 1H) H_6; δ=6.98 ppm, (t, ^3J= 8 Hz, 1H) H_7; δ= 7.22 ppm, (t, ^3J= 7.6 Hz, 1H) H_8; δ=7.16 ppm, (d, ^3J= 7.6 Hz, 1H) H_9; δ= 7.97 ppm, (d, ^3J=8.4 Hz, 2H) $H_{2',6'}$; δ= 7.29 ppm, (d, ^3J=8.4 Hz, 2H) $H_{3'5'}$; δ= 12.85 ppm, (s, 1H) -COOH.

^{13}C NMR, DMSO-d_6: δ ppm 12.5 (-CH_2), 41.5 (-CH_3), 127.1 (C_1), 129.3 (C_2), 130.1 (C_3), 126.8 (C_4), 124.6 (C_{4a}), 122.8 (C_{5a}), 115.8 (C_6), 123.1 (C_7), 127.9 (C_8), 115.2 (C_9), 143.1 (C_{9a}), 160.6 (CH=N), 155.5 ($C_{1'}$), 130.5 ($C_{2',6'}$) 121 ($C_{3'5'}$), 121.9 ($C_{4'}$), 167.2 (COOH).

4-Chloro-3-((10-ethyl-10H-phenothiazin-3-yl)methyleneamino)benzoic acid 3.b.

3-formyl-10-ethyl-phenothiazine 0.5g (1.9mmol) and 3-amino-4-chloro-benzoic acid 0.266g (1.9mmol) were were stirred at 78℃ for 24 hours in isoamyl-alcohol. The product was purified by recrystallization from ethyl acetate. A light green coloured solid precipitate, with melting point 209℃, was co llected by filtration. Yield 50%.

MS: m/z= 408/410(73%) $M^{+\cdot}$

^{1}H NMR, 400 MHz, DMSO-d_6: δ= 3.97 ppm (q, ^3J=7 Hz, 2H) CH_2; δ= 1.33 ppm (t, ^3J=7 Hz, 3H) CH_3; δ= 7.14 ppm, (d, ^3J=8.4 Hz, 1H) H_1; δ= 7.79 ppm, (d, ^3J=8.4 Hz, 1H) H_2, δ=8.51 ppm, (s, 1H) CH=N; δ=7.69 ppm, (s, 1H) H_4; δ=7.05 ppm, (d, ^3J=8.4 Hz, 1H) H_6; δ=6.98 ppm, (dd, ^3J=8.4 Hz, ^3J=8 Hz, 1H) H_7; δ= 7.21 ppm, (dd, ^3J= 9.2 Hz, ^3J=8 Hz, 1H) H_8; δ=7.12 ppm, (d, ^3J= 9.2 Hz, 1H) H_9, δ= 7.71 ppm (s, 1H) $H_{2'}$; δ= 7.76 ppm, (d, ^3J= 8.4 Hz, 1H) $H_{6'}$; δ= 7.63 ppm, (d, ^3J= 8.4 Hz, 1H) $H_{5'}$.

^{13}C NMR, DMSO-d_6: δ ppm: 12.2 (-CH_2), 41.5 (-CH_3), 126.7 (C_1), 129.2 (C_2), 130.6 (C_3), 161.5 (C=N), 129.9 (C_4), 127.3 (C_{4a}), 122.6 (C_{5a}), 115.8 (C_6), 122.9 (C_7), 126.8 (C_8), 115.6 (C_9), 142.8 (C_{9a}), 144.8 (C_{10a}), 148.6 ($C_{3'}$), 127.3 ($C_{4'}$), 120.4 ($C_{5'}$), 121.7 ($C_{6'}$), 131.8 ($C_{1'}$), 147.2 ($C_{2'}$), 166.2 (COOH).

4-methoxy-N-((10-ethyl-10*H*-phenothiazin-3-yl)methylene)aniline 3.c.

3-formyl-10-ethyl-phenothiazine 0.5g (1.9mmol) and p-metoxy-aniline 0.246g (2.1mmol) were refluxed in ethyl alcohol for 24 hours. The product was purified by recrystallization from ethanol. A lemon-yellow coloured solid precipitate was collected by filtration, with melting point 108℃. Yield 76%.

MS: m/z= 360 (76%) $M^{+\cdot}$

^{1}H NMR, 400 MHz, DMSO-d_6: δ= 3.93 ppm (q, ^3J=7 Hz 2H) -CH_2; δ= 1.41 ppm (t, ^3J=7 Hz 3H) CH_3; δ= 6.86 ppm, (d, ^3J= 8.40 Hz, 1H), H_1; δ= 7.58 ppm, (d, ^3J= 8.40 Hz, 1H) H_2: δ=8.30 ppm, (s, 1H) CH=N; δ=7.63 ppm, (s, 1H) H_4; δ=7.09 ppm, (d, ^3J= 8 Hz 1H) H_6; δ=6.91 ppm, (t, ^3J= 8 Hz, 1H) H_7; δ= 7.58 ppm, (t, ^3J= 8 Hz, 1H) H_8; δ= 6.84 ppm, (d, ^3J= 8.4 Hz 1H) H_9, δ= 6.90 ppm (d, ^3J= 8.8 Hz, 2H) $H_{2',6'}$; δ= 7.18 ppm, (d, ^3J= 8.8 Hz, 2H) $H_{3',5'}$.

^{13}C NMR, DMSO-d_6 δ ppm: 12.9 (CH_2), 42.1 (CH_3), 55.4 (OCH_3)114.6 (C_1), 128.3 (C_2), 130.9 (C_3), 153.8 (C=N), 126.9 (C_4), 124.4 (C_{4a}) 123.6 (C_{5a}), 127.3 (C_6), 122.8 (C_7), 127.3 (C_8), 115.2 (C_9), 143.8 (C_{9a}), 147.2 (C_{10a}), 144.9 ($C_{1'}$), δ= 114.3 ($C_{2',6'}$), 122.1 ($C_{3',5'}$), 158.0 (C_4).

4-((10-methyl-10Hphenothiazin-3yl)-methylenamino)benzoic acid 4.a.

3-formyl-10-methyl-phenothiazine 0.5g (2.0mmol) and p-amino-benzoic acid 0.28g (2.0mmol) were refluxed in ethyl alcohol for 24 hours. The product was purified by recrystallization from toluene. After filtration an orange yellow coloured solid precipitate was collected by filtration, with melting point 256℃. Yield 70%.

MS: m/z= 360 (68%) $M^{+\cdot}$

^{1}H NMR, 400 MHz, DMSO-d_6: δ= 3.5 ppm (s, 3H) CH_3; δ= 6.99 ppm, (d, ^3J= 5.2 Hz, 1H) H_1; δ= 7.71 ppm, (d, ^3J= 5.2 Hz, 1H) H_2, δ=8.51 ppm, (s, 1H) CH=N; δ=7.70 ppm (s, 1H) H_4; δ=7.19 ppm, (d, ^3J= 6.4 Hz, 1H) H_6; δ=7.03 ppm, (dd, ^3J= 6.4 Hz,

^3J= 8.2 Hz 1H) H_7; δ= 7.24 ppm, (t, ^3J= 8.2 Hz, ^3J= 7.6 Hz, 1H) H_8; δ=7.02 ppm, (d, ^3J= 7.6 Hz, 1H) H_9; δ= 7.26 ppm, (d, ^3J= 8.4 Hz, 2H), $H_{3',5'}$; δ= 7.98 ppm, (d, ^3J= 8.4 Hz, 2H) $H_{2',6}$; δ= 9.80 ppm, (s, 1H) -COOH.

^{13}C NMR, DMSO-d_6 δ ppm**:** 35.5 (-CH_3), 114.6 (**C_1**), 159.5 (C=N), 126.8 (C_4), 126.5 (C_{4a}), 126.9 (C_6), 129.5 (C_7), 121.2 (C_8), 142.5 (C_{9a}), 144.8 (C_{10a}), 118,4 (C_{5a}), 155.5 ($C_{1'}$), 130.5 ($C_{2',6'}$), 121 ($C_{3'5'}$), 121.9 ($C_{4'}$), 167 (COOH).

4-chloro-3-((10-methyl-10H-phenothiazin-3-yl)methyleneamino)benzoic acid 4.b.

3-formyl-10-methyl-phenothiazine 0.5g (2.0mmol) and 3-amino-4-chloro-benzoic acid 0.53g (2.0mmol) were heated at 78℃ in isoamyl -alcohol under stirring for 24 hours. The product was purified by recrystallization from ethyl acetate. After filtration an orange yellow coloured solid precipitate was collected by filtration, with melting point 243-244℃. Yield 80%.

MS: m/z= 394/396 (72%) $M^{+\cdot}$

^{1}H NMR, 300 MHz, DMSO-d_6: δ= 3.38 ppm (s, 3H) **-**CH_3; δ= 7.02 ppm, (d, ^3J= 7.8 Hz, 1H) H_1; δ= 7.81 ppm, (d, ^3J= 7.8 Hz, 1H) H_2; δ=8.51 ppm, (s, 1H) CH=N; δ=7.70 ppm, (s, 1H) H_4; δ=7.19 ppm, (d, ^3J= 8.1 Hz, 1H) H_6; δ=6.99 ppm, (t, ^3J= 8 Hz,1H) H_7; δ= 7.24 ppm, (t, ^3J= 8 Hz, 1H) H_8; δ=7.08 ppm, (d, ^3J= 8.4 Hz, 1H) H_9, δ= 7.60 ppm, (d, ^3J= 8.1 Hz, 1H) $H_{5'}$; δ= 7.76 ppm, (d, ^3J= 8.1 Hz, 1H) $H_{6'}$; δ= 7.73 ppm, (s, 1H) $H_{2'}$.

4-Chloro-N-((10-methyl-10H-phenothiazin-3-yl)methylene)aniline 4.c.

3-formyl-10-methyl-phenothiazine 1g (4.14mmol) and 4-chloroaniline 0.53g (4.14mmol) were refluxed in ethanol for 6 hours. After filtration an orange yellow coloured solid precipitate with melting point 125℃ was collected. Yield 98%.

MS m/z= 349/401 (100%) $M^{+\cdot}$

^{1}H NMR, 300 MHz, $CDCl_3$: δ= 3.42 ppm (s, 3H) CH_3; δ= 6.82 ppm (d, ^3J= 8.4 Hz, 1H) H_1; δ= 7.63 ppm (d, ^3J= 8.4 Hz, 1H) H_2; δ=8.29 ppm (s, 1H) CH=N; δ=7.70 ppm, (s, 1H) H_4; δ=7.22 ppm (d, ^3J= 7.0 Hz, 1H) H_6; δ=6.98 ppm, (t, ^3J= 7.2 Hz, 1H) H_7; δ= 7.23 ppm (t, ^3J= 7.2 Hz, 1H) H_8; δ=6.85 ppm (d, ^3J= 8.4 Hz, 1H) H_9; δ= 7.35 ppm (d, ^3J= 8.6 Hz, 2H) $H_{2',6'}$; δ= 7.14 ppm, (d, ^3J= 8.6 Hz, 2H) $H_{3',5'}$.

^{13}C NMR, $CDCl_3$ δ ppm**:** 35.6 (-CH_3), 126.9 (C_1), 129.1 (C_2), 130.5 (C_3), 159.2 (C=N), δ= 129.2 (C_4), 122.7 (C_{5a}), 114.5 (C_6), 123.1 (C_7), 123.9 (C_8), 114.5 (C_9), 144.7 (C_{9a}), 144.8 (C_{10a}), 118,5 (C_{4a}) 148.6 (C_1), 127.2 ($C_{2',6'}$), 122.2 ($C_{3'5'}$), 150.6 ($C_{4'}$).

***N,N'*-(10-methyl-10*H*-phenothiazine-3,7-diyl)bis(methan-1yl-1-ylidene)bis (4-methoxyaniline) 5.a.**

3,7-diformyl-10-methyl-phenothiazine 0.5g (1.86mmol) and 4-methoxy-aniline 0.45g (3.7mmol) were refluxed in ethanol under stirring for 16 hours. After filtration an orange yellow coloured solid was obtained, melting point 234℃. Yield 68%.

MS m/z= 479 (100%) $M^{+\cdot}$

^{1}H NMR, 300 MHz, $CDCl_3$: δ= 3.47 ppm (s, 3H) CH_3; OCH_3 δ= 3.85 ppm, (s, 6H); δ= 6.86 ppm, (d, ^3J= 8.4 Hz, 2H) $H_{1,9}$; δ= 7.64 ppm, (d, ^3J= 8.4 Hz, 2H) $H_{2,8}$; δ=8.36 ppm, (s, 2H) CH=N; δ=7.71 ppm, (s, 2H) $H_{4,6}$; δ= 6.94 ppm, (d, ^3J= 8.8 Hz, 4H) $H_{2'2'',6'6''}$; δ= 7.23 ppm, (d, ^3J= 8.8 Hz, 4H) $H_{3'3''5'5''}$.

^{13}C NMR, $CDCl_3$ δ (ppm)**:** 35.9 (-CH_3), 55.5 (-OCH_3); 126.7 ($C_{1,9}$), 128.7 ($C_{2,8}$), 131.6 ($C_{3,7}$), 158.1 (C=N), 122.2 ($C_{4,6}$), 124.4 ($C_{4a,5a}$) 147.2($C_{9a,10a}$) 114.8 ($C_{2'2'',6'6''}$), 148.1 ($C_{1'1''}$), 124.8 ($C_{3'3''5'5''}$), 156.7 ($C_{4'4''}$).

***N,N'*-(10-methyl-10*H*-phenothiazine-3,7-diyl)bis(methan-1yl-1-ylidene)bis (4-bromoaniline) 5.b.**

3,7-diformyl-10-methyl-phenothiazine 0.5g (1.86mmol) and 4-bromoaniline 0.64g (3.72mmol) were refluxed in ethanol was stirred for 10 hours at 78℃.. After filtration an orange yellow coloured solid precipitate was obtained, with melting point 222-224℃. Yield 58%.

MS m/z= 575/577/579 (100%) $M^{+\cdot}$

^{1}H NMR, 300 MHz, $CDCl_3$: δ= 3.49 ppm (s, 3H) CH_3; δ= 6.88 ppm, (d, ^{3}J= 8.4 Hz, 2H) $H_{1,9}$; δ= 7.65 ppm, (d, ^{3}J= 8.4 Hz, 2H) $H_{2,8}$; δ=8.31 ppm, (s, 2H) CH=N; δ=7.72 ppm, (s, 2H) $H_{4,6}$; δ= 7.51 ppm, (d, ^{3}J= 8.6 Hz, 4H) $H_{2',2''6'6''}$,; δ= 7.09 ppm, (d, ^{3}J= 8.6 Hz, 4H) $H_{3'3''5'5''}$.

^{13}C NMR, $CDCl_3$ δ (ppm)**:** 30.9 (-CH_3); 126.9 ($C_{1,9}$), 129,2 ($C_{2,8}$), 131.2 ($C_{3,7}$), 158.9 (C=N), 122.6 ($C_{4,6}$), 118.2 ($C_{4a,5a}$) 144.8 ($C_{9a,10a}$) 114.8 ($C_{2'2'',6'6''}$),147,5 ($C_{1'1''}$), 124.8 ($C_{3'3''5'5''}$), 122.3 ($C_{4'4''}$).

***4,4'*-(10-methyl-10*H*-phenothiazine-3,7-diyl)bis(methan-1yl-1-ylidene)bis(aza-1-yl-1-ylidene)dibenzoic acid 5.c.**

3,7-diformyl-10-methyl-phenothiazine 0.39g (1.4mmol) and p-amino-benzoic acid 0.39g (2.8mmol) in ethyl alcohol was refluxed for 24 hours at 78℃. The product was purified by recrystallization from ethanol. An orange coloured solid precipitate was collected by filtration, with melting point 308℃ (decomp.). Yield 75%.

^{1}H NMR, 400 MHz, DMSO-d6: δ= 3.38 ppm (s, 3H) CH_3; δ= 6.66 ppm, (d, ^{3}J= 8.4 Hz, 2H) $H_{1,9}$; δ= 7.61 ppm, (d, ^{3}J= 8.4 Hz, 2H) $H_{2,8}$; δ=8.30 ppm, (s, 2H) CH=N; δ=7.65 ppm, (s, 2H) $H_{4,6}$; δ= 7.981 ppm, (d, ^{3}J= 7.6 Hz, 4H) $H_{2',2''6'6''}$,; δ= 7.29 ppm, (d, ^{3}J= 7.6 Hz, 4H) $H_{3'3''5'5''}$.

^{13}C NMR, DMSO-d6: δ (ppm)**:** 35.6 (-CH_3); 115.3 ($C_{1,9}$), 120,9 ($C_{2,8}$), 131.2 ($C_{3,7}$), 159 (C=N), 125.8 ($C_{4,6}$), 124.6 ($C_{4a,5a}$), 147.8, 143.1 ($C_{9a,10a}$), 130.6 ($C_{2'2'',6'6''}$), 138.8 ($C_{1'1''}$), 121.0 ($C_{3'3''5'5''}$), 128.5 ($C_{4'4''}$).

4,4'-methylene*bis*(N-(10*H*-phenothiazin-3-yl)methylene)aniline)-4,4'-methylenedianiline 6

3-formil-10*H*-phenothiazine 0.6g (2.6mmol) and *p,p'*-diamino-diphenyl-methane 0.26g (1.3mmol) in ethyl alcohol was refluxed for 6 hours. The product was filtered and then purified by recrystallization from toluene. A lemon yellow coloured solid precipitate was collected by filtration, with melting point 310℃. Yield 65%. m/z= 616 ($M^{+\cdot}$, rel. int. 100%)

^{1}H NMR, 400 MHz, DMSO-d_6: δ= 3.95 ppm, (s, 2H) –CH_2-; δ= 6.73 ppm, (d, ^{3}J= 8.4 Hz, 2H) H_1; δ= 6.93 ppm, (d, ^{3}J= 8.4 Hz, 2H) H_2; δ=8.36 ppm, (s, 2H) CH=N; δ=7.43 ppm, (s, 2H) H_4; δ=7.51 ppm, (d, ^{3}J= 8.4 Hz, 2H) H_6; δ=6.79 ppm, (t, ^{3}J= 8.4 Hz, 2H) H_7; δ= 7.10 ppm, (t, ^{3}J= 8.4 Hz, 2H) H_8; δ=6.70 ppm, (d, ^{3}J= 8 Hz, 2H), H_9; δ= 7.14 ppm, (d, ^{3}J= 8.4 Hz, 4H), $H_{2'2'',6'6''}$; δ= 7.25 ppm, (d, ^{3}J= 8.4 Hz, 4H) $H_{3'3'',5'5''}$; δ= 9.01 ppm, (s, 2H) NH.

^{13}C NMR, DMSO-d_6: δ ppm: 114.1 (C_1), 125.2 (C_2), 158.4 (C=N), 126.1 (C_4), δ128.9 (C_6), 122.5 (C_7), 127.7 (C_8), 114.7 (C_9), 144.5 (C_{9a}), 148.3 (C_{10a}), 122.9 (C_{5a}) 123.9 (C_{4a}) 138.7 ($C_{1',1''}$), 121.0 ($C_{2'2'',6'6''}$), 130.6 ($C_{3'3'',5'5''}$), 138.7 ($C_{4',4''}$), 40,9 (CH_2).

ACKNOWLEDGMENTS

Financial support from Roumanian Ministery of Education, Research and Inovation, for Coop. Bil. 40/10.06.08 Ro-Ua is greatly acknowledged.

REFERENCES

1. S. Patai Ed., "The Chemistry of the Carbon-Nitrogen Double Bond", J. Wiley & Sons, London, **1970**.
2. U. Spichiger-Keller, "Chemical Sesors and Biosensors for Medical and Biological Applications", Wiley-VCH, Weinheim, **1998**.
3. E. Jungreis, S. Thabet, "Analytical Applications of Schiff bases", Marcell Dekker, New York, **1969**.
4. N. I. Mohamed, E. Salah, A. Sharif, *E-Journal of Chemistry http://www.e-journals.net,* **2007**, *4* (4), 531.
5. a) Z. Cimerman, Z. Stefanac, *Polyhedron*, **1985**, *4,* 1755; b) N. Galic, Z. Cimerman, V. Tomisic, *Anal*. *Chim*. *Acta*, **1997**, *343*, 135.
6. V.A. Skorodumov, S.V. Zhuravlev, *Russian J. Org. Chem.,* **1965,** *2* (1), 363.
7. D. Simov, Ek.M. Simova, *Doklady Bolgarskoi Akademii Nauk,* **1958**, *11*, 407.
8. M. Jitaru, G. Petrica, L.I. Gaina, C. Cristea, T. Lovasz, I.A. Silberg, *Rev. Roum. Chim.,* **2002**, *47* (3-4), 249.
9. D.S. Belei, I. Ciocoiu, C. Ciocoiu, E. Bacu, *Anal. St. Univ. "Al. I. Cuza" Iasi, Chimie*, **2001**, *9*, 155.
10. L. Gaina, T. Lovasz, I.A. Silberg, C. Cristea, S. Udrea, *Heterocycl. Commun.*, **2001**, *7* (6), 549.
11. W. Kremers, J.W. Steele, *Can. J. Chem.,* **1967**, *45*, 745
12. K. Rehse, T. Siedel, *Arch. Pharm*., **1992**, *325*, 235.
13. W. Jeon, Y. Kwon, J.J. Baek, L.S. Park, E.W. Lee, Y.S. Han, H.T. Kim., *J. Nonlinear Opt. Phys. Mater.*, **2005**, *14* (4), 545.
14. Y.S. Han, S.D. Kim, Y. Kwon, K.H. Choi, L.S. Park, *Mol. Cryst. Liq. Cryst.,* **2006**, *459*, 119.
15. L. Gaina, C. Cristea, C. Moldovan, D. Porumb, E. Surducan, C. Deleanu, A. Mahamoud, J. Barbe and I.A. Silberg, *Int. J. Mol. Sci*., **2007**, *8*, 70.
16. L. Yang, J.K. Feng, A.M. Ren, *J. Org. Chem*., **2005**, *70*, 5987.

STUDIA UNIVERSITATIS BABEŞ-BOLYAI, CHEMIA, LIV, 4, 2009

ON OMEGA POLYNOMIALS OF C_{40n+6} FULLERENES

MARYAM JALALI[a] AND MODJTABA GHORBANI[a]

ABSTRACT. The Omega polynomial is defined as $\Omega(G,x)=\sum_s m\cdot x^s$ where m(G,s) is the number of ops strips of length s. Also, the Sadhana polynomial is defined as $Sd(G,x)=\sum_s m(G,s)\cdot x^{|E|-s}$. This last polynomial has been defined to evaluate the Sadhana index of a molecular graph. In this paper, the Omega and Sadhana polynomials of an infinite family of fullerenes is computed for the first time.

Keywords: Fullerene, Omega and Sadhana Polynomials, Sadhana Index.

INTRODUCTION

Fullerenes are polyhedral molecules, consisting solely of carbon atoms. Fullerenes C_n can be drawn for n = 20 and for all even $n \geq 24$. They have n carbon atoms, 3n/2 bonds, 12 pentagonal and n/2-10 hexagonal faces. The most important member of the family of fullerenes is C_{60} [1, 2].

Let G = (V, E) be a connected bipartite graph with the vertex set V = V(G) and the edge set E = E(G), without loops and multiple edges. Two edges e = (u,v) and f = (x,y) of a graph G are called equidistant if the two ends of one edge show the same distance to the other edge. However, the distance between edges can be defined in several modes, as presented below. The distance from a vertex z to an edge e = (u,v) is taken as the minimum distance between the given point and the two endpoints of that edge [3]:

$$d(z,e)=\min\{d(z,u),d(z,v)\} \quad (1)$$

Then, the edge $e=(u,v)$ is equidistant to $f=(x,y)$ if:

$$d(x,e)=d(y,e) \quad (2)$$

Or the edges e = (u, v) and f = (x, y) are equidistant if:

$$d(x,e)=d(y,e) \text{ and } d(u,f)=d(v,f) \quad (3)$$

[a] *Department of Mathematics, Faculty of Science, Shahid Rajaei Teacher Training University, Tehran, 16785–136, I R. Iran; Ghorbani30@gmail.com; Institute of Nanoscience and Nanotechnology, University of Kashan, Kashan 87317-51167, I. R. Iran*

A second definition for equidistant edges joins the conditions for (topologically) parallel and perpendicular edges [4]:

$$d(v,x) = d(v,y) + 1 = d(u,x) + 1 = d(u,y), \text{ for } \square \text{ edges} \quad (4)$$

$$d(u,x) = d(u,y) = d(v,x) = d(v,y), \text{ for } \perp \text{ edges} \quad (5)$$

Omega Polynomial

Two edges e = (u, v) and f = (x, y) of G are called codistant (briefly: e co f) if they obey the topologically parallel edges relation (4).

For some edges of a connected graph G there are the following relations satisfied [5, 6]:

$$e \text{ co } e \quad (6)$$

$$e \text{ co } f \Leftrightarrow f \text{ co } e \quad (7)$$

$$e \text{ co } f \;\&\; f \text{ co } h \Rightarrow e \text{ co } h \quad (8)$$

though the relation (8) is not always valid.

Let $C(e) := \{f \in E(G); f \text{ co } e\}$ denote the set of edges in G, codistant to the edge $e \in E(G)$. If relation co is an equivalence relation (i.e., all the elements of C(e) satisfy the relations (6) to (8), then G is called a co-graph. Consequently, C(e) is called an orthogonal cut oc of G and E(G) is the union of disjoint orthogonal cuts: $E(G) = C_1 \cup C_2 \cup ... \cup C_k$ and $Ci \cap Cj = \emptyset$ for $i \neq j$, and $i, j = 1, 2, .., k$. Observe co is a Θ relation, (Djoković-Winkler [7,8], relations (6) to (8)), and G is a co-graph if and only if it is a partial cube [9], as Klavžar correctly stated in a recent paper [10].

If any two consecutive edges of an edge-cut sequence are topologically parallel within the same face of the covering, such a sequence is called an opposite edge strip ops, which is a quasi-orthogonal cut qoc strip. This means the transitivity relation (8) of the co relation is not necessarily obeyed. Any oc strip is an ops but the reverse is not always true.

Let m(G,s) be the number of ops of length s (i.e., the number of cut-off edges) in the graph G; for the sake of simplicity, m(G,s) will hereafter be written as m. The counting polynomials, defined on the ground of ops strips, [3, 5, 11-14] are as follows:

$$\Omega(G,x) = \sum_s m \cdot x^s \quad (9)$$

$$Sd(G,x) = \sum_s m x^{(|E(G)|-s)} \quad (10)$$

In a counting polynomial, the first derivative (in x=1) defines the type of property which is counted:

$$\Omega'(G,1) = \sum_s m \cdot s = e = |E(G)| \quad (11)$$

$$Sd'(G,1) = \sum_s m(|E(G)| - s) = Sd(G) \quad (12)$$

The Sadhana index Sd(G) of a graph G was defined by Khadikar *et al*. [12, 13] while the Sadhana polynomial by Ashrafi *et al*. [14]. From the definition of Omega polynomial, one can obtain the Sadhana polynomial by replacing x^s with $x^{|E(G)|-s}$ in Omega polynomial. Then the Sadhana index will be the first derivative of Sd(G,x) evaluated in x=1 [14]. Our notations are standard as taken from the textbooks and articles on Graph Theory [15-24].

Example 1. Suppose K_n denotes the complete graph on n vertices (see Figure 1). Then we have:

$$\Omega(K_n, x) = \binom{n}{2} x = (1/2)n(n-1)x\,; \quad Sd(K_n, x) = (1/2)n(n-1)x^{(1/2)(n^2-n-2)}$$

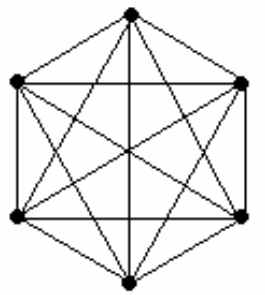

Figure1. Complete graph K_6.

Example 2. Let C_n denotes the cycle of length n. Then we have:

$$\Omega(C_n, x) = \begin{cases} \frac{n}{2} x^2 & 2 \mid n \\ nx & 2 \nmid n \end{cases}; \quad Sd(C_n, x) = \begin{cases} \frac{n}{2} x^{n-2} & 2 \mid n \\ nx^{n-1} & 2 \nmid n \end{cases}.$$

Example 3. Let T_n be a tree on n vertices. We know that $|E(T_n)| = n-1$. Thus, $\Omega(T_n, x) = (n-1)x;\ Sd(T_n, x) = (n-1)x^{n-2}$.

RESULTS AND DISCUSSION

The aim of this section is to compute the counting polynomials of equidistant edges (Omega and Sadhana polynomials) of an infinite family C_{40n+6} of fullerenes with 40n+6 carbon atoms and 60n+9 bonds (the graph in Figure 2 is n = 2).

Theorem. The omega polynomial of fullerene graph C_{40n+6} is as follows:

$$\Omega(G,x)=\begin{cases} a(x)+4x^{2n}+4x^{2n+1}+4x^{4n-1}+2x^{4n} & 5\mid n \\ a(x)+2x^{4n+3}+8x^{2n-2}+2x^{4n+4}+2x^{4n+1} & 5\mid n-1 \\ a(x)+8x^{2n}+4x^{2n-1}+2x^{4n}+2x^{4n+2} & 5\mid n-2 \\ a(x)+4x^{2n-2}+4x^{2n+2}+4x^{4n-1}+2x^{4n+2} & 5\mid n-3 \\ a(x)+4x^{2n-2}+4x^{2n-1}+4x^{2n}+2x^{4n+3}+x^{8n+6} & 5\mid n-4 \end{cases}$$

in which $a(x)=x+9x^2+4x^3+2x^4+(2n-3)x^{10}$.

Proof. By Figure 2, there are ten distinct cases of ops strips. We denote the corresponding edges by e_1, e_2, …, e_{10}. By using Table 1 and Figure 3 the proof is completed.

Corollary. The Sadhana polynomial of the fullerene graph C_{40n+6} is as follows:

$$Sd(G,x)=\begin{cases} b(x)+4x^{|E|-2n}+4x^{|E|-2n-1}+4x^{|E|-4n+1}+2x^{|E|-4n} & 5\mid n \\ b(x)+2x^{|E|-4n-3}+8x^{|E|-2n+2}+2x^{|E|-4n-4}+2x^{|E|-4n-1} & 5\mid n-1 \\ b(x)+8x^{|E|-2n}+4x^{|E|-2n+1}+2x^{|E|-4n}+2x^{|E|-4n-2} & 5\mid n-2 \\ b(x)+4x^{|E|-2n+2}+4x^{|E|-2n-2}+4x^{|E|-4n+1}+2x^{|E|-4n-2} & 5\mid n-3 \\ b(x)+4x^{|E|-2n+2}+4x^{|E|-2n+1}+4x^{|E|-2n}+2x^{|E|-4n-3}+x^{|E|-8n-6} & 5\mid n-4 \end{cases}$$

in which $b(x)=x^{|E|-1}+9x^{|E|-2}+4x^{|E|-3}+2x^{|E|-4}+(2n-3)x^{|E|-10}$

and $|E|=60n+9$.

Table 1. The number of opposite edges of e_i, $1\le i\le 10$.

No.	Number of opposite edges	Type of Edges
1	1	e_1
9	2	e_2
4	3	e_3
2	4	e_4
2n-3	10	e_5

2	$\begin{cases} 2n+1 & 5 \mid n \\ 4n+3 & 5 \mid n-1 \\ 2n & 5 \mid n-4, n-2 \\ 2n+2 & 5 \mid n-3 \end{cases}$	e_6
$\begin{cases} 2 \\ 4 \\ 4 \end{cases}$	$\begin{cases} 4n-1 & 5 \mid n-3 \\ 2n & 5 \mid n, n-2 \\ 2n-2 & 5 \mid n-1, n-4 \end{cases}$	e_7
$\begin{cases} 4 \\ 4 \\ 2 \end{cases}$	$\begin{cases} 2n-2 & 5 \mid n-1, n-3 \\ 2n-1 & 5 \mid n-2, n-4 \\ 4n-1 & 5 \mid n \end{cases}$	e_8
$\begin{cases} 1 \\ 2 \\ 2 \\ 2 \end{cases}$	$\begin{cases} 8n+6 & 5 \mid n-4 \\ 4n+2 & 5 \mid n-3 \\ 4n+4 & 5 \mid n-1 \\ 4n & 5 \mid n, n-2 \end{cases}$	e_9
2	$\begin{cases} 4n-1 & 5 \mid n, n-3 \\ 4n+1 & 5 \mid n-1 \\ 4n+2 & 5 \mid n-2 \\ 4n+3 & 5 \mid n-4 \end{cases}$	e_{10}
2	$\begin{cases} 2n+1 & 5 \mid n \\ 2n & 5 \mid n-2, n-4 \\ 2n+2 & 5 \mid n-3 \end{cases}$	e_{11}

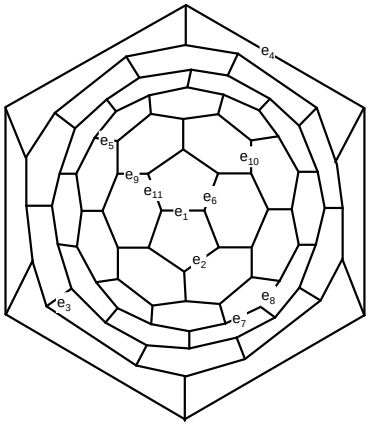

Figure 2. The graph of fullerene C_{40n+6} for n=2.

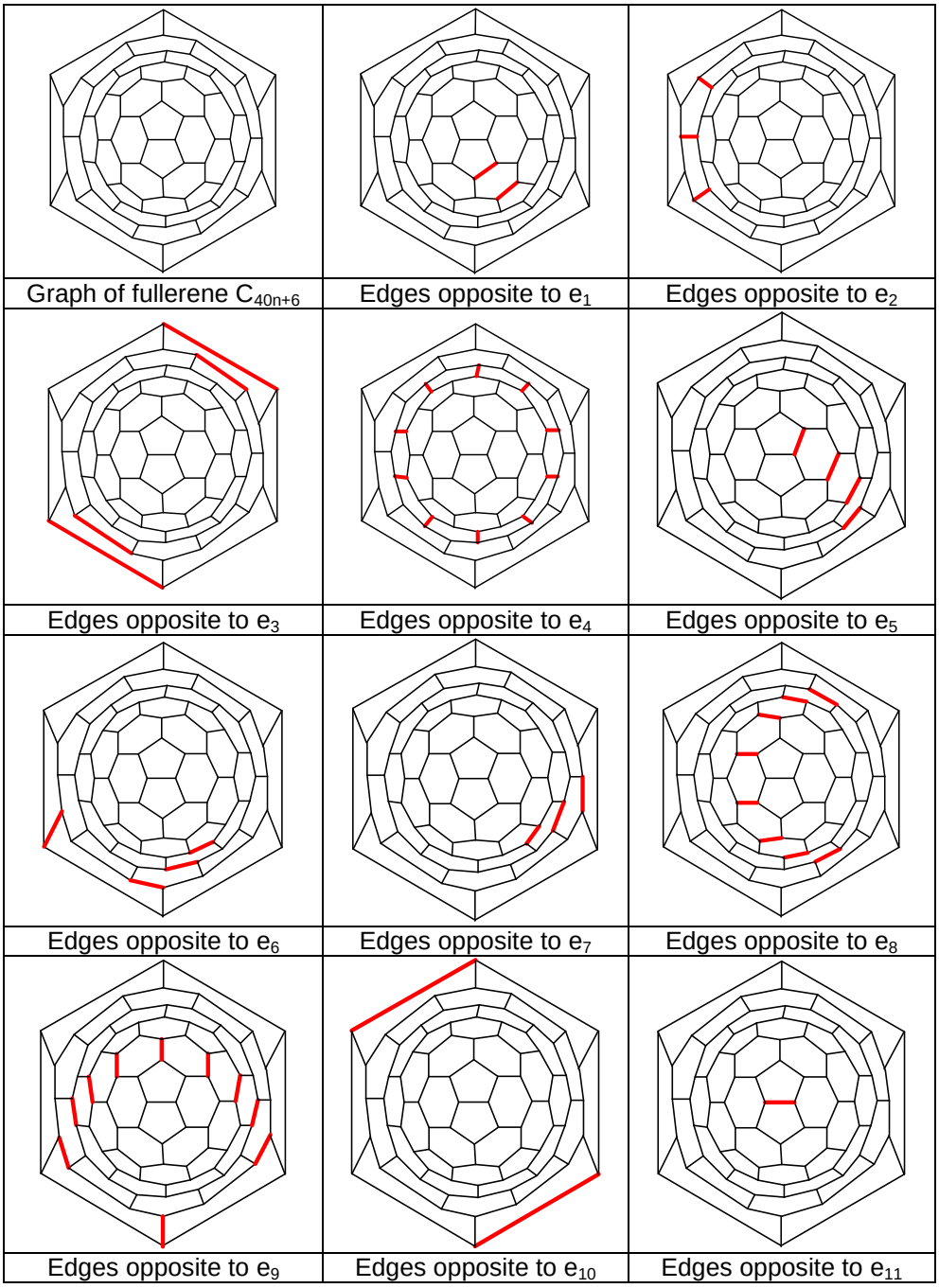

Figure 3. The main cases of opposite edge strips ops in fullerenes C_{40n+6}

CONCLUSIONS

The Omega polynomial was defined by M. V. Diudea in view of counting the opposite edge strips of any length in the graph. He also computed this polynomial for some nanostructures. In this paper, the Omega and the related Sadhana polynomials of an infinite class of fullerenes of formula C_{40n+6} was computed for the first time.

REFERENCES

1. H.W. Kroto, J.R. Heath, S.C. O'Brien, R.F. Curl, R.E. Smalley, *Nature*, **1985**, *318,* 162.
2. H.W. Kroto, J.E. Fichier, D.E. Cox, The Fullerene, Pergamon Press, New York **1993**.
3. M.V. Diudea, S. Cigher, P.E. John, *MATCH Commun. Math. Comput.*, **2008**, *60,* 237.
4. P.E. John, A.E. Vizitiu, S. Cigher, M.V. Diudea, *MATCH Commun. Math. Comput. Chem.*, **2007**, *57,* 479.
5. M.V. Diudea, *Carpath. J. Math.,* **2006**, *22,* 43.
6. M.V. Diudea, S. Cigher, A.E. Vizitiu, O. Ursu, P.E. John, *Croat. Chem. Acta*, **2006**, *79,* 445.
7. D.Ž. Djoković, *J. Combin. Theory Ser. B*, **1973**, *14,* 263.
8. P.M. Winkler, *Discrete Appl. Math.*, **1984**, *8*, 209.
9. S. Ovchinikov, arXiv: 0704.0010v1 math CO. 31 Mar, **2007**.
10. S. Klavžar, *MATCH Commun. Math. Comput. Chem.*, **2008**, *59,* 217.
11. M.V. Diudea, S. Cigher, A.E. Vizitiu, M.S. Florescu and P.E. John, *J. Math. Chem*., **2009**, *45*, 316.
12. P.V. Khadikar, *Nat. Acad. Sci. Letters*, **2000**, *23,* 113.
13. P.E. John, P.V. Khadikar, J. Singh, *J. Math. Chem.*, **2007**, *42,* 37.
14. A.R. Ashrafi, M. Ghorbani and M. Jalali, *Ind. J. Chem.*, **2008**, *47A,* 535.
15. N. Trinajstic, "Chemical Graph Theory", CRC Press, *Boca Raton, FL*, **1992**.
16. A.R. Ashrafi, M. Jalali, M. Ghorbani, M.V. Diudea, *MATCH Commun. Math. Comput. Chem.*, **2008**, *60,* 905.
17. M. Ghorbani, A.R. Ashrafi, *J. Comput. Theor. Nanosci.*, **2006**, *3, 1*.
18. A.R. Ashrafi, M. Ghorbani and M. Jalali, *J. Theor. Comput. Chem.*, **2008**, *7,* 221.
19. A.R. Ashrafi, M. Ghorbani, *MATCH Commun. Math. Comput. Chem.*, **2008**, *60,* 359.
20. M. Ghorbani, and M. Jalali, *Digest Journal of Nanomaterials and Biostructures*, **2008**, *3* (4), 269.
21. M. Ghorbani and M. Jalali, *MATCH Commun. Math. Comput. Chem.*, **2009**, *62*, 353.

22. A.R. Ashrafi, M. Jalali, M. Ghorbani and M.V. Diudea, *MATCH Commun. Math. Comput. Chem.,* 2008, *60* (3), 905.

23. A.R. Ashrafi, M. Ghorbani and M. Jalali, *Digest Journal of Nanomaterials and Biostructures*, **2008**, *3* (4), 245.

24. M. Jalali and M. Ghorbani*, Studia Universitatis Babes-Bolyai, Chemia*, **2009**, *2,* 145.

STUDIA UNIVERSITATIS BABEŞ-BOLYAI, CHEMIA, LIV, 4, 2009

PHENOL REMOVAL FROM WATER USING CARBON AEROGEL AS ADSORBENT

ANDRADA MĂICĂNEANU[a], COSMIN COTEȚ[a], VIRGINIA DANCIU[a], MARIA STANCA[a]

ABSTRACT. This paper presents experimental results obtained in the process of phenol adsorption from synthetic wastewaters in batch conditions using a carbon aerogel (CA) as adsorbent. Influence of the phenol initial concentration and contact type over the process efficiency was studied. The carbon aerogel adsorbent was prepared by polycondensation of resorcinol and formaldehyde followed by drying in supercritical condition with liquid CO_2 and a pyrolysis step. Morpho-structural characteristics of carbon aerogel were investigated using transmission electron microscopy (TEM), scanning electron microscopy (SEM), X-ray diffraction (XRD) and specific surface area determination using nitrogen adsorption (BET method). Obtained carbon aerogel proved to be an efficient adsorbent for phenol from wastewaters. Adsorption efficiencies up to 94.32% were reached.

Keywords: carbon aerogel, phenol, adsorption

INTRODUCTION

The presence of phenol and phenolic compounds in wastewaters can result in the contamination of both surface and ground waters with important negative consequences over the environment. The choice of treatment, in case of wastewaters polluted with phenol and phenolic compounds, depends on the concentration, which can varies from 0.1 to 6800 mg/dm^3 depending on the wastewater source (pulp and paper industry, refineries, coking operations, coal processing) [1], economics, efficiency, easy control and reliability [2].

Adsorption technology is a widely used technique, efficient for the removal of organic pollutants from wastewaters. The most usual adsorbents for organic pollutants removal from wastewaters are activated carbons, which proved to have excellent adsorption capacities [1,3,4]. Due to their high initial cost and the need for an expensive regeneration [3,4] alternative adsorbents or low-cost sources for the preparation of activated carbons were considered. As non-conventional low-cost adsorbents of phenol and phenolic compounds from wastewaters, were tested: (a) natural materials such as clay minerals (raw or modified), siliceous materials (e.g. perlite, dolomite, glasses), zeolites,

[a] *Universitatea Babeş-Bolyai, Facultatea de Chimie şi Inginerie Chimică, Str. Kogălniceanu, Nr.1, RO-400084 Cluj-Napoca, România, andrada@chem.ubbcluj.ro*

apatite, rectorite, attapulgite [3-13]; (b) bioadsorbents such as chitin, chitosan, peat, coal, plants and dead or living microorganisms (bacteria, fungi, yeast, algae) [3,4,14-17]; (c) agricultural and industrial by-product or waste materials (sawdust, rice husk, bark, fly ash, sludge, red mud), [3,4,18-20]. Synthetic zeolites and different type of polymeric resins were also considered as an alternative to activated carbons for phenol adsorption [1,4,21-28]. Activated carbons used as adsorbents for phenol removal can be prepared from solid wastes and coal based materials. Because there are renewable, abundant, inexpensive and require little processing, agricultural wastes are considered to be very important materials in the obtaining of activated carbons. Corn cob, nut shells, apricot stone shell, coffee grounds, coconut shell, olive stones or oil-palm shells are just a few examples of materials that can be transformed in activated carbons [3,4,29-35]. Novel adsorbents such as carbon nanotubes, hybrid xerogels, Mg Al layered double hydroxides, or macromolecule grafted on SiO_2 can be also used to remove phenol form aqueous solutions [36-39].

Due to their high surface area, high open porosity and controllable morpho-structural characteristics, carbon aerogels, could be considered as attractive materials for adsorption of organic pollutants (*e.g.* phenol) from wastewaters [40,41]. These materials can be obtained by carbonization of organic aerogels, which are prepared from the sol–gel polycondensation of certain organic monomers, such as resorcinol and formaldehyde in Na_2CO_3 catalysis [41-43]. The skeletal structure of resulted wet gels is maintained by a supercritical drying with CO_2. Before the pyrolysis process, monolithic solids with high porosity and specific surface areas are obtained.

This paper presents experimental results obtained in the process of phenol adsorption from synthetic wastewaters in batch conditions using a carbon aerogel (CA) as adsorbent. Influence of the phenol initial concentration and contact type over the process efficiency was studied. The morpho-structural characteristics of the carbon aerogel were investigated using transmission electron microscopy (TEM), scanning electron microscopy (SEM), X-ray diffraction (XRD), specific surface area and porosity determinations using nitrogen adsorption-desorption isotherms (BET method).

RESULTS AND DISCUSSION

Carbon aerogel morpho-structural characterization

By TEM (figure 1) and SEM (figure 2) images, the nanostructure and mesoporosity of the carbon aerogel framework are evidenced.

The analysis of XRD patterns shows an amorphous structure for carbon aerogel sample, with two large peaks at about $2\theta = 24^o$ and 44^o (figure 3).

Specific surface area and pore size distribution of the prepared carbon aerogel, were 850 m^2/g and 20-50 nm, respectively.

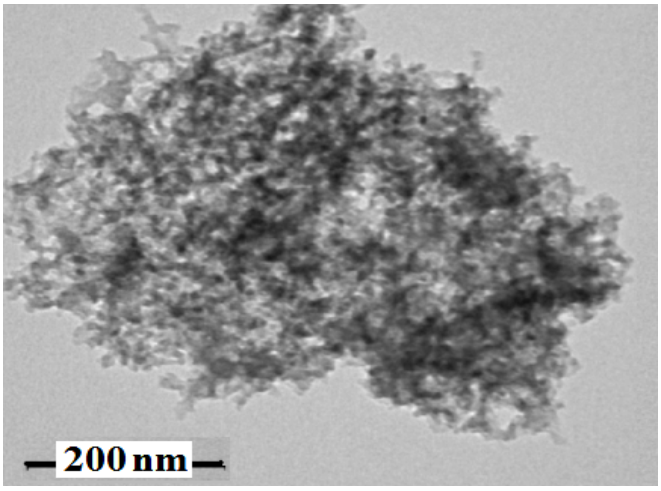

Figure 1. TEM image of the carbon aerogel sample.

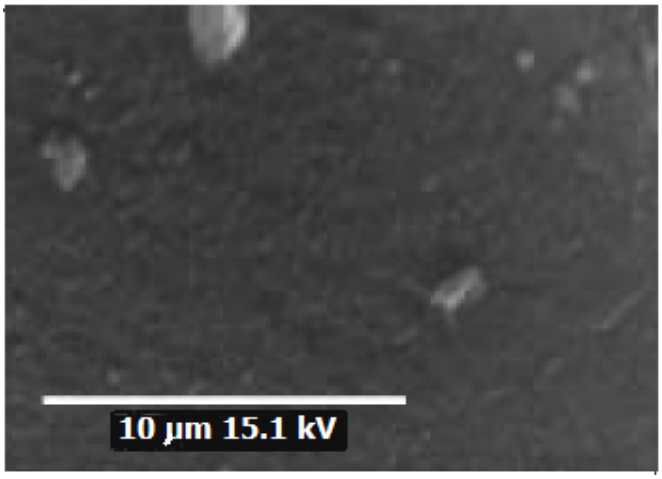

Figure 2. SEM image of the carbon aerogel sample.

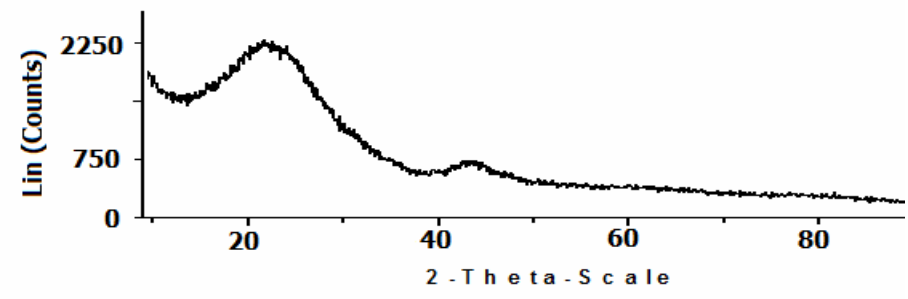

Figure 3. XRD patterns of the carbon aerogel sample.

Phenol adsorption results

Results obtained in case of carbon aerogel (CA) adsorbent and phenolic wastewater as ***immobile phases*** in a batch reactor (static conditions) are presented in figures 4 and 5.

Adsorption efficiency evolutions in time for the three more diluted phenolic wastewaters (5, 10 and 25 mg phenol/L) are presented in figure 4. A slowly increase of the adsorption efficiency is observed in the first 30 minutes reaching to equilibrium. Equilibrium was reached after 30 minutes for all three solutions, while the maximum adsorption efficiency was calculated to be 72.46% for 25 mg/L solution. In case of the two more concentrated phenolic wastewaters, 50 and 100 mg/L, equilibrium was reached in 8 hours, while the adsorption capacity increased with 15% for 100 mg/L solution.

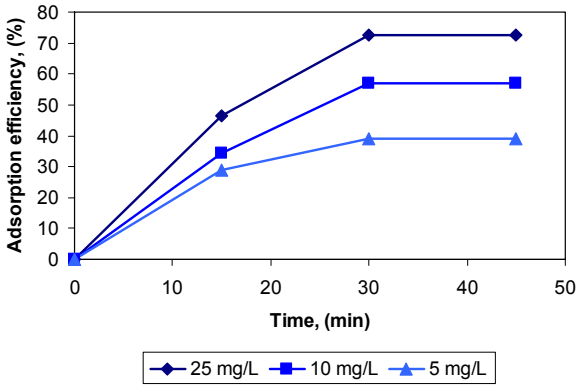

Figure 4. Adsorption efficiency evolution in time during phenol removal process on CA adsorbent (0.1 g), in static conditions, for C_i = 5, 10 and 25 mg phenol/L (100 cm^3).

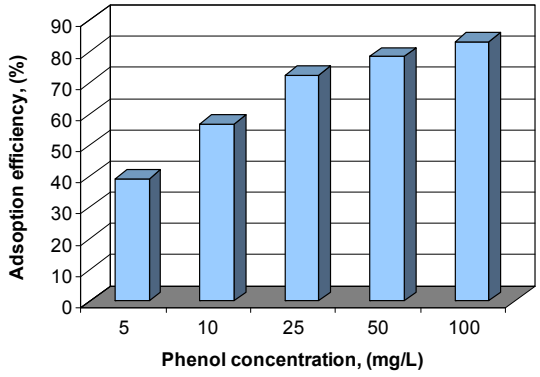

Figure 5. Influence of the initial phenol concentration over the maximum adsorption efficiency, during phenol removal process on 0.1 grams CA adsorbent in static conditions.

Influence of the initial phenol concentration over the maximum adsorption efficiency, during phenol removal process on 0.1 grams CA adsorbent in static conditions is presented in figure 5. It can be observed that with an increase of the initial concentration of phenol, adsorption efficiency increases up to 83.28% which is the maximum value calculated for 100 mg/L solution.

Results obtained in case of carbon aerogel (CA) adsorbent and phenolic wastewater as ***mobile phases*** under magnetic stirring in a batch reactor (dynamic conditions) are presented in figures 6, 7 and 8.

Adsorption efficiencies evolution in time for the two sets of solutions is presented in figures 6 and 7. In case of the more diluted phenolic wastewaters, maximum adsorption efficiency was reached after 10 minutes (equilibrium), with values very close to those obtained after 5 minutes (figure 6). Maximum adsorption efficiency was calculated to be 88.30% for 25 mg/L solution. In case of 50 and 100 mg/L solutions, figure 7, equilibrium was reached slower, after 60 minutes, while adsorption efficiency increased with around 7% for 100 mg/L solution.

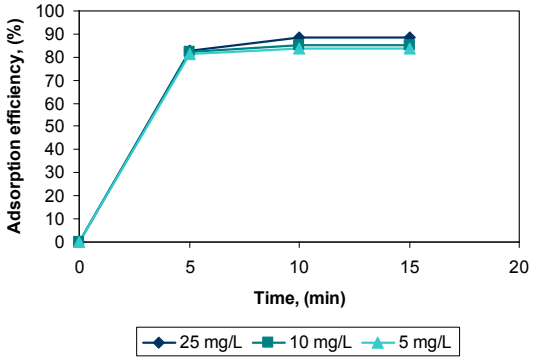

Figure 6. Adsorption efficiency evolution in time during phenol removal process on CA adsorbent (0.1 g), in dynamic conditions, for C_i = 5, 10 and 25 mg phenol/L (100 cm^3).

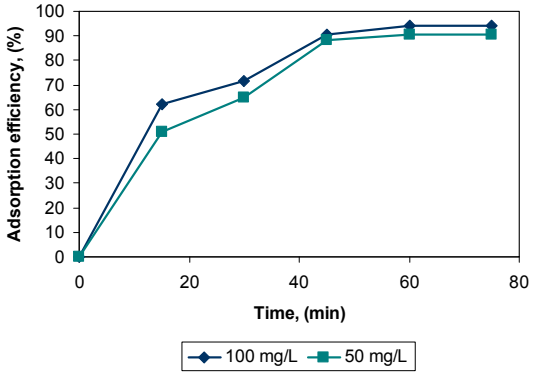

Figure 7. Adsorption efficiency evolution in time during phenol removal process on CA adsorbent (0.1 g), in dynamic conditions, for C_i = 50 and 100 mg phenol/L.

If we compare the maximum adsorption efficiencies calculated for all five initial concentrations, same evolution as in case of static conditions was observed, figure 8. A closer inspection of the adsorption efficiency values lead us to the conclusion that dynamic conditions are more efficient for the adsorption of phenol from synthetic wastewaters, figures 5 and 8, due to the elimination of diffusion limitations.

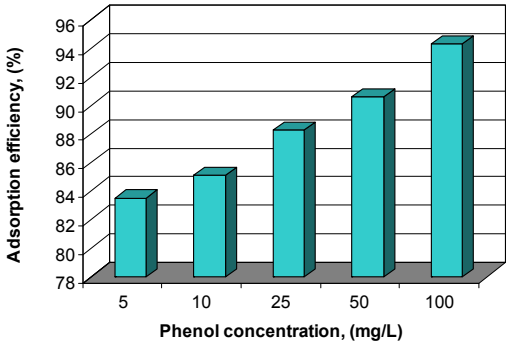

Figure 8. Influence of the initial phenol concentration over the maximum adsorption efficiency, during phenol removal process on 0.1 grams CA adsorbent in dynamic conditions.

EXPERIMENTAL SECTION

Carbon aerogel preparation

Using resorcinol (98% purity), formaldehyde (37% solution), Na_2CO_3 (99.9% purity), all from Aldrich, and deionised water, a resorcinol-formaldehyde wet gel was prepared. Resorcinol (0.29 moles) was dissolved in deionised water at a certain ratio (R/W = 0.2 g/cm^3). Solution of formaldehyde was added to the resorcinol solution (R/F = 0.5) in vigorous stirring. After that, Na_2CO_3 in 0.1 M aqueous solution was added as catalyst (C) to the previous mixture (R/C = 50). The solution was placed into tightly closed glass moulds (7 cm – length $\times$ 1 cm – internal diameter) and cured: 1 day at room temperature, 1 day at 50^{o}C and 3 days at 70^{o}C. The resorcinol-formaldehyde gel obtained in this way was washed with acetone and dried with CO_2 in supercritical conditions, when a resorcinol-formaldehyde aerogel was formed. This organic aerogel was then pyrolysed in N_2 atmosphere for 2 h at 850^{o}C with the formation of the carbon aerogel (CA) [41].

Carbon aerogel morpho-structural investigations

Transmission electron microscopy (TEM) of the metal doped carbon aerogels was performed with a Hitachi H-7000 microscope operating at 125 keV.

Scanning electron microscopy investigation was performed with a JSM-6400 (Scanning Microscope).

X-ray diffraction patterns were recorded in a θ–2θ Bragg–Bretano geometry with a Siemens D5000 powder diffractometer with Cu-K_α incident radiation (λ = 1.5406 Å) and a graphite monochromator.

Specific surface area determinations were performed using Brunauer-Emmett-Teller (BET) method using an ASAP 2000 surface area analyzer (Micrometrics Instruments Corp.). Prior to determination, samples of approximately 0.03 g were heated to 130°C under vacuum (10^{-5} Torr) for at least 18 h to remove all adsorbed species.

Phenol adsorption – working conditions

Phenol adsorption was realised in a batch reactor with adsorbent and phenolic wastewater as immobile phases (static conditions) and with adsorbent and phenolic wastewater under magnetic stirring (dynamic conditions) at room temperature. 0.1 g carbon aerogel, brought at a grain size of d < 250 μm using an appropriate sieve, were contacted with 100 cm^3 synthetic wastewater containing phenol – 5, 10, 25, 50 and 100 mg phenol/L. During the experiment, determination of the organic compounds in solution was carried out every 15 minutes (5, 10, 25 mg phenol/L) and 1 or 3 hours (50, 100 mg phenol/L) in static conditions, and every 5 minutes (5, 10, 25 mg phenol/L) and 15 minutes (50, 100 mg phenol/L) in dynamic conditions until equilibrium was reached. Taking in account the fact that in this stage of the research we were interested to see how this type of material acts as adsorbent for phenol, we used $KMnO_4$ chemical oxygen demand, CCO-Mn, method in order to establish the final concentration of the organics in solution. This determination is currently used in environmental laboratories for wastewaters characterization (STAS 3002/85, SR ISO 6060/96) according to Romanian legislation [44].

The evolution of phenol removal process was followed by means of adsorption efficiency (calculated using chemical oxygen demand values as CCO-Mn at a moment *t* and the initial CCO-Mn value), eq. (1).

$$\mathbf{E_{ads} = \frac{C_i - C_t}{C_i} \cdot 100} \quad (1)$$

where,

C_i is the CCO-Mn initial value, in mg $KMnO_4/dm^3$

C_t is the CCO-Mn value at moment *t*, in mg $KMnO_4/dm^3$.

CONCLUSIONS

A carbon aerogel sample was prepared by polycondensation of resorcinol and formaldehyde followed by drying in supercritical condition with CO_2 and a pyrolysys step. Morpho-structural characterization (TEM, SEM, XRD, BET method) of the prepared carbon aerogel proved that this is a amorphous mesoporous nanomaterial with a high specific surface area.

The influence of the working conditions (static and dynamic) and phenol concentration in wastewater were studied in order to establish their influence over the phenol adsorption process on carbon aerogel. An increase in the concentration and the utilization of the magnetic stirring led to an increase of the adsorption efficiency. Prepared carbon aerogel proved to be an efficient adsorbent for phenol from wastewaters. Adsorption efficiencies up to 94.32% were reached.

Further studies will be performed in order to establish the optimum working conditions for adsorption of phenol using carbon aerogel and also to establish kinetic and adsorption equilibrium models.

ACKNOWLEDGMENTS

Authors would like to thank EU Marie Curie Training Site Grant HPMT-CT-2000-0006, Romanian National University Research Council Grant CNCSIS Td 402/2006-2007, and also to research group of Prof. Elies Molins and Dr. Anna Roig from Institut de Ciencia de Materials de Barcelona (Spain).

REFERENCES

1. G. Busca, S. Berardinelli, C. Resini, L. Arrighi, *Journal of Hazardous Materials*, **2008**, *160*, 265.
2. A. Alejandre, F. Medina, A. Fortuny, P. Salagre, J.E. Sueiras, *Applied Catalysis B: Environmental*, **1998**, *16*, 53.
3. Md. Ahmarizzaman, *Advances in Colloid and Interface Science*, **2008**, *143*, 48.
4. S-H. Lin, R-S. Juang, *Journal of Environmental Management*, **2009**, *90*, 1336.
5. U.F. Alkaram, A.A. Mukhlis, A.H. AlDujaili, *Journal of Hazardous Materials*, **2009**, *169*, 324.
6. A. Bahdoda, S. El Asria, A. Saoiabia, T. Coradinb, A. Laghzizila, *Water Research*, **2009**, *43*, 313.
7. Y. Huang, X. Ma, G. Liang, H. Yan, *Chemical Engineering Journal*, **2008**, *141*, 1.
8. J. Huang, X. Wanga, Q. Jina, Y. Liua, Y. Wangb, *Journal of Environmental Management*, **2007**, *84*, 229.
9. L. Xu, L. Zhu, *Colloids and Surfaces A*, **2007**, *307*, 1.
10. M. Sprynskyy, T. Ligor, M. Lebedynets, B. Buszewski, *Journal of Hazardous Materials*, **2009**, *169*, 847.
11. S. Richards, A. Bouazza, *Applied Clay Science*, **2007**, *37*, 133.
12. Z. Rawajfih, N. Nsour, *Journal of Colloid and Interface Science*, **2006**, *298*, 39.
13. R. Liu, R.L. Frost, W.N. Martens, Y. Yuan, *Journal of Colloid and Interface Science*, **2008**, *327*, 287.

14. H. Polat, M. Molva, M. Polat, *International Journal for Mineral Processing*, **2006**, *79*, 264.
15. H. Cherifia, S. Haninia, F. Bentaharb, *Desalination*, 2009, *244*, 177.
16. A.Y. Dursun, C. Seda Kalayci, *Journal of Hazardous Materials*, **2005**, *B123*, 151.
17. A.E. Navarro, R.F. Portales, M.R. Sun-Kou, B.P. Llanos, *Journal of Hazardous Materials*, **2008**, *156*, 405.
18. A.T. Mohd Din, B.H. Hameed, A.L. Ahmad, *Journal of Hazardous Materials*, **2009**, *161*, 1522.
19. G. Dursun, H. Cicek, A.Y. Dursun, *Journal of Hazardous Materials*, **2005**, *B125*, 175.
20. S.P. Kamble, P.A. Mangrulkar, A.K. Bansiwal, S.S. Rayalu, *Chemical Engineering Journal*, **2008**, *138*, 73.
21. M. Carmona, A. De Lucas, J.L. Valverde, B. Velasco, J.F. Rodrıguez, *Chemical Engineering Journal*, **2006**, *117*, 155.
22. J-H. Huang, K-L. Huang, A-T. Wang, Q. Yang, *Journal of Colloid and Interface Science*, **2008**, *327*, 302.
23. W. Zhang, Q. Dua, B. Pan, L. Lv, C. Honga, Z. Jianga, D. Konga, *Colloids and Surfaces A*, **2009**, *346*, 34.
24. X. Zeng, Y. Fan, G. Wu, C. Wang, R. Shi, *Journal of Hazardous Materials*, **2009**, *169*, 1022.
25. M-C. Xu, Y. Zhou, J-H. Huang, *Journal of Colloid and Interface Science*, **2008**, *327*, 9.
26. B. Pan, B. Pan, W. Zhang, Q. Zhang, Q. Zhang, S. Zheng, *Journal of Hazardous Materials*, **2008**, *157*, 293.
27. P.A. Mangrulkar, S.P. Kamblea, J. Meshramb, S.S. Rayalua, *Journal of Hazardous Materials*, **2008**, *160*, 414.
28. F-Q. Liu, M-F. Xia, S-L. Yao, A-M. Li a, H-S. Wu, J-L. Chen, *Journal of Hazardous Materials*, **2008**, *152*, 715.
29. N. El Hannafi, M.A. Boumakhla, T. Berrama, Z. Bendjama, *Desalination*, **2008**, *223,* 264.
30. B.H. Hameed, A.A. Rahman, *Journal of Hazardous Materials*, **2008**, *160*, 576.
31. Z. Ioannou, J. Simitzis, *Journal of Hazardous Materials*, **2009**, in press, corrected proof, on-line
32. V. Srihari, A. Das, *Desalination*, **2008**, *225*, 220.
33. K.P. Singh, A. Malik, S. Sinha, P. Ojha, *Journal of Hazardous Materials*, **2008**, *150*, 626.
34. D. Richard, M. de Lourdes Delgado Nunez, D. Schweich, *Chemical Engineering Journal*, **2009**, *148*, 1.
35. A.C. Lua, Q. Jia, *Chemical Engineering Journal*, **2009**, *150*, 455.
36. K. Haghbeen, R.L. Legge, *Chemical Engineering Journal*, **2009**, *150*, 1.
37. P.E. Diaz-Flores, F. Lopez-Urıas, M. Terrones, J. R. Rangel-Mendez, *Journal of Colloid and Interface Science*, **2009**, *334*, 124.

38. S. Chena, Z.P. Xub, Q. Zhangc, G.Q. Max Lub, Z.P. Haod, S. Liub, *Separation and Purification Technology*, **2009**, *67*, 194.

39. F. An, B. Gao, *Journal of Hazardous Materials*, **2008**, *152*, 1186.

40. S.A. Al-Muhtaseb, J.A. Ritter, *Advanced Materials,* **2003**, *15*, 101.

41. L.C. Cotet, A. Roig, I.C. Popescu, V. Cosoveanu, E. Molins, V. Danciu, *Revue Roumaine de Chimie*, **200**7, *52*, 1077.

42. R.W. Pekala, US patent 4873218, **1989**.

43. R.W. Pekala, C.T. Alviso, F.M. Kong, S.S. Hulsey, *Journal of Non-Crystalline Solids*, **1992**, *145*, 90.

44. Law 458/2002, 311/2004, 107/1996, 311/2004, 112/2006, HG 188/2002, HG 352/2005.

STUDIA UNIVERSITATIS BABEŞ-BOLYAI, CHEMIA, LIV, 4, 2009

THE DEVELOPMENT OF A MPC CONTROLLER FOR A HEAT INTEGRATED FLUID CATALYTIC CRACKING PLANT

MIHAELA-HILDA MORAR[a] AND PAUL ŞERBAN AGACHI[a]

ABSTRACT. The use of the advanced control techniques is necessary because, now, the PID control is no more competitive in the 20% of the industrial applications when special dynamics are involved. By implementing an advanced control system one can push the process unit to a more profitable region without affecting the operation constraints. In previous works an industrial FCC plant from a Romanian refinery was studied from the point of view of heat integration and steady state performance of the new heat exchanger network (HEN) design. In this study the improvement of the same FCC plant was done by implementing an advanced control scheme capable to maintain stabilized the heat transfer through the plant. Model Predictive Control (MPC) is one of the most used advanced control techniques in process control. A MPC controller was developed for an industrial fluid catalytic cracking (FCC) plant using Aspen HYSYS. The developed MPC controller results enable to establish that the strategy of the advance control imposed is a very efficient one in case of a FCC heat integrated plant.

Keywords: fluid catalytic cracking, heat integration, model predictive control, dynamic state.

INTRODUCTION

Due to its complexity the interest of solving problems related to the FCC process is worldwide spread. There has been a continuous effort to improve the efficiency and yield of the FCC unit during the time. There are many articles that present the problem of the FCC process modeling, simulation and control the most significant being [1] - [12] and just a few articles in which the study is related to the problem of energy integration [15].

The FCC process description is very difficult due to several reasons: the complexity of the chemical reactions mechanism, complex hydrodynamics, strong interaction between the operation of the main reactor and of the regenerator and due to the operation constrains imposed by the new HEN.

The aim of our research was to develop a MPC control scheme capable to control the FCC plant with the new HEN design obtained in a previous

[a] *Universitatea Babeş-Bolyai, Facultatea de Chimie şi Inginerie Chimică, Str. Kogălniceanu, Nr. 1, RO-400084 Cluj-Napoca,Romania, mmorar@chem.ubbcluj.ro*

work [13], [14]. The implementation of a MPC control scheme can provide a high stability of the plant knowing that the heat integration induces more instability in the process.

For reaching the purpose of this research, a FCC plant dynamic simulator was build in Aspen HYSYS using real industrial data related to material fluxes, temperatures, pressures, equipments size and geometry, etc. The data have been provided by a Romanian refinery.

MODEL PREDICTIVE CONTROL

The Model Predictive Control (MPC) is one of the most used advanced control technique in process control. In 1980s it was developed to meet the specialized control needs of power plants and petroleum refineries (ex. [15], [16]). Nowadays, can also be found in a wide variety of application areas like: chemicals, food processing, automotive, aerospace, metallurgy, pulp and paper, etc.

As it can be seen in Figure 1, the main idea of MPC is to choose the control action by repeatedly solving an optimal control problem. Therefore, MPC is based on iterative, finite horizon optimization of a plant model. At time "t", the current plant state is analyzed and a "cost minimizing" control strategy is computed, using a numerical minimization algorithm (Euler-Lagrange numerical method), for a very short time horizon in the future.

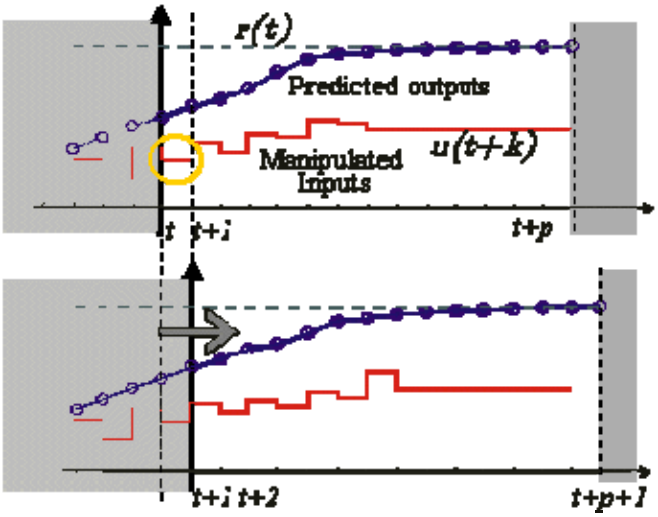

Figure 1. The MPC finite horizon

The MPC is also called receding horizon control because the prediction horizon keeps changing forward.

In Figure 2 the basic structure of MPC is presented. The model predictive control algorithm uses the models and current plant measurements in every moment in time to calculate the future moves for the safety.

Consequently, the process model plays an important role in the controller. The chosen model must be able to catch the process dynamics in order to predict the future outputs with high precision. Also, the model must be simple to be implemented and understood.

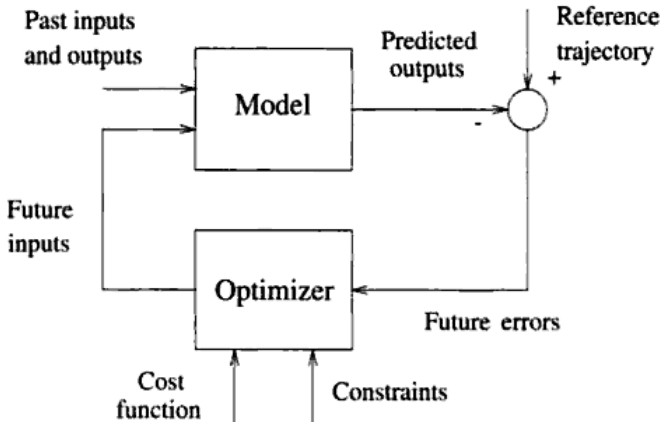

Figure 2. The basic MPC structure [16]

There are many types of models used in different formulations such as truncated impulse response model, step response model, state space model, transfer function model, etc. A typical MPC contains the behavior of multiple Single Input Single Output (SISO) controllers and de-couplers and uses a process model like first order model or step response model.

Comparing with the PID controller, the MPC controller main difference is represented by the necessity to build the process model that has to be implemented in the MPC controller structure.

THE DEVELOPMENT OF THE MPC CONTROLLER

The dynamic simulations performed revealed that only 5 controllers of PID type are necessary in order to obtain a proper stability of the FCC column. The stability of the column is reflected in the quality of heat transfer through the HEN. The development of the MPC controller for controlling the FCC column is based on the data provided by those 5 controllers that were able to settle the FCC column behavior at normal functioning conditions. The PID control scheme of the FCC column is presented in Figure 3.

MPC controller from the Aspen HYSYS object palette allows implementing up to a maximum 12 pairs of controlled variables (CV) and manipulated variables (MV). At the moment, the only MPC Control Algorithm that is implemented in the Aspen HYSYS software is the unconstrained MPC. This algorithm does not consider constraints on either controlled or manipulated variables.

In this case, 5 inputs (process /controlled variable – PV/CV) and 5 outputs (output target objects/manipulated variable – OP/MV) MPC is developed.

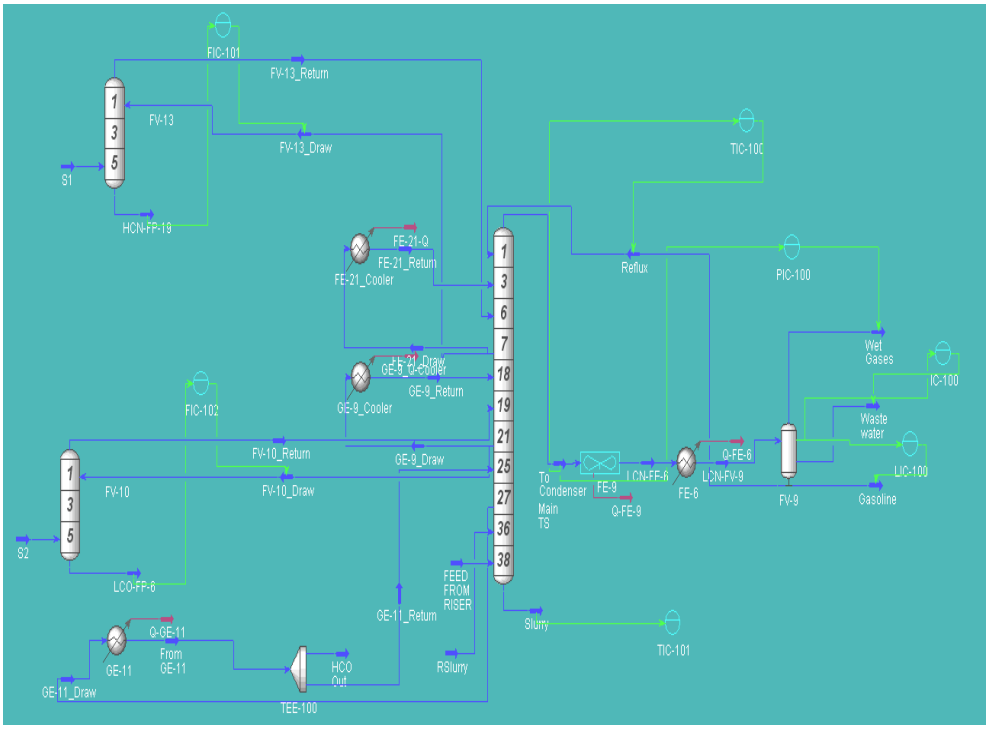

Figure 3. The PID control scheme of the FCC column

The controlled and the manipulated variables are summarized in Table 1.

Table 1. MPC control scheme selected variables

Controlled Variable		Manipulated Variable	
CV1	To Condenser stream temperature	**MV1**	Reflux flow rate
CV2	Condenser Liquid % Level	**MV2**	Gasoline flow rate
CV3	FV-13 bottom HCN flow rate	**MV3**	FV-13 HCN feed flow rate
CV4	FV-10 bottom LCO flow rate	**MV4**	FV-10 LCO feed flow rate
CV5	Slurry temperature	**MV5**	Column recycle slurry flow rate

"To Condenser" stream represents the top column output stream that passes two heat exchangers and enters in the condenser. The FV-10 and FV-13 (see Figure 3) are the side strippers of the FCC column. The stream which represents the bottom product of FV-13 (HCN stripper) is named HCN-FP-19. The stream which represents the bottom product of FV-10 (LCO stripper) is named LCO-FP-6. The Slurry stream is the bottom product of the FCC column.

Having all these specified the way of the MPC strategy implementation is presented as follows.

The Aspen HYSYS has implemented two options to specify the MPC controller model: the Step response model and the First order model. The model used in this case, for the MPC is the First Order model.

The first order model implementation is possible if the process gain (Kp), the process time constant (Tp) and the delay are known. With these process parameters it is possible to obtain the step response matrix necessary to build the internal MPC model.

The identification of those parameters could be realized by developing step response tests for each manipulated variable using the implemented PID control scheme from the dynamic state model. Consequently, a +10% step was used for each manipulated variable and the effect on the controlled variable was registered.

The step response tests provided the process gains, the time constants and the delays necessary for building the MPC controller. These parameters are presented in Table 2.

Table 2. First order model process parameters

MV / CV	MV1	MV2	MV3	MV4	MV5
CV1	Kp = -2.35 T = 2.56 τ = 0	Kp = 0.567 T = 15.66 τ = 0	Kp = -1.5182 T = 45.83 τ = 6.66	Kp = -1.5526 T = 77.083 τ = 0	Kp = -0.9611 T = 16.183 τ = 0
CV2	Kp = -0.15685 T = 3.033 τ = 0	Kp = -0.312 T = 8.33 τ = 0	Kp = -0.068 T = 58.75 τ = 0	Kp = -0.0775 T = 58.583 τ = 0	Kp = -0.0738 T = 20.016 τ = 0
CV3	Kp = -0.2043 T = 29.03 τ = 0	Kp = 0.1147 T = 32.16 τ = 0	Kp = 1.41 T = 0.01 τ = 0	Kp = -0.061 T = 113.5 τ = 7.33	Kp = -0.00456 T = 42.316 τ = 0
CV4	Kp = -0.66 T = 34.783 τ = 0	Kp = 0.39 T = 24.08 τ = 0	Kp = 0.437 T = 21.75 τ = 1.583	Kp = 7.436 T = 0.01 τ = 0	Kp = -0.1452 T = 26.85 τ = 0
CV5	Kp = -0.3741 T = 14.06 τ = 0	Kp = 0.32 T = 12.33 τ = 0	Kp = 0.28 T = 8.916 τ = 0	Kp = 1.156 T = 6.5 τ = 0	Kp = -1.151 T = 4.28 τ = 0

The process parameters were used to determine the 5x5 MPC step response matrix necessary for implementation of the MPC controller internal model. The dimensions of the generated step response matrix are 50x25.

After establishing the MPC controlled and manipulated variables and after determining the internal MPC model, the MPC controller was implemented in the FCC heat integrated plant dynamic model.

RESULTS AND DISCUSSIONS

The MPC control performances were analyzed in order to verify if the MPC controller was properly developed.

In order to perform the MPC performance analysis, several diagrams were developed in which the colors established for the variables are: red – the setpoint, green – the controlled variable, blue – the manipulated variable.

During the performance analysis it was observed that the MPC controller can not entirely stabilize the LCO-FP-6 flow rate, but the control action is good enough in order to have a proper operation of the HEN. The Figure 4 shows the behavior of the LCO-FP-6 flow over the time.

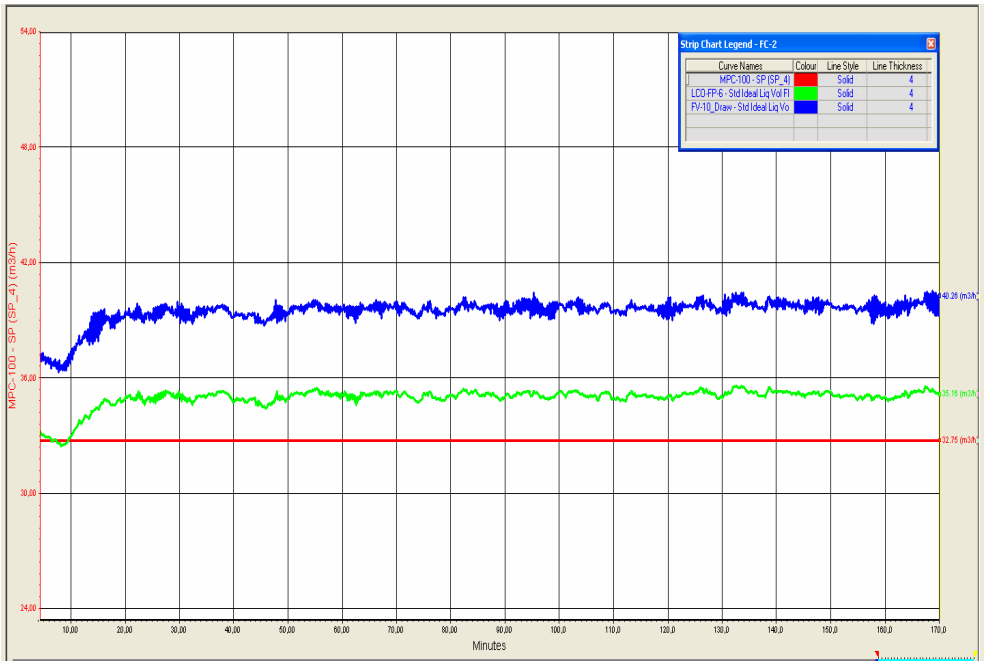

Figure 4. The performance of the LCO FP-6 flow control

As it can be seen in Figure 5, despite the LCO-FP-6 flow variation after stopping the noise amplification, the HCN-FP-19 flow control, which was the most affected by the noise, presents a good behavior and time stability. The HCN-FP-19 stream represents the bottom product stream of the FV-13 side-stripper which enters in the FE-24 heat exchanger.

The MPC control could reach the setpoint from industry for the Slurry temperature meaning that the controller model was successfully developed.

Further analysis regarding the HEN operation suggested that working at the set point value for the slurry temperature destabilizes the heat transfer of the HEN. This because working at the setpoint the quantity of the slurry entering in the HEN is not sufficient enough to sustain an efficient heat transfer as it was imposed in order to have a successfully heat integrated plant. This problem appears, as has been explained before, due to the geometrical data implemented in the FCC column model. Those data are not entirely the one that the real FCC column has. In order to solve the problem with the optimum heat transfer in the HEN, the system was operated near the value of the setpoint which assure the quantity of the slurry needed for an optimum operation of the heat exchangers. In these conditions the slurry temperature is approaching the setpoint and is stabilized at the value of 352^0C as can be seen in Figure 6.

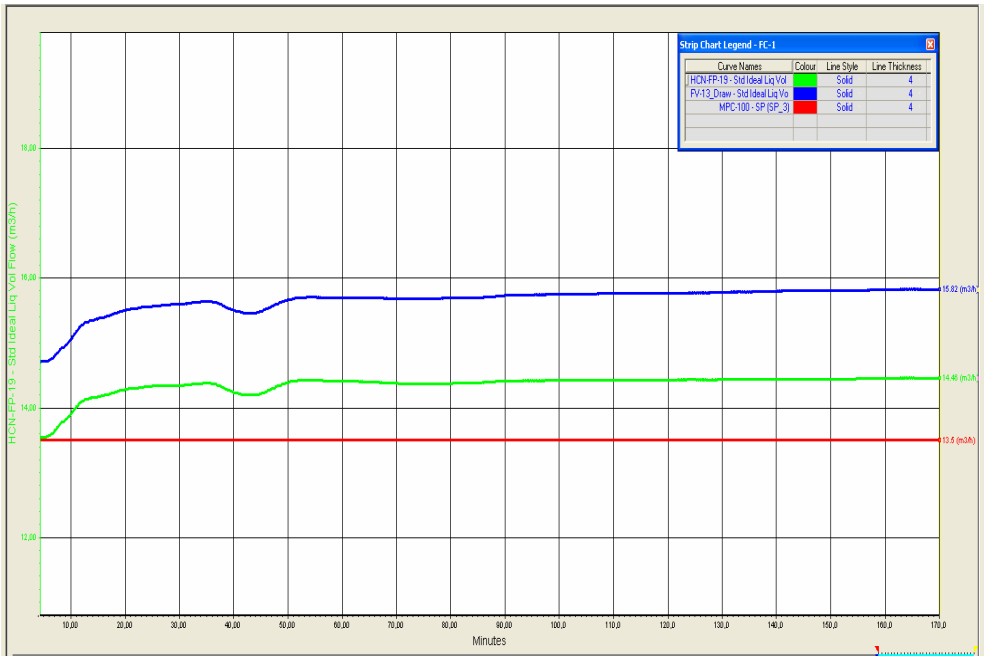

Figure 5. The performance of the HCN-FP-19 flow control

Beside the negative impact on the heat exchangers, the decreasing of the RSlurry flow rate presents another inconvenience. The role of the RSlurry stream in the column is to cool the effluent vapor stream from the riser that enters at the bottom of the column. If the cooling is not sufficient the column fractionation efficiency decreases considerably. The quality of the column products is compromised. Therefore, it is vital to have sufficient RSlurry quantity to handle the vapors proper cooling.

Consequently, the RSlurry flow control valve was set to the following values: 0% opening – 200.1 m^3/h and 100% opening – 346.8 m^3/h.

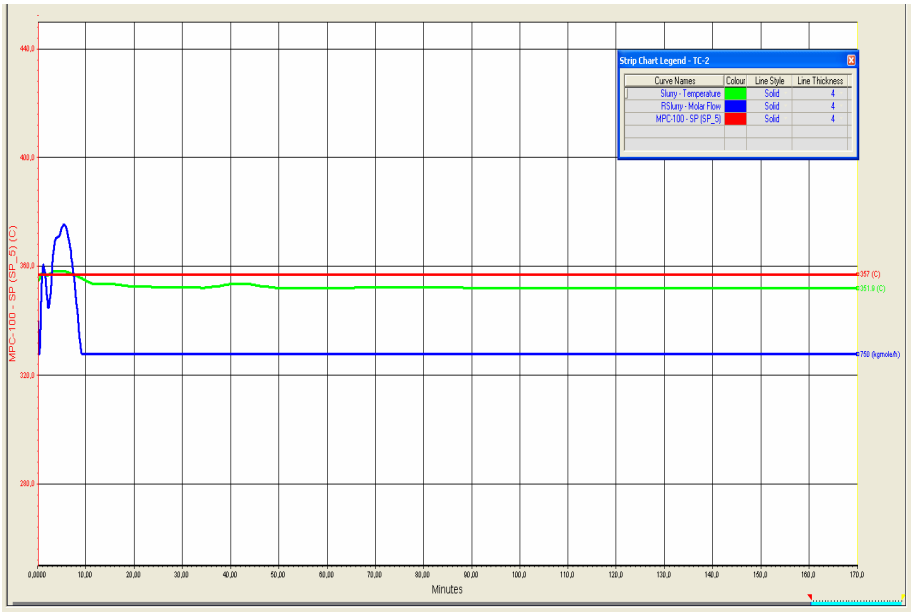

Figure 6. The performance of the Slurry temperature control

However, it is known from the real plant that the range of temperature for the slurry stream, in order to have a proper operation, is 345 – 360^{0}C. This means that the obtained value of the slurry temperature (352^{0}C) is an appropriate one. In these conditions the approach adopted is correct. The goal of maintaining an optimum heat transfer in the HEN has been realized. Another observation is that even if a lower temperature than the setpoint of the slurry stream is used this doesn't affect the heat transfer in the HEN.

Comparing with the PID control, the MPC provides better results in controlling the temperature of the top output stream of the column (To Condenser). The PID temperature controller – TIC-100 achieves the set point after 30 minutes from starting the simulation. Meanwhile, as it can be seen in Figure 7, the MPC controller needs only 10 minutes from the simulation start to attain the setpoint.

Also, better control performance can be observed in controlling the liquid percent level of the FV-9 condenser. The MPC control has faster response than the PID level controller LIC-100 which follows the set point line after 40 minutes. The MPC controller needs only 25 minutes to bring the level at the setpoint. The MPC liquid level control performance is presented in Figure 8.

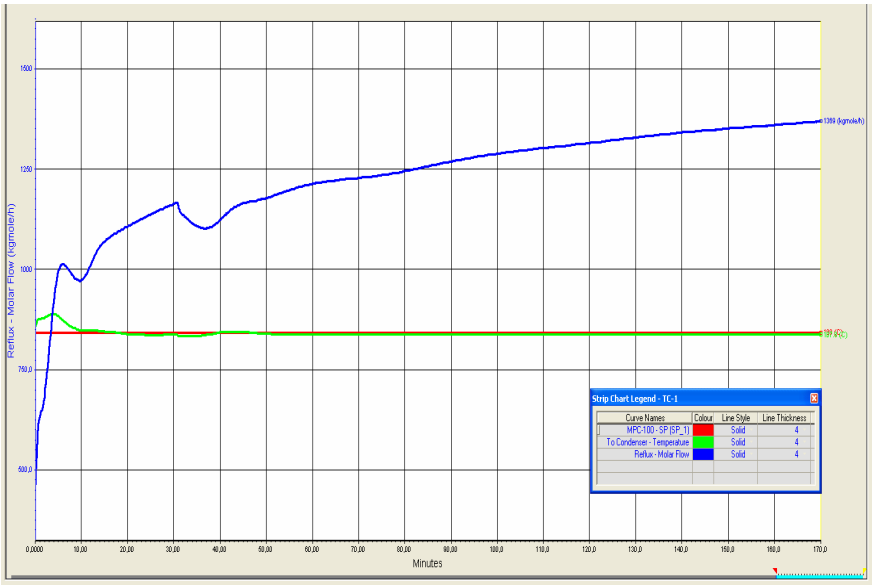

Figure 7. The performance of the temperature control of the column top product

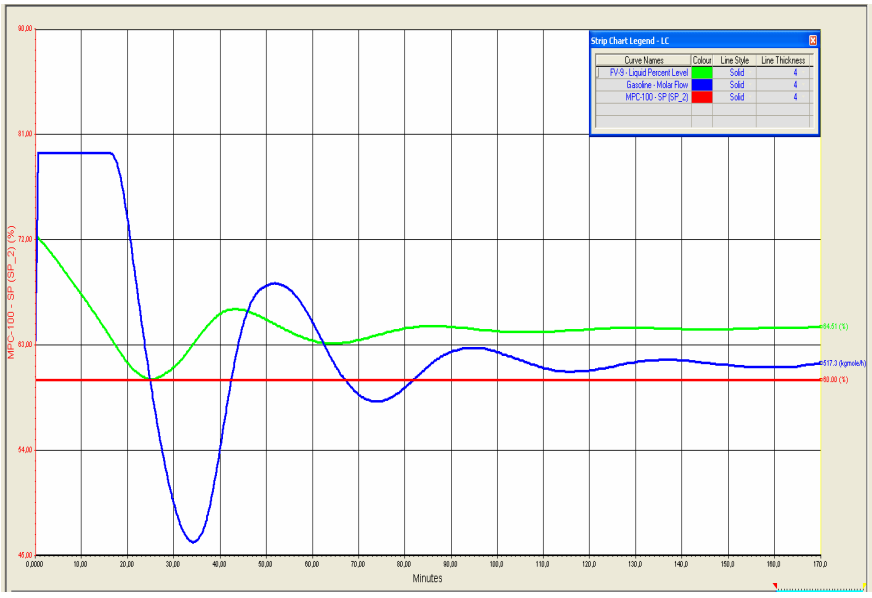

Figure 8. The performance of the condenser liquid percent level control

The liquid level from the condenser can be exactly maintained at 60% neither by PID controller nor by MPC controller because it is dependent on the column calculation of the output streams composition. The level reaches the steady state at around 65%.

The performance analysis of the MPC controller revealed that this controller is very efficient in case of the FCC heat integrated plant model proposed in this research.

CONCLUSIONS

In the last years, the model predictive control (MPC) has become a preferred control strategy for a large number of processes. This advanced control method was developed to meet the specialized control needs especially of the petroleum refineries.

The MPC can decrease the operating costs with approximately 2% - 6% [17] of the existing operating cost related to the real PID control scheme of a real plant because a MPC controller is capable to maintain the variation of the controlled variables much closer to the setpoint than PID controllers. Therefore, the plant is exploited at its maximum capacity.

Comparing with the PID controller, the MPC controller presents the necessity to build a process model. Many types of models such as truncated impulse response model, step response model, state space model, transfer function model, etc. can be used.

Based on the control demands of the heat integrated FCC plant and on the results obtained with PID control strategy, 5x5 MPC controller was developed using the First Order model.

In this case the estimation of model states and parameters is critical. The successful implementation of the MPC controller depends on them.

The identification of the process parameters that are needed for the first order model development (the process gain - Kp, the process time constant - Tp and the delay) was realized by developing step response tests for each manipulated variable.

After the parameter were calculated they were used to build the 5x5 MPC step response matrix necessary for determining the MPC controller internal model. In this way arise a new MPC controller capable to handle the control of the FCC column. The developed MPC controller results enable to establish that the strategy of the advanced control imposed is a very efficient one in case of a FCC heat integrated plant.

Regarding the MPC controller development, the novelty is using an easy method for the internal MPC model development. This method is fast and very useful in implementing an advanced control scheme at industrial scale. The step response tests in the real plant are insecure and costly especially in a continuous process. Any kind of these step control tests are able to compromise the quality of the products and to destabilize the industrial plant followed by undesirable incidents and costs.

LIST OF ABREVIATIONS

CV	controlled variable
FCC	fluid catalytic cracking
HCN	heavy cat naphta
HEN	heat exchanger network
LCO	light cycle oil
MPC	model predictive control
MV	manipulated variable
OP	output target object
PID	proportional-integral-derivative
PV	process variable
SISO	single input single output

REFERENCES

1. A. Arbel, I.H. Rinard, R. Shinnar, *Industrial & Engineering Chemistry Research*, **1996**, *35*, 2215.
2. P. Grosdidier, A. Mason, A. Aitolahti, P. Heinonen, V. Vanhamäki, *Computer and Chemical Engineering*, **1993**, *17*, 165.
3. I.S. Han, C.B. Chung, *Chemical Engineering Science*, **2001**, *56*, 1951.
4. I.S. Han, J.B. Riggs, C.B. Chung, *Chemical Engineering and Processing*, **2004**, *43*, 1063.
5. S.M. Jacob, B. Gross, S.E. Voltz, V.M. Weekman, *AIChE Journal*, **1976**, *22*, 701.
6. H. Kurihara, "Optimal Control of Fluid Catalytic Cracking Processes", PhD. Thesis, MIT, **1967**.
7. E. Lee, F.R. Jr. Groves*, Transactions SOC. Comput. Simulation*, **1985**, *2*, 219.
8. W. Lee, A.M. Kugelman, *Industrial and Engineering Chemistry Process Design and Development*, **1973**, *12*, 197.
9. M. Hovd, S. Skogestad, *AIChE Journal*, **1993**, *39*, 1938.
10. R.C. McFarlane, R.C. Reineman, "Multivariable optimizing control of a model IV fluid catalytic cracking unit", AIChE Spring National Meeting, Orlando, FL., **1990**.
11. R.C. McFarlane, R.C. Reineman, J.F. Bartee, C. Georgakis, *Computer and Chemical Engineering,* **1993**, *17*, 275.

12. V.W. Weekman, D. M. Nace, *AIChE Journal*, **1970**, *16*, 397.
13. E. Jara-Morante, M. Morar, P.Ş. Agachi, Heat integration of an industrial fluid catalytic cracking plant, *Studia Universitatis Babes-Bolyai Chemia*, **2009**, *LIV(1),* 69.
14. M. Morar, P.S. Agachi, *Computer Aided Chemical Engineering*, **2009**, *26*, 465.
15. R.A. Abou-Jeyab, Y.P. Gupta, *Industrial & Engineering Chemistry Research* **1996**, *35*, 3581.
16. A.K. Jana, A.N. Samanta, S. Ganguly, *Computers & Chemical Engineering*, **2009**, *33*, 1484.
17. J.S. Anderson, Process control opportunities and benefits analysis, *Proc. Advanced Control for the Process Industries*, Cambridge, 9-11th Sept., **1992**.
18. A.B. Al-Riyami, J. Klemes, S. Perry, *Applied Thermal Engineering*, **2001**, *21*, 1449.
19. E.F. Camacho, C. Bordons, "Model Predictive Control", Springer-Verlag London, **2004**.
20. P.S. Agachi, Z.K. Nagy, M.V. Cristea, A. Imre-Lucaci, "Model Based Control. Case Studies in Process Engineering", Wiley – VCH, **2008**.
21. N. Alsop, J.M. Ferrer, "Step-test free APC implementation using dynamic simulation", Process Control Spring National Meeting, Orlando, FL, April 24-27, **2006**.
22. A. Kalafatis, K. Patel, M. Harmse, Q. Zheng, M. Craik, *Hydrocarbon Processing*, **2006**, February issue, 93.
23. G.A. Kautzman, W. Korchinski, M. Brown, *Hydrocarbon Processing*, **2006**, October issue.
24. R. Lien, J. Deshmukh, Y. Zhu, "How much can we increase the efficiency of MPC identification?", NPRA Decision Support and Automation Conference, September, San Antonio, **2003**.

STUDIA UNIVERSITATIS BABEŞ-BOLYAI, CHEMIA, LIV, 4, 2009

THE CONSTRUCTION AND CALIBRATION OF A ROTATING VISCOMETER

NICU BORŞ[a], ANDRA TĂMAŞ[b], ZENO GROPŞIAN[b]

ABSTRACT. The paper describes the construction and calibration of a modified Couette rotating rheometer for the study of the hydraulic effects that are specific to the motion in ring-shaped spaces limited by two glass concentric cylinders; the inner cylinder is mechanically driven, the outer one is positioned by the balance which is established between the viscous friction force and the torsion force developed in the elastic muff used for its fixation.The measurement and adjustment of the rotation speed by modulating the frequency of the electric current are presented, as well as the measurement of the torsion moment on the outer cylinder, at different elongation forces and elastic muff thicknesses, in correlation with constructive-functional characteristics.

Keywords: coaxial cylinders, rotational rheometer, sheear rate, shear stress, torsion, viscosity

INTRODUCTION

The liquids rotational motion is especially encountered to the devices working from chemical industry: centrifugal pumps, vessels with stirring, centrifugal separators, some types of evaporators, rotating columns (for absorption, rectification, extraction). The hydrodynamic regime of the flow process is expressed by Reynolds criteria (Re), defined as the ratio of inertia forces to viscous forces, or by Taylor number (Ta), which represents the ratio of centrifugal and viscous forces. The flow characterization in ring-shaped spaces is expressed by the Reynolds-Taylor criteria [1,2] which depends on the cylinders geometry, the liquid nature and the intensity of rotational motion (revolution n, angular velocity Ω):

$$\mathrm{Re}=\frac{n\cdot d^2\cdot\rho}{\eta};\ Ta=\frac{\pi\cdot n\cdot\left(r_o^2-r_i^2\right)\cdot\rho}{\eta};\ Ta_{\mathrm{Re}}=\frac{\Omega\cdot r_i\cdot(r_o-r_i)\cdot\rho}{\eta} \qquad (1\text{-a,b,c})$$

The effect of deformation forces of concentric liquid layers, moving at different velocities, leads to the friction forces appearance that are in direct correlation with the nature of the substance (its viscosity). Determination of

[a] *Dinkelberg Analitics GmbH Germany, nicu.bors@online.de*
[b] *Universitatea "Politehnica"din Timişoara, Facultatea de Chimie Industriala si Ingineria Mediului, P-ta Victoriei Nr.2, RO-300006 Timisoara, andra.tamas@chim.upt.ro*

flow regime, particularly the transient one, has special importance on these forces; their reduction (Toms effect) through the addition of small quantities (ppm) of specific substances (surfactants [3], linear polymers [4-6], fibers), leads to energy consumption decreasing.

The liquids rotational motion is specific to rotational viscometers (Couette, Rheotest and modified Couette) that, alongside rheological characterization, assure the detailed study of the transient regime and the turbulence, defining the Taylor-Couette flow.

The rheometer that was made and tested (modified Couette type) contains two concentric glass cylinders; the inner cylinder is rotated around its axis by an asyncronous electric motor with adjustable rotation speed using a transmission; the outer cylinder is elastically fixed with a rubber tube which allows a partially rotation with a central angle $\Delta\theta$; this angle is the measure of the torsion moment M_t [4]. The rubber tube provides the hydraulic closure of the ring-shaped space where the liquid is introduced to study its rheological behavior. This cylinder is suspended to the upper side through a torsionable thread which assures the centering and controlled straining of the elastic tube-cylinder-thread system [3, 4]. The viscometer's Duran glass cylinders have the following characteristics: height H= 290mm; inner radius r_i= 40mm, outer radius r_o= 42mm, ring-shaped thickness $\Delta r= r_o-r_i$= 2mm; r_o/r_i=1.05.

The driving shaft is provided with a sealing system and a disk for measuring the rotation speed; the entire cylinder system is placed in a controlled temperature environment.

RESULTS AND DISCUSSION

The measurement of the inner cylinder rotation speed

The rotor rotation speed n_r is calculated using equations (2a, b, c) as a function of its slide s as compared with the synchronism rotation n_s determined by the triphasic currents system (p- the number of winding pole pairs):

$$n_r = n_s \cdot (1-s); \qquad s = \frac{n_s - n_r}{n_r}; \qquad n_s = 60 \cdot \frac{\nu}{p}; \tag{2-a,b,c}$$

At synchronism, the shaft will have the rotation speed n_{Ax-s} (eq.3a):

$$n_{Ax-s} = n_s \cdot R_t = 60 \cdot \frac{\nu}{2} \cdot \frac{1}{3} = 10 \cdot \nu; \tag{3a}$$

The real rotation speed of the device shaft n_{Ax} (eq. 3b):

$$n_{Ax} = (1-s) \cdot n_{Ax-s} = 10 \cdot (1-s) \cdot \nu; \tag{3b}$$

The factor f represents the ratio between these two rotation speeds (eq. 4):

$$f = \frac{n_{Ax}}{n_{Ax-s}} = \frac{(1-s)\cdot n_{Ax}}{n_{Ax-s}} = (1-s); \tag{4}$$

By modifying the electric current frequency, the values of the f factor (the ratio between the real and the synchronism rotations) have been experimentally determined, which is shown in Figure 1, both for the no-load situation (without friction to the sealing system) and for the loaded situation. This factor tends to 0.97 (in no-load situation) and 0.9, respectively. The rotation speeds actually used are between 30 and 200 rpm and can be reached for frequencies between 5 and 20Hz (0.65 < f < 0.9).

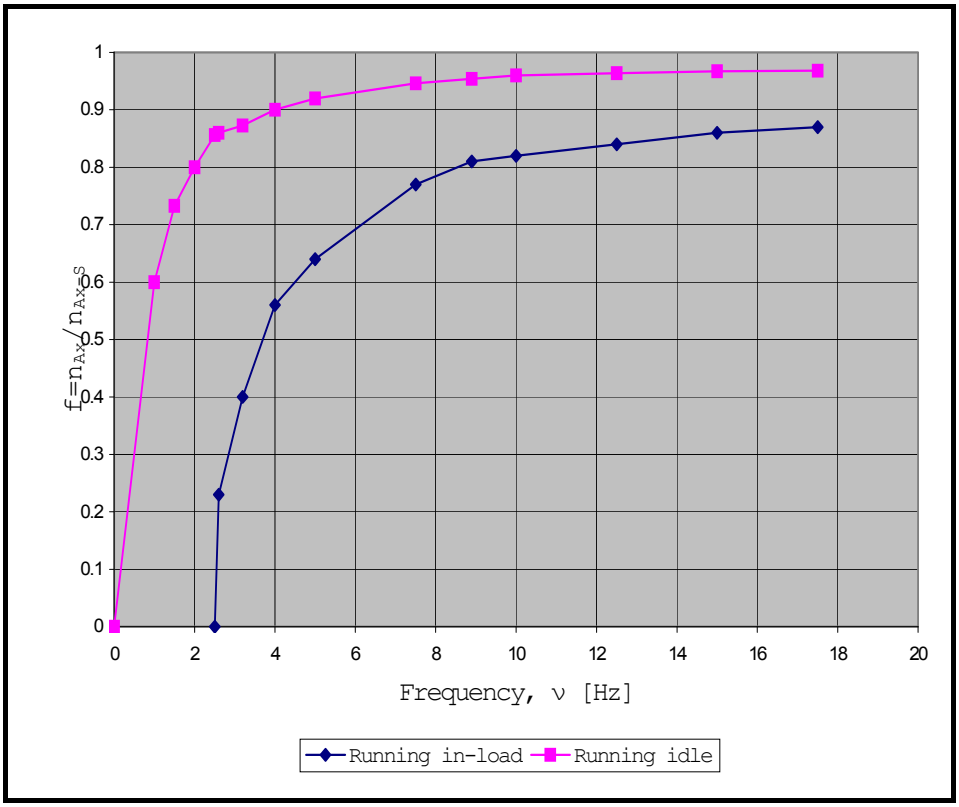

Figure 1. The influence of feed current frequency on the rotation ratio.

Depending on the inner cylinder rotation speed and the geometrical dimensions of the two cylinders, the functional sizes which define the rheological behavior can be calculated (Table 1).

Table 1. Rheometer functional sizes.

Size	General relation	Characteristic relation**
Shear rate, γ [s^{-1}]	$\gamma = \frac{2 \cdot \pi \cdot r_o^2}{r_o^2 - r_i^2} \cdot n$	$\gamma = 67.5 \cdot n$
Shear stress*, τ [Pa]	$\tau = \eta \cdot \gamma$	$\tau = 67.5 \cdot \eta \cdot n$
Friction force, F_f [N]	$F_f = 2 \cdot \pi \cdot H \cdot r_o \cdot \tau$	$F_f = 5.17 \cdot \eta \cdot n$
Torsion moment, M_t [N.m]	$M_t = F_f \cdot r_o$	$M_t = 0.22 \cdot \eta \cdot n$

* For Newtonian fluids: η - dynamic viscosity, $Pa \cdot s$; n - rotation speed, s^{-1}.

** For rheometer dimensions, m : $r_i = 0.04$, $r_o = 0.042$, $H = 0.29$.

The measurement of muff elongation force

The outer glass cylinder is attached to the gasket body by means of a rubber muff with the following characteristics: material – natural rubber/ butadiene-styrene; hardness 40±5 Shore A; inner diameter 90mm; wall thickness 0.5, 1.0 and 1.5mm, muff length 180mm, Figure 2.

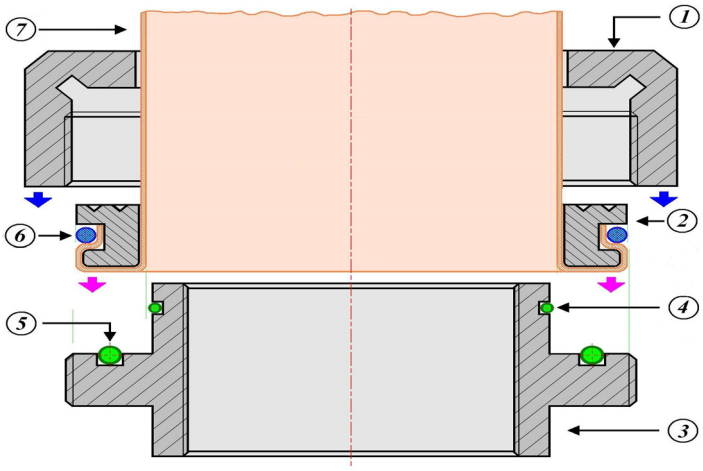

Figure 2. The fitting of rubber elastic muff
1- nut; **2**- aluminium ring; **3**- fixing socket; **4**, **5, 6**- fittings O-Ring; **7**- rubber muff.

The cylinder is suspended to the upper side by means of a torsionable thread which assures the cylinders centering and the control of system straining. The elongation is achieved either using an electric system (stepper motor) or through a screw system.

The measurement of the elongation force is assured by a bimetal force sensor (KD24S type); the obtained results can be locally displayed (digital size) or transmitted to a computer.

The torsion measurement of the outer cylinder

The torsion measurement of the outer cylinder is achieved by using a linear measure magnetic system, without contact, composed of a magnetic belt fixed on the outer surface of an aluminium disk, solidary fitted with the outer cylinder and a magnetic sensor fixed on the viscometer body to a distance between 0.1 and 2mm in comparison with the magnetic tape.

The magnetic belt moving in front of the sensor generates impulses that can be counted (experimentally was obtained 224.4 impulses/rotation or 0.028 radian/impulse). The correlation between the torsion angle of the outer cylinder $\Delta\theta$ and the torsion moment M_t was achieved using two torsion balances (Figure 3a, b) for different elongation forces and thicknesses of the elastic muff. The results are shown in Figure 4a, b, c.

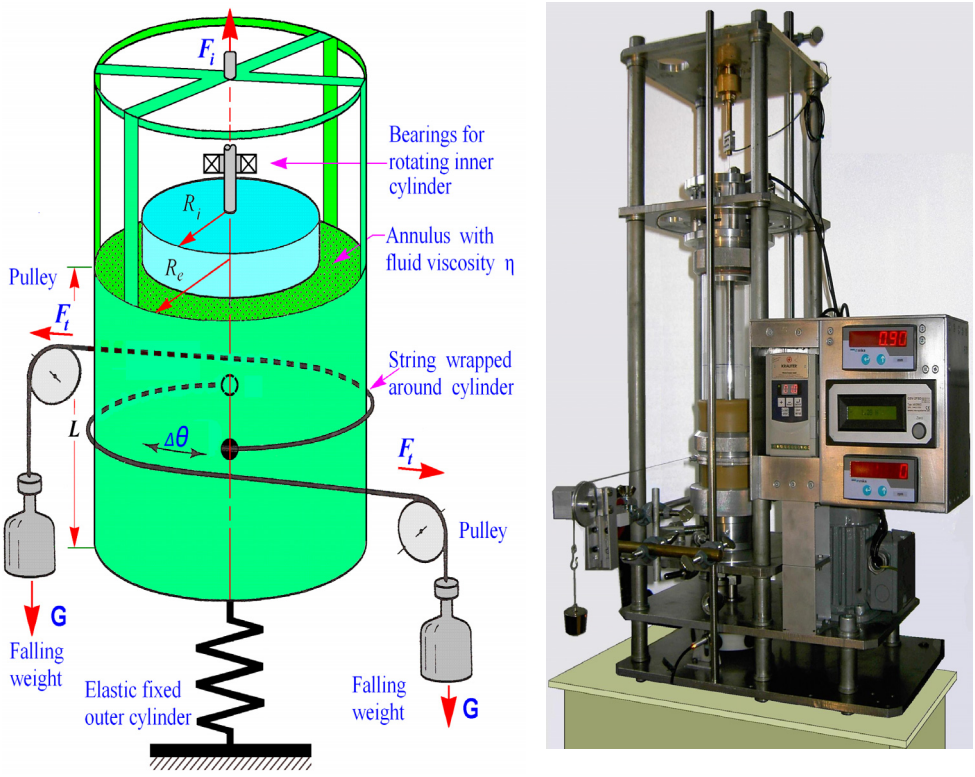

Figure 3a, b. The torsion measurement of the outer cylinder.

From these pictures presented it is found that an increase of muff thickness assures a better stability against the elongation force modification (Figure 4a and 4b), as well as a good linearity (Figure 4c).

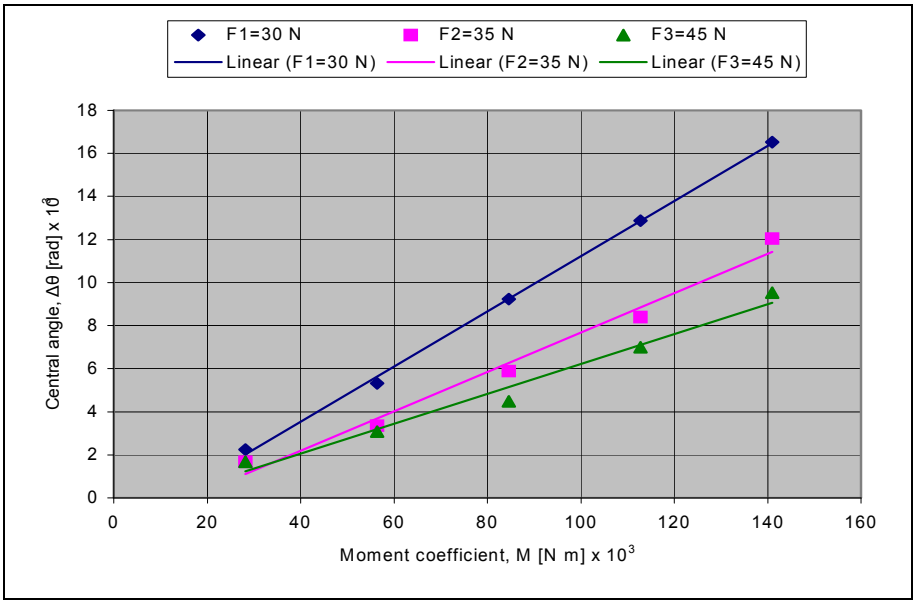

Figure 4a. $\Delta\theta = f(M_t)$ dependence, at different elongation forces, for δ_m= 1mm.

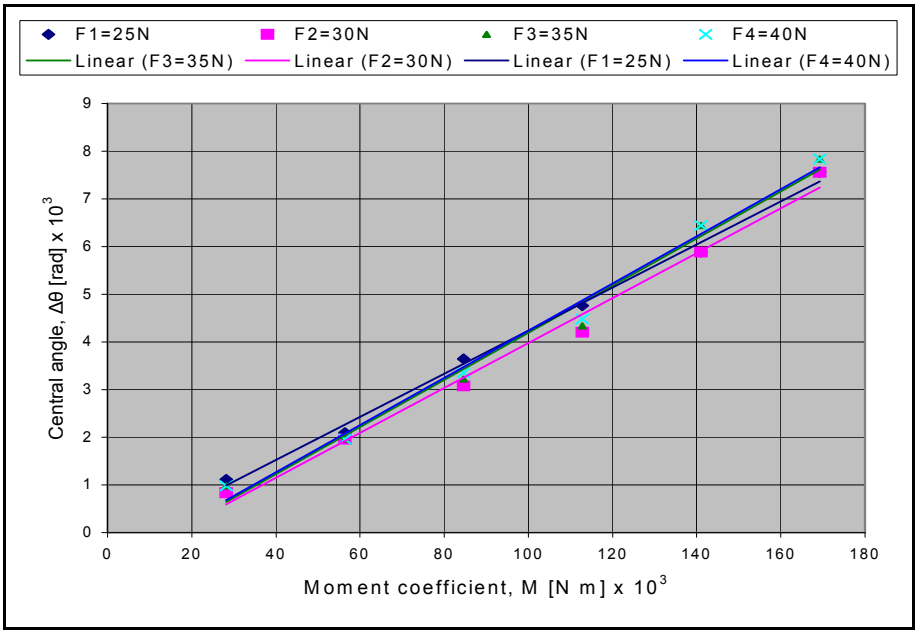

Figure 4b. $\Delta\theta = f(M_t)$ dependence, at different elongation forces, for δ_m= 1.5mm.

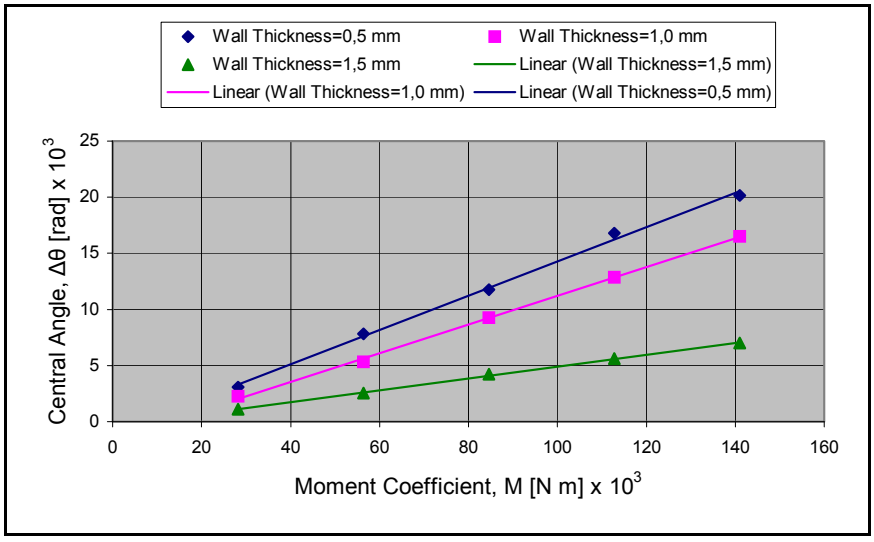

Figure 4c. $\Delta\theta = f(M_t)$ dependence, at different elastic muff thicknesses, for elongation force F= 30N.

CONCLUSIONS

A modified Couette type rotational viscometer with two glass concentric cylinders has been designed and realised.

The rotation speed adjustment is obtained through the electric current frequency modulation; the standardization curve frequency-revolution was experimentally traced;

It was experimentally established the effect of the torsion moment caused by the viscous friction force on the rotation angle of the outer cylinder assembled using an elastic muff.

The correlation between the torsion moment and the rotation angle was determined for different elongation force values and elastic muff thicknesses so as to determine the domain which is nearest to linearity.

EXPERIMENTAL

The rheometer constructive-functional scheme is presented in Figure 5.

The shaft is driven by using an asincron motor with power P= 180W and rotation speed n= 1360 rpm (at 50Hz); the transmission ratio $R_t = 1/3$, frequency domain $1 < \nu < 120Hz$, frequency step $\Delta\nu = 0.1Hz$. It is thus possible to achieve rotation speeds of the inner cylinder $6 < n_{Ax} < 1080$ rpm.

The inner cylinder revolution is measured using an inductive proximity detector; the data are digitally indicated and it is possible to transfer them to a computer.

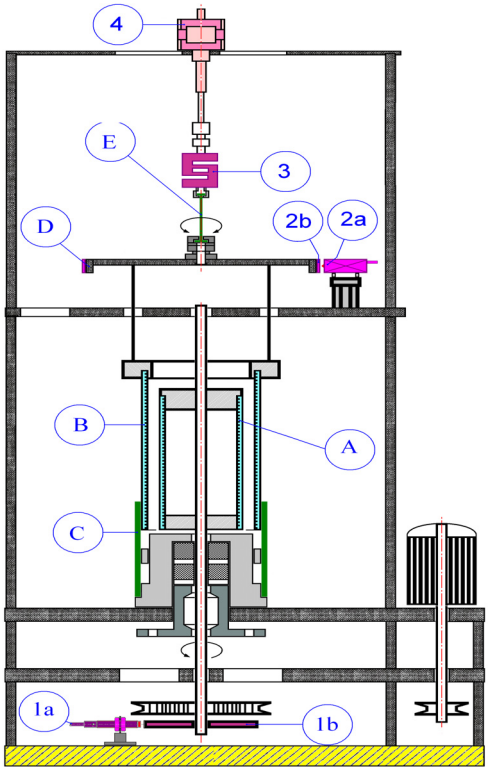

Figure 5. The scheme of experimental device
A- inner cylinder; **B**- outer cylinder; **C**- elastic tube; **D**- device for the free height regulation of the elastic tube; **E**- elongation thread; **1a**- inductive proximity detector IE 5260 (rotation sensor); **1b**- camp late E89010 (accessory to 1a); **2a**- magnetic measurement system for cylinder torsion; **2b**- magnetic tape; **3**- force detector KD24S; **4**- elongation system driven by a stepper motor.

REFERENCES

1. M.A. Couette, *Annales de Chimie et de Physique,* **1890***, 21*, 433.
2. N. Latrache, A. Ezersky, I. Mutabazi, 13th International Couette-Taylor Workshop, Barcelona, July 3-5, **2003**.
3. A. Tamas, N. Bors, R. Minea, *Buletinul Universitatii Petrol-Gaze din Ploiesti,* Seria Tehnica*,* **2008***, LX,* 4B*,* 105.
4. N. Bors, A. Tamas, Z. Gropsian, *Buletinul Stiintific al Universitatii Politehnica Timisoara,* Seria Chimie si Ingineria Mediului, **2008**, *53*, 1-2, 16.
5. J.L. Lumley, *J. Polymer Science, Macromol. Reviews,* **1973**, *7*, 263.
6. A. Gyrand, H.-W. Bewersdorff, “Drag Reduction of Turbulent Flows by Additives”, Kluwer Academic Publishier, Dordrecht, The Nederlands, **1995**.

STUDIA UNIVERSITATIS BABEŞ-BOLYAI, CHEMIA, LIV, 4, 2009

CHEMICAL CONTENTS IDENTIFICATION ON GC-MS FROM SELECTED SPECIES OF MACROMYCETES

DUMITRU RISTOIU[a], EMOKE-DALMA KOVACS[b], MARCEL PÂRVU[b], LUMINIȚA SILAGHI-DUMITRESCU[c]

ABSTRACT. Edible (Xerula radicata), inedible (Russula foetens), semi-edible (Lactarius piperatus) and poisonous mushrooms (Amanita phalloides) were analyzed on gas chromatography-mass spectrometry for its chemical contents. Analysis performed on GC-MS shown a high content of phenolic compounds in these basidiomycete species. Differences between chemical contents with 45 % were observed between young and mature species. Content of selected phallotoxins was determined in Amanita phalloides species.

Keywords: volatile compounds, organic fractions, basidiomycetes, GC-MS

INTRODUCTION

Mushrooms in the division of basidiomycota are worldwide distributed. Four species such as Xerula radicata, Russula foetens, Lactarius piperatus and Amanita phalloides, found in Faget forest, were studied for chemical compounds content.

Edible basidiomycetes such as Xerula radicata, commonly known as the rooting shaker or beech rooter is an edible basidiomycete fungus of the genus Xerula. As many researches shown, *Xerula radicata* is appreciated due to its medicinal properties as antihypertensive effects due to contain oudenone ((S)-2-[4,5-dyhydro-5-propyl-2-(3H)-furylidene]), an antihypertensive molecule. This molecule is a fungal metabolite and was reported as a strong inhibitor of catecholamine biosynthesis, inhibiting the enzymes phenylalanine and tyrosine hydroxylase (1). Different study has shown that the physiological effect of this enzyme inhibition is the reduction of blood pressure (2). Also Xerula radicata has been shown to contain an antibiotic named oudemansin X (E-β-methoxyacrylate oudemansin X, antifungal metametabolite), which lacked antibacterial activity against various organisms tested, but showed a good antifungal activity (3). *Lactarius piperatus* also known as the peppery milk cap is a semi-edible

[a] *Universitatea Babeş-Bolyai, Facultatea de Ştiința Mediului, Str. Fântânele, Nr. 30, RO-400294 Cluj-Napoca,Romania*
[b] *Universitatea Babeş-Bolyai, Facultatea de Biologie si Geologie, Str. Gh. Bilascu, Nr. 44, RO-400015 Cluj-Napoca, Romania*
[c] *Universitatea Babeş-Bolyai, Facultatea de Chimie şi Inginerie Chimică, Str. Kogălniceanu, Nr. 1, RO-400084 Cluj-Napoca, Romania*

(depending on regions from world, for example in Romania this mushroom is consumed by many people) basidiomycete fungus of the genus Lactarius. It's known also to have some antioxidant activity, based on its chemical content (4). *Russula foetens* named also as Fetid russula is an inedible fungus of genus Russula, but recent medical studies shown that due to its polysaccharides content present antitumoral effects (5, 6, 7). As poisonous mushroom, Amanita Phalloides was studied, known also with Death cap name. These species of Amanita genus is a seriously poisonous basodiomycetes fungus, its toxicities is thanks to presence of two main group of toxins such as amatoxins and the phallotoxins, both multicyclic peptides, spread throughout the mushroom tissue (8).

RESULTS AND DISCUSSION

The volatile fractions were obtained from the fresh mushrooms fruiting bodies and analyzed as described in experimental section. The results obtained for the four species studied are presented in table 1.

Table 1. Volatile compounds present in the four basidiomycetes studied (Percent of the total ion current, GC-MS*,**)

Compounds	Xerula r. (%)	Lactarius p. (%)	Russula f. (%)	Amanita ph. (%)
Phenol	0.8	0.9	1.1	2.9
Hexanal	0.5	-	0.4	0.8
2.4-decadienal	-	-	0.2	0.5
2-undecanone	0.1	0.1	0.2	0.2
Acetic acid	1.2	1.1	1.2	2.1
Hydroxy acetic acid	-	-	-	0.1
Hexadecanoic acid	1.1	0.8	0.7	1.3
Hydroxyquinone monopryl ether	0.5	0.4	1.2	2.8
Acetic acid phenyl ether	0.1	0.1	0.5	0.3
Hexadecanoic acid ethyl ester	1.5	1.8	0.9	2.2

*) The ion current generated depends on the characteristics of the compound concerned and is not a true quantification.

**) All matching (as percentages) of mass spectrometry data with literature data were in the range of 83 – 98 %.

The most founded compounds in all mushroom samples were the phenolic compounds. These results in quietly normal, based on the several researches reported in the last decades. They also suggested that the production of phenolic compounds originates from an evolutionary ancestral biochemical shift. Some research sustain that these phenolic compounds may be involved in a chemical mechanism against insects and microorganisms (9).

After the comparison of chemical contents results in each parts of the analyzed mushroom it was observed that in the cap and flesh higher value with 20 – 30 % were determined than in the stem of the same basidiomycete's species. Also for volatile compounds the levels were higher in the young mushrooms species with 15 % than in the mature mushrooms (for the same species), but the content of some organic compounds (such as urea, tyrosine, proline, glycine, resorcinol and catechol) were lower with almost 45 % than in the mature mushrooms as shown in table 2.

Table 2. The main organic fraction constituents in xerula radicata and Lactarius piperatus basidiomycetes as a comparation between young and mature mushrooms (Percent of the total ion current, GC-MS*,**)

Compounds	Xerula r.		Lactarius p	
	Young sp.	***Mature sp.***	***Young sp.***	***Mature sp.***
Urea	3.5	4.9	3.3	5.0
Tyrosine	-	-	-	0.1
Proline	0.3	0.7	0.2	0.5
Glycine	-	0.2	-	-
Resorcinol	0.2	0.3	-	0.2
Catechol	0.3	1.2	0.1	0.4
Valine	-	0.3	-	0.2
Leucine	0.1	0.4	-	-

*) The ion current generated depends on the characteristics of the compound concerned and is not a true quantification.

**) All matching (as percentages) of mass spectrometry data with literature data were in the range of 83 – 98 %.

In Amanita phalloides were also identified α-amanitin, β-amanitin, amanin and amanullin in an average of 0.5 % in mature species. Also compounds such as phalloidin, phalloicin and prophalloin belonging to phallotoxin class, characteristic for these species was determinate in an average of 0.8 % in mature mushrooms.

CONCLUSIONS

The results obtained add new stocks to the knowledge on the chemical composition of the selected species mushrooms belonging basodiomycetes division studied in this work. These dates help to provide further explanation for their reported toxicity or positive medical effects in some health anomaly.

EXPERIMENTAL SECTION

Collection of samples: The four basidiomycetes were collected from Faget forest, near Cluj-Napoca, Romania in June 2009.

Extraction: The fresh fruiting bodies of basidiomycetes were separated as: cap, gills, flesh and stem. All of these parts were cut again in very small species as possible, and from them 10 g from every group was put to leach with trichloromethane for 1 hour in order to establish volatile compounds content for each species of basidiomycetes. Also the same think was done but with ethanol and for 24 hour in order to establish the organic compounds content in each mushroom species. After soak they were extracted with headspace heated ultrasound apparatus (Elmasonic S 10 H) for 1 hour for separate the volatile compounds. The solid phase microextractiom technique was performed on each sample in order to analyze the organic compounds contents from mushroom samples.

Analysis of volatile organic compounds: They were analyzed by gas chromatography with electron capture detector (ECD) and flame ionization detector (FID) with Trace GC Ultra apparatus and DSQ II quadupole mass spectrometry. TR-V1 cyanopropylphenyl polysiloxane based phase capillary column (30 m $\times$ 0.53 mm ID $\times$ 3.0 μm) was used to perform all analysis. The FID detector temperature was set at 300 °C and the ECD detector at 250 °C. The mixture was heated at 80 °C for 30 minutes. The temperature program was programmed from 40 – 220 °C at a rate of 7 °C min^{-1}, and nitrogen was used as carrier gas.

Analysis of organic compounds: They were analyzed on gas chromatography coupled to an guadrupole mass spectrometer (DSQ II – FOCUS GC) with columns Thermo TR-WaxMS (30 m $\times$ 0.25 mm ID $\times$ 0.25 μm). The ion source was set at 270 °C and the ionization voltage at 70 eV. The column temperature program was set from 40 °C with 5 °C min^{-1} to 100 °C, with 3 minutes hold time and after that continued with 10 °C min^{-1} to 280 °C and maintained at this temperature for 7 minutes. Helium was used as carrier gas.

REFERENCES

1. M. Ohno, M. Okamoto, N. Kawabe, H. Umezawa, T. Takeuchi, H. Iinuma, S. Takahash, *Journal of American Chemical Society*, **1971**, *93*(5), 1285.
2. T. Nagatsu, I. Nagatsu, H. Umezawa, T. Takeuchi, *Biochem Pharmacol*, **1971**, *20*(9), 2505.
3. T. Anke, A. Werle, M. Bross, W. Steglich, *Journal of Antibiotics (Tokyo)*, **1990**, *43*(8), 1010.
4. L. Barros, P. Baptista, ICFR Ferreira, *Journal of Food Chem Toxicology*, **2007**, *45*, 1731.
5. S. Ohtsuka, S. Ueno, C. Yoshikumi, F. Hirose, Y. Ohmura, T. Wada, T. Fujii, E. Takahashi, *UK Patent 1331513*, **1973**.
6. XN, Wang, JH. Shen, JC. Du, JK. Liu, *Journal of Antibiotics (Tokyo)*, **2006**, *59*(10), 669.
7. XN. Wang, F. Wang, JC. Du, HM. Ge, RX. Tan, JK. Liu, *Journal of Chemical Science*, **2005**, *60*(10), 1065.
8. J. Vetter, *Journal of Toxicon*, **1998**, *36*(1), 13.
9. A. Del signore, F. Romeo, M. Giaccio, *Mycol Res*, **1997**, *101*, 552.

STUDIA UNIVERSITATIS BABEŞ-BOLYAI, CHEMIA, LIV, 4, 2009

CO-CRYSTALLIZATION OF MERCAPTO-1,3,4-THIADIAZOLE DERIVATIVES WITH *ORTHO*-FUNCTIONALIZED PYRIDINES AND SPECTRAL CHARACTERIZATION IN SOLID STATE

ANDREA E. PASCUI[a], MONICA M. VENTER[a]*, VASILE N. BERCEAN[b]

ABSTRACT. Co-crystallization of 2,5-dimercapto-1,3,4-thiadiazole (DMTD) and (3*H*-2-thioxo-1,3,4-thiadiazol-2-yl)thioacetic acid (H_2L) with *ortho*-functionalized pyridines in 1:1 molar ratio produced three molecular complexes: DMTD·2,2'-bipy (1), H_2L·2,2'-bipy (2) and H_2L·2-H_2NPy (3), respectively. The structure of compounds 1–3 was characterized in solid state by microanalysis and FT-IR, FT-Raman and electronic spectroscopy. The spectral data suggest the formation of proton transfer molecular complexes (1) or association products (2, 3). Acid-base C=O···HN and C=O···HO intermolecular interactions are enphasized for compounds 2 and 3.

Keywords: mercapto-1,3,4-thiadiazole derivatives, co-crystallization, spectroscopy

INTRODUCTION

The co-crystallization products have been also named co-crystals and this term has been extensively used as well as criticized in recent years. There were published different interpretations of its meaning, from common multi-component crystals to multiple crystal systems.[1] The latest interpretation was given by Desiraju[2] who also pointed out the term's ambiguity and recalled that "*(…) it would do one good to remember that we had (and still have) a perfectly good word to describe multi-component crystals, which have specific noncovalent interactions between the distinct molecules, and this is molecular complex".* It is the molecular complex formation and characterization that concerns our present work.

Initially, molecular complexes have been constructed mainly through heteromeric N–H···O, O–H···O and N–H···N hydrogen bonds. Recently, high order systems have been generated through combination of these strong and directional non-covalent connectivities and other interactions, such as halogen-bonding.[3]

[a] *"Babeş-Bolyai" University, Faculty of Chemistry and Chemical Engineering, RO-400028 Cluj-Napoca, Romania. monica@chem.ubbcluj.ro*

[b] *"Politehnica" University, Faculty of Industrial Chemistry and Environment Engineering, RO-300006 Timişoara, Romania.*

Our studies in the field of supramolecular chemistry have focused on heterocyclic thione donors containing at least one thioamide group. Compounds such as 2,4,6-trimercaptotriazine (TMT) or mercapto-1,3,4-thiadiazole derivatives (MTD) proved valuable candidates for building supramolecular structures through hydrogen bonding and S···S interactions.[4,5] In addition, Rao et al. successfully co-crystallized TMT with melamine, tricyanuric acid or 4,4'-bipyridine, engineering channel-type nanostructured crystals. Some of these compounds have proved excellent zeolitic properties.[6-9] In spite of the plethora of publications discussing co-crystallization of organic acids and bases, there are very few reports on molecular complexes containing MTD moieties. For example, there is one crystallographic evidence concerning the co-crystallization ability of MTD compounds and refers to (4,4'-bipyridine)·(5-amino-1,3,4-thiadiazole-2(3*H*)-thione) in 1:2 ratio.[10]

In several of our recent works we reported synthetic procedures and spectral studies on (3*H*-2-thioxo-1,3,4-thiadiazol-2-yl)thioacetic acid, $C_2HN_2S_3CH_2COOH$ (H_2L) and related metal complexes. The neutral H_2L consists of a 2,5-dimercapto-1,3,4-thiadiazole, $C_2H_2N_2S_3$ (DMTD) skeleton extended with one pendant acetic fragment (Fig. 1).

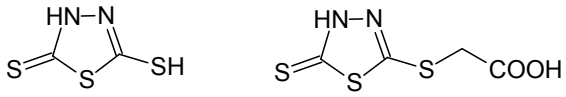

DMTD **H_2L**

Figure 1. Schematic drawing of 2,5-dimercapto-1,3,4-thiadiazole (DMTD) and (3*H*-2-thioxo-1,3,4-thiadiazol-2-yl)thioacetic acid (H_2L).

Both compounds reveal acidic behaviour. Thus, first step deprotonation of DMTD and H_2L leads to monoanions, which have been identified in metal salts and complexes. The remaining proton is located on the nitrogen[11-13] or sulphur atom[14] in the case of DMTD and on the nitrogen atom in the case of H_2L.[15-17] Further deprotonation of the title acids leads to dianions, also present in several metallic derivatives.

The aim of this work is to study the co-crystallization versatility of H_2L by comparison with that of DMTD using 2-aminopyridine (2-H_2NPy) and 2,2'-bipyridyl (2,2'-bipy) as acceptors. Thus, here we report the preparation of three molecular complexes DMTD·2,2'-bipy (**1**), H_2L·2,2'-bipy (**2**) and H_2L·2-H_2NPy (**3**). The co-crystallization ratio was elucidated by microanalysis. Due to the lack of suitable crystals for single-crystal X-ray diffraction, the structure of the molecular complexes (**1**–**3**) and the acid-base association was investigated in solid state by FT-IR, FT-Raman, and electronic spectroscopy. Similar studies on molecular complexes containing acceptors of higher symmetry (i.e. *para*-functionalized pyridines), as well as structural studies in solution are in progress.

RESULTS AND DISCUSSION

Co-crystallization of DMTD and H_2L with 2,2'-bipy and 2-H_2NPy in 1:1 molar ratio, produced three molecular complexes: DMTD·2,2'-bipy (**1**), H_2L·2,2'-bipy (**2**) and H_2L·2-H_2NPy (**3**). All the reactions worked in methanol solution, at room temperature or gentle heating. The products are stable during recrystallization from methanol, except compound **1** which shows traces of decomposition products during purification. All complexes are air and light stable in solid state.

The co-crystallization ability of the acids can be roughly estimated from the difference in pK_a between the conjugate acid of the base and the acid. According to literature, the proton transfer should occur for $\Delta pK_a > 3.75$.[18] Taking into account the pK_a values of DMTD (-1.36 and 7.5)[19] and the pK_b values of 2,2'-bipy (9.5 and 14.1) we can predict a single proton transfer from DMTD to 2,2'-bipy ($\Delta pK_a = 5.8$). Unfortunately, no acidity data could be found for H_2L in order to do similar calculations.

The FT-IR and Raman spectra of DMTD, H_2L and the corresponding molecular complexes **1**–**3** were recorded in solid state, in the 4000–400 and 3500–200 cm^{-1} spectral ranges, respectively. The spectra of the products are presented in Fig. 2. The most relevant spectral data are listed in Table 1 and 2. Assignments of the starting material vibrational modes were made according to literature data.[20-24] The vibrational behaviour of DMTD and related compounds was extensively investigated by F. Hipler et al.[20,21] as both matrix isolated species (IR) and bulk material (Raman). Their assignments support our IR and Raman data recorded for DMTD in solid state. As it concerns the H_2L derivative, we have already reported a brief vibrational characterization[23] and we will use our assignments in further discussions.

DMTD as free and co-crystallized acid: One of the main structural characteristics of DMTD is the co-existence of the thione (HNC=S) and thiol (NC-SH) tautomeric forms in the same molecule, as proved by spectral and crystallographic evidences.[20,21,25] The thione tautomer of DMTD is characterized in the IR and Raman spectra by the assignment of the ν(NH) and δ(NH) vibrational modes. Thus, the IR spectrum of pure DMTD shows a complicated broad feature in the 3200–2700 cm^{-1} spectral range, characteristic for the ν(NH) fundamental of poliazolic heterocycles.[22] However, the assignment of the ν(NH) stretching vibration at 3051 cm^{-1} is in good agreement with literature data.[20,21] The NH group deformation is well represented by the first two thioamide bands: ν(C=N)/δ(NH) (1502 cm^{-1}) and δ(NH) (1450 cm^{-1}). It is worth mentioning that the position and relative intensity of these bands change significantly in the absence of the thione tautomer.

For example, the spectra of the symmetrically S-substituted derivative 2,5-bis(*tert*-butyldithio)-1,3,4-thiadiazole, reveal only the ν(C=N) fundamentals in the 1471–1442 cm^{-1} region.[21]

The IR and Raman spectra of the co-crystallized product (**1**) exhibit the expected ν(NH) modes in the 3075–3042 cm^{-1} spectral range. However, the assignment of these bands to the thiadiazole and/or – in case of proton transfer – to the pyridinium NH groups is ambiguous.

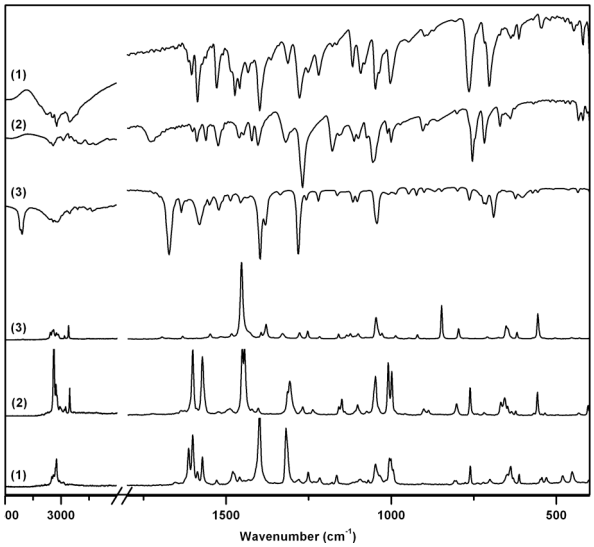

Figure 2. The IR and Raman spectra of DMTD·2,2'-bipy (**1**), H_2L·2,2'-bipy (**2**) and H_2L·2-H_2NPy (**3**).

Table 1. Selected vibrational data (cm^{-1}) for **DMTD** and DMTD·2,2'-bipy (**1**)

DMTD		DMTD·2,2'-Bipy (1)		Vibrational Assignment
IR	**Raman**	**IR**	**Raman**	
3051 s,br	3056 w	3042 s	3040 ms	ν(NH)
2471 m,br	2489 m,br			ν(SH)
		1587 s	1585 m	$\nu(ring)_{Py}$
1502 vs	1512 mw	1528 s	1530 w	ν(CN) / δ(NH)
1450 m	1453 vs	1472 s	1479 m	δ(NH) + $\nu(ring)_{Py}$
		1457 s	1458 w	
1260 vs	1283 mw	1281 s	1281 mw	ν(CN)
1075 mw	1080 m			ν(CS) / δ(SH)
1048 s	1042 m	1047 s	1048 m	ν_{as}(S=C-S)
		1002 s	1006 ms	$\nu(ring)_{Py}$
939 mw	942 w			δ(SH)
		763 s	761 ms	$\delta(CH)_{Py}$
712 s	716 w	703 s	701 w	ν_{as}(CSC)
658 mw	659 vs	640 w	638 ms	ν_s(CSC)

Abbreviations: w – weak, mw – medium weak, m – medium, ms – medium strong, s – strong, vs – very strong, ν - stretching, δ - bending, br – broad, Py – pyridyl ring.

Table 2. Selected vibrational data (cm^{-1}) for **H_2L**, $H_2L{\cdot}2,2'$-bipy (**2**) and $H_2L{\cdot}2\text{-}H_2NPy$ (**3**).

H_2L[23]		$H_2L{\cdot}2,2'$-Bipy (2)		$H_2L{\cdot}2\text{-}H_2NPy$ (3)		Vibrational Assignment
IR	**Raman**	**IR**	**Raman**	**IR**	**Raman**	
				3346 s		$\nu(NH_2)$
3093 ms,br	3103 w	3071 m,br	3070 vs	3070 m	3073 m	$\nu(NH)$
2950 ms	2953 m	2984 mw	2965 w		2975 w	$\nu_{as}(CH_2)$
2903s	2915 s	2926 w	2928 m	2939 mw	2939 m	$\nu_s(CH_2)$
1693 vs	1693 m	1725 m,br	1724 vw	1672 vs	1697 w	$\nu(C=O)$
				1635 m	1634 w	$\delta(NH_2)$
		1587 m	1574 vs	1579 s		$\nu(ring)_{Py}$
		1561 m		1549 mw	1549 mw	
1494 vs	1497 w	1521 m	1522 w	1522 m	1519 vw	$\nu(CN) / \delta(NH)$
		1460 m	1491 w	1487w	1485 w	$\nu(ring)_{Py}$
1448 mw	1453 vs	1449 m	1446 vs	1454 mw	1456 vs	$\delta(NH)$
		1423 m	1443 vs	1434 w		$\nu(ring)_{Py}$
1293 s	1303 w	1269 vs	1270 mw	1281 vs	1279 mw	$\nu(CN)$
1051 vs	1051 s	1057 s	1050 s	10413 s	1048 s	$\nu_{as}(S=C\text{-}S)$
		1002 ms	1001 s	1005 w		$\nu(ring)_{Py}$
		754 s	764 ms	764 m	798 m	$\delta(CH)_{Py}$
724 s	726 w	715 m	719 w	719 m	710 w	$\nu_{as}(CSC)_{endo}$
670 m	678 s	666 mw	670 m	690 s	654 m	$\nu_s(CSC)_{endo}$

Abbreviations: w – weak, mw – medium weak, m – medium, ms – medium strong, s – strong, vs – very strong, br – broad, ν - stretching, δ - bending, endo – endocyclic, Py – pyridyl ring.

The same ambiguity may arise from the assignment of the second thioamide band of the acid in the 1479–1457 cm^{-1} region, due to the closeness of the ν(C=N)/ν(C=C) stretching vibration of the pyridyl ring. On the other hand, the first thioamide band of the co-crystallized DMTD can be clearly located (1528 cm^{-1}) and reveals a positive shift by 26 cm^{-1} when compared to the homologue value of the free acid. This vibrational behaviour may suggest an additional and/or stronger involvement of the NH groups into hydrogen bonding during co-crystallization.[24]

The thiol tautomer of DMTD is characterized in the IR and Raman spectra by the assignment of the ν(SH) and δ(SH) fundamentals. Thus, the spectra of pure DMTD show medium, broad bands assigned to ν(SH) mode at 2489–2471 cm^{-1}. In addition, the SH group deformation can be found in the 1080–1075 and 942–939 cm^{-1} narrow ranges. The IR and Raman spectra of the co-crystallized product (**1**) do not exhibit any of the previously mentioned bands. As a consequence, the acid may be present in the molecular complex either as thione-thione or thione-thiolate tautomer.

H_2L as free and co-crystallized acid: The donor ability of H_2L is governed by the presence of the thiadiazole heterocycle and the carboxylic group of the pendant arm. Similarly to DMTD, the heterocyclic fragment could exist as thione or thiol tautomer but in this case we have proved that the thione tautomeric form settles in solid state.[23] Thus, it was possible to assign the ν(NH) fundamental despite the complicate structure of the broad band (3100–2500 cm^{-1}) produced by the carboxylic OH group vibrations. The same ν(NH) mode was located in the IR and Raman spectra of **2** and **3** around 3070 cm^{-1}, suggesting that the H_2L molecule saves its thione tautomeric form during co-crystallization. In addition, none of the Raman spectra reveals characteristic ν(SH) bands for the free and co-crystallized acid. This structural feature is even more obvious when we analyse the pattern of the first two thioamide bands. The IR spectrum of the pure H_2L shows a very strong ν(C=N)/δ(NH) band (1494 cm^{-1}) and a medium-to-weak δ(NH) band (1448 cm^{-1}). In the corresponding Raman spectrum, the two bands switch relative intensities. This spectral feature is very well reproduced by the IR and Raman spectra of **2** and **3** confirming that the heterocycle remains protonated. In addition, the positive shift of the ν(C=N)/δ(NH) mode in the spectra of **2** and **3** by up to 28 cm^{-1} suggests an additional and/or stronger involvement of the NH groups into intermolecular interactions.[24]

The carboxylic fragment of the pendant chain is best characterized by the ν(C=O) vibrational mode assignment at 1693 cm^{-1} as a very strong IR band. The position of this band is significantly shifted in the spectra of the molecular complexes towards higher wavenumbers by 32 cm^{-1} (**2**) or lower wavenumbers by 21 cm^{-1} (**3**). The negative shift of the ν(C=O) band does not reach the values reported for the related ν_{as}(COO) fundamental (1641–1577 cm^{-1}) in the IR spectra of metallic derivatives containing the acid as carboxylato monanion.[15-17] As a

consequence, the carboxyl group of H_2L saves its protonated form during co-crystallization. According to literature data, the location of the ν(C=O) mode in the approx. 1730–1700 cm^{-1} region may suggest C=O···H-N interactions, while the location in the approx. 1700–1660 cm^{-1} region could be the result of C=O···H-O interactions.[26] However, the IR spectrum of **3** lacks the medium-to-strong, broad band in the 955–915 cm^{-1} range, assigned to the δ_{op}(OH···O) mode in carboxylic acid dimmers.[24]

Ortho-functionalized pyridine acceptors: The IR and Raman spectra of the molecular complexes **1**–**3** show characteristic frequencies for the 2,2'-bipy and 2-H_2NPy acceptors. Among the most important vibrational modes, the ν(ring) and δ(CH) were located in the 1600–1400 and 800 – 750 cm^{-1}, respectively. In addition, the $\nu(NH_2)$ and $\delta(NH_2)$ fundamentals of 2-H_2NPy were found in the expected spectral regions. The positive shift of the $\delta(NH_2)$ modes in the IR spectrum of **3** by 7 cm^{-1} suggests a strengthen of the hydrogen bonds involving this group.[24]

The electronic spectra of the molecular complexes **1**–**3** along with those of the corresponding starting materials were recorded in solid state, in the 200–800 nm spectral range (Fig. 3). The spectra reveal different patterns depending on the nature of the donor acid. Thus, the spectrum of compound **1** consists of a large band which broadens towards visible domain by approx. 100 and 200 nm when compared to the spectra of DMTD and 2,2'-bipy, respectively. Several electronic studies on solutions of molecular complexes and salts containing functionalized pyridinium moieties (i.e. 2- and 4-H_2NPyH^+, 4,4'-bipyH_2^{2+}) have revealed bathochromic shifts of the UV-bands when compared with those of the neutral pyridine derivatives and donor acids.[27-30] Moreover, in the case of pyridine-2,6-bis(monothiocarboxylic) acid · 2-aminopyridine proton transfer complex the electronic spectrum shows the formation of a new peak in the longer wavelength domain besides the red-shift of the expected bands.[27] In this respect, we can afford to suggest that the electronic behaviour of **1** is a result of the proton transfer from DMTD to 2,2'-bipy and the consequent interaction between the resulting charged species.

On the opposite, the spectra of **2** and **3** show no such significant changes in the shape and position of the initial bands. More specific, the spectrum of **2** consists of a large band (200-400 nm) which reveals four peaks at 216, 262, 304 and 355 nm. These peaks meet their correspondence in the spectra of starting materials, except the 304 nm maximum which seams to mediate the 293 nm transition of H_2L and the 319 nm transition of 2,2'-bipy. Similarly, the spectrum of **3** shows a UV band with four broad maximums at 216, 239, 297, 338-357 nm. These values are also comparable with those found for the starting materials, except the 297 nm maximum which is slightly red-shifted by 4 nm.

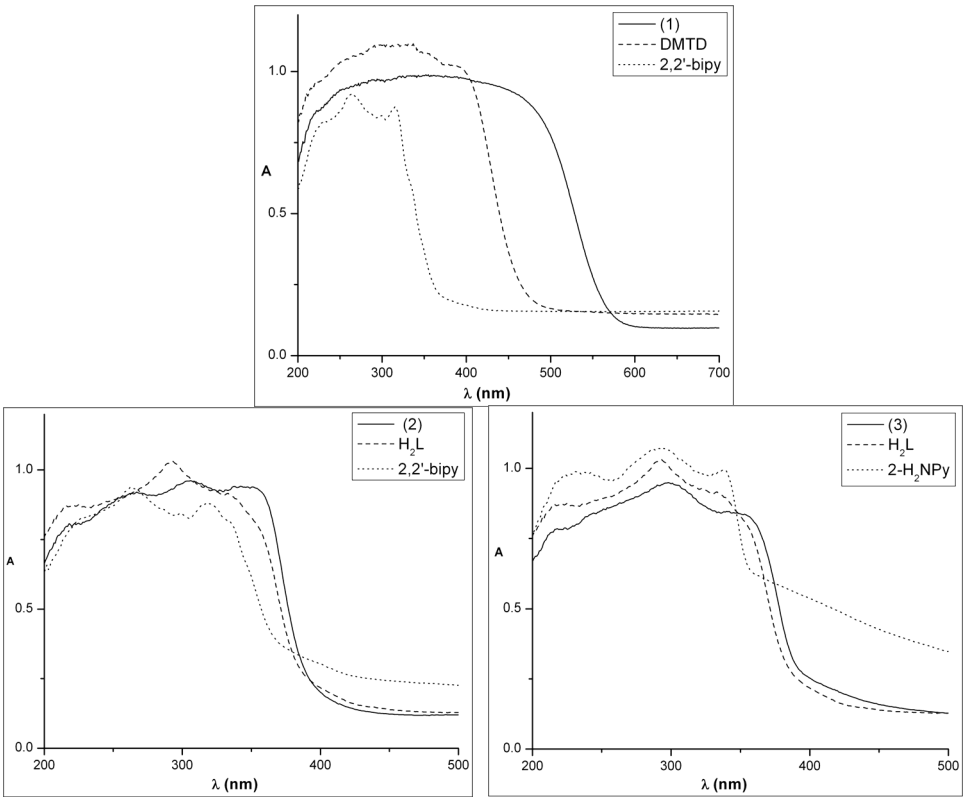

Figure 3. The electronic spectra of DMTD·2,2'-bipy (**1**), H_2L·2,2'-bipy (**2**), H_2L·2-H_2NPy (**3**) and the corresponding starting materials.

CONCLUSIONS

The co-crystallization of DMTD and H_2L with *ortho*-functionalized pyridines in 1:1 molar ratio allows the formation of molecular complexes **1**–**3**.

The vibrational behaviour of DMTD·2,2'-bipy (**1**) is consistent with the thione-thione or thione-thiolato tautomeric form of the DMTD moiety. Taking into account the major bathochromic shift in the electronic spectrum of **1**, as well as the prediction of the ΔpK_a rule, we suggest an ionic structure containing the thione-thiolato DMTD anion and the monoprotonated 2,2'-bipy cation.

The spectral investigation of H_2L·2,2'-bipy (**2**) and H_2L·2-H_2NPy (**3**) clearly shows that these molecular complexes cannot be the result of a proton transfer, but a simple association process. According to the vibrational data, we may predict different acid-base association scenarios for the two compounds (Fig. 4). Thus, for compound **2** N-H···O hydrogen bonding is suggested between the carbonyl and the NH groups of H_2L. This interaction leaves the possibility

of N_{Py}···H-O connections between the base and the acid. The vibrational data of **3** suggests intermolecular O-H···O hydrogen bonding between the carboxyl groups of neighboring acids. Consequently, the most probable acid-base connection could be the N-H··· N_{Py} interaction.

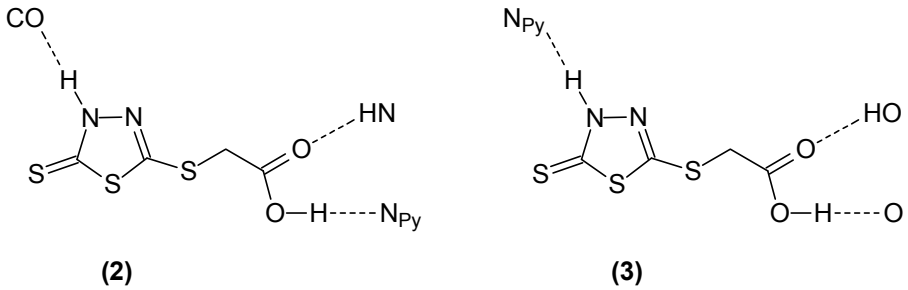

(2) **(3)**

Figure 4. Proposed acid-base association patterns for compounds H_2L·2,2'-bipy (**2**) and H_2L·2-H_2NPy (**3**)

EXPERIMENTAL SECTION

Methods and materials: Elemental analyses were obtained on a VarioEL apparatus from Elementar Analysensysteme GmbH. Melting points (uncorrected) were measured in the 30-360°C range using a KRUSS KSPI digital apparatus. FT-IR and FT-Raman spectra on solid samples were recorded using a Bruker FT-IR Equinox 55 spectrometer with an integrated FRA 106 S Raman module. The excitation of the Raman spectra was performed using the 1064 nm line from a Nd:YAG laser with an output power of 250 mW. An InGaAs detector operating at room temperature was used. FT-IR spectra were also recorded on KBr pellets using a FT-IR JASCO 600 Spectrometer. The spectral resolution was 2 cm^{-1}. Electronic spectra were recorded on solid samples at room temperature, in the 200-800 nm spectral range, using a Jasco V-670 UV/VIS/NIR spectrophotometer.

The starting materials and solvents were purchased from commercial sources (Merck and Reagents Com.) as analytical pure substances and were used with no further purification or drying. The preparation of (3*H*-2-thioxo-1,3,4-thiadiazol-5-yl)thioacetic acid (**H_2L**) was reported elsewhere.[23]

Synthesis: Methanol solutions of donors and acceptors in 1:1 molar ratio were mixed for 30 min. at room temperature (**2** and **3**) or gentle heating (**1**). Compounds **1** and **2** were crystallized from the reaction mixture at low temperature (approx. 5°C). Compound **3** precipitated from the reaction mixture as white powder. Reaction and purification details as well as brief characterization of the products are given bellow:

2,5-Dimercapto-1,3,4-thiadiazole·2,2'-bipyridyl·CH_3OH (1). The product crystallized from the reaction mixture as orange microcrystalline solid of analytical purity. Recrystallization from methanol shows traces of decomposition products. Yield: 0.57 g, 93%; mp: 120-2°C. Microanalysis: found (calc. for $C_{12}H_{10}N_4S_3·CH_4O$, MW 338.48) C 46.21 (46.13), H 3.91 (4.17), N 16.96 (16.55).

(3*H*-2-thioxo-1,3,4-thiadiazol-2-yl)thioacetic acid·2,2'-bipyridyl·0.25H_2O (2). The product recrystallized from MeOH as colorless fine needles. Yield: 0.57 g, 78%; mp: 118-20°C. Microanalysis: found (calc. for $C_{14}H_{12}N_4O_2S_3·0.25H_2O$, MW 368.978) C 45.46 (45.57), H 3.07 (3.41), N 15.20 (15.18).

(3*H*-2-thioxo-1,3,4-thiadiazol-2-yl)thioacetic acid·2-aminopyridine (3). The product recrystallized from hot MeOH as colorless fine needles. Yield: 0.57 g, 93%; mp: 226-30°C (dec.). Microanalysis: found (calc. for $C_9H_{10}N_4O_2S_3$, MW 302.403) C 35.82 (35.75), H 2.87 (3.33), N 18.02 (18.53).

ACKNOWLEDGMENTS

The authors thank The National University Research Council Romania for financial support during the course of this work (Grant CNCSIS-A/2007-2008, 14-25/1449) and the "Babes-Bolyai" University Cluj-Napoca for a Performance Research Fellowship (A.E. Pascui). M.M. Venter thanks Prof.Dr. Mircea Darabantu for useful discussions.

REFERENCES

1. A.D. Bond, *CrystEngComm*, **2007**, *9*, 833.
2. G.R. Desiraju, *CrystEngComm*, **2003**, *5*, 466.
3. C.B. Aakeroy, J. Desper, M Fasulo, I. Hussain, B. Levina, N. Schultheiss, *CrystEngComm*, **2008**, *10*, 1816.
4. V. Bercean, C. Crainic, I. Haiduc, M.F. Mahon, K.C. Molloy, M.M. Venter, P.J. Wilson, *J. Chem. Soc., Dalton Trans*., **2002**, 1036.
5. M.F. Mahon, K.C. Molloy, M.M. Venter, I. Haiduc, *Inorg. Chim. Acta*, **2003**, *348*, 75.
6. A. Ranganathan, V.R. Pedireddi, S. Chatterjee, C.N.R. Rao, *J. Mater. Chem.*, **1999**, *9*, 2407.
7. S. Ahn, J.P. Reddy, B.M. Kariuki, S. Chatterjee, A. Ranganathan, V.R. Pedireddi, C.N.R. Rao, K.D.M. Harris, *Chem.-Eur.J.,* **2005**, *11*, 2433.
8. V.R. Pedireddi, S. Chatterjee, A. Ranganathan, C.N.R. Rao, *J. Am. Chem. Soc.,* **1997**, *119*, 10867.
9. A. Ranganathan, V.R. Pedireddi, C.N.R. Rao, *J. Am. Chem. Soc.,* **1999***, 121*, 1752.
10. Q.-J. Deng, M.-X. Yao, M.-H. Zeng, *Acta Crystallogr.,* **2005***, E61*, o2239.

11. P. Mura, B.G. Olby, S.D. Robinson, *Inorg. Chim. Acta,* **1985***, 97*, 45.
12. H. Tannai, K. Tsuge, Y. Sasaki, O. Hatozaki, N. Oyama *Dalton Trans.,* **2003***,* 2353.
13. V. Wee L. Ng, S.L. Kuan, Z. Weng, W.K. Leong, J.J.Vittal, L.L. Koh, G.K. Tan, L.Y. Goh, *J. Organomet. Chem.,* **2005***, 690*, 2323.
14. P. Mura, S.D. Robinson, *Eur. Cryst. Meeting,* **1982***, 7*, 208.
15. M.M. Venter, V. Chis, S. Cinta Pinzaru, V.N. Bercean, M. Ilici, I. Haiduc, *Studia Univ. Babes-Bolyai, Ser. Chem*., **2006**, *LI(2),* 65.
16. M.M. Venter, A. Pascui, V.N. Bercean, S. Cinta Pinzaru, *Studia Univ. Babes-Bolyai, Ser. Chem.*, **2007**, *LII(1),* 55.
17. M.M. Venter, V.N. Bercean, M. Ilici, S. Cinta Pinzaru, *Rev. Roum. Chim*., **2007**, *52(1-2)*, 75.
18. B.R. Bhogala, S. Basavoju, A. Nangia, *CrystEngComm*, **2005**, *7*, 551.
19. L. Huang, F. Tang, B. Hu, J. Shen, T. Yu, Q. Meng, *J. Phys. Chem. B,* **2001**, *105,* 7984.
20. F. Hipler, R.A. Fischer, J. Müller, *J. Chem. Soc*., *Perkin Trans.,* **2002**, *2*, 1620.
21. F. Hipler, M. Winter, R.A. Fischer, *J. Molec. Struct*., **2003**, *658*, 179.
22. H.G.M. Edwards, A.F. Johnson, E.E. Lawson, *J. Molec. Struct*., **1995**, *351*, 51.
23. M.M. Venter, S. Cinta Pinzaru, I. Haiduc, V. Bercean, *Studia Univ. Babes-Bolyai, Physica*, **2004**, *XLIX(3),* 285.
24. G. Socrates, "Infrared and Raman Characteristic Group Frequencies. Tables and Charts", 3rd ed., Wiley, Chichester, 2001, chapter 9,10 and 12.
25. J.W. Bats, *Acta Cristallogr.*, **1976**, *B32*, 2866.
26. Z. Gu, R. Zambrano, A. McDermott, *J. Am. Chem. Soc*., **1994**, *116*, 6368.
27. A. Moghimi, S.M. Moosavi, D. Kordestani, B. Maddah, M. Shamsipur, H. Aghabozorg, F. Ramezanipour, G. Kickelbick, *J. Molec. Struct*. **2007**, *828*, 38.
28. B.B. Ivanova, M.G. Arnaudov, H. Mayer-Figge, *Polyhedron*, **2005**, *24*, 1624.
29. B.B. Koleva, T. Kolev, T. Tsanev, S. Kotov, H. Mayer-Figge, R.W. Seidel, W.S. Sheldrick, *J. Molec. Struct*., **2008**, *881*, 146.
30. T. Dorn, C. Janiak, K. Abu-Shandi, *CrystEngComm*, **2005**, *7*, 633.

STUDIA UNIVERSITATIS BABEŞ-BOLYAI, CHEMIA, LIV, 4, 2009

MECHANISTIC STUDY OF SE AND GE SEMICONDUCTORS ELECTRODEPOSITION

BOGDAN TUTUNARU[a], ADRIANA SAMIDE[a], MIRCEA PREDA[a]

ABSTRACT. The electrodeposition and mechanism of nucleation of Se and Se-Ge films was studied in this work. The employed experimental techniques were potentiostatic polarization and chronoamperometry. The initial deposition of Se film by potentiostatic polarization shows that the crystallization potential of -0,40 V and corresponding densities linearly depends on the H_2SeO_3 concentration and potential scan rate. The simultaneous presence of both species in the bath composition produced a new peak at -0,50 V. The chronoamperometric study indicate a 3D complex mechanism for Se and Se-Ge electrodeposition. The morphological changes in surface of working electrode was analysed with an Euromex microscope.

Keywords: Semiconductors, Se and Se_2Ge electrodeposition, nucleation mechanism

INTRODUCTION

Selenium is essential for life when consumption of foods contain 0,1 mg kg^{-1} of this element, and is toxic when dietary levels are above 1 mg kg^{-1} [1]. In the human body, selenium is bond by covalent carbon-selenium bonds and some inorganic selenium salts have powerful cancer chemopreventive effects.

Semiconductors were found that they can replace or compete with monocrystalline materials in photoelectrochemical cells [2]. The photo-induced changes observed in semiconductor compounds are attributed to the amorphous state [3]. Selenium has played an important role in the production of metal selenides (ZnSe, MgSe, FeSe, PbSe, SnSe, CdSe etc.) [4-8]. This kind of compounds presents interesting applications such as optical filters, solar cells, laser materials [9,10].

One of the most adequate method to obtain a thin film of semiconductor or metal-selenide compound is electrodeposition [11]. Selenium electrodeposition is a side reaction in the cathodic synthesis of metal selenides [12].

To our knowledge, electrodeposition of Se-Ge has not been reported in the literature. Hence, we have attempted in the present study to deposit a Se-Ge thin film by electrodeposition.

[a] *Faculty of Chemistry, University of Craiova, Calea Bucureşti, no. 107i, Craiova, Romania*

RESULTS AND DISCUSSION

In the electrochemical deposition of Se the electrodeposition potential and the corresponding densities were found to depend on sweep rate and concentration of the electrolyte. Figure 1 shows the cathodic curves obtained in solutions containing H_2SeO_3 at three different concentrations.

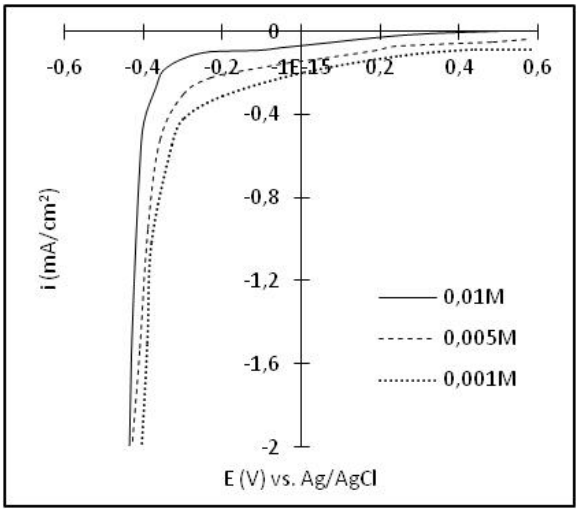

Figure 1. Cathodic curves obtained during selenium deposition onto Pt electrode from 0,01; 0,005 and 0,001 M H_2SeO_3 aqueous solutions, pH=2.

The potential scan was initiated in the negative direction from open circuit potential vs. Ag/AgCl. The reduction wave starts at -0.40 V vs. Ag/AgCl when selenous acid is present in the electrolyte with 0.01 M concentration.

In the case of selenium the crystallization potential and the corresponding current densities linearly depends on the concentration of H_2SeO_3 in solution.

Further analysis at various scan rates (fig. 2) showed clearly a linear variation of the crystallization potential with different scan rate (insert of figure 2).

The current densities are proportional to the scan rate and the crystallization potential is moving to the more positive direction, these features are characteristic for an irreversible system [13,14].

Reduction of the selenium species without the germanium precursor in the electrolyte, starts at -0,4 V vs. Ag/AgCl according to reaction:

$$SeO_3^{2-} + 3H_2O + 4e \rightarrow Se + 6HO^- \quad (E^0 = -0{,}366\ V) \qquad (1)$$

Metallic selenium electrodeposition is also indicated by the purplish colour of the deposit.

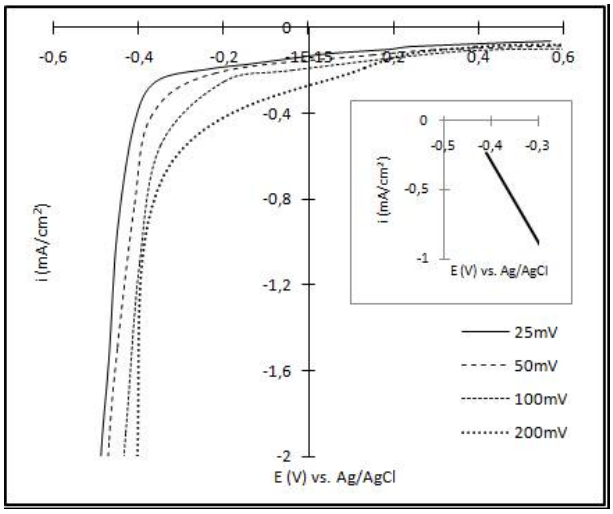

Figure 2. Cathodic polarization curves for Pt electrode at different scan rates in plating bath, H_2SeO_3 0,005 M, pH=2.

We performed a chronoamperometric study in order to examine the nucleation of selenium and selenium-germanium electrodeposition. Figure 3 shows a set of potentiostatic current transients for 0, 10, 30 and 50 mV overcharges obtained during the electrochemical deposition of selenium onto platinum electrode from a 0,005 M H_2SeO_3 solution.

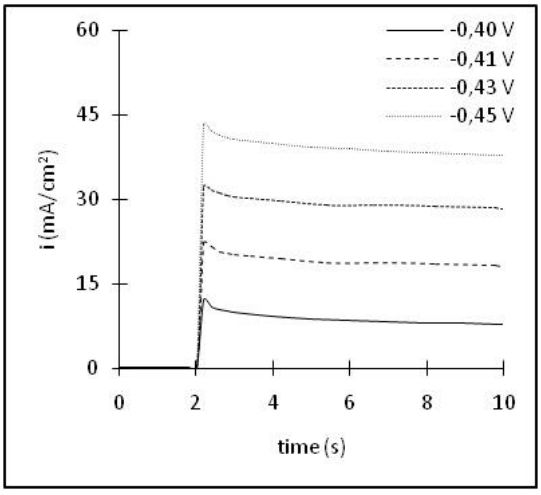

Figure 3. Potentiostatic current transients for the electrodeposition of selenium onto Pt electrode from 0,005 M H_2SeO_3, pH=2.

Experimental current transients are presented in a nondimensional form by ploting i/i_{max} vs. t/t_{max} (2D) and $(i/i_{max})^2$ vs. t/t_{max} (3D) and compared with theoretical values for instantaneous and progressive nucleation, respectively (fig. 4).

As can observe from figure 4, one can affirm that the selenium electrodeposition on the platinum electrode, in the given experimental conditions, take place after a combinatorial kinetic of 3D nucleation.

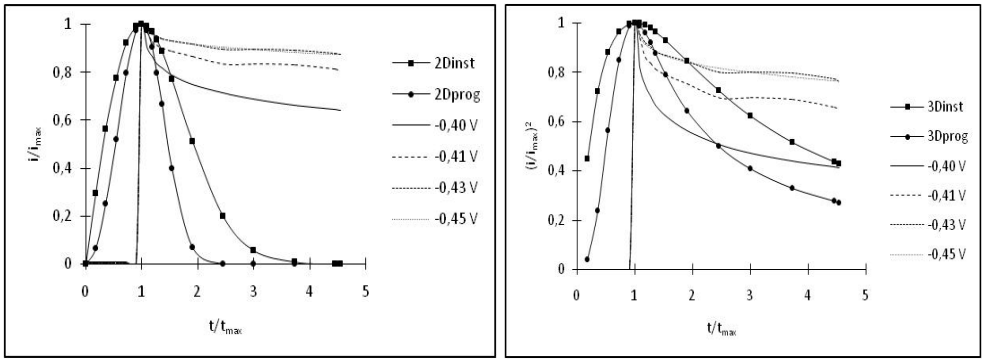

Figure 4. Comparison of the theoretical nondimensional plots for 2D (fig. 4a) and 3D (fig. 4b) for instantaneous and progressive Se nucleation to the experimental current transients in fig. 3.

The simultaneous presence of both species in the bath composition produced noticeable changes in the cathodic response. It can be seen in fig. 5 that a new peak appears during the scan in the negative direction at -0,50 V vs. Ag/AgCl.

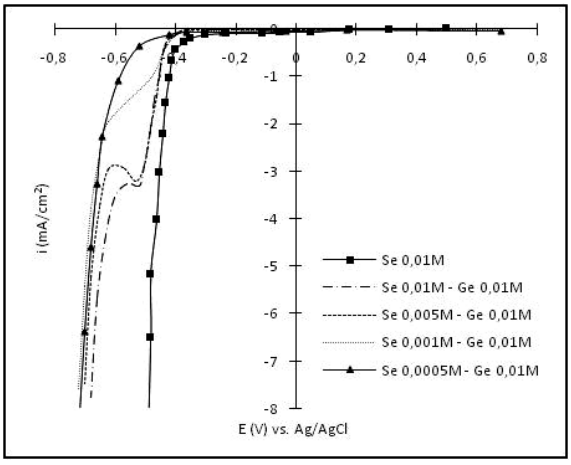

Figure 5. Cathodic curves for Pt electrode obtained during Se and Se-Ge electrodeposition.

We note that the cathodic current densities of this peak are decreasing with the Se concentration decrease. This peak may be ascribed to the formation of Se-Ge on the substrate. The $GeCl_4$ is hydrolyzed with distilled water to produce GeO_2; in this conditions we have to consider the possibility that this peak can be atributed to the GeO_2 reduction to GeO (E^0 = -0.370 V). At more negative potentials further reductions of the deposited selenium to H_2Se and/or germanium species to H_4Ge are possible. Selenium being nobler, it is expected to be deposited first. At selenium concentrations of $5 \cdot 10^{-4}$ M or smaller this peak is not more evident.

The nucleation mechanism of selenium-germanium electrodeposition was study by the chronoamperommetry methode. The corresponding potentiostatic current transients for 0, 10, 30 and 50 mV overpotentials obtained during the electrochemical deposition of selenium-germanium onto platinum electrode from a 0,005 M H_2SeO_3, 0,01 M $GeCl_4$ solution are presented in figure 6.

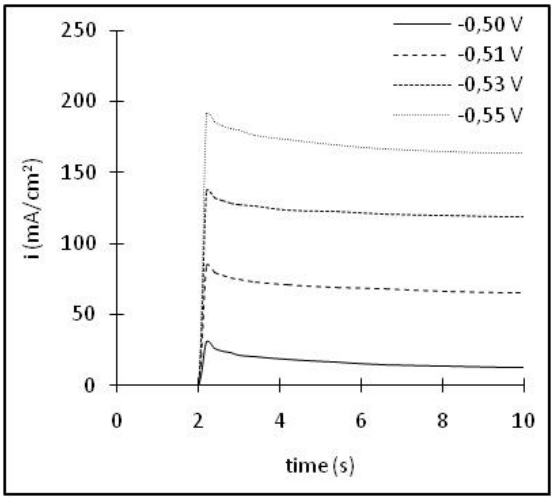

Figure 6. Potentiostatic current transients for the electrodeposition of selenium-germanium onto Pt electrode from 0,005 M H_2SeO_3, 0,01 M $GeCl_4$, pH=2.

From fig. 6 it may be observed that at shorter times there is a maximum current transient that, in this case, can be associated with a process where diffusion-controlled nucleation of selenium and germanium occurs simultaneously at the platinum electrode surface. After this maximum current, in each case the i-t plot passes through a falling current and then approaches to the limiting diffusion current to a planar electrode.

Experimental current transients compared with theoretical one for selenium-germanium instantaneous and progressive nucleation are presented in fig. 7.

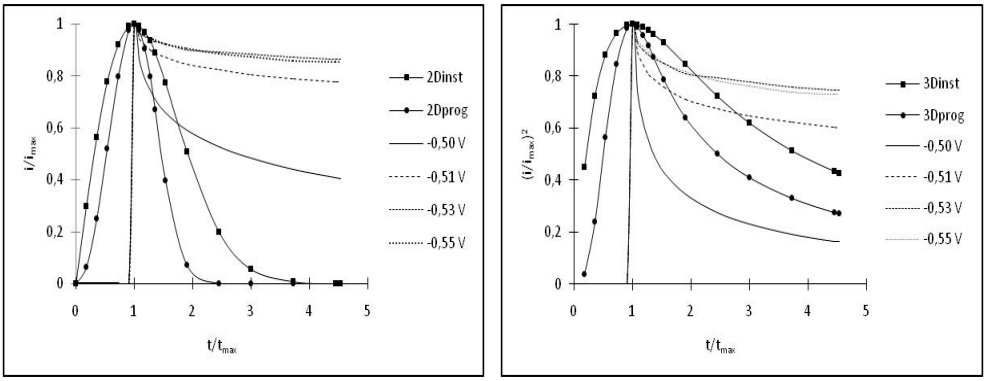

Figure 7. Comparison of the theoretical nondimensional plots for 2D (fig. 7a) and 3D (fig. 7b) for instantaneous and progressive Se-Ge nucleation to the experimental current transients in fig. 6.

Similar to selenium electrodeposition, when the both species are present in the electrolyte composition, at nucleation potential the mechanism fallow the progressive one and at higher overpotentials is changing to instantaneous.

The morphological changes in surface electrode were observed with an Euromex microscope. Figure 8a presents the surface morphology of Pt electrode before electrodeposition; figure 8b presents the surface morphology of deposited selenium and figure 8c presents the selenium-germanium deposit morphology.

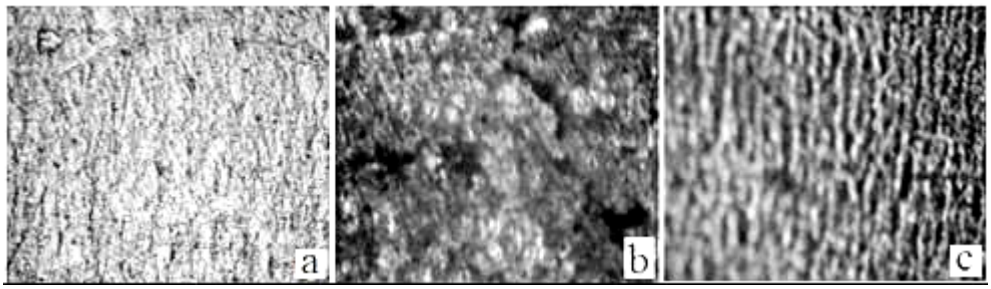

Figure 8. Surface morphology of: Pt electrode before electrodeposition (a), Se (b) and Se-Ge (c) deposited layer.

CONCLUSIONS

The Se and Se-Ge films were deposited onto Pt surface by potentiostatic polarization.

In the electrochemical deposition of Se, the electrodeposition potential and corresponding densities were found to depend on sweep rate and concentration of the electrolyte.

Selenium and selenium-germanium electrodeposition on the platinum electrode, in the given experimental conditions, take place after a combinatorial kinetic of instantaneous and progressive 3D nucleation.

EXPERIMENTAL SECTION

All electrochemical measurements were performed with the Keithley 2420 3A SourceMeter potentiostat/galvanostat. Experimental data recording was carried out in a standard electrochemical cell with three electrodes. The Ag/AgCl, KCl (saturated) was used as the reference electrode to which all potentials are quoted. The working and auxiliary electrodes were made from platinum foils with 1,0 cm^2 geometric area. The Se and Se-Ge films were deposited onto Pt surface by potentiostatic polarization.

All the chemicals used in this work were of analytical grade (99,5%) excepting H_2SeO_3 which was of standard purity (99,99%).

The electrolyte bath for Se deposition comprised of H_2SeO_3 solution, pH = 2 ± 0,05 (by adding HNO_3) and the working temperature was of 20 ± 2 ˚C. The pH of the electrolytic bath was measured using digital pH-meter (HANNA instruments). In order to analyse the influence of H_2SeO_3 concentration, three values of electrolyte concentration were used 0,01; 0,005 and 0,001M.

In the electrolyte bath for Se-Ge electrodeposition, the concentration of H_2SeO_3 was varied from 0,01M to 0,005; 0,001 and 0,0005M while the concentration of $GeCl_4$ was kept constant at 0,01M.

The chronoamperometry methode was used to analyse the nucleation mechanism of Se and Se-Ge electrodeposition.

After the deposition, the films were washed, dried and their morphology were analysed by an Euromex microscope.

REFERENCES

1. O. Wada, N. Kurihara, N. Yamazaki, *Jap. J. Nutr. Assesss.*,**1993**, *10*, 199.
2. V. Plaskov, Solar Energy Conversion, Springer, Berlin, **1990**.
3. P. Nagels, E. Sleeckx, R. Callaerts, L. Tichy, *Solid Stade Commun.*, **1995**, *94*, 49.
4. R. Kowalik, P. Zabinski, K. Fitzner, *Electrochim. Acta*, **2008**, *53*, 6148.
5. T. Mahaligam, A. Kathalingam, C. Sanjeeviraja, R. Chandramohan, J.P. Chu, Y.D. Kim, S. Velumani, *Materials Characterization*, **2007**, *58*, 735.
6. S. Thanikaikarasan, T. Mahalingam, S. Sundaram, A. Kathalingam, Y.D. Kim, T. Kim, *Vacuum*, **2009**, *83*, 1066.
7. M.F. Cabral, H.B. Suffredini, V.A. Perosa, S.T. Tanimoto, S.A.S. Machado, *Appl. Surf. Sci.*, **2008**, *254*, 5612.

8. Z. Zainal, A.J. Ali, A. Kasim, M.Z. Hussein, *Solar Energy & Solar Cells*, **2003**, *79*, 125.
9. W.Z. Wang, Y. Geng, P. Yan, F.Y. Liu, Y. Xie, Y.T. Qian, *J. Am. Chem. Soc.*, **1999**, *121*, 4062.
10. W.B. Zhao, J.J. Zhu, H.Y. Chen, *J. Cryst. Growth*, **2003**, *252*, 587.
11. K. Rajeshwar, *Adv. Mater.*, **1992**, *4*, 1.
12. M.S. Kazacos, B. Miller, *J. Electrochem. Soc.*, **1980**, *127*, 869.
13. Southampton Electrochemitry Group, Instrumental Methods in Electrochemistry, Ellis Horwood, Chichester, UK, **1985**.
14. R.H. Wopschall, I. Shain, *Anal. Chem.*, **1976**, *39*, 1514.

STUDIA UNIVERSITATIS BABEŞ-BOLYAI, CHEMIA, LIV, 4, 2009

ARTIFICIAL NEURAL NETWORKS USED FOR THE SIMULATION OF THE BATCH FERMENTATION BIOREACTOR

VASILE MIRCEA CRISTEA[a], IMRE LUCACI ARPAD[a], ŞIPOŞ ANCA[b], BRĂTFĂLEAN DORINA[a], PAUL ŞERBAN AGACHI[a]

ABSTRACT. The paper presents the modelling results of the batch alcoholic fermentation bioreactor using both the first principle and the Artificial Neural Networks (ANN) approach. For the nonlinear fermentation process the first principle model validated with experimental data considers for the biomass the Monod and for substrate the Bovée and Strehaiano models, including the temperature influence. It has been used for the ANN model development. A design and training methodology is proposed for statistical modelling based on artificial neural networks. Comparison between the two models is performed revealing the incentives of the ANN modelling method for reducing the computational time and sparing the computer resources.

Keywords: alcoholic fermentation, Artificial Neural Networks, modelling

INTRODUCTION

Winemaking technology is a complex process implying a succession of operations affected by the large variety of must and microbiota. The grape juice transformation into wine is substantially influenced by the wine makers' tradition and processing techniques are usually emerged from their experience [1]. Investigation of the mechanisms and phenomena lying behind the alcoholic fermentation is difficult as the stoichiometry and kinetics of the biochemical processes are only possible by lumping the numerous involved components and due to the need for simplifying the biomass characterization [2]. The oenologists claim that organoleptic properties of the wine are also dependent on the alcoholic fermentation in a very complex relationship [3, 4].

The alcoholic fermentation of wine is a biochemical process of transforming the sugar into alcohol and CO_2. Metabolites are the result of enzymatic reactions for the different metabolic paths [5]. Kinetics of the enzymatic reactions, as well as of the chemical reactions, is influenced by a set of factors. The most important of them are: composition of the culture medium, concentration of the limiting substrate, temperature, pH, concentration of the dissolved oxygen and stirring intensity. Setting optimal conditions for the

[a] *Babeş-Bolyai University of Cluj-Napoca, Faculty of Chemistry and Chemical Engineering, 11 Arany Ianos Street, 400028, Cluj-Napoca, Romania, mcristea@chem.ubbcluj.ro*

[b] *Lucian Blaga University of Sibiu, Faculty of Food Industry, 7-9 Dr. Ion Rațiu Street, 550024 Sibiu, Romania*

development of the fermentative process is directly related to the knowledge of the way of influencing the enzymatic reactions. Interaction between variables is strong as the change of a single parameter may affect the all the others [6].

Due to all these aspects the need for building reliable models is obvious and is highly appreciated as they may serve for better understanding the intrinsic processes and consequently, for optimizing the wine production according to the desired criteria [7, 8]. The first principle modelling allows logical description and interpretation of the involved phenomena, on the expense of a substantial modelling effort and with possible errors. Development of the analytical models is complex and time consuming as they imply a good knowledge of the phenomena and processes taking place inside the modelled system. Statistical mathematical models (such as the Artificial Neural Networks models) are based on observation data and measurements originating from the process. The statistical models require less effort and may reduce the modelling errors if an appropriate set of data is available [9-11].

In this paper a new statistical model based on Artificial Neural Networks (ANN) is proposed as an alternative to the first principle modelling of the alcoholic fermentation process performed in a batch bioreactor. Comparison between the first principle and ANN modelling results is performed, showing the benefits of the proposed ANN approach.

RESULTS AND DISCUSSION

A previously developed first principle model was available and used to generate the sets of input-target data further employed for training the ANN. The detailed analytical model used in the present work is described in [12]. This model has been validated with experimental data. Each of the biomass latent, exponential growing and decline phase has been described. Consequently, specific kinetic models of the biomass, substrate and alcohol have been considered. For substrate consumption the Bovée and Strehaiano model has been used [13]. Heat balances for the bioreactor vessel and jacket have been also accounted for.

This ANN based modelling approach has been considered as the first step for investigating the capability of designing and training an ANN model of the fermentation bioreactor. The developed ANN model design and training procedure may be considered as a prerequisite for the future step consisting in building the ANN dynamic simulator based on pure experimental data.

As the aim of the study bas been the development of a dynamic simulator of the alcoholic fermentation process, the following main process variables have been selected to demonstrate the time evolution of the process: substrate (glucose) concentration, biomass (Saccharomyces cerevisiae) concentration, alcohol concentration, reactor temperature and jacketed reactor cooling agent temperature. The ANNs based models have been designed and trained for revealing the dynamics of the five previously mentioned process variables, as a result of starting from different initial conditions of the batch fermentation

process. These initial conditions are specified by the subsequent variables: reactor inventory initial temperature, substrate initial concentration and biomass initial concentration. A sampling time of 3 hours has been considered for all process variables. One distinct ANN has been developed for each of the five process variables. Each of these ANNs has 3 inputs (the initial conditions) and 68 outputs. The outputs are the values of the respective process variable at the 68 moments of time multiples of the sampling time (starting with moment 0 h and finishing with moment 201 h). Two hidden layers with 3 and 4 neurons were used.

The set of training and testing data consists in 546 *input-desired output* pairs of data. The main part (75%) of the available set of data has been used for the training and validation step of the ANN model building. A quarter (25%) of the set of data has been used for testing the already trained ANN. Training and validation subset of data has been further divided: 75% of data was used for training and the rest for validation [14].

Following the training and validation step, the first testing step has been performed in order to assess the quality of the trained ANN. This testing step has been carried out on the set of input-desired output pairs of testing data not involved in the first training and validation step. Results obtained by the trained ANN on the set of testing data show a good quality of the training phase, as the correlation coefficients (R-value) for the set of ANN simulated and desired output (targets) sets of data are close to unity. They are not presented in the paper due to space saving reasons and to the next more comprehensive test.

The second testing step and more ample assessment of the prediction ability of the trained ANN have been performed for a new set of input data not yet used during the previous training-validation-testing steps and comparison with the analytical simulation results has been accomplished. These comparative first principle and ANN model simulations used random chosen initial conditions consisting in the following particular values: reactor inventory initial temperature $T_0=299\ K$, substrate initial concentration $S_0=190\ g/l$ and biomass initial concentration $X_0=0.75\ g/l$.

The comparative results between the analytical simulation and ANN simulation results, obtained for the five investigated process variables, are presented in Figures 1 to 5.

The simulation results reveal a good training procedure of the ANN, demonstrated by very close values of the bioreactor main process variables obtained with the first principle and the ANN models. For the substrate concentration, alcohol concentration and reactor inventory temperature the simulated evolutions of the variables are almost identical. For the biomass concentration and cooling agent temperature variables almost identical values have been also obtained for the periods of time when the change of these variables is reduced. For the time interval when the two previously mentioned variables have large changes in time, such as the time interval between 30h and 45 h, some differences may be noticed. But these differences, featuring in fact reduced relative errors, are mainly caused by the use of a relative large

sampling time compared to the time interval when the involved variables show large changes in time. It is expected that by reducing the sampling time these not essential differences to become smaller. According to the obtained results it may be appreciated the good fit between the ANN model and first principle model behaviour.

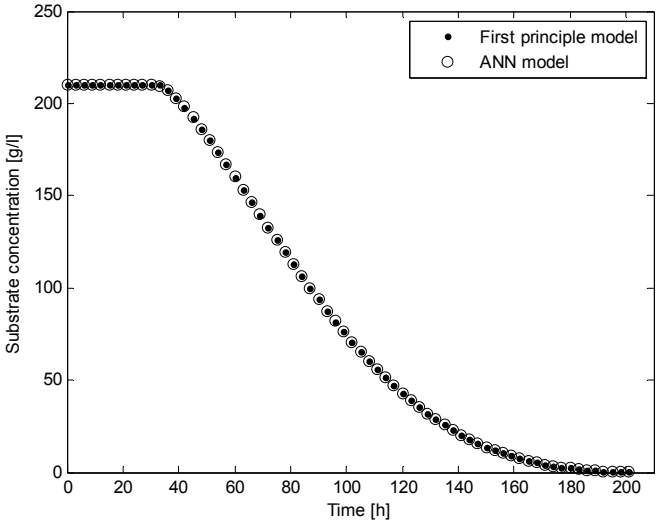

Figure 1. Comparative simulation results obtained by the first principle model and the ANN model, for the substrate concentration variable

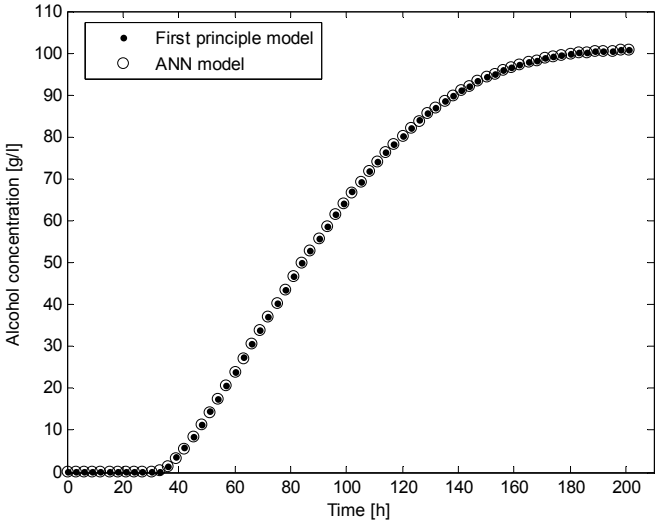

Figure 2. Comparative simulation results obtained by the first principle model and the ANN model, for the alcohol concentration variable

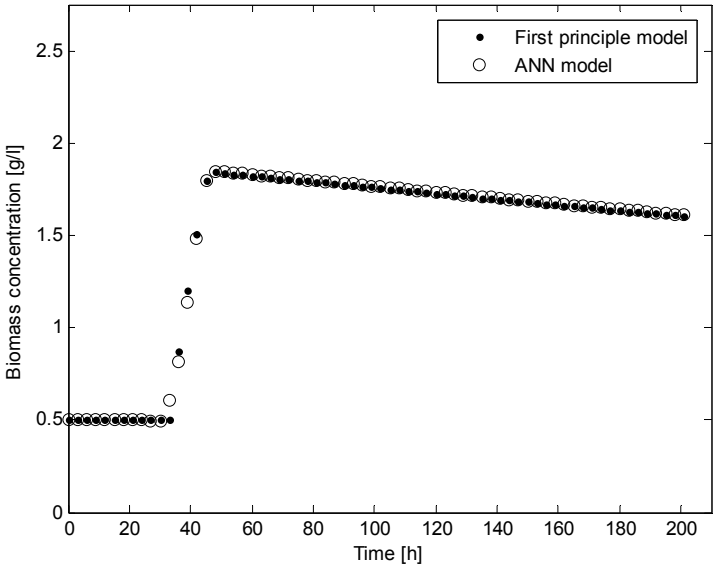

Figure 3. Comparative simulation results obtained by the first principle model and the ANN model, for the biomass concentration variable

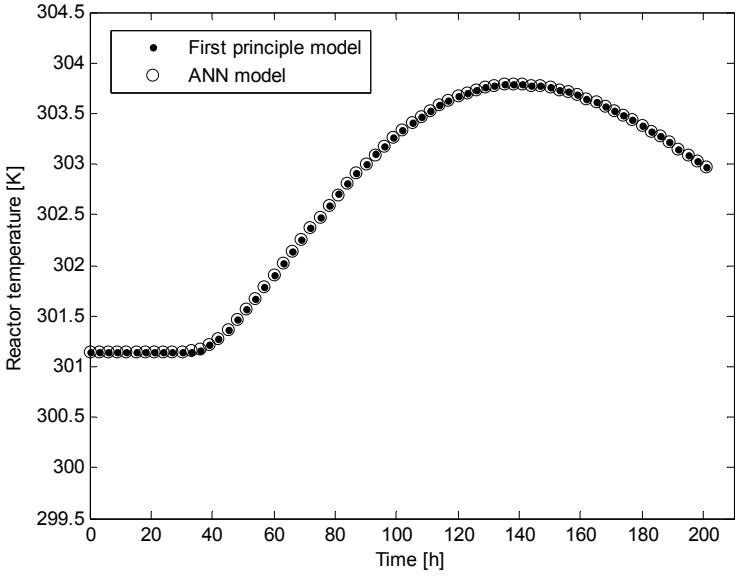

Figure 4. Comparative simulation results obtained by the first principle model and the ANN model, for the reactor temperature variable

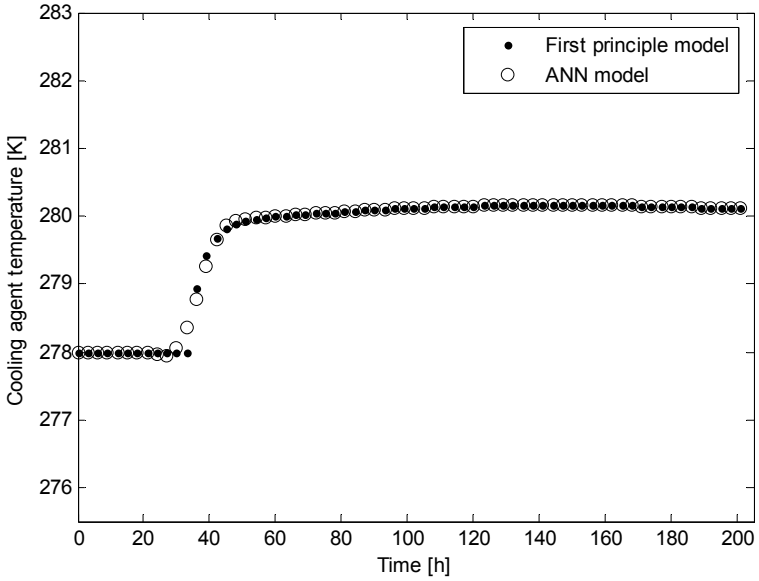

Figure 5. Comparative simulation results obtained by the first principle model and the ANN model, for the reactor cooling agent temperature variable

CONCLUSIONS

The paper presents the simulation results of successfully using Artificial Neural Networks for modelling the dynamic behaviour of the alcoholic fermentation bioreactor main process variables. The way the ANN has been designed and subsequently trained proved to be efficient for obtaining a useful dynamic simulator. The reduced relative errors proved by the good fit between the desired process outputs and the ANN simulated outputs are proofs of the ANN performance. Incentives of the ANN based model consist in the development of an efficient methodology of building the ANN model of the complex alcoholic fermentation bioreactor associated to the reduced modelling effort. The ANN model may exclusively rely on experimental data and implicitly does not imply comprehensive knowledge of the detailed physical, chemical and biological first principle description.

Another main advantage of the ANN based modelling consists in the important reduction of the simulation time (exceeding one order of magnitude), hence resulting in an efficient management of the computing resources. This incentive may become much appreciated for its potential use in bioreactor real time control applications based on mathematical models where implementation feasibility is very challenging.

EXPERIMENTAL SECTION

The ANN architecture for the batch alcoholic fermentation process consists in a feedforward ANN having four layers (one input, two hidden and one output layers), for which the weights and biases have been trained according to the backpropagation training algorithm [15]. The number of neurons in the hidden layers (4 and 3) has been set on the basis of a heuristic procedure, as a consequence of the errors analysis performed during the repeated training steps. The neurons transfer function in the hidden layers has been selected to be *tansig* (hyperbolic tangent sigmoid) and for the output layer *purelin* (linear). The quasi-Newton type Levenberg-Marquardt algorithm has been used for training the ANN. Overfitting has been avoided by early stopping, improving the generalization capability of the ANN.

During the repeated training sequences, random initial values have been used for the ANN weights and biases in order to prevent convergence to local minima. The input and desired output sets of data have been scaled (based on minimum and maximum values) and principal component analysis has been used for improving the computation precision and training performance.

ACKNOWLEDGMENTS

Funding from the grant PNCDI II 100CP/I, CAPACITATI 142 and 71-006 is gratefully acknowledged by the authors.

REFERENCES

1. J. Blouin, E. Peynaud, Connaissance et travail du vin, Dunod, Paris, **2001**, 87.
2. M. A. J. Torija, N. Rozès, M. Poblet, J.M. Guillamón, A. Mas, *International Journal of Food and Microbiology*, **2003**, *80*, 47.
3. C. Flanzy, Œnologie - Fondements scientifiques et techniques, **1999**, Techniques & Documentation, Paris.
4. P. Ribéreau-Gayon, D. Dubourdieu, B. Donèche, A. Lonvaud, Handbook enology. The microbiology of wine and vinifications, Vol. I, **2000**, Wiley, West Sussex, 49.
5. H. Fariha, A. A. Shah, A. Hameed, *Enzyme and Microbial Technology*, **2006**, *39*, 235.
6. A. Houde, A. Kademi, D. Leblanc, *Applied Biochemistry and Biotechnology*, **2004**, *118*, 155.
7. W. Wiechert, *Journal of Biotechnology*, **2002**, *94*, 37.
8. B. Srinivasan, S. Palanki, D. Bonvin, *Computers and Chemical Engineering*, **2003**, *27*, 1.

9. M.T Hagan, M.H. Menhaj, T, *IEEE Transaction on Neural Networks*, **1994**, *5*, 989.
10. V. M. Cristea, S. P. Agachi, *Studia Universitatis Babes-Bolyai*, **2005**, *L, 2*, 65.
11. S. Haykin, Neural Networks: A Comprehensive Foundation, **1994**, MacMillan College Publshing Co., New-York, Chapter 6.
12. A. Sipos, X.M. Meyer, P. Strehaiano, *Acta Alimentaria*, **2007**, *36*, 429.
13. J. P. Boveé, P. Strehaiano, G. Goma, Y. Sevely, *Biotechnology and Bioengineering*, **1984**, *26*, 328.
14. V. M. Cristea, R. Roman, P. S. Agachi, **2009**, *Studia Universitatis Seria Chemia*, *1*, 125.
15. Neural Networks Toolbox 6.0.1.User Guide, **2008**, Matlab 7.7, MathWorks Inc.

STUDIA UNIVERSITATIS BABEŞ-BOLYAI, CHEMIA, LIV, 4, 2009

SYNTHESIS, SPECTROSCOPIC AND ELECTROCHEMICAL CHARACTERIZATION OF A NEW CHROMIUM (III) SUBSTITUTED DAWSON POLYOXOMETALATE

ADRIAN-RAUL TOMŞA[a], DANIELA CIOLOBOC[a], ANA MARIA TODEA[a,b], RADU SILAGHI-DUMITRESCU[b], GRIGORE DAMIAN[c] AND MARIANA RUSU[b]

ABSTRACT. A new chromium (III) substituted Dawson 2-molybdo-15-tungsto-2-phosphate $K_7[Cr(H_2O)P_2Mo_2W_{15}O_{61}]\cdot 17H_2O$ was synthesized by reaction of Cr(III) chloride with monolacunary Dawson molybdo-tungsto-diphosphates $[P_2Mo_2W_{15}O_{61}]^{10-}$ in aqueous solution. The complex has been characterized using spectroscopic and electrochemical techniques. The FT-IR spectroscopic data indicate that the polyanion overall symmetry is restored after the coordination of Cr(III). Coordination of chromium (III) is further supported by the ^{31}P-NMR, EPR and UV-Vis electronic absorption spectroscopy results. Cyclic voltammograms of the chromium (III) complex exhibit three pairs of oxidation/reduction waves with negative $\varepsilon^{0`}$values. These waves were assigned to two molybdenum-centered single electron redox processes and one tungsten-centered two electrons process. A positive shift of these waves when going from Dawson monolacunary complex to its Cr(III) complex. A modified Dawson structure was inferred from the results for the new chromium (III) complex, in which the chromium and molybdenum atoms are located to the same cap of the anion.

Keywords: polyoxometalate, Dawson structure, chromium, FT-IR spectroscopy, UV-Vis spectroscopy, NMR-spectroscopy, EPR-spectroscopy

INTRODUCTION

Polyoxometalates (POMs) comprise a rich and diverse family of metal-oxygen clusters of the early transition metals in high oxidation states, most commonly V(V), Mo(VI) and W(VI), with unique versatility in terms of shape, polarity, redox potentials, surface charge distribution, acidity, and solubility [1-4].

These compounds have promising applications in various domains, including catalysis [5,6], electrocatalysis [7], medicine [8,9], molecular conduction [10-12], magnetism [13], photochemistry [14,15], luminescence [16], analytical chemistry [17] and materials science [18].

[a] *"Babeş-Bolyai" University, "Raluca Ripan" Institute for Research in Chemistry, 30 Fântânele St., Cluj-Napoca, Romania, rtomsa@yahoo.com*

[b] *"Babeş-Bolyai" University, Faculty of Chemistry and Chemical Engineering, 11 Arany Janos St., RO-400028, Cluj-Napoca, Romania, mrusu@chem.ubbcluj.ro*

[c] *"Babeş-Bolyai" University, Faculty of Physics, 1 Mihail Kogălniceanu St., RO-400084, Cluj-Napoca, Romania*

The synthesis of polyoxometalates is mostly rather simple and straightforward, once the proper reactions conditions have been identified. However, the mechanism of formation of polyoxometalates is not yet well understood and is commonly described as self-assembly. Therefore, the design of novel polyoxometalates remains a challenge for synthetic chemists.

The most rational synthesis of new polyoxometalates uses the lacunary precursors prepared from the corresponding complete polyoxometalate species, by loss of one or more **MO_6** octahedra. Reaction of a stable lacunary polyoxometalate with transition metal ions mostly leads to a product in which the polyoxometalate framework remains unchanged.

For instance, under hydrolytic conditions, in the presence of Na_2CO_3, the α-$[P_2W_{18}O_{62}]^{6-}$ Dawson polyoxometalate loses three capping WO_6 octahedra, yielding a Dawson trilacunary polyoxotungstate derivative [α-$P_2W_{15}O_{56}]^{12-}$ [19]. Furthermore, the reaction of the trilacunary derivative [α-$P_2W_{15}O_{56}]^{12-}$ with molybdate, carried out in mild conditions, allows the selective addition of two molybdenum atoms in an apical site of [α-$P_2W_{15}O_{56}]^{12-}$ [20]. Complexes of the resulting monolacunary Dawson polyanion, [α_2-$P_2Mo_2W_{15}O_{61}]^{10-}$, with a first row transition metal cation are of particular interest for their electrocatalytic properties [21-23].

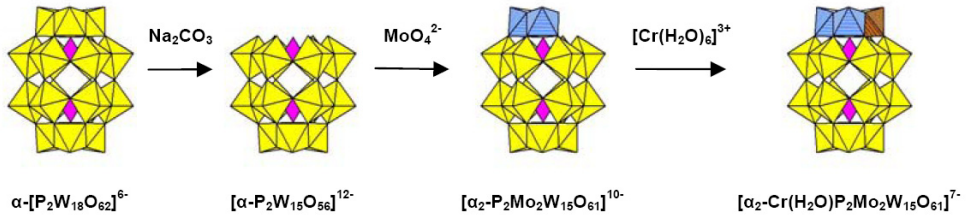

Figure 1. The preparation scheme of **α_2-$CrP_2Mo_2W_{15}$**.

Herein we report the synthesis, spectroscopic and electrochemical characterization of a new chromium (III) complex of Dawson monolacunary polyoxometalate [α_2-$P_2Mo_2W_{15}O_{61}]^{10-}$, as aqueous soluble potassium salt. The $K_4Li_3[\alpha_2$-$Cr(H_2O)P_2Mo_2W_{15}O_{61}]\cdot 17H_2O$ complex (**α_2-$CrP_2Mo_2W_{15}$**) has been characterized by elemental and TG-DSC analysis, UV-Vis, FT-IR and ^{31}P-NMR spectroscopy, EPR, as well as by electrochemical measurements.

RESULTS AND DISCUSSION

The new chromium (III) polyoxometalate complex was synthesized in aqueous solution by reacting the potassium salt of the monolacunary Dawson polyoxometalate $K_{10}[\alpha_2$-$P_2Mo_2W_{15}O_{61}]\cdot 18H_2O$ (**α_2-$P_2Mo_2W_{15}$**) with chromium (III) chloride. In order to avoid the migration of molybdenum atoms, which may

give numerous isomers, the synthesis must be performed in acidic solution heated to 40°C. Isolation of the products as potassium salts resulted in relatively good yields of the polyoxometalate complex.

The thermal stability of **α_2-$CrP_2Mo_2W_{15}$** was investigated by TG-DSC. The differential scanning calorimetry curve for **α_2-$CrP_2Mo_2W_{15}$** shows four endothermic and one exothermic processes in the region from 20°C to 650°C (Figure 2).

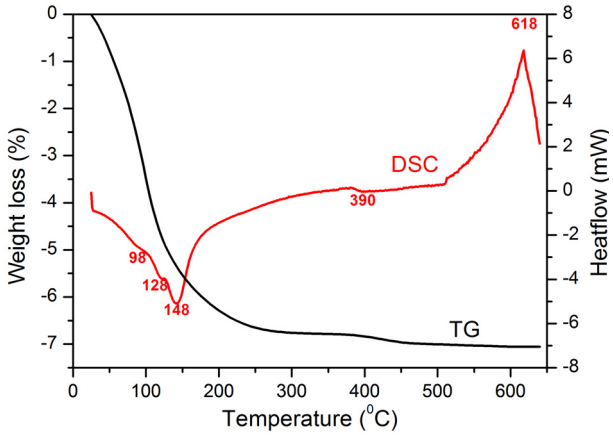

Figure 2. TG and DSC curves of **α_2-$CrP_2Mo_2W_{15}$**.

The three endothermic processes from ~25°C to 200°C are attributed to the desorption of 17 water molecules from the lattice structure. The endothermic process from ~380°C to 450°C is assigned to the loss of the coordination water molecule attached to Cr(III). The exothermic process observed from 500°C to 650°C coresponds to the collapse of the polyoxometalate framework. This assignement is also supported by FT-IR spectra, which show significant changes in the P-O and M-O (M= Mo, W) stretching modes after heating to 650°C (Figure 3).

The FT-IR spectrum of chromium (III) complex **α_2-$CrP_2Mo_2W_{15}$** in the P-O and M-O stretching region is shown in Figure 3, along with those of the monolacunary ligand **α_2-$P_2Mo_2W_{15}$** and complete Dawson polyoxometalate, $K_6[P_2W_{18}O_{62}]\cdot 14H_2O$ (**α-P_2W_{18}**).

As expected, in the FT-IR spectrum of the ligand **α_2-$P_2Mo_2W_{15}$**, the P-O vibration band, recorded between 1200 and 1000 cm^{-1}, is split, due to the decrease of the local symmetry. When Cr (III) fills the vacancy, the symmetry is restored. As a consequence, the FT-IR spectra of **α_2-$CrP_2Mo_2W_{15}$** and **α-P_2W_{18}** are similar. However, the spectrum of **α_2-$CrP_2Mo_2W_{15}$** exhibits an additional vibration band, recorded at 686 cm^{-1}, which was assigned to the stretching vibration $\nu_{(Cr\text{-}O)}$ [24,25].

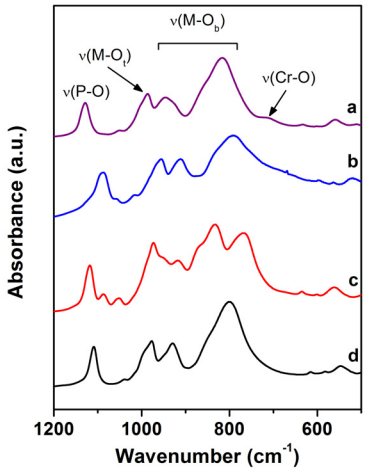

Figure 3. FT-IR spectra of **α_2-$CrP_2Mo_2W_{15}$** (a), **α_2-$CrP_2Mo_2W_{15}$** heated to 650ºC (b) **α_2-$P_2Mo_2W_{15}$** (c) and **α-P_2W_{18}** (d).

The vibrations in the 1000-700 cm^{-1} range were assigned to the asymmetric stretching of the bridges (M-O$_b$-M) and of the terminal bonds (M-O$_t$) [26]. Mention should be made of the fact that the stretching vibrations are shifted towards higher wavelengths, after the coordination of Cr(III), thus suggesting an increase of the polyoxoanion cohesion [26].

In the UV spectrum of **α_2-$CrP_2Mo_2W_{15}$,** the two characteristic bands, assigned to the dπ-pπ charge transfer transitions M←O$_t$ and M←O$_b$ (M is Mo or W; O$_t$ is a terminal oxygen and O$_b$ is a bridging oxygen), were recorded at ~50000 cm^{-1} and ~35273 cm^{-1} [27, 28] (Figure 4a).

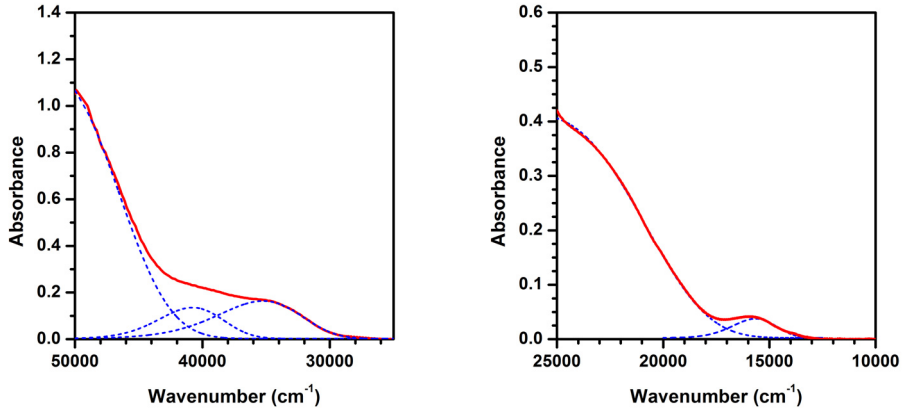

Figure 4. The UV (a) and visible (b) electronic spectra of **α_2-$CrP_2Mo_2W_{15}$** recorded in aqueous solution. The Gaussian components are represented with dashed lines.

The visible spectrum provides information about the local environment of Cr(III) (Figure 4b). Two bands characteristic of the chromium complexes, registered at 15650 cm^{-1} and 23446 cm^{-1} were assigned to $^4T_{2g}(F) \leftarrow {}^4A_{2g}(F)$ (v_1) and $^4T_{1g}(F) \leftarrow {}^4A_{2g}(F)$ (v_2) transitions, respectively. The v_3 band, assigned to $^4T_{1g}(P) \leftarrow {}^4A_{2g}(F)$ transition [29], overlaps the dπ-pπ charge transfer transitions $M \leftarrow O_t$ and $M \leftarrow O_b$ specific to the polyoxometalate structure, and appear as a shoulder at 40703 cm^{-1}. This assignment is supported by the calculation of the spectral parameters according to the method proposed by Lever (Dq= 1565 cm^{-1}, Dq/B=1.25, v_3/B=32.51, B=1252 cm^{-1}) [30].

While the ^{31}P-NMR of the ligand **α_2-$P_2Mo_2W_{15}$** shows a clean two-line spectrum with signals at -3.15 and -11.97 ppm, the spectrum of the Cr(III) complex **α_2-$CrP_2Mo_2W_{15}$** shows only a broadened peak at -11.58 ppm (Figure 5), which was assigned to P(2), the farthest phosphorus atom from the Cr(III) coordination site [31,32]. The phosphorus atom which is closest to the site of Cr(III) incorporation, P(1), was not observed probably because of the strong interaction with the paramagnetic ion.

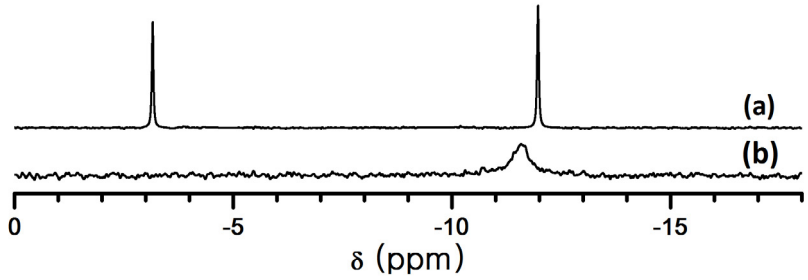

Figure 5. ^{31}P NMR spectra of **α_2-$P_2Mo_2W_{15}$** (a) and **α_2-$CrP_2Mo_2W_{15}$** (b), recorded in D_2O.

The EPR spectrum of **α_2-$CrP_2Mo_2W_{15}$** is shown in Figure 6. Low-temperature EPR spectra of other Cr(III)-substituted polyoxometalates reported before at 77K [24] show rhombic signals with features centered at 1500, 2000 and 3500 G, which are suggestive of a rhombohedrally distorted CrO_6 octahedron. Similarly, in our case, the low-field resonances in a range of g=3-6 indicate the presence of isolated Cr(III) species in orthorhombically distorted octahedral environments with S=3/2. The best fit of the simulated experimental spectrum at low field (1000-2000 G) was obtained assuming a Lorenzian line shape and two magnetic non- equivalent sites of chromium ions in a 0.55 to 0.45 ratio. The parameters for the first species were g_x= 5.11, g_y= 5.09, g_z= 5.0, and A_x= 251, A_y= 442, A_z= 494, which are characteristic of orthorhombically distorted symmetry. The parameters of the second species, g_x=4.1, g_y=3.53, g_z=3.22, and A_x=195, A_y=124, A_z=127, are characteristic of octahedral local symmetry [33]. These two magnetically- non-enequivalent species of Cr(III) are assigned to two different crystalline form of the polyoxometalate complex.

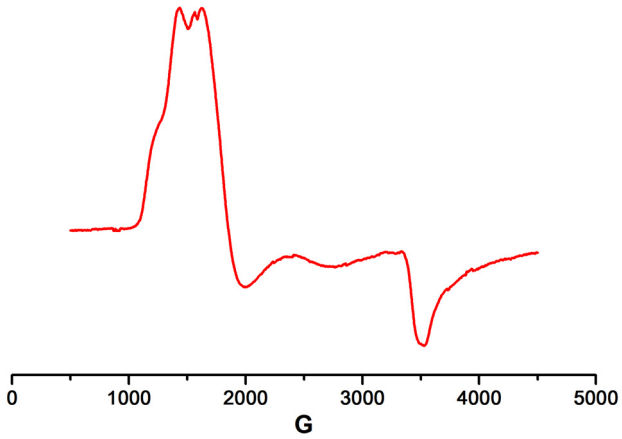

Figure 6. Low-temperature X-band EPR spectrum of **α_2-$CrP_2Mo_2W_{15}$**.

The electrochemical response of **α_2-$CrP_2Mo_2W_{15}$** in aqueous solution consists of three successive redox peak pairs in the negative potential range (Figure 7).

Peaks I and II were assigned to two molybdenum-centered single electron redox processes, while peak III corresponds to a two electrons tungsten-centered process [34]. The recorded cyclic voltammogram for the chromium (III) complex is very similar to those of **α_2-$P_2Mo_2W_{15}$**. Only a slight negative shift in the peak potentials was observed for **α_2-$CrP_2Mo_2W_{15}$** relative to the monolacunary ligand.

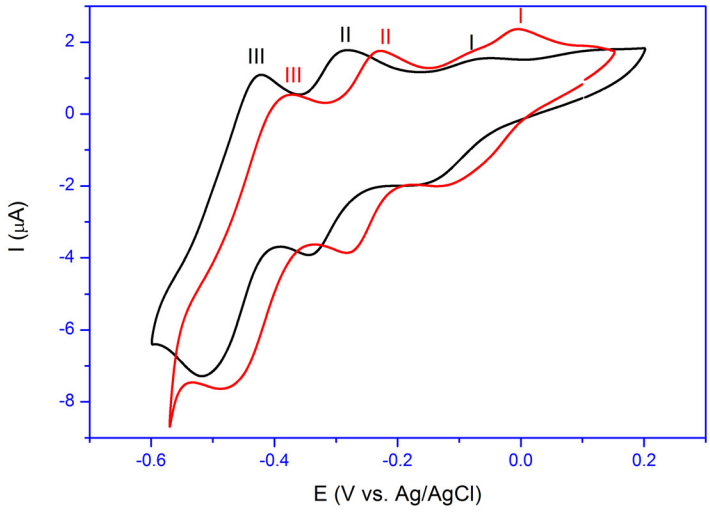

Figure 7. Cyclic voltammograms of **α_2-$CrP_2Mo_2W_{15}$** (black) and **α_2-$P_2Mo_2W_{15}$** ligand (red), recorded in 0.5 M HSO_4^- buffer solutions (pH= 3.0), sweep rate 10 mV s^{-1}.

Table 1. CV data for the chromium (III) complex and the parent Dawson monolacunary polyoxometalate.

Process	E_{pa} (V)	E_{pc} (V)	$\varepsilon^{0'}$ (V)	ΔE_p (V)
α_2-$P_2Mo_2W_{15}$				
I	-0.003	-0.102	-0.0525	0.099
II	-0.234	-0.279	-0.2565	0.045
III	-0.374	-0.485	-0.4295	0.111
α_2-$CrP_2Mo_2W_{15}$				
I	-0.052	-0.114	-0.0830	0.062
II	-0.287	-0.329	-0.3080	0.042
III	-0.419	-0.514	-0.4665	0.095

E_{pa}, oxidation potential; E_{pc}, reduction potential; $\varepsilon^{0'}$, formal standard potential estimated as the average of anodic and cathodic peak potentials; ΔE_p the difference between the redox peak potentials. Experimental conditions: 0.5 M HSO_4^- buffer solution; pH= 3.0, 25°C; glassy carbon working electrode; scan rate 10 mV s^{-1}; c=10^{-3} M, potentials recorded vs Ag/AgCl.

The formal standard potential $\varepsilon^{0`}$ (estimated as the average value of anodic and cathodic peak potentials) shows a negative shift with increasing values of pH (Figure 8a). For all three peaks, the $\varepsilon^{0`}$ versus pH dependences are linear, with slopes of 102.01 (I), 75.06 (II) and 73.96 (III) mV/ΔpH. The anodic to cathodic peak separation values (Δ*E*) and the described pH dependence are probably consistent with the fact that a single electron as well as one proton are involved in each redox process I and II, while two electrons and two protons are involved in the redox process III [32, 35-38].

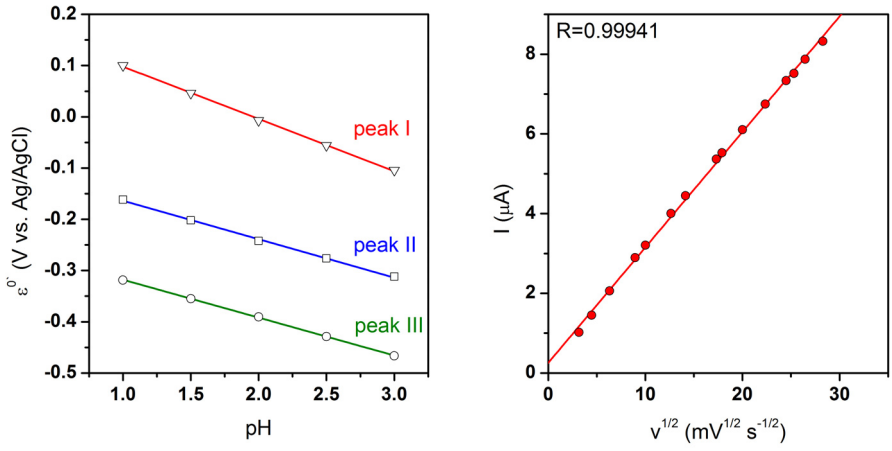

Figure 8. Dependence of the formal standard potentials on the pH for **α_2-$CrP_2Mo_2W_{15}$** (a); dependence of cathodic peak II current on the scan rate (b).

The linear relationship between peak currents and the square root of scan rates for cathodic peak II (Figure 8b) provides evidence for a diffusion controlled process [39].

CONCLUSIONS

The spectroscopic and electrochemical investigations of **α_2-$CrP_2Mo_2W_{15}$** provide evidence for the coordination of Cr(III) by the $[\alpha_2\text{-}P_2Mo_2W_{15}O_{61}]^{10-}$ Dawson monolacunary polyoxometalate. Both chromium and molybdenum atoms are located to the same cap of the anion. Cr(III) ion binds to five oxygen atoms, surrounding the vacancy of the ligand **α_2-$P_2Mo_2W_{15}$**, and to one water molecule. The electrochemical behavior of **α_2-$CrP_2Mo_2W_{15}$** illustrates the influence exerted by chromium upon the redox character of **α_2-$P_2Mo_2W_{15}$**. The redox behavior of the new chromium (III) derivative **α_2-$P_2Mo_2W_{15}$** recommends it as a promising mediator (electrocatalyst) in indirect electrochemical reactions.

EXPERIMENTAL SECTION

1. Materials

The monolacunary polyoxometalate $[P_2Mo_2W_{15}O_{61}]^{10-}$ was prepared according to the published method [19], starting from the Dawson polyoxometalate $[P_2W_{18}O_{62}]^{6-}$ (see Figure 1). The identity of precursors was established by ^{31}P-NMR and FT-IR spectra.

1.1. Preparation of $K_4Li_3[Cr(H_2O)P_2Mo_2W_{15}O_{61}]\cdot 17H_2O$

A sample of 1.33 g (5 mmol) of $CrCl_3\cdot 6H_2O$ was dissolved in 110 mL of molar acetic acid - lithium acetate buffer (pH=3.5), and 25.00 g (5.25 mmol) of $K_{10}[P_2Mo_2W_{15}O_{61}]\cdot 21H_2O$ was added with stirring. The mixture was heated at 40°C for 1 hour while the colour changed from green to brown, and then the clear solution was treated with 150 mL saturated KCl. The white precipitate was removed by filtration over a synthered glass frit and the brown filtrate was kept at 5°C. After three days, brown needle-like crystals appeared which were collected by filtration over a synthered glass frit, washed with ethanol and ether, and dried in air. Yield: 15 g (64.7%). Calcd. for $K_4Li_3[Cr(H_2O)P_2Mo_2W_{15}O_{61}]\cdot 17H_2O$: K 3.43, Li 0.46, Cr 1.14, P 1.36, Mo 4.30, W 60.70. Found: K 3.05, Li 0.40, Cr 1.12, P 1.44, Mo 4.05, W 62.08. FT-IR (cm^{-1}, KBr pellets, polyoxometalate region): 1093, 1014, 953, 912, 779, 686, 598, 565, 525, 476. ^{31}P NMR (D_2O, δ): -11.58 (s).

2. Methods

Elemental analysis was performed by inductively coupled plasma atomic emission spectroscopy on an ICP-OES Perkin Elmer Optima 3500 DV spectrometer. The water content was determined thermogravimetrically, with a METTLER-TOLEDO TG/SDTA 851 thermogravimeter (Pt crucible, 20 mL/min nitrogen flow, 5ºC/min heating rate).

A JASCO 610 FTIR spectrophotometer was used to record the FT-IR spectra (KBr pellets).

UV-Vis spectra were recorded on a Shimadzu UV-3101PC instrument using Teflon-stoppered quartz cells with a path length of 1 cm. A 10 μM aqueous solution of **α_2-$CrP_2Mo_2W_{15}$** was used to record the UV spectrum, while for the Vis spectrum was used a 1mM aqueous solution of **α_2-$CrP_2Mo_2W_{15}$**.

^{31}P-NMR spectra were recorded at 101.2561380 MHz using an ARX 250 spectrometer. Chemical shifts are reported in ppm using D_3PO_4 as external reference.

A Bruker EMX Micro spectrometer with a liquid nitrogen cooling system was employed for EPR spectra. Instrument conditions were: microwave frequency 9.43 GHz, microwave power 15.89 mW, modulation frequency 100 kHz, modulation amplitude 5 G, sweep rate 22.6 G/s; time constant 81.92 ms, average of three sweeps for each spectrum, temperature 100 K. To find the magnetic parameters, the experimental spectrum was simulated using the program POWFIT (http://epr.niehs.nih.gov/).

Electrochemical measurements were performed using a computer controlled AUTOLAB PGSTAT302N potentiostat. A conventional (single-compartment) three electrode electrochemical cell was used, with a Metrohm planar platinum counter electrode and a Metrohm Ag/AgCl reference electrode. Glassy carbon (Metrohm, Φ~ 3mm) was used as a working electrode (WE). This was polished with 0.3 μm alumina, followed by sonication for 3 min. in purified water before each run. The WE was polarized in a 10^{-3} M solution of the complex in 0.5 M HSO_4^- buffer (pH = 1.0 - 3.0) with a scan rate between 10 and 900 mV s^{-1}. Solutions were deoxygenated using purified N_2 gas (99.9%). While recording the voltammograms, N_2 was passed over the solution surface. All measurements were performed at room temperature.

ACKNOWLEDGMENTS

The authors gratefully acknowledge the financial support from the Romanian National Council for Scientific Research (PNCDI II - IDEI, Project No. 329/2007). We also thank Dr. Laura Elena Mureşan for TG-DSC measurements and Ioana Mihaela Perhăiță for elemental analysis.

REFERENCES

1. M.T. Pope, A. Müller (Eds.), “Polyoxometalates: From Platonic Solid to Antiretroviral Activity”, Kluwer Academic Publishers, Dordrecht, **1994**.
2. M.T. Pope, A. Müller (Eds.), “Polyoxometalate Chemistry: From Topology via Self-Assembly to Applications”, Kluwer Academic Publishers, Dordrecht, **2001**.
3. T. Yamase, M.T. Pope (Eds.), “Polyoxometalate Chemistry for Nano-Composite Design”, Kluwer Academic Publishers, Dordrecht, **2002**.

4. J.J. Borrás-Almenar, E. Coronado, A. Müller, M.T. Pope (Eds.), "Polyoxometalate Molecular Science", Kluwer Academic Publishers, Dordrecht, **2004**.
5. M. Misono, *Chemical Communications*, **2001**, 1141.
6. N. Mizuno, M. Misono, *Chemical Reviews*, **1998**, *98*, 199.
7. M. Sadakane, E. Steckhan, *Chemical Reviews,* **1998**, *98*, 219.
8. J.T. Rhule, C.L. Hill, D.A. Judd, *Chemical Reviews*, **1998**, *98*, 327.
9. T. Yamase, *Journal of Materials Chemistry*, **2005**, *15*, 4773.
10. E. Coronado, C. Giménez-Saiz, C.J. Gómez-García, S.C. Capelli, *Angewandte Chemie, International Edition,* **2004**, *43*, 3022.
11. E. Coronado, P. Day, *Chemical Reviews*, **2004**, *104*, 5419.
12. E. Coronado, C. Giménez-Saiz, C.J. Gómez-García, *Coordination Chemistry Reviews*, **2005**, *249*, 1776.
13. E. Coronado, J.R. Galán-Mascarós, C. Giménez-Saiz, C.J. Gómez-García, S. Triki, *Journal of American Chemical Society*, **1998,** *120,* 4671.
14. E. Papaconstantinou, *Chemical Society Reviews*, **1989**, *16*, 1.
15. A. Hiskia, A. Mylonas,E. Papaconstantinou, *Chemical Society Reviews*, **2001**, *30*, 62.
16. T. Yamase, *Chemical Reviews*, **1998**, *98*, 307.
17. D.P. Smith, M.T. Pope, *Analytical Chemistry*, **1968**, *40*, 1906.
18. D.E. Katsoulis, *Chemical Reviews*, **1998**, *98*, 359.
19. B.J. Hornstein, R.G. Finke, *Inorganic Chemistry*, **2002**, *41*, 2720.
20. M. Abbessi, R. Contant, R. Thouvenot, G. Hervé, *Inorganic Chemistry*, **1991**, *30*, 1695.
21. B. Keita, L. Nadjo, R. Contant, *Journal of Electroanalytical Chemistry,* **1998**, *443*, 168.
22. B. Keita, Y. Jean, B. Levy, L. Nadjo, R. Contant, *New Journal of Chemistry* **2002**, *26*, 1314.
23. B. Keita, Y.W. Lu, L. Nadjo, R. Contant, M. Abbessi, J. Canny, M. Richet, *Journal of Electroanalytical Chemistry*, **1999**, *477*, 146.
24. K. Wassermann, R. Palm, H.J. Lunk, J. Fuchs, N. Steinfeldt, R. Stösser, R., *Inorganic Chemistry*, **1995**, *34*, 5029.
25. K. Wassermann, H.J. Lunk, R. Palm, J. Fuchs, N. Steinfeldt, R. Stösser, R., M.T. Pope, *Inorganic Chemistry*, **1996**, *35*, 3273.
26. C. Rocchiccioli-Deltcheff, R. Thouvenot, *Spectrochimica Acta*, **1976**, *32A*, 587.
27. H. So, M.T. Pope, *Inorganic Chemistry*, **1972**, *11*, 1441.
28. A.R. Tomşa, D. Cioloboc, A.M. Todea, L. Mureşan, V. Paşcalău, M. Rusu, *Studia Universitatis Babeş-Bolyai, Seria Chemia*, **2009**, *LIV*, 33.
29. A.B.P. Lever, "Inorganic Electronic Spectroscopy", Elsevier, New York, 2nd edn., **1984.**
30. A.B.P. Lever, *Journal of Chemical Education*, **1968**, *45*, 711.
31. D.K. Lyon, W.K. Miller, T. Novet, P.J. Domaille, E. Evitt, D.C. Johnson, R.G. Finke, *Journal of American Chemical Society*, **1991**, *113*, 7209.
32. C. Rong, F.C. Anson, *Inorganic Chemistry*, **1994**, *33*, 1064.

33. R.P.S. Chakradhar, J.L. Rao, G. Sivaramaiah, N.O. Gopal, *Physica Status Solidi (b)* **2005**, *242*, 2919.
34. M. Sadakane, E. Steckhan, *Chemical Review*, **1998**, *98*, 219.
35. S. Dong, X. Xi, M. Tian, *Journal of Electroanalytical Chemistry*, **1994**, *385*, 227.
36. X. Xi, G. Wang, B. Liu, S. Dong, *Electrochimica Acta*, **1995**, *40*, 105.
37. L. David, C. Crăciun, M. Rusu, O. Cozar, P. Ilea, D. Rusu, *Polyhedron*, **2000**, *19*, 1917.
38. A.R. Tomşa, L. Mureşan, A. Koutsodimou, P. Falaras, M. Rusu, *Polyhedron*, **2003**, *22*, 2901.
39. A.J. Bard, L.R. Faulkner, "Electrochemical Methods Fundamentals and Applications", Wiley, New York, **2001**.

STUDIA UNIVERSITATIS BABEŞ-BOLYAI, CHEMIA, LIV, 4, 2009

PREDICTIVE ROLE OF ANALYTICAL INVESTIGATIONS ON THE BIOCHEMICAL HOMEOSTASIS IN YOUTH NOTE I. LIPID METABOLITES RELATED TO SOMATOMETRY

GARBAN GABRIELA[a], AUMÜLLER CORINA[b], GARBAN ZENO[b]

ABSTRACT: Research concerning the homeostasis of lipid metabolites elicits interest due to its predictive value of the pathobiochemical risk.

In this context the investigations were performed on a number of 423 subjects aged between 10-18 years (174 boys and 248 girls), pursuing the status of lipid metabolites in blood serum, i.e. triacylglycerols and total cholesterol. Also, the analytical data were correlated with the body mass index (BMI) – a somatometric index. Thus, it was possible to identify the overweight subjects (BMI over 95 percentile) as well as the overweight subjects with homeostatic disturbances (dyshomeostasis). As these adolescents might develop cardiovascular and/or other related diseases in adulthood, they were included in a preventive monitoring system.

Keywords: chemical investigations on lipid metabolites in human blood serum – dyshomeostasis, pathobiochemistry

INTRODUCTION

Biochemical homeostasis in human organism is fundamental for the maintenance of its morphophysiological status [1], [2]. Analytical and bio-analytical chemistry offer means for the investigation of various metabolites, e.g.: carbohydrates, lipids, proteins and electrolytes.

In metabollomics theoretical concepts and applicative chemical investigations are more and more developed in relation with biomarkers. In biochemistry and clinical chemistry such markers define the normal functioning of tissues and organs.

Dyshomeostasis is defined as a decrease or increase in the concentration of various metabolites. These changes can occur, among others, as a consequence to malnutrition (lack or excess of nutrients), the presence of different chemical xenobiotics from the environment. [3], [4].

[a] *Laboratory of Environment and Nutrition, Institute of Public Health Timisoara, Bd. Dr. V. Babes Nr.16, RO-300 242 Timisoara, Romania, garban_g@yahoo.com;*

[b] *Department Biochemistry and Molecular Biology, Faculty of Food Products Technol., University Agricultural Sciences and Veterinary Medicine of Banat Timisoara, Calea Aradului Nr. 119, RO-300 645 Timişoara, Romania, zeno_garban@yahoo.com*

The problem of lipid metabolites presents interest from different point of view: e.g.: nutritional (hypercaloric foods), medical (pathobio-chemistry of cardiovascular system), social (stress in human activity) and others.

Investigations were performed successively on the concentration of the main serum lipid metabolites: triacylglycerols, total cholesterol and correlated with the body mass index - BMI (Note I); on HDL-cholesterol, LDL-cholesterol and extended to blood metallograms - regarding Ca and Mg (Note II). On the whole, peculiarities of the biochemical homeostasis in young people were monitored.

MATERIALS AND METHODS

Investigations included a group of 423 healthy young people from a school collectivity and is the first study in this domain in Romania. Youth were divided in two groups: group n_1 – including 174 boys and group n_2 – including 249 girls. The age limits of subjects were between 10-18 years which, according to WHO, covers the period of adolescence.

In the first step the weight and height of young people were measured, thus obtaining the somatometric data. Then blood samples were collected for biochemical analysis (lipids, lipoproteins and some metals).

This paper presents the results obtained on serum lipid fractions: triacylglycerols (TAG) and total cholesterol (T-Chol). The analytical results were correlated with the somatometric data expressed in body mass index (BMI) in order to evidence the subjects with risk to develop cardiovascular or other diseases [5], [6].

Analytical determinations were made by using a LABSYSTEM-901 analyzer and specific Clinilab reagents. The method of Fossatti and Prencipe [7] was used for triacylglycerols and the method of Allain et al. [8] for total cholesterol determination.

Serum triacylglycerols determined by the enzymatic spectrophoto-metric method has the following principle: serum triacylglycerols are transformed, in the presence of lipoproteinlipase, into glycerine-3-phosphate. Finally, the measurements were performed at the wavelength 540 nm.

Total cholesterolemia determined by the enzymatic spectrophotometric method was based on the following principle: the transformation of cholesterol ester in cholesterol and fatty acids in the presence of cholester-esterase. Final determinations were made at the wavelength 500 nm.

The analytical data were statistically processed; for each age group the mean value (X) and the standard deviation (SD) were calculated.

RESULTS AND DISCUSSIONS

Blood triacylglycerols result mainly from the catabolism of dietary glycerides and in a more reduced amount from the conversion of carbohydrates and of some aminated acids (in the frame of specific biochemical pathways of the tricarboxylic acid cycle).

The obtained data on triacylglycerolemia are presented in Table 1. These are mentioned for gender groups (noted n_1 the boys and n_2 the girls) and within gender groups for age categories – see Table 1. Comparative data regarding triacylglycerolemia (in mg / dL) in the studied boy and girl groups.

Table 1. Comparative data regarding triacylglycerolemia (in mg/dL) in the studied boy and girl groups

Age groups (years)	Group (boys)		Group (girls)		ΔX (X_1-X_2)
	n_1	$X_1 \pm DS$	n_2	$X_2 \pm DS$	
10	15	66.07 ± 33.92	14	69.50 ± 35.65	+ 3.43
11	23	86.09 ± 37.25	33	78.21 ± 42.28	- 7.88
12	29	76.72 ± 44.14	45	78.82 ± 48.77	+ 2.10
13	35	59.06 ± 25.14	26	87.73 ± 59.48	+ 28.77
14	30	52.83 ± 23.88	36	78.86 ± 45.03	+ 26.03
15	13	62.46 ± 26.41	36	73.77 ± 31.27	+ 11.31
16	18	67.56 ± 23.33	25	72.48 ± 34.32	+ 4.92
17	8	76.75 ± 20.44	16	91.56 ± 35.92	+ 14.81
18	3	80.33 ± 46.48	18	76.22 ± 32.52	- 4.11

According to the method for triacylglycerolemia determination the normal values range between 50-160 mg/dL in boys and between 45-140 mg/dL for girls. In this context the resulted mean values were in normal limits.

As seen in Table 1 the highest values of triacylglycerolemia in boys were found at 11 years age and the lowest at 14 years age. In girls the values were higher than in boys excepting age groups of 11 and 18 yrs.

A similar study was performed in Greece by Schulpis and Karikas [9] on a number of 7767 subjects (3980 boys and 3785 girls) aged between 6-14 years. Their results showed a maximum level for triacylglyceridemia in boys aged 11 yrs and a diminishing to age13 yrs. The same results were revealed in girls with the observation that in the group of 10 yrs and 14 yrs old girls the values were over the normal limit.

Another study performed by Khalil et al. [10] on the serum lipid profile in a number of 410 healthy Indian subjects aged 3-12 years revealed no significant difference between genders. The mean value for triglycerides was 91.1 mg/dL and for total cholesterolemia 134.5 mg/dL. It is to mention that the mean value of triacylglycerols was higher than in our study but total cholesterolemia was much lower.

Bistrizer et al. [11] evaluated the serum lipids profile in 107 children and their parents (40 families) in which the father had a myocardial infarction or coronary heart disease (CHD) before age 40 years. Regarding the results for children, significant hyperlipidaemia were found in 42%.

Studies performed by Tamir et al. [12] and Williams et al. [6], evidenced the complex influence of morphophysiologic factors in adolescents.

The American Heart Association set guidelines for serum triacylglycerol levels (values were expressed in mg/dL), thus: normal < 150 (no risk); borderline high 150-199; high 250-499; very high > 500 (high risk)

In the human organism augmented levels of triacylglycerols in the bloodstream have been linked to atherosclerosis, even in the absence of hypercholesterolemia, and, by extension the risk of heart disease and stroke.

Between the causes of hypertriacylglycerolemia one can mention obesity, high intakes of fat and concentrated sweets, genetic predisposition and others. The values found by us indicate changes related to age and maturation which could reflect the influence of sex hormones on serum lipoprotein metabolism [13], [14].

Homeostasis changes in cholesterolemia originate in the metabolic disturbances of sterides – macronutrients present in diet [15], [16]. In table 2 there are presented the values of the T-Chol in the studied groups.

Normal values according to the used method for cholesterolemia range between 160-199 mg/dL. Thus, in our subjects the mean values did not exceed normal limits, but in girls the values are higher, except for girls aged 14 and 15 years.

The 1987 report of National Cholesterol Education Program, suggest the total serum cholesterol level should be: < 200 mg/dL normal serum cholesterol, 200–239 mg/dL borderline-high, > 240 mg/dL high cholesterol [17]. Nowadays, the link between cholesterol and atherosclerosis is accepted by the majority of medical scientists [18].

Table 2. Comparative data regarding cholesterolemia (in mg/dL) in the studied boy and girl groups

Age groups (years)	Group n_1 (boys)		Group n_2 (girls)		ΔX (X_1-X_2)
	n_i	$X_1 \pm DS$	n_i	$X_2 \pm DS$	
10	15	150.50 ± 24.79	14	159.14 ± 34.87	+ 8.64
11	23	143.60 ± 29.54	33	155.82 ± 30.10	+ 12.22
12	29	147.70 ± 32.35	45	155.27 ± 32.57	+ 7.57
13	35	131.70 ± 20.29	26	141.42 ± 24.08	+ 9.72
14	30	140.50 ± 29.25	36	138.11 ± 20.25	- 2.39
15	13	147.80 ± 27.66	36	143.81 ± 29.18	- 3.99
16	18	136.10 ± 24.36	25	157.40 ± 22.61	+ 21.30
17	8	122.40 ± 26.12	16	146.56 ± 32.25	+ 24.16
18	3	137.70 ± 16.29	18	146.06 ± 35.42	+ 8.36

Investigations concerning cholesterolemia is of great importance because this steroid compound is present in blood, bile and brain tissue. In metabolic processes cholesterol is a precursor in the synthesis of bile acids, steroid hormones and vitamine D [19], [20]. The level of T-Chol in blood serum is associated with metabolic processes and their disturbances in some cardiovascular disease and infections [21]. There are also experimental studies on young subjects [22], [23].

Genetics play an important role in determining adolescents`s cholesterol level. Also, the family lifestyle and diet will have an important effect on an adolescent's cholesterol.

Cholesterol and other cardiovascular risk factors often persist from childhood to adulthood. Autopsy studies demonstrated that aortic and coronary atherosclerosis are commonly seen before age 20 years. High total cholesterolemia, LDL-Chol, VLDL-Chol and low HDL-Chol are correlated with extent of early atherosclerotic lesions in adolescent and young adult [12], [24].

Usually, dyshomeostasis of TAG and T-Chol in youth give evidence of „metabolic syndrome" which develops in time to atherosclerotic processes [25].

Based on somatometric data (weight and height) the body mass index (BMI) - an anthropometric index, defined as the individual`s body weight in kilograms divided by the square of his or her height, were calculated. BMI is widely used to define overweight and obesity, because it correlates well with accurate measures of body fatness.

Using the BMI-for-age gender specific charts recommended by Center for Disease Control and Prevention – Atlanta, USA, the adolescents were classified as: under-weighted - BMI < 5th percentile; normal weighted - BMI between 5 < 85 percentile; at risk of overweight - BMI between 85 < 95 percentile or overweighted - BMI > 95 percentile [26]. The obtained results are presented in Table 3.

Having in view the somatometric criteria, exactly the BMI and assessing the distribution of subjects in the percentile limits, there were revealed 14 boys and 16 girls between 85-95 percentile, and 6 boys and 12 girls over 95 percentile.

Recent studies indicate an increasing prevalence of overweight and obesity in childhood in developed and developing countries, e.g. the prevalence among children and adolescents in USA has doubled in the past two decades [27], [28].

It is known that obesity is associated with significant health problems in childhood and adolescence and is an important early risk factor for much of adult morbidity and mortality [29], [30]. In obese children and adolescents the cardiovascular system is affected (e.g. hypercholes-terolemia, dyslipidemia, hypertension) – see [31], [32]. At the same time, perturbations were found in endocrine system (hyperinsulinism, insulin resistance, impaired glucose tolerance, type 2 diabetes mellitus, menstrual irregularity) and mental health (depression).

Table 3. Distribution of the studied subjects according to percentile (BMI-for-age) evaluation

Age group	Scale of BMI in boys					Scale of BMI in girls				
	< 5	5-85	85-95	> 95	Total	< 5	5-85	85-95	> 95	Total
10	0	12	1	2	**15**	0	13	1	0	**14**
11	2	15	3	3	**23**	1	30	0	2	**33**
12	3	23	3	0	**29**	3	35	6	1	**45**
13	4	28	3	0	**35**	0	24	1	1	**26**
14	4	24	1	1	**30**	1	26	5	4	**36**
15	2	9	2	0	**13**	3	29	2	2	**36**
16	1	16	1	0	**18**	1	22	1	1	**25**
17	1	7	0	0	**8**	1	15	0	0	**16**
18	0	3	0	0	**3**	2	15	0	1	**18**
Total	**17**	**137**	**14**	**6**	**174**	**12**	**209**	**16**	**12**	**249**

Detailed results on TAG and T-Chol determination for overweighted subjects (18 cases) with high risk for “metabolic syndrome” – i.e. category of subjects over 95 percentile of BMI, are presented in Table 4.

Table 4. Serum TAG and T-Chol (mg/dL) in boys and girls with BMI over 95

Gender	Age (years)	Identified subjects		TAG	T-Chol
		No.	Cases		
Boys (6)	10	1.	CS	**164**	167
		2.	TD	89	171
	11	3.	BA	**193**	176
		4.	CA	50	137
		5.	MA	83	116
	14	6.	SM	49	136
Girls (12)	11	1.	NI	**191**	117
		2.	CA	**194**	195
	12	3.	TA	56	**211**
	13	4.	CV	**259**	158
	14	5.	BS	**251**	173
		6.	PR	84	153
		7.	PM	68	147
		8.	KA	84	127
	15	9.	RB	101	146
		10.	MI	72	174
	16	11.	TM	48	162
	18	12.	FC	61	**201**

Regarding the obtained analytical results of TAG and T-Chol in overweighted subjects, high values (over the normal limits) were observed in 8 cases (2 boys and 6 girls). In boys 2 cases of hypertriacyl-glycerolemia were evidenced. In girls 4 cases of hypertriacyglicerolemia and 2 cases of hypercholesterolemia were found. The values over the normal limits are evidenced in table 4 by using bold.

Vanhala et al. [33] found that obese children who went on to be obese adults had a threefold increased risk of developing the metabolic syndrome compared with those who became obese as adults.

The probability of childhood obesity persisting into adulthood is estimated to increase from approximately 20% at 4 years of age to approximately 80% by adolescence [34]. In addition, it is probable that comorbidities will persist into adulthood [35].

In light of the literature data, in order to prevent the development of cardiovascular and other related diseases all the young subjects found with BMI over 95 and high values of TAG and T-Chol will be monitored.

CONCLUSIONS

Investigations on some serum lipid fraction by using methods based on bioanalytical chemistry, the values of TAG and T-Chol were determined in 423 adolescents (174 boys and 248 girls) aged 10-18 years. Also, the somatometric index, i.e. body mass index (BMI), for each subject was calculated. Thus, a number of 18 adolescents (6 boys and 12 girls) was detected with BMI over 95 (considered as overweight). This category of young people is exposed to pathobiochemical risk in time.

When correlated the BMI of the 18 overweight adolescents with their analytical findings only a number of 8 subjects were find with hyper-lipidemia: 2 boys and 4 girls with hypertriacylglycerolemia and 2 girls with hypercholesterolemia. The subjects with hyperlipidemia will be included in a monitoring system with a strict treatment (diet and medication) in order to reduce body weight and to decrease TAG and T-Chol values, thus preventing the development of cardiovascular and/or other related diseases.

The identified 10 subjects (4 boys and 6 girls) only with BMI over 95 percentile will be included also in a preventive monitoring program in order to reduce their body weight, e.g. with energy-restricted diet (lowered lipid and carbohydrate nutrients in ratio), increase of physical activity, and others.

Using methods which are specific for analytical chemistry in lipidology and calculations to obtain the somatometric index, permitted the identification of subjects with “metabolic syndrome”. These subjects have a major risk to develop biochemical injuries characteristic to atherosclerosis. In order to prevent adulthood diseases in these subjects they must be monitored.

REFERENCES

1. T. Brody T., „Nutritional biochemistry", Academic Press, San Diego, **1994**.
2. J. W. Marshall, K. S. Bangert, „Clinical Biochemistry. Metabolic and clinical aspects", Churchill Livingstone, New York-Edinburgh-London-Madrid, **1995**.
3. A. G. Gornall (Ed.), „Applied Biochemistry of Clinical Disorders", J. B. Lippincott Company Philadelphia, **1986**.
4. G.A. Kaplan, A. J. Pesce, S.C. Kazmierczak (Eds.), "Clinical chemistry: theory, analysis and correlation", 4th ed., C.V. Mosby Comp., St. Louis-Toronto-Princeton, **2002**.
5. R. Monge-Rojas, *Arch. Latinoam. Nutr*., **2001**, *51*, 236.
6. C. L. Williams, L. L. Hayman, S. R. Daniels, T. N. Robinson, J. Steinberger, S. Paridon, T. Bazzarre, *Circulation*, **2002**, *106*, 143.
7. P. Fossati, L. Prencipe, *Clin. Chem*., **1982**, *28*, 2077.
8. C.C. Allain, L. S. Poon, C. S. Chan, W. Richmond, P. C. Fu, *Clin. Chem*., **1974**, *20*, 470.
9. Kleopatra Schulpis, A.G. Karikas, *Pediatrics*, **1998**, *101*(5), 861.
10. A. Khalil, R. Gupta, A. Madan, M. Venkatesan, *Indian Pediatr.*, **1995**, *32*, 1177.
11. T. Bistritzer, L. Rosenzweig, J. Barr, S. Mayer, E. Lahat, H. Faibel, Z. Schlesinger, M Aladjem - *Arch Dis Child*., **1995**, *73,* 62.
12. I. Tamir, G. Heiss, C. J. Glueck, B. Christensen, P. Kwiterovich, B. M. Rifkind, *J. Chron. Dis*., **1981**, *34*, 27-39.
13. T.B. Newman, A.M. Garber, N.A. Holtzman, S.B. Hulley, *Arch. Pediatr. Adolesc. Med*., **1995**, *149*, 241-247.
14. Gabriela Garban, Corina Aumüller, Z. Garban, *Physiology*, Supplement, **2006** (16), 39.
15. W.W. Christie, „Lipid Analysis", 3rd edition, Oily Press, Bridgwater, **2003**.
16. Corina Aumüller, Gabriela Garban, Z. Garban, *Journal of Agroalimentary Processes and Technologies*, **2006**, *12*(2), 557.
17. S.S. Gidding, W. Bao, S.R. Srinivasan, G.W. Berenson, *J Pediatr.***1995**, *127*, 868.
18. *** *Arch. Intern. Med.,* **1987**, *148* (1), 36.
19. J. A. Morrison, I. de Groot, B.K. Edwards, *Pediatrics*, **1978**, *62*, 990.
20. M. T. Pugliese, F. Lifshitz, G. Grad, P. Fort, M. Marks-Katz, *N. Engl. J. Med*., **1983**, *309*, 513.
21. M.H. Steiner, L.S. Neinstein, J. Pennbridge, *Pediatrics*, **1991**, *88*, 269-278.
22. L. Gallo, C. Bennett, S. Myers, G. Vanouny, *J. Lipid Res*., **1984**, *25*, 604.
23. Y.B. Park, S.M. Jeon, S.J. Byun, H.S. Kim, M.S. Choi, *Life Sci.*, **2002**, *70*, 1849.
24. G.S. Berenson, S.R. Srinivasan, J.L. Cresanta, T.A. Foster, L.S. Webber, *Am. J. Epidemiol*., **1981**, *113*, 157.
25. Ana Carolina R. Vieira, Marlene M. Alvarez, S. Kanaan, Rosely Sichieri, Gloria V. Veiga, *Rev. Saúde Pública*, **2008**, *42(6),* 1.

26. *** Centers for Disease Control and Prevention, BMI for children and teens, 2003. http://www.cdc.gov/nccdphp/dnpa/bmi/bmi-for-age.htm.
27. J.H. Himes, W.H. Dietz, *Am J Clin Nutr.*, **1994**, *59*, 307.
28. *** US Dept Health and Human Services. *The Surgeon General's Call to Action to Prevent and Decrease Overweight and Obesity.* Rockville, MD: US Department of Health and Human Services, Public Health Service, Office of the Surgeon General; **2001**.
29. D.S. Freedman, W.H. Dietz WH, S.R. Srinivasan, G.S. Berenson, *Pediatrics,* **1999**, *103*, 1175.
30. A. Must, P.F. Jacques, G.E. Dallal, C.J. Bajema, W.H. Dietz, *N. Engl. J. Med.,* **1992**, *327*, 1350.
31. J.A. Morrison, P.M. Laskerzewski, J.L. Rauh, *Metabolism,* **1979**, *28*, 641.
32. D. Steinberg, *The Cholesterol Wars: The Cholesterol Skeptics vs the Preponderance of Evidence*, 2007, Boston, Academic Press.
33. M. Vanhala, P. Vanhala, E. Kumpusalo, P. Halonen, J. Takala, *BMJ,* **1998**, *317*, 319.
34. S.S. Guo, W.C. Chumlea, *Am J Clin Nutr.,* **1999**, *70(suppl)*, 145S.
35. W. Wisemandle, L.M. Maynard, S.S. Guo, R.M. Siervogel, *Pediatrics,* **2000**, *106(1)* Available at: http://www.pediatrics.org/cgi/content/full/106/1/e14

STUDIA UNIVERSITATIS BABEŞ-BOLYAI, CHEMIA, LIV, 4, 2009

SYNTHESIS, CHARACTERIZATION AND OPTIMUM REACTION CONDITIONS FOR NANOSTRUCTURED ZINC OXIDE

OANA CADAR[a], CECILIA ROMAN[a], LUCIA GAGEA[b], ILEANA CERNICA[c], ALINA MATEI[c]

ABSTRACT. In the present paper were established the optimum conditions for the synthesis of Ag-doped ZnO nanopowders. The 0.05% Ag-doped ZnO nanopowders were successfully synthesized by coprecipitation, followed by a washing-drying-calcination treatment. It was found that the optimum conditions for the preparation with high yield and high surface area were as follows: pH value 6.9-7.1, calcination temperature 400 - 500 °C and calcination time 2 h, respectively. The obtained nanopowders were investigated by X-ray diffraction (XRD), Fourier transform infrared spectroscopy (FTIR) and specific surface. The silver doping improves the antibacterial activity of ZnO nanopowders. Therefore the materials based on the obtained nanopowders represent an attractive opportunity for the construction industry.

Keywords: zinc oxide, silver, synthesis, coprecipitation, characterization.

INTRODUCTION

In the past decades, the synthesis and characterization of “so-called” nanoparticles have attracted much attention, not only for the fundamental scientific interest, but also for many technological applications [1–4]. These particles have distinctly different electrical, optical, mechanical and chemical properties in comparison with their corresponding bulk material.

The interior mould attack has become a problem of increasing importance. The medical researchers and phisicians have been observing more and more respiratory and allergic complaints arising from exposure to moulds. Also, paint on outside attack must be taken into account [5, 6].

In recent years, ZnO and ZnO-based powders have been extensively studied due to their properties and technological applications [7]. As well known, zinc oxide has a long history of usage for pigments and protective coatings on metals [8]. Zinc oxide is a very important material due to the interesting

[a] *INCDO-INOE 2000 Institutul de Cercetări pentru Instrumentație Analitică, Str. Donath, Nr. 67, RO-400293 Cluj-Napoca, România, icia@icia.ro*
[b] *Universitatea Babeş-Bolyai, Facultatea de Chimie şi Inginerie Chimică, Str. Kogălniceanu, Nr. 1, RO-400084 Cluj-Napoca, România, gagea@chem.ubbcluj.ro*
[c] *Institutul Național de Cercetare – Dezvoltare pentru Microtehnologie, Str. Erou Iancu Nicolae Nr. 126A, RO-077190 Bucureşti, România, ileanac@imt.ro*

characteristics (fluffy white, density 5.61 g/cm^3, melting point 1975^{o}C) [9]. ZnO is cheaper than other white oxides and insoluble in water, a very important property of the quality of a pigment.

As well known, silver and silver ions exhibit an excellent antibacterial activity against many types of bacteria, even at lower concentrations, and do not cause adverse health effects [10, 11]. Recently, several inorganic antibacterial materials containing silver and silver ions have been successfully prepared and some of them are already commercialized products. These materials are more chemically durable, discharge slowly the silver ion and more slowly affected by light. Therefore, it is rational that introduction of silver ions into ZnO may improve antibacterial capacity of ZnO.

Until now, several methods, such as the mechanical mixing method [12], sol-gel process [13, 14], thermal hydrolysis [15] and coprecipitation [16] have been used to prepare metal-doped ZnO nanopowders.

The coprecipitation method seems to be the most attractive due to its easy control, without requiring expensive and complex equipments. Coprecipitation is the process whereby the fractional precipitation of a specified ion in a solution results in the precipitation not only of the target ion but also of other ions existing in the solution. The additional precipitation of unwanted ions represent an impediment to the analytical process [17]. Some of the most commonly substances used in coprecipitation operations are hydroxides, carbonates, sulfates and oxalates. pH is evidently an important factor in this type of process.

During last years our interests were focused on the preparation and characterization of new ZnO-based nanopowders [18]

The objective of the present study is to continue our research related to determining the optimum parameters for the synthesis of Ag-doped ZnO nanopowders *via* coprecipitation and the properties of the obtained nanoparticles. The obtained nanopowders have a low doping metal content (0.05 wt.%) in order to avoid cytotoxicity and not to affect the white color of the powders. The materials that incorporate these nanopowders may be used in construction industry, increasing the security of living, durability and comfort.

RESULTS AND DISCUSSION

Preparation

Establishing the adequate conditions for complete precipitation from zinc solution is not a simple process due to the amphoter character of Zn. In order to obtain the desired material, the zinc hydroxide is dissolved in a small excess of sodium or potassium hydroxide resulting in the corresponding alkali metal zincate. Because the zinc hydroxide is soluble in the presence of ammonium ions, different complex ions resulted too. Therefore, the solution pH is an important factor for the process.

The zinc hydroxide in the presence of alkaline carbonates form some basic zinc carbonates as $(CO)_3Zn_4(OH)_2$. Thus, it was appeal to the simultaneous precipitation of Zn^{2+} and Ag^{+} using an alkaline carbonate. The obtained carbonates were calcinated at an appropriate temperature resulting in a homogenous mixture of oxides containing particles of small dimensions.

The degree of precipitation control was realized by titration of the unprecipitated cation from the solution resulted after filtration, at controlled pH values. Thus, the quantity of precipitated Zn^{2+} could be calculated as the difference between initial and final content from the filtrate filled up to constant volume. The experiments were realized at different pH values, *i.e*. 6.0-8.0. In Figure 1 are presented the values for the zinc remained unprecipitated in solution. The optimum precipitation pH value is 6.9-7.1.

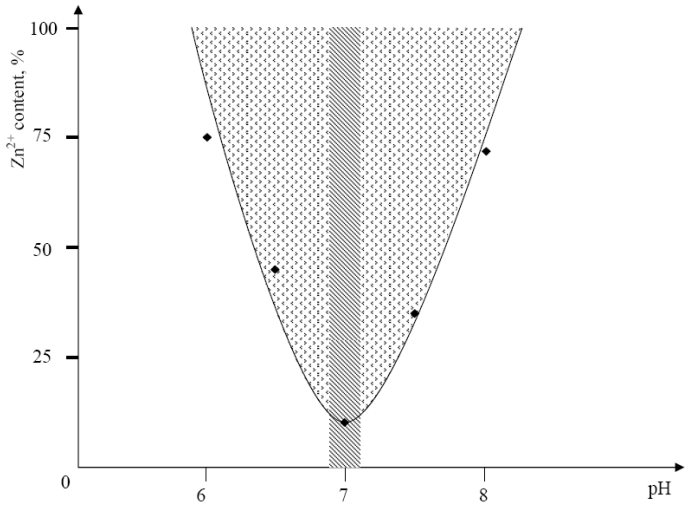

Figure 1. Relationship between the pH of solution and Zn^{2+} content.

It was found experimentally that the optimal synthesis method can be divided into two parts: one is the preparation of the precursor by the coprecipitation method and the other one is the formation of silver doped ZnO nanopowders by calcination (Figure 2) [18].

The zinc oxide diffraction peaks start to appear after the powder was calcinated at 380^{o}C. With the increase of thermal treatment temperature, the microcrystallites are formed more obviously and also the diffraction peaks become more intense.

The commercial ZnO has a wurtzite crystal structure. Literature data demonstrate that ZnO crystals begin to nucleate at about 380^{o}C, and then ZnO crystal growth is completed at about 800^{o}C [19].

At 600ºC X-ray diffraction analysis of the prepared Ag-doped ZnO nanopowder show sharp diffraction peaks corresponding to the hexagonal wurtzite structure: 31.8º (1 0 0), 34.5º (0 0 2), 36.4º (1 0 1), 47.7º (1 0 2), 56.7º (1 1 0), 62.9º (1 0 3), 66.4º (2 0 0), 68.2º (1 1 2) and 69.3º (2 0 1).

The typical silver diffraction peaks were not observed, mainly because the low dosage of silver ions.

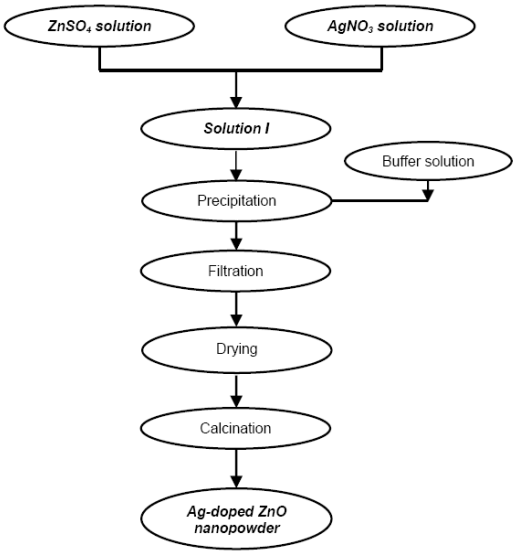

Figure 2. Flow diagram for the synthesis of Ag-ZnO nanopowders.

Structural characterization

X-ray diffraction spectra

Figure 3 shows the XRD patterns of the samples calcinated at different temperatures.

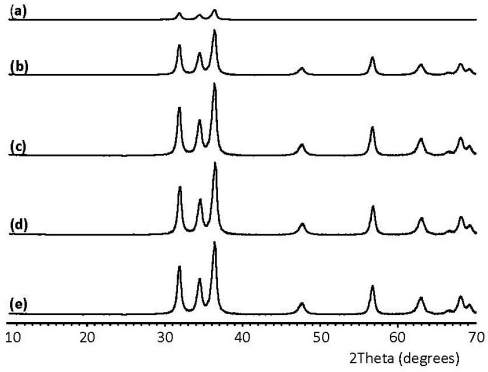

Figure 3. XRD patterns of the ZnO nanopowders calcinated at different temperatures: (a-e) 300, 380, 400, 450 and 600ºC, respectively.

Specific surface

The temperature heat treatment is the factor that mostly influences the formation and growth of crystalline particles obtained from precipitates after calcination. The diffusion in solids, the mobility of constituent particles and their possibility of migration to interfaces increase as temperature increases. The control of particle size increasing is realized indirectly by determining specific surface of the calcinated product at the temperatures of interest.

The studies were realized on precipitates calcinated at 300, 400 and 600°C. The results of the specific surface area analyses are reported in Table 1.

Table 1. Specific surface area of the powders calcinated at different calcination temperatures.

Temperature (°C)	Specific surface area (m^2/g)	Average diameter (nm)
300	70.8-74.3	14.39-15.10
400	49.8-51.5	20.90-21.39
600	20.46-28.6	52.27-62.40

Fourier transform infrared spectroscopy

In FTIR spectra of the samples undoped and doped ZnO (calcinated at 400°C) were observed bands with maximum well defined, centred at 593, 555, 547, 522, 517, 503, 500, 490 cm^{-1} (Figure 4).

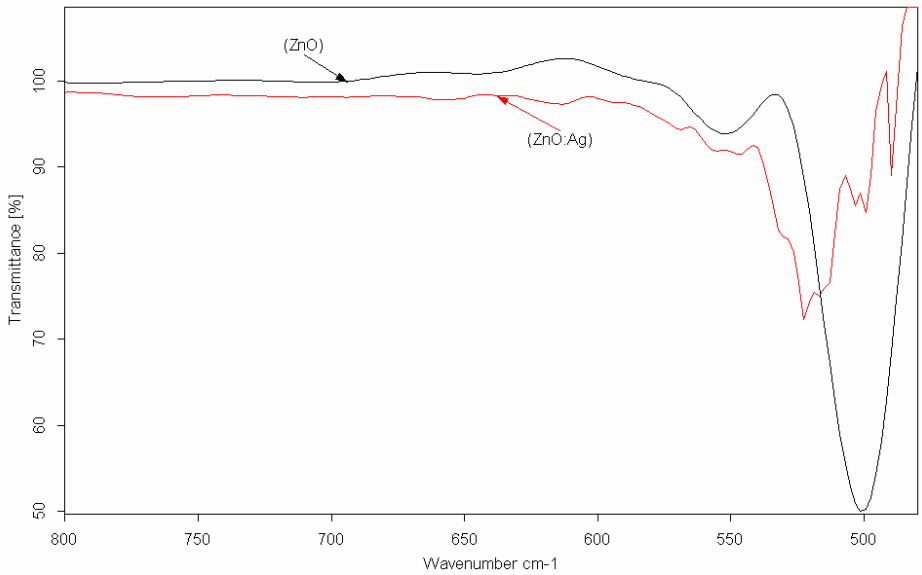

Figure 4. FT-IR spectra of undoped ZnO and Ag - doped ZnO nanopowder, calcinated at 400ºC.

The FTIR spectra of undoped ZnO powders show a high intensity broad band around 490 cm^{-1} due to the stretching mode of Zn–O bond. A similar band was also observed in doped ZnO powder.

The absorption bands observed in the low energy region is formed by the stretching vibration modes of Zn–O and Ag–O bonds (593 and 490 cm^{-1}) [20].

In the FTIR spectra for doped ZnO sample, in comparison with undoped ZnO spectra, we can see a slight displacement of characteristic Zn-O band, concurrent with modification of the peaks and appearance of the new bands which can be attributed to the Zn-O-Ag bonds.

The broad absorption band from 490-600 cm^{-1} indicates the presence of Ag in the ZnO powder and this could be due to a small concentration of silver.

The materials based on these nanopowders could be used in public spaces which necessitate high quality standards and special technical requirements (hospitals, surgeries, bathrooms, food processing facilities, storage rooms, laboratories, nurseries, schools, sport rooms, etc.). General advantages and benefits in the use of materials based on these nanopowders are: environmentally friendly, significant reduction of moos and algae, improvement of the air quality, housing comfort and healthy dwelling, inexpensive, long-term prevention, convenient and easily synthesizable.

CONCLUSIONS

The synthesis of Ag-doped ZnO samples by coprecipitation is simple, stable, repeatable and inexpensive. Several parameters that may influence the synthesis have been discussed. It has been concluded that the optimum reaction conditions are: pH: 6.9-7.1, calcination temperature: 400-500 °C and calcination time: 2 h. The silver concentration must be enough small not to influence the pigment color. The characterization of the obtained samples by specific techniques clearly indicates nano-sized particles.

These nanopowders may be incorporated into a coating in order to obtain materials with superior characteristics for the construction industry.

EXPERIMENTAL SECTION

The Ag-doped ZnO nanopowders were prepared by the coprecipitation method similar to that one previously reported [18].

All reagents were purchased from commercial suppliers and used without further purification. There were used precipitant solution of different pH values, *i.e*. 6.0-8.0) and the calcination temperatures were: 300, 380, 400, 450 and 600ºC, respectively).

The obtained powders were investigated using powder X-ray diffraction (XRD), Fourier transform infrared spectroscopy (FTIR) and specific surface studies. X-ray diffraction (XRD) patterns of these powders were measured on

the SHIMADZU 6000 diffractometer using a CuKα radiation source (40.0 KV, 30.0 mA) and a graphite monochromator. The samples were characterized by FTIR measurements using a model Tensor 27 Bruker spectrometer, in the wavelength range 4000-400 cm^{-1}, after 64 scans, with resolution of 4 cm^{-1}. The specific surface was determined using a modified BET installation.

The detailed preparation process can be described as follows: firstly, under vigorous stirring, the aqueous solution of zinc sulfate was added into silver nitrate aqueous solution. Subsequently, a buffer solution was used to adjust the pH of the reaction system to about 6.9-7.1. The resulted precursor of Ag-doped, $Zn_5(CO_3)_2(OH)_6$ precipitate, was thoroughly washed with distilled water and dried at room temperature (for more than 24 h) and then thermally decomposed under static air atmosphere to give silver doped zinc oxide. The calcination temperature was relatively low, in the range of 400-500 ^oC and the calcination time was 2 h, after which the material was cooled in the furnace and a white powder was obtained. A similar procedure was used for other pH and calcination conditions.

REFERENCES

1. G. Schmid, "Nanoparticles: From Theory to Application", Wiley-VCH, Weinheim, **2004**.
2. K.J. Klabunde, "Nanoscale Materials in Chemistry", Wiley-Interscience, New York, **2001**.
3. A.P. Alivisatos, *Science*, **1996**, *271*, 933.
4. Zhong Lin Wang, *J. Phys.: Condens. Matter*, **2004**, *16*, 829.
5. S. E. Henshon, "Mildew on the Wall", Royal Fireworks Publishing Company, New York, **2004**.
6. F.H. Kayser, K.A. Bienz, J. Eckert, R.M. Zinkernagel, "Medical Microbiology", Ed. Georg Thieme Verlag, Stuttgart, **2005**.
7. S.R. Dhagea, R. Pasrichab, V. Ravia, *Materials Letters*, **2005**, *59*, 779.
8. G.E. Weismantel, "Paint Handbook", Ed. McGraw-Hill, New York, **1981**.
9. C.G. Macarovici, D. Macarovici, "Chimia oxizilor dubli si utilizarile lor", Ed. Academiei Republicii Socialiste Romania, Bucuresti, **1975**.
10. A. Panacek, L. Kvitek, R. Prucek, M. Kolar, R. Vecerova, N. Pizurova, V.K. Sharma, T. Nevecna, R. Zboril, *J. Phys. Chem. B*, **2006**, *110*, 16248.
11. H.J. Lee, S.Y. Yeo, S.H. Jeong, *J. Mater. Sci.*, **2003**, *38*, 2199.
12. P.B. Joshi, N.S. S. Murti, V.L. Gadgeel, V.K. Kaushik, P. Ramakrishnan, *Journal of Materials Science Letters*, **1995**, *14*, 1099.
13. B. Houng and C.-J. Huang, *Surf. Coat. Technol.*, **2006**, *201*, 3188.
14. M.J. Alam, D.C. Cameron, *J. Vac. Sci. Technol.*, A, *Vac. Surf. Films*, **2001**, *19*, 1642.

15. Y. Liu, C. Liu, Q. Rong, Z. Zhang, *Appl. Surf. Sci.,* **2003**, *220*, 7.
16. O.D. Jayakumar, H.G. Salunke, R.M. Kadam, M. Mohapatra, G. Yaswant, S.K. Kulshreshthaa, *Nanotechnology*, **2006**, *17*, 1278.
17. P. Patnaik, "Dean's Analytical Chemistry Handbook", 2nd ed. McGraw-Hill, **2004**.
18. O. Cadar, C. Roman, L. Gagea, I. Cernica, A. Matei, *Revista Romana de Materiale*, **2007**, *37 (4)*, 316.
19. T. Masaki, S.J. Kim, H. Watanabe, K. Mizamoto, M. Ohno, K.H. Kim, *J. Cer. Proces. Res.*, **2003**, *4 (3)*, 135.
20. A.S. Tas, P. J. Majewski, F. Aldinger, *J. Am. Ceram. Soc.*, **2000**, *83*, 2954.

STUDIA UNIVERSITATIS BABEŞ-BOLYAI, CHEMIA, LIV, 4, 2009

CHLORINATED SOLVENTS DETECTION IN SOIL AND RIVER WATER IN THE AREA ALONG THE PAPER FACTORY FROM DEJ TOWN, ROMANIA

VANCEA SIDONIA[a], KOVACS MELINDA HAYDEE[b], DUMITRU RISTOIU[b], SILAGHI-DUMITRESCU LUMINITA[c]

ABSTRACT. Considerable amounts of chlorinated solvents compounds were identified and measured in raw water and soil samples collected during several month studies, along the Somes River near Dej city region of Romania. The most common organochlorine solvents detected were trichloroethylene (C_2HCl_3), tetrachloroethylene (C_2Cl_4), carbon tetrachloride (CCl_4) and chloroform ($CHCl_3$) with the range between 3.05 – 68.92 μg L^{-1}, 5.62 – 55.48 μg L^{-1}, 2.11 – 29.45 μg L^{-1} and 0.37 – 80.29 μg L^{-1}. They were detected using a mass spectrometer coupled at a gas chromatograph with electron capture detector and quantified using chlorinated solvent standards. Organochlorine compounds have different chemical properties that lead into a broad range to uses. Many of them have significant biological activities and some of them can be very toxic for plant, animals and humans. Because of that they present seriously environmental concern. This study presents the source of the pollution and also the levels of these pollutants in river water and the soil.

Keywords: chlorinated solvents, environmental pollution, GC-MS, GC-ECD.

INTRODUCTION

Starting with October 2006 it was observed in several water sample collected from Somes River Basins a high level of some chlorinated solvents. The aim of this study was to identify the chlorinated solvent species presence in river water and established the amount of them. Starting with results obtained from river water analysis was supposed also the possibility of soil contamination, so in the same time were analyzed even the soil sampled near the Somes River. Another goal of this study was to identify the possible pollution source. As shown previous medical and environmental researches, these compounds can induce serious adverse effects to humans and environment [1]. Chlorinated solvents are associated with a series of adverse human health effects such

[a] *Garda de Mediu, Comisariatul Judetean Cluj, str. G-ral T. Mosoiu, nr. 49, Cluj-Napoca, Romania*
[b] *Babes Bolyai University of Cluj-Napoca, Faculty of Environmental Science, Str. P-ta Stefan cel Mare, no.4, 400084, Cluj-Napoca, email: dristoiu@enviro.ubbcluj.ro*
[c] [c]*Universitatea Babeş-Bolyai, Facultatea de Chimie, str. Arany Janos, nr.11, 400068, Cluj-Napoca, Cluj-Napoca*

as toxicity of central nervous system, reproductive, liver and kidney and also carcinogenicity [2 - 5]. Several chlorinated solvents are used in large volume amount in industry because they own a batch proper chemical and physical property [6 - 9]. They are widely used as solvents for fats, oils, waxes and resins or adhesives solvent, in dry cleaning operations, cleaning printed circuit boards, vapour degreasing, parts cleaning, engine cleaner or degreasing agent and paint remover. Many times they are used primarily to produce other chemicals or as chemical intermediate, also are used in organic synthesis, fluorocarbon and polymer manufacture, aerosol propellant and foam plastic blowing agents.

Dej is a small city located at 60 km from Cluj-Napoca town where Somesul Mic River meet Somesul Mare River. At the outlying of Dej city is water making factory. It is known as the pulp and paper industry has been consuming much water. The simple process of paper making is almost the same as the method of Cailun who is the invitatory of paper in ancient China. In Dej paper making factory, the Kraft process is the main process applied in the paper production. The main chemicals are sodium hydroxide (NaOH) for pulping and chlorine for bleaching. The production of paper can be divided in seven steps: a. raw material selection and preparation; b. digestion; c. washing; d. bleaching; e. washing; f. refining or beating and g. paper making – as shown in scheme 1. This paper making unit (g) consists of many unit operations such as: sheet forming, transferring, pressing, and drying. Finally is obtained the paper.

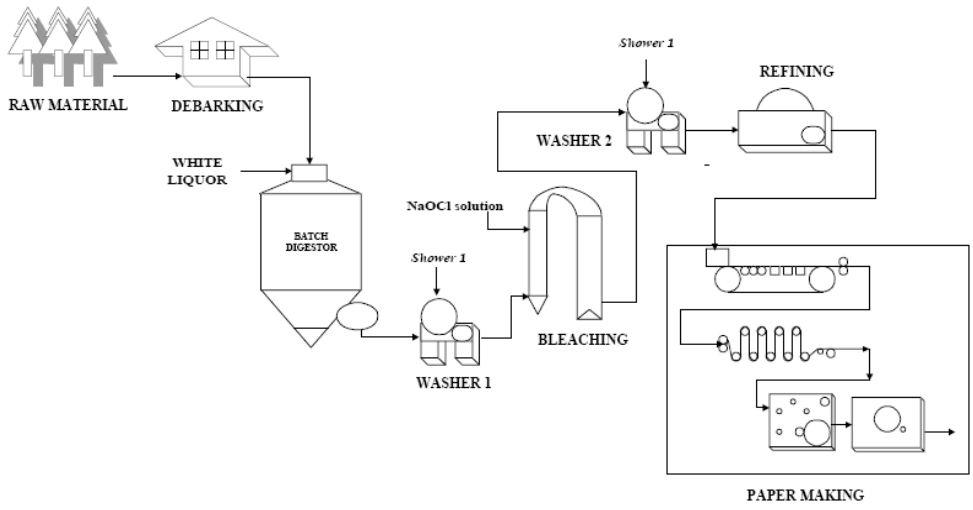

Scheme 1

RESULTS AND DISCUSSION

Organochlorine are organic compounds and from it class make part chlorinated solvents. Some of chlorinated solvents are volatile organic compounds. The most common organochlorine and chlorinated solvents founded in Somes river water were: carbon tetrachloride, 1,2-dichloroethane, 1,1-dichloroethylene, cis-1,2-dichloroethylene, trans-1,2-dichloroethylene, methylene chloride, tetrachloroethylene, 1,1,1-trichloroethane, trichloroethylene, vinyl chloride and chloroform, dichlorobromomethane, dibromochloromethane.

Chlorinated solvents are widely used in industry such as in the paper making factory and also in common household products. These chemicals are used as degreasing fluids for many different purposes such as dry-cleaning clothes, de-caffeinate coffee, cleaning metal machinery, dissolving grease build up in septic tanks and in making paper industry.

Because some of the organochlorine compounds are volatile organic compounds (VOCs) they can move easily through the environment. If improperly discarded onto the ground, these chemicals can travel downward through the soil and eventually end up in the groundwater. Organochlorine compounds such as chloroform, trichloroethylene or tetrachloroethene are not usually found in river water because they tend to evaporate from the water into the air but they can appear in river just if exist a source of man made pollution. Even that in all sample collected from Somes River was found such of kind's organochlorine compounds and in the high concentration level. That could de explain by the fact that near the Somes River outlying Dej district is located the paper factory where in the paper making process is used high amount of chlorine based solvents. Actually in the bleaching steps from the paper making process – where the purposes of this process are to whiten the pulps is used high amount of organochlorine solvents. In that process unbleached pulps are loaded to the bleaching tanks (see scheme 1), the common bleaching chemicals used normally are sodium hypochlorite or calcium hypochlorite. Also in the washing steps the bleacher bark is transferred to the concrete tanks for washing. This washing steps in performed 2 - 5 times or until the smell of chlorine disappears. The factory evacuates that water in Somes River. It was observed that after the closing of factory for two weeks the concentration level of these compounds started to decreased – table1.

When the factory was closed organochlorine compounds concentration was followed every day in the water sample during October. In the middle of the month the factory was closed (in 15 October the factory was closed to 28 October when the factory was opened again). Our measurement show that the concentration for the followed compounds started to decreased after the factory was closed. Before the concentration for chloroform was between 65 – 85 μg/l and after that the factory was closed the concentration was between 35 – 55 μg/l – see figure 1. The same situation was observed for trichloroethylene and tetrachloroethene, their concentration decreasing with 30 -50 %, after that the factory was closed.

Table 1. Chloroform and trichloroethylene concentration variation when factory are working on and after that the factory was closed

Observation	Data of sampling	$CHCl_3$ μg L^{-1}	C_2HCl_3 μg L^{-1}
Factory on working	1	77.42	66.79
	2	78.65	48.59
	3	68.88	56.73
	4	61.26	50.12
	5	65.94	55.08
	6	66.05	57.49
	7	71.19	49.37
	8	79.05	69.28
	9	78.01	66.35
	10	79.53	68.11
	11	80.42	52.94
	12	86.79	48.97
	13	88.29	54.26
	14	87.41	54.92
	15	85.23	51.05
Factory are closed	16	76.48	44.11
	17	68.99	42.68
	18	60.27	35.16
	19	54.29	29
	20	59	11.59
	21	53.84	24.61
	22	54.59	30.94
	23	58.93	22
	24	49.02	21.54
	25	52.61	13.98
	26	43.27	10
	27	38.75	14.29

It is known that are several natural sources that may contribute significantly to the chlorocarbons in the environment [8]. For example chloroform is a major contributor to natural gaseous chlorine. It was found to be emitted by several anthropogenic and natural sources including the terrestrial areas. The origin of chloroform in the terrestrial environment can be anthropogenic point sources, atmospheric deposition, released by vegetation and production directly in the soil. Among terrestrial sources, forest has recently been identified as contributing to the release of chloroform into the environment [9]. But in our case it was found that the major chlorinated compounds detected in the Somes river are industrial origin alone, once due the factory that evacuate the dirty used water directly in the river and on the other hand due to atmospheric pollution that is an important source of contamination of surface water and soil by rain [9].

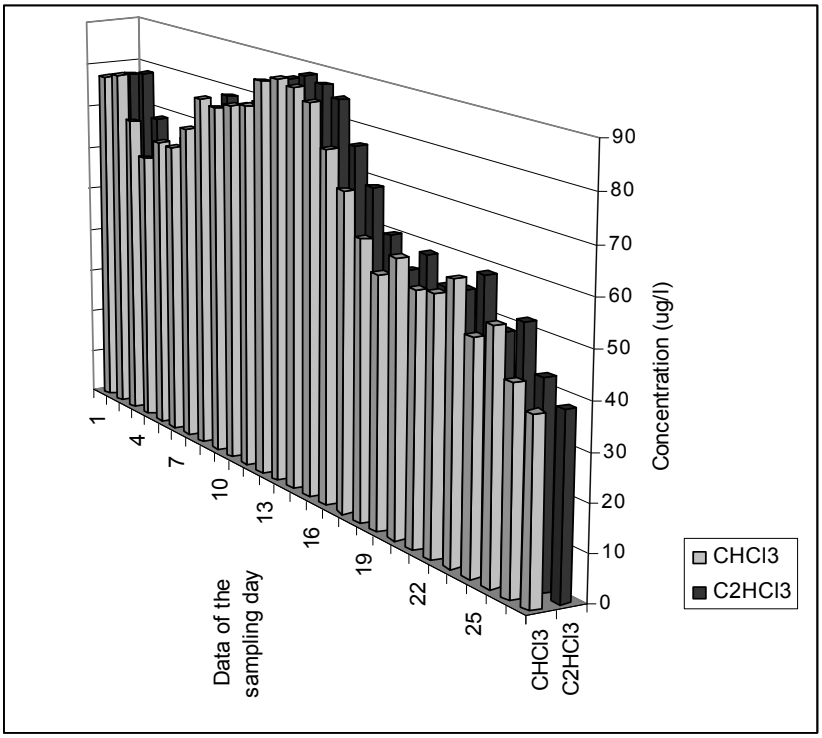

Figure 1. Trichloroethylene (C_2HCl_3) concentration (µg L^{-1}) and $CHCl_3$ concentration (µg L^{-1}) measured in Somes river water sample in October when the paper factory was working and after that the factory was closed.

In analysis of the water sample and soil sample the main found organochlorine were chloroform, TCE and PCE (see table 2 and 3). The presence of chloroform in terrestrial natural sources is still poorly investigated.

Table 2. Chloroform, trichloroethene and tetrachloroethene concentration value (µg/l) during May – October 2007 from soil sample from Dej sampling point.

Month	Chloroform (µg/l)	Trichloroethylene (µg/l)	Tetrachloroethylene (µg/l)
May	57.92	36.09	27.66
June	66.29	33.26	54.37
July	79.5	52.1	76.28
August	86.22	44.68	69.45
September	74.92	43.95	35.82
October	43.95	29.41	39

Table 3. Chloroform, trichloroethylene and tetrachloroethene concentration value (μg/l) during May – October 2007 from raw water sample.

Month	Chloroform (μg/l)	Trichloroethylene (μg/l)	Tetrachloroethylene (μg/l)
May	22.14	25.09	18.26
June	15.92	28.71	34.08
July	28.34	18.44	42.08
August	19.05	37.09	44.51
September	11.53	28.69	27.63
October	14.02	19.48	20.49

The formation and emission of chloroform by forest soil and observed large variation seen between sampling areas to the question of whether a seasonal variation exist (see figure 2 and 3). This may be expected if the production is biologically catalyzed.

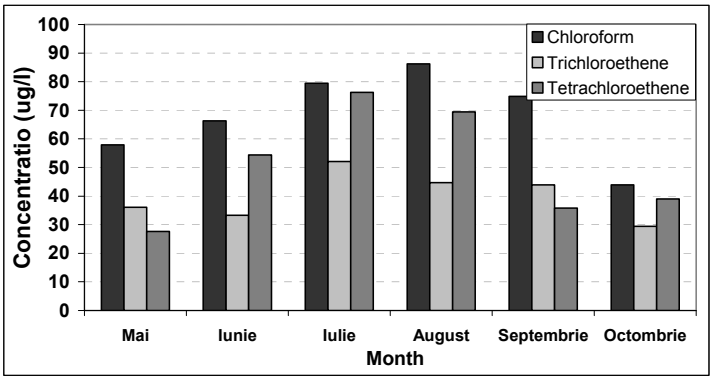

Figure 2. Chloroform, trichloroethene and tetrachloroethene variation during May – October 2007 from soil sample.

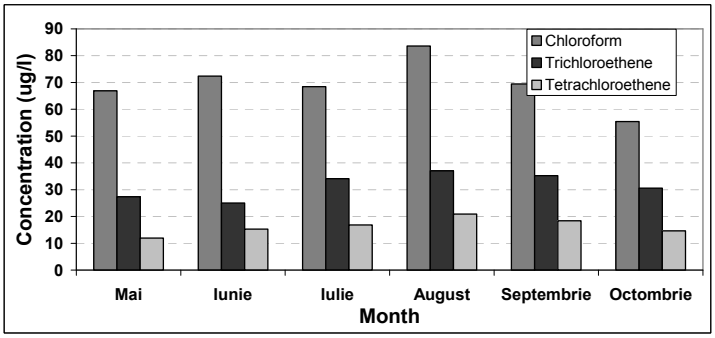

Figure 3. Chloroform, trichloroethene and tetrachloroethene variation during May – October 2007 from surface water sample.

CONCLUSIONS

The measurements of the Somes river water samples have shown that the industrial pollution is the most important sources of the chloroform, trichloroethylene and tetrachloroethene in the environment.

The major identified organocglorine compounds in the water and soil sample was chloroform, trichloroethen and tetrachloroethene. The presence of TCE and PCE can be explained by human hand made pollution of the environmental especially in Dej city where in the sample were measured higher concentration of this compounds. That could be caused from the factory that leased the used water in the Somes River. Also they used in their work process substances like TCE and $CHCl_3$. But also the natural source for chloroform exists and makes a contribution to the global sources. While chloroform alone may play a minor role in the global chlorine cycle, it may play be worth considering more seriously when taken together with other naturally – produced chlorocarbons. During the different month it was observed a highly seasonally variability for that compounds. That can be explaining by the fact that when the temperature increases, reaction is faster. In the winter months it is wait to be less concentration of these compounds because in some case ice cover protects surface of raw water and soil, and in that case the concentration of TCE, PCE and $CHCl_3$ found in nature due to their anthropogenic source are lower due to lower temperature and natural organic matter.

Also the results have shown that the concentration measured for the chloroform, trichloroethylene and tetrachloroethene was high in the period when the factory was on working. After that the factory was shot down the concentration for the followed compounds start to decrease. The difference between the concentration measured in the period of function of factory and in the period when the factory was close is high (almost 50%) – see figure 1. The major pollution of the soil and waste water is due to the paper factory.

EXPERIMENTAL SECTION

Water samples: were collected in 40 mL screw cap glass vials equipped with PTFE-faced single use septa. Prior to use the vials were washed with hot soapy water then rinse thoroughly with ultrapure water. After that, all cleaned vials were dry at 200 °C for 6 – 10 hours in an oven. All water samples were collected in duplicate and preserved. Phosphate buffer were used to inhibit base catalyzed degradation of some chlorinated solvents and to standardize the pH of all samples. The buffer were prepared as a dry homogenous mixture of 1 % Na_2HPO_4/99 % KH_2PO_4, from that mixture 0.8 g were add to all 40 mL vials before sampling. Water sample or extract were store at 4 °C in a freezer until the analysis. All extracts of the samples were analyzed within 14 days after sampling. The primary dilution standard

was prepared in 50 mL buffered reagent water, from it 500 μL with acetone were add in a 50 mL volumetric flask. This yields a final concentration in water of 10 μg/L and this solution were fortified into the aqueous sample prior to extraction. The chlorinated solvents were extracted from water samples with MTBE (high purity) after addition of surrogate analyte fortification solution. 10 g NaCl were add to the water sample before extraction. The NaCl/MTBE/water sample mixture was shaking vigorously and consistently by hand. After that the separator funnel was invert for 3-5 minutes to allow the water and MTBE phases to separate. 1 mL from the solvent phase was transferred to analysis vial and it analysis was done on gas chromatography equipped with an electron capture detector (GC-ECD) and splitless injector. The column used for analysis was Trace TR-V1 cyanopropylphenyl based phase, 30 mm x 0.53 mm ID x 3.0 μm film and with temperature program 40 °C (hold time 7 minutes), 2 °C/minutes to 80 °C (hold time 3 minutes), 7 °C/minutes to 120 °C (hold time 2 minutes), 15 °C/minutes to 180 °C (hold time 10 minutes).

The *soil samples* (25 g) were centrufugated for 5 minutes at 3000 rpm to remove the excess water. The samples were wetted with 30 mL MeOH/Acetone. The extraction was done with hexane (50 mL) with 20 mL MeOH/Acetone and was shaken manual for 30 minutes at room temperature. The extractions were repeated tree times with hexane.

Identification of the compounds was confirmed by a quadrupole mass spectrometer (DSQ II MS - Termo Electron Corporation) coupled to gas chromatograph (GC) with a split/splitless injector, using the Selective Ion Monitoring (SIM) modality. Cromatographyc separation on GC-MS was achieved using TR-5MS, 5% Phenyl (equiv) Polysilphenylene-siloxane column (Thermo Finnegan, USA). The operation condition is shown in table 4. All injection was done with TriPlus HS autosampler. It working condition are presented in table 4. Quantification was performed using the standard stock solution for organochlorine compounds and based on peak area.

Table 4. GC – ECD, MS-GC and TriPlus HS operation conditions.

MS - GC
Carrier gas flow: helium (He_2) 10 mL min^{-1}
Split ratio: splitless
Injector temperature: 200^0C
Detector temperature: 300^0C
Oven temperature: 40^0C (hold time 7 minutes), 2^0C/minutes to 80^0C (hold time 3 minutes), 7^0C/minutes to 120^0C (hold time 2 minutes), 15^0C/minutes to 180^0C (hold time 10 minutes)
Solvent delay: 1.5 minutes
MS scan program: 40 – 750 m/z
Ionization: 70 eV electron impact

GC - ECD
Carrier gas flow: nitrogen (N_2) 30 mL min^{-1} Make up: nitrogen (N_2) 30 mL min^{-1} Split ratio: 1:5 Injector temperature: 200^0C Detector temperature: 300^0C Oven temperature: 35^0C (hold time 3 minutes), 15^0C/minutes to 200^0C (hold time 3 minutes)
TriPlus HS
Incubation time: 45 min Incubation mode: constant Agitator temperature: 60^0C Agitator on – 20 sec/ Agitator off – 20 sec Syringe temperature: 80^0C Injection depth: 35 mm Injection speed: 40 mL/min Filling volume: 1.2 mL Filling counts: 1 /Filling delay: 0 sec Post injection syringe flush: 30 sec

The organochlorine compounds after analysis were shown in chromatograms obtain after the water sample analysis on GC-MS – see figure 4.

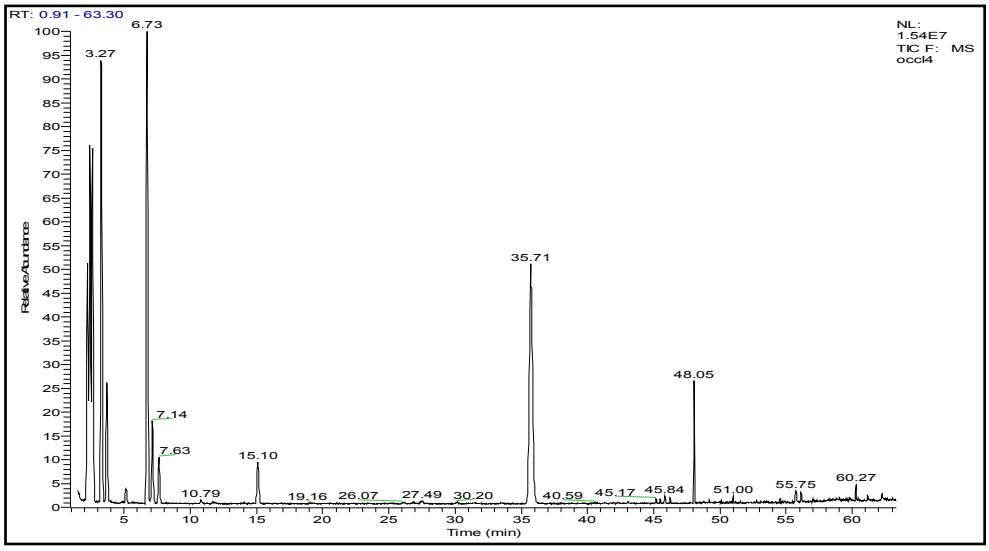

Figure 4. Chromatogram obtained after analysis of water sample on GC-MS with SIM method.

REFERENCES

1. A. Blair, P. Hartage, P.A. Stewart, M. McAdams, J. Lubin, *J. of Occupational Environmental Medicine*, **1998**, *55*, 161.
2. G.C. Windham, D. Shusterman, S.H. Swan L. Fenster, B. Eskenazi, *American Journal of Industrial Medicine,* **1991**, *20*, 241.
3. M. Sallmwn, M-L. Lindbohm, P, Kyyronen, *American Journal of Industrial Medicine*, **1995**, *27*, 699-713.
4. D. H. Garabrant, J.V. Lacey, T.J. Laing, B.W. Gillespie, M.D. Mayes, B.C. Cooper, D. Schottenfeld, *American Journal of Epidemiology*, **1999**, *157* (6), 493.
5. M. Dosemeci, P. Cocco, W.H. Chow, *American Journal of Industrial Medicine,* **1999**, *36*, 54.
6. E.F. Heihneman, P. Cocco, R.M. GOMEZ, M. DOSEMECI, P.A. STEWART, R.B. Hayes, S.H. Zahm, T.L. Thomas, A. Blair, *American Journal of Industrial Medicine*, **1994**, *26*, 155.
7. A. Anttila, E. Pukkala, M. Sallmen, S. Hernberg, K. Henminki, *J. of Occupational Environmental Medicine*, **1995**, *37* (7), 797.
8. G.W. Gibbs, J. Amsel, K. Soden, *J. of Occupational Environmental Medicine*, **1996**, *38*, 693.
9. S. F. Lanes, K. J. Rothman, N. A. Dreyer K. J. Soden, *Scandinavian Journal of Work, Environment and Health*, **1993**, *19*, 426.

STUDIA UNIVERSITATIS BABEŞ-BOLYAI, CHEMIA, LIV, 4, 2009

KINETIC MODEL FOR CHLORINE DECAY AND DISINFECTION BY-PRODUCTS FORMATION USING ABTS METHOD AND DPD METHOD

KOVACS MELINDA HAYDEE[a], DUMITRU RISTOIU[a], SIDONIA VANCEA[b], LUMINIȚA SILAGHI-DUMITRESCU[c]

ABSTRACT. The kinetics of chlorine decay of the pre-treated water collected once a month from the Gilau Water Treatment Plant after one of the sand filters was investigated. The chlorine species reacts with ABTS (2,2-azino-bis(3-ethylbenzothiazoline)-6-sulfonicacid-diamonium salt) to yield a green colour product that is measured at 405 nm wavelength with a spectrophotometer. The second method used for the investigation of chlorine consumption was by means of DPD (N,N-diethyl-p-phenylenediamine), where chlorine oxidizes DPD which takes on a red colour. The absorption is measured with a spectrophotometer at a wavelength of 515 nm. Both methods are useful for the determination of chlorine consumption in the treated water from distribution systems.

Keywords: Disinfection by-products, ABTS method, Chlorine consumption, THM formation.

INTRODUCTION

Chlorine is mostly used in water treatment plants from Romania for water disinfection. The regulation and monitoring of disinfection by-products has become a current issue after Romania's entry to the UE and after many previous studies have shown the possible adverse health effects on humans of this compounds [1, 2]. Their formation in treated water depends by the type of disinfection process and the type of disinfectant agent that is used.

Chlorine's popularity is not only due to lower cost, but also to its higher oxidizing potential which provides a minimum level of residual chlorine throughout the distribution systems and protects against microbial recontamination [2, 3]. For that, over of many years, chlorine became the most popular disinfecting agent due to its ability to kill most pathogens. In 1974 was finding that after adding of chlorine to water in order to disinfect it, this resulted the formation of compounds such as chloroform (one of the component of trihalomethanes class) due to

[a] *Babes Bolyai University of Cluj-Napoca, Faculty of Environmental Science, Str. P-ta Stefan cel Mare, no.4, 400084, Cluj-Napoca*
[b] *Garda de Mediu, Comisariatul Judetean Cluj, str. G-ral T. Mosoiu, nr. 49, Cluj-Napoca, Romania*
[c] *Universitatea Babeş-Bolyai, Facultatea de Chimie, str. Arany Janos, nr.11, 400068, Cluj-Napoca, Cluj-Napoca*

reaction of chlorine with the organics present in the water. After then hundreds of additional disinfection by-products have been identified including haloacetic acids and haloacetonitriles [4, 5]

Trihalomethanes (THMs) is the class of disinfection by-products that are most identified in treated water. Usually chloroform is the most commonly THMs compound in drinking water and it is present in the highest concentration.

Many parameters have an important influence on the formation of THMs. Previous research studies have shown that the major variables that affect THM formation are chlorine dose, concentration and nature of natural organic matter, contact time, pH, temperature of water and the presence of inorganic ions like bromide [3, 4].

The major factor that influence the THMs formation is the organic matter present in water supplies, they reacts with chlorine and leads to the formation of THMs. The type and characteristics of organic precursors directly affect the formation of THMs. Naturally occurring humic and fulvic substances which constitute a large fraction of the organic matter in water are the major THMs precursors [6]. Increase of chlorine dose has been reported to have positive influence of disinfection by-products yield. The same is true for increased concentrations of natural organic matter and increased temperature. The presence of bromine ions shifts the speciation of disinfection by-products to more brominated analogues, while increased pH can enhance the formation of some categories of disinfection by-products, ex. THMs and inhibits the formation of some others, ex. haloacetonitriles and haloketones [3]. Higher THM concentrations are expected at higher levels of the above mentioned parameters [7,8].

RESULTS AND DISCUSSION

Total chlorine (including all species: $HOCl$, NH_2Cl, ClO_2 and ClO_2^- react rapidlly with ABTS or DPD and it is impossible to have a distinction between the different species (relations 1, 2):

$$ClO_2 + ABTS + 2\,H^+ \rightarrow ClO^- + ABTS^+ \quad (1)$$

$$ClO_2^- + 4\,ABTS + 4\,H^+ \rightarrow Cl^- + 4\,ABTS^+ + 2\,H_2O \quad (2)$$

To determine NH_2Cl both HOCl and ClO_2 are destroyed by the addition of nitrite prior to ABTS addition. Nitrite rapidly reacts with ClO_2 and HOCl but only slowly with NH_2Cl. Nitrite does not react with ABTS and does not interfere in the determination of NH_2Cl fraction [6, 7, 8]. Four minutes are sufficient for a complete destruction of ClO_2 and HOCl. The concentration of free chlorine is calculated by subtracting monochloramine from total available chlorine fraction. Table 1. shows the concentration ($mg \cdot L^{-1}$) obtained for total chlorine, free chlorine and NH_2Cl in laboratory kinetic experiments with both methods: ABTS and DPD.

It is observed a slightly small difference between the results.

Table 1. Comparison between results obtained with ABTS and DPD method for determination of total chlorine, free chlorine and NH_2Cl.

Time (minutes)	ABTS method			DPD method		
	Total chlorine (mg/l)	Free chlorine (mg/l)	NH_2Cl (mg/l)	Total chlorine (mg/l)	Free chlorine (mg/l)	NH_2Cl (mg/l)
0.333	1.62	1.6	0.03	1.73	1.68	0.04
0.666	1.32	1.2	0.06	1.35	1.26	0.08
1	1.26	1.2	0.07	1.29	1.24	0.10
3	1.1	1	0.07	1.14	1. 7	0.11
6	0.92	0.8	0.12	0.98	0.84	0.15
15	0.81	0.5	0.21	0.85	0.67	0.28
40	0.7	0.4	0.21	0.74	0.55	0.23
60	0.62	0.36	0.17	0.68	0.39	0.19
90	0.56	0.3	0.17	0.60	0.37	0.17
120	0.52	0.3	0.17	0.54	0.34	0.16
240	0.46	0.28	0.14	0.48	0.29	0.13
600	0.26	0.2	0.08	0.29	0.22	0.06
690	0.19	0.14	0.06	0.23	0.18	0.05
780	0.12	0.1	0.04	0.15	0.13	0.04

The advantages of these methods are:

- they are easy to use and can determine with a high precision the total chlorine, free chlorine and NH_2Cl concentration.
- can help us to try to predict the potential formation of chlorination by-products, such as trihalomethanes – see figure 1.
- help in the prediction of chloroform formation in the distribution system if we respect the water condition (Chlorine dose, pH, temperature).

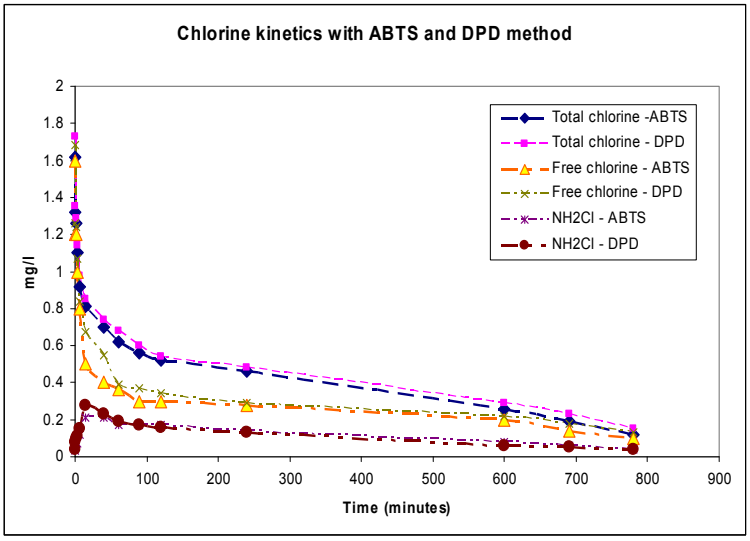

Figure 1. Total Cl_2 and NH_2Cl concentration vs. reaction time for both methods (ABTS and DPD).

In figure 2.a., is shown the result of chlorine kinetics experiment in laboratory and in figure 1.b., is shown the chloroform kinetics formation obtained from chlorine kinetics experiment. At each desired reaction time, in the water sample was injected thiosulfate solution to quench chlorine and stop the THM formation.

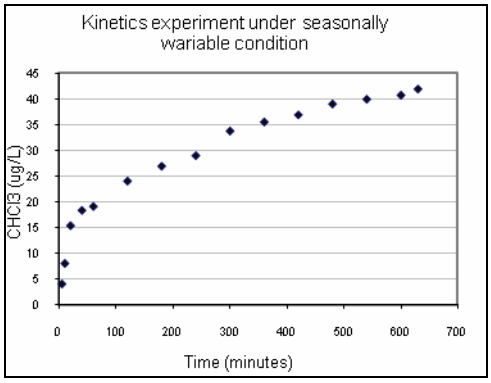

Figure 2.a.: represent the chlorine kinetics experiment (total chlorine kinetics, free chlorine and NH_2Cl kinetics.

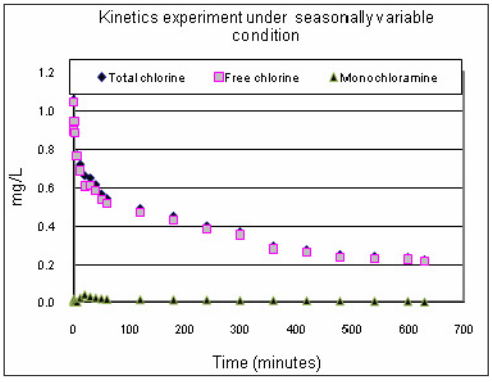

Figure 2.b.: Show the chloroform formation kinetics from experiments.

To assess the possibility to simulate the THM formation in the distribution system, $CHCl_3$ formed in laboratory experiments was compared with $CHCl_3$ concentration measured in the distribution system on the sampling day – see table 2.

Table 2. Chloroform formation in laboratory experiment and the chloroform value measured in the sampling point.

Sampling point	Chloroform concentration ($\mu g \cdot L^{-1}$) in water sample taken from Gilau Water Treatment Plant – Cluj (a) and chloroform ($\mu g \cdot L^{-1}$) concentration obtained in laboratory experiment (b) for different month									
	1a	**1b**	**2a**	**2b**	**3a**	**3b**	**4a**	**4b**	**5a**	**5b**
A	0.6		0		0		0		0	
B	4.9	2.1	0	0	0	0	0	0	0	0
C	12.4	13.2	8.4	7.8	2.22	3.8	8.09	7.9	8.22	7.9
D	18.7	19.1	47.7	50.1	9.34	11.0	16.71	15.98	20.81	21.14
E	28.4	29.6	47.0	49.3	6.36	7.8	18.70	19.03	29.26	30.06
F	35.2	36.6	66.9	70.4	27.77	26.8	18.99	19.8	27.12	28.24
G	37.1	38.3	66.6	69.3	21.08	20.9	20.90	21.14	32.41	33.56
H	23.2	24.8	71.1	72.8	28.17	29.3	21.60	22.05	33.86	34.09

The sampling was started from Gilau water treatment plant to distribution system in Cluj Napoca (A – raw water, B – filtrated water, C – exit reservoir, D – Sapca Verde, E – Beer factory, F – Chemistry faculty, G – Environmental

science faculty, H – Institute of public health) in different month (1a –$CHCl_3$ concentration in July in the water take from sampling point, 1b – $CHCl_3$ concentration in July in laboratory kinetics experiment which correspond in time with the water that arrived to the sampling point; the same is for 2a and 2b but for September water sample; 3a, 3b – December; 4a, 4b – March; 5a, 5b - May).

CONCLUSIONS

Both colorimetric methods are easy to use and give precise results. The difference between the two different methods was very small (3 %). The difference between ABTS and DPD method is, ABTS method is easier to apply in comparison with DPD for a long experiment like a kinetics experiment.

The two methods give really information between the chlorine consumption and the $CHCl_3$ formation. That helps us in the future to make the prediction of total THMs formation. The results of measured THMs show that $CHCl_3$ is the main THMs formed in distribution system and its amount is in the range 0.6 – 73 $\mu g \cdot L^{-1}$, value that is under the maximum permissible level according to the EU drinking water safety regulation.

EXPERIMENTAL SECTION

Sampling: Pre-treated water was collected at the treatment plant after one of the sand filters once a month and stored in 5 L plastic bottles at 4 ^0C until the chlorination experiments. pH and water temperature were measured at the sampling site when the sample were taken.

Reagents: $NaNO_2$, NaB_7O_5 and $Na_2S_2O_3$ were purchased from Reactivul Bucuresti (Bucharest, Romania). KI (purissim p.a.) was purchased from Merk (Darmstadt, Germany). NaH_2PO_4 used was from BPH Chemicals (Poole, England). ABTS (2,2-azino-bis(3-ethylbenzothiazoline)-6-sulfonicacid-diamonium salt) was purchased from Fluka (Buchs, Switzerland). DPD (N,N-diethyl-p-phenylenediamine) was taking from Merk (Darmstadt, Germany). Aqueous chlorine dilution was prepared from a chlorine solution for cleaning purposes (2-5 %, Sun Industries, Ilfov, Romania). NaOH, H_2SO_4 and KIO_3 were purchased from Fluka (Buchs, Switzerland).

Chlorine experiments: The chlorine dose in the water treatment plant from Gilau (where was collected the filtrated water) is regulated manually to achieve a free chlorine concentration at the exit reservoir (where the water arrives approximately 15 minutes after chlorination) of 0.5 – 0.7 $mg \cdot L^{-1}$ Cl_2 in winter and 0.7 – 0.9 $mg \cdot L^{-1}$ Cl_2 in summer. Chlorination experiments were carried out monthly with raw water collected at the treatment plant after one of the sand filters. To assess the influence of the seasonal variances in the water matrix, kinetic experiments with filtrated water will be performed monthly under the two conditions.

The experiments were conducted under two conditions:

- *Base line conditions* (pH 7, 21^{0}C, 2.5 mg/l Cl_2) to gain information about the change of the organic matter in the raw water, and seasonally variable conditions to simulate the actual process at the treatment plant.
- Experiments under *seasonally variable conditions* were carried out with pH and temperature as measured in the pretreated water on the sampling day and an initial chlorine dose according to a free chlorine concentration after 15 minutes as prescribed in the guidelines of the water treatment plant.

The chlorine concentration was determined by the ABTS method at a wavelength of 405 nm and ε has a value of 28 500 M^{-1} cm^{-1} (see figure 3.a.), and also with DPD method at a wavelength of 515 nm (see figure 3.b.). In laboratory experiment the chlorine dose added to filtrate water was the same that in the sampling day, also the temperature and the pH. The kinetics experiment time was 13 hour (is the time for the water to arrive from Gilau water treatment plant to the centre of city). The THM samples taken from kinetics experiment were preserved with sodium thiosulfate. The experiment results in the first one will give information about the seasonal variance of NOM and its influence on the THM formation potential, while the second one is an attempt to simulate the conditions at the WTP which will give information about the actual process.

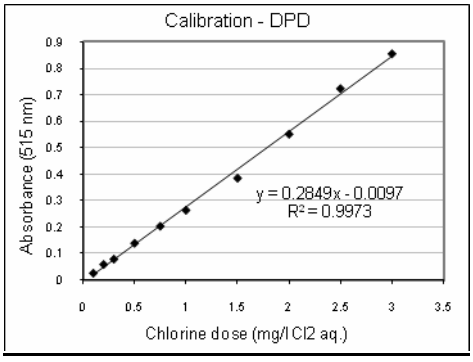

Figure 3.a.: Present the calibration curve of Cl_2 with DPD method.

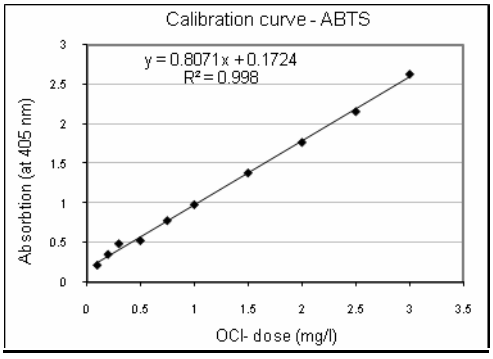

Figure 3.b.: Represent the calibration curve of OCl^- with ABTS method.

Monochloramine, total and free chlorine are measured with the ABTS method. Monochloramine and HOCl react with ABTS to a green coloured product, which can be measured at a wavelength of 405 nm.

Instrumental measurements: For the *kinetic studies* chlorine was measured colorimetrically according to standard method 8021 DPD method (powder pillow) for free chlorine determination and standard method 8167 DPD method (powder pillows) for total chlorine determination using a Hach Dr 2800 analyzer. A 25-ml cell was filled with samples and added DPD free chlorine reagent (powder pillow). After mixing, chlorine was read at a wavelength of 530 nm wavelength. Also, the chlorine concentration was determined by the ABTS method at a wavelength of 405 nm with a molar absorption coefficient ε of 28 500 M^{-1} cm^{-1}. Monochloramine, total and free chlorine are measured with the ABTS method. Monochloramine and HOCl react with ABTS to a green coloured product, which can be measured at a wavelength of 405 nm.

Trihalomethanes analysis: THMs were measured by a Thermo Finningan U.S. Trace GC Ultra gas chromatography system with an electron capture detector (GC-ECD) equipped with a TriPlus HS auto sampler. The analysis was made using headspace technique. 10 ml of sample was filled into 20 ml headspace vials and closed with Teflon lined screw caps. After that, the samples were equilibrated in an oven at 60^0C for 45 minutes. 1 ml of the headspace was then injected into the GC (Cyanopropylphenyl Polysiloxane column, 30 m x 53 mm, 3 μm film thickness, Thermo Finnigan, USA). The column program was 35^0C (hold time 3 minutes), 15^0C/minutes to 200^0C (hold time 3 minutes).

REFERENCES

1. USEPA, Toxicological review of Chloroform, **2001**, EPA /635/R-01/00.
2. WHO: Background document for development of WHO Guidelines for Drinking-water Quality, **2005**, WHO/SDE/WSH/ 05.08/64.
3. EU, Official Journal of the European Community, **1998**, L 330, Directive 98/83/Ec.
4. USEPA, National Primary drinking water Regulation: Disinfectants and Disinfection Byproducts, **1998**, Federal Register *63* (241): 69390-69476, 115.
5. WHO Guidelines for drinking water quqlity,Third edition, **2006**, 138.
6. U. Gunten, A. Driedjer, H. Gallard, E. Salhi, *Water Resources*, **2001**, *35*, 2095.
7. L. Clesceri, A. Greenberg, D. Eaton, *American Water Works Association*, **1999**,109.
8. U. Pinkernell, B. Nowark, H. Gallard, U. VonGunten, *Water Resources*, **2006**, *34*, 4343.

STUDIA UNIVERSITATIS BABEŞ-BOLYAI, CHEMIA, LIV, 4, 2009

OPTIMIZATION OF METHODS FOR THE DETERMINATION OF DISINFECTION BY-PRODUCTS IN DRINKING WATER

MELINDA HAYDEE KOVACS[a], DUMITRU RISTOIU[a]

ABSTRACT. Chlorination is the most widely disinfection process of drinking water in Romania. The goal of the water disinfection is to protect it in the distribution systems against microbial contamination and to prevent and control re-growth of microorganism in the distribution system. The presence of DBPs in drinking water is a matter of concern for human health and can also produce unpleasant organoleptic taste. Under Stage I of the Disinfectants/Disinfection By-products (D/DBP) Rule, USEPA sets maximum contaminant levels (MCLs) for total trihalomethanes (chloroform, bromodichloromethane, dibromochloromethane and bromoform) at 80 $\mu g \cdot L^{-1}$; for a total of five haloacetic acids (monochloroacetic, dichloroacetic, trichloroacetic, monobromoacetic and dibromoacetic acids) at 60 $\mu g \cdot L^{-1}$; for bromate at 10 $\mu g \cdot L^{-1}$ and for chlorite 1.0 $mg \cdot L^{-1}$. Other DBPs have been added to the US Environmental Protection Agency's Candidate Contamination List (CCL), which is the list from which future regulated drinking water compounds will be selected. In Europe, the 98/83/CEE Directive is less restrictive than that applied in the USA. The only DBPs that must be controlled are the four trihalomethanes, and their proposed maximum level being 100 $\mu g\ l^{-1}$. Due to the fact that their identification and quantization have become extremely important to drinking water companies in order to reduce or remove their presence, other analytical methods different from those proposed by U.S. EPA have been optimized and are now commented in this article.

Keywords: disinfection by-products, gas chromatography-electron capture detector, headspace extraction.

INTRODUCTION

A particularly significant group of water pollutants consists of volatile organic compounds (VOCs). This group includes compounds, which are insoluble or sparingly soluble in water, with boiling points up to 200 °C and molecular masses between 16 and 250 Dalton [1, 2]. The compounds vary greatly in their structures and properties, e.g. hydrocarbon halogen derivatives, aliphatic hydrocarbons, aromatic hydrocarbons, alcohols, ketones, esters, ethers, amines, phenols, etc [3]. Many of them are toxic or considered carcinogenic,

[a] *Babes Bolyai University of Cluj-Napoca, Faculty of Environmental Science, Str. Fantanele, no.30, 400294, Cluj-Napoca, email: haydee_kovacs@yahoo.com*

mutagenic or teratogenic [4]. VOCs group include also some disinfection by products. They appear after the reaction of disinfectant agent with organic matter from water.

In many state, like in Romania, chlorine is the most usually disinfectant agent use for water disinfection due to its ability to kill most pathogens. However, in 1974 it was discovered that the chlorination of drinking waters resulted in the production of trihalomethanes (THMs) due to reaction of chlorine with organics in the water [1]. Since 1980's THMs raised significant concern due to evidence of their adverse human health effects, in particular cancer and reproductive disorders [5, 6]. THMs are the organohalogen compounds that are most monitored by protection agencies from treated water. Usually chloroform is the THM most commonly found in drinking water and in most of case is present in the highest concentration [7].

In choosing an appropriate analytical procedure to analyze the DBPs from water sample, it must be taken into account are not only precision, accuracy, selectivity, detectability, and reproducibility, but also limiting the time, labour and other costs involved in the procedure. The aim is also to determine a number of components of various properties in a single analytical cycle [8]. Automation of analytical procedures and making field determinations possible is also of importance. Reduction in the use of solvents in the analytical procedure and to in the amount of environment-threatening waste produced is becoming essential [9].

RESULTS AND DISCUSSION

The THMs were extracted from water sample by two different procedures, one LLE and the second HSE. In that case of HSE, the head space devices is connected directly to gas chromatography (GC) coupled with ECD.

In the analysis of THMs samples using TriPlus HS auto sampler the four peaks belonging to the four THM compounds were well separated, see figure 1.

Accuracy (%) for the four THMs compounds were in the range of 0.0003 – 0.2634 % in case of HSE and in the range of 0.52 – 4.2 % for LLE. The accuracy was determinate for every THMs compounds on 7 different samples and for the follow concentration 1 $\mu g \cdot L^{-1}$, 10 $\mu g \cdot L^{-1}$ and 100 $\mu g \cdot L^{-1}$.

The detection limit (MDLs) for $CHCl_3$, $CHCl_2Br$, $CHClBr_2$ and $CHBr_3$ were 0.3, 0.2, 0.3 and 0.6 $\mu g \cdot L^{-1}$ respectively (n=7). The RSD of 1 $\mu g \cdot L^{-1}$, 20 $\mu g \cdot L^{-1}$ and 80 $\mu g \cdot L^{-1}$ spiked samples were between 0.05 – 3.7 % after HSE and between 2.1 – 6.4 % after LLE.

The results regarding the methods performance show us good values in case of HSE than in case of LLE. Also it can be observed that the precision increase using the TriPlus HS and the incubation with agitation. That permit a better separation of the THMs compounds by the sample matrix (see table 1). The recovery in the two cases for 1 $\mu g \cdot L^{-1}$, 20 $\mu g \cdot L^{-1}$, and 80 $\mu g \cdot L^{-1}$ are

in the range 93-120 % and also the limit of detection for THMs compounds were: $CHCl_3$ is 0.3 μg/l, $CHCl_2Br$ is 0.2 $\mu g \cdot L^{-1}$, $CHClBr_2$ is 0.3 $\mu g \cdot L^{-1}$ and $CHBr_3$ is 0.6 $\mu g \cdot L^{-1}$.

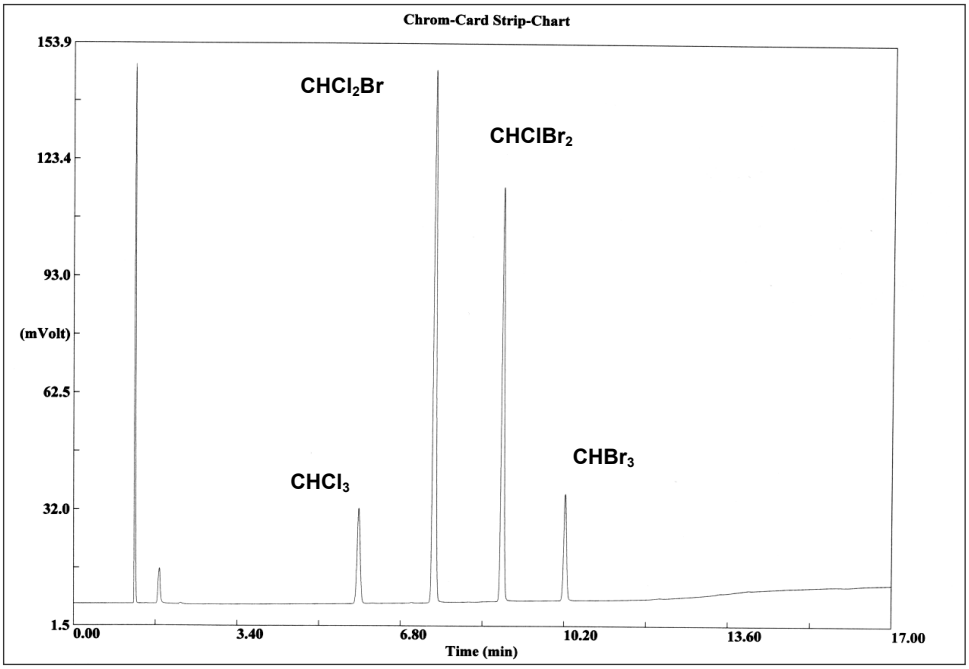

Figure 1. Chromatogram obtained after analysis of water sample – the four trihalomethanes compounds

Table 1. Relative standard deviation using the two procedures for the four THMs compounds analysis.

Compounds	TriPlus HS Autosampler		LLE Manually Injection	
	Relative standard deviation %		Relative standard deviation %	
	20 μg/l	***80 μg/l***	***20 μg/l***	***80 μg/l***
$CHCl_3$	1.43	1.17	2.05	1.91
$CHCl_2Br$	2.28	1.51	2.77	2.35
$CHClBr_2$	1.86	1.06	2.53	1.89
$CHBr_3$	2.40	1.92	3.21	2.97

CONCLUSIONS

The method of headspace extraction compared with liquid-liquid extraction has been presented in case of THMs analysis from water. HSE allows direct, trace analysis of components without disrupting the natural equilibrium established between the gas phase and the liquid phase of sample.

This method provides a better statistical accuracy. Collecting just the headspace eliminates the need to dispose of the liquid or solid sample. Present the best possible statistical accuracy. Using this method in analysis of disinfection by products on chromatography we obtain better sensitivity for THMs compounds and better statistical accuracy.

HSE sample preparation and analysis with GC-ECD can be used well for quantitative analysis of disinfection by products in environmental samples. Using it, for THMs were found good results for relative standard deviation, recovery and detection limit for each THMs compounds. Also the time necessary to perform the THMs analysis from water samples is less than in case of LLE.

EXPERIMENTAL SECTION

Sampling: Several treated and untreated water were collected in the period of January – December 2008 from Gilau and Dej Water Treatment Plant in every month. The collection and the preparation of water samples make up the most important element of every analytical procedure, which directly affects the quality and accuracy of final results. The basic problem is preserving the representative character (original composition) of the collected water sample to be analyzed in the laboratory avoiding positive deviations such as contamination under operation or negative deviation like losses of the target compounds. In order to avoid any possible contamination the sample were collected in duplicate in 40 mL vials that were previously cleaned with Millipore water and dried in oven at 150 °C for 10 hour. Also in order to keep out the possibility to miss of these compounds from our water sample all vials were full filed with sample and closed with Teflon lined screw cap. Because the THMs are formed after the reaction of chlorine with the natural organic matter present in water, every sample was preserved with sodium thiosulfate ($Na_2S_2O_3$) to quench residual chlorine. Samples were stored at 4 °C for a maximum 7 days until analysis.

Methods: Tree methods of extraction were used to determine the THMs presence in the water sample. These extraction methods were performed in order to compare these methods and to establish the most exactly and easily practicable method for analysis of these compounds. After extraction THMs were carried out by Thermo Finningan U.S.S. Trace GC Ultra gas chromatography with electron capture detector (GC-ECD). In case of head space analysis was used a TriPlus HS auto sampler.

Liquid-liquid extraction: The most commune extraction method for disinfection by-products is liquid-liquid extraction (LLE). After sampling, in laboratory 2 mL of hexane (extraction solvent) was added to ten mL of water sample in a separator funnel. The partitioning is then brought to equilibrium

by shaking the separator funnel for 5 minutes vigorously and allows it to stand. Then 1 µL of aliquot of the organic layer was removed with a microsyringe for gas chromatographic analysis.

Head-space extraction: One of the most common techniques used for the isolation of THMs from water samples is extraction into the gaseous phase. Headspace analysis techniques are based on the phenomenon of partition of analytes between the liquid and the gaseous phase. The gaseous phase (headspace) is analyzed together with the volatile compounds freed from the liquid sample (see Figure 2). In this figure is presented with G the gas phase (headspace) and with S the sample phase. The gas phase is commonly referred to as the headspace and lies above the condensed sample phase. The sample phase contains the compound(s) of interest. It is usually in the form of a liquid or solid in combination with a dilution solvent or a matrix modifier.

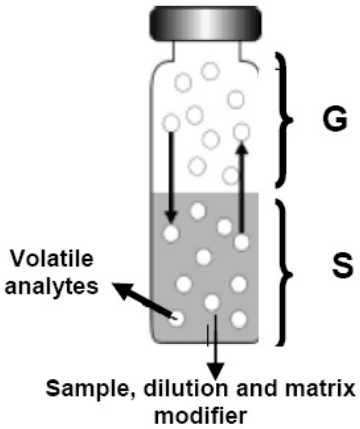

Figure 2. Schematic presentation of headspace process.

The equipment necessary for this type of analysis is very simple. The determination limit of the headspace analysis technique in a static system depends, besides the sensitivity of the detector employed, on the value of its coefficient of partition between the liquid and gaseous phase. For some compounds, the value of partition coefficient can be increased even by two orders of magnitude by varying temperature, pH, and salt effect (usually NaCl).

The analysis was made using headspace technique. 10 ml of sample was filled into 20 ml headspace vials and closed with Teflon lined screw cap. The agitator temperature was set at 60^0C, and the agitator on and the agitator off were set at 20 seconds and respectively 20 seconds. The incubation time was 30 minutes. Also the syringe was set at 80^0C. On GC the column

temperature program was 35^0C (hold time 3 minutes), 15^0C/minutes to 200^0C (hold time 3 minutes). The inlet was set at 200^0C. After this process 1 ml of the headspace was then injected into the GC (Cyanopropylphenyl Polysiloxane column, 30 m x 53 mm, 3 μm film thickness, Thermo Finnigan, USA). The column program was 35^0C (hold time 3 minutes), 15^0C/minutes to 200^0C (hold time 3 minutes). The inlet was set at 200^0C. In case of LLE extraction the same column and column program was used.

REFERENCES

1. H. A. Duong, M. Berg, M. H. Hoang, H.V. Pham, H. Gallard, W. Giger, U. Gunten, *Water Research*, **2003**, *37*, 3242.
2. J. Huang, C.G. Smith, *Journal of American Water Works Association*, **1984**, *76*(4) 168.
3. T.F. Marhaba, M.B. Washington, *Advances in Environmental Research*, **1998**, *2*, 103.
4. A.D. Nikolau, M.N. Kostopolou, T.D. Lekkas, *Global Nest: The International Journal,* **1999**, 1(3), 143.
5. USEPA, *Alternative Disinfectants and Oxidants Guidance Manual,* USEPA, **1999**, EPA 815-R-99-014.
6. USEPA, *National primary drinking water standards*, USEPA; **2001**, 816-F-01-007.
7. J.J. Rook, *Water Works Association*, **1976**, *68*(3), 168.
8. Standard Methods for the Examination of Water and Wastewater, 20th Edition, APHA, AWWA, WEF, **1998**, Washington DC, USA.
9. C. Vogt, S. Regli, *Journal of American Water Works Association*, **1981**, *73*(1), 33.

STUDIA UNIVERSITATIS BABEŞ-BOLYAI, CHEMIA, LIV, 4, 2009

SYNTHESIS AND STRUCTURAL ANALYSIS OF SOME NEW STERICALLY HINDERED DIENES

FLAVIA PIRON[a], ELENA BOGDAN[a], CRINA CISMAŞ[a], ANAMARIA TEREC[a], ION GROSU[a]

ABSTRACT. The good yields synthesis of some new tetrabromo and tetraiodo dienes obtained via the Hay homo coupling reaction of two polyethyleneoxy terminal alkynes and the structural investigations on these sterically hindered compounds are reported.

Keywords: dienes, axial chirality, atropenantiomers, coupling reactions, diynes

INTRODUCTION

Compounds with axial chirality are of high interest in the field of chiral catalysts and chiral discriminators. Many biphenyl and binaphtyl derivatives [1] are commercially available as single enantiomers.

Besides the very well known atropenantiomeric compounds with biaryl units many other unexpected compounds (e.g. styrenes I [2], 2-aryl,2-methyl-1,3-dioxanes II [3], *EE*-tetrahalogeno-1,3-butadienes III [4,5]; Scheme 1) exhibit axial chirality and atropenantiomers.

The atropisomers of *EE*-1,3-butadienes are due to the hindrance of the rotation around the formal simple bond C^2-C^3. These compounds prefer the conformation with perpendicular arrangement of the double bonds, which insures the highest distance between the large substituents at positions 2 and 3 (**III**, Scheme 1). The racemization of the atropenantiomers (*aR*⇆*aS*) occurs by the rotation of the molecule around the C^2-C^3 bond, via either the *s-trans* isomer (*transoid*) or the *s-cis* structure (*cisoid*) of the 1,3-butadiene core. The barrier via the *transoid* conformation is considerably lower and the compounds prefer this itinerary for the racemisation reaction.

The values of the barriers of racemization depend of X and R groups (named internal substituents). The reported barriers were measured either by dynamic NMR [6], DHPLC [4] or using polarimetry measurements [7]. The R^1 groups (named external substituents) are not involved directly in the hindrance of the rotation around the C^2-C^3 bonds, but if they are large they increase the barrier of rotation by the *buttressing* effect. [8]

[a] *Universitatea Babeş-Bolyai, Facultatea de Chimie şi Inginerie Chimică, Str. Kogălniceanu, Nr. 1, RO-400084 Cluj-Napoca,Romania, igrosu@chem.ubbcluj.ro*

We considered of interest to develop the investigations in the field of chiral dienes and to obtain new compounds exhibiting a tetrahalogeno-1,3-butadiene core, to determine their structure and to estimate the hindrance of the rotation around the formal simple bond of the 1,3-butadiene unit.

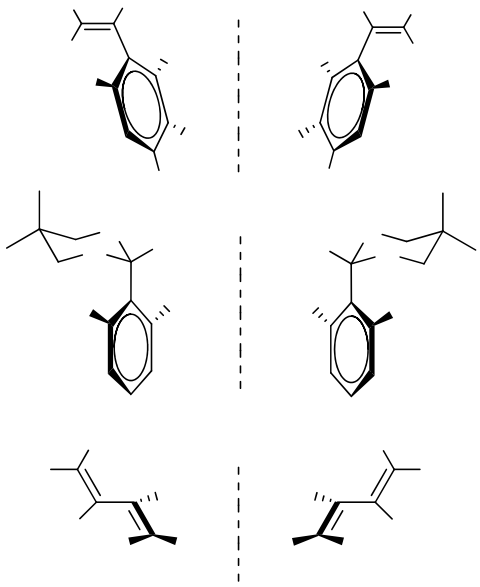

Scheme 1

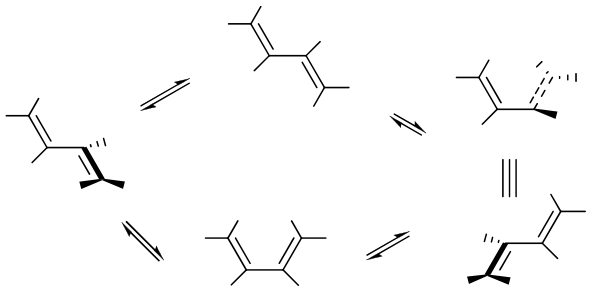

Scheme 2

RESULTS AND DISCUSSION

New tetrahalogeno dienes (**3**-**6**) were synthesized by halogen addition reactions to the corresponding diynes (**1** and **2;** Scheme 3). The reactions underwent stereoselectively with the formation of the *EE* isomers.

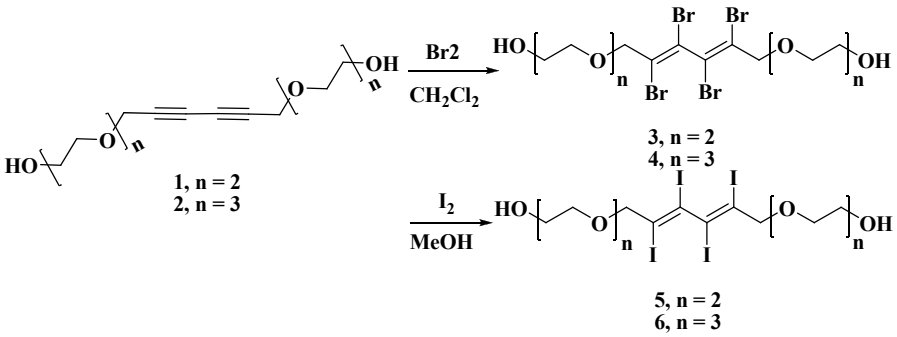

Scheme 3

Diynes **1** and **2** were synthesized by the coupling reaction of the monoalkyne alcohols **7** and **8** (Scheme 4) which were obtained by the reaction of the corresponding polyethyleneglycols (**9** and **10**) with propargyl bromide (Scheme 5). Even if compounds **7** and **8** are known [9] and their synthesis has been reported, they could be obtained in good yields only by adapting a procedure described in the literature for similar compounds [10].

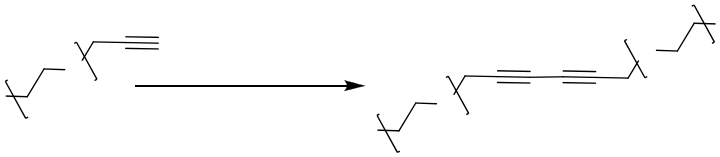

Scheme 4

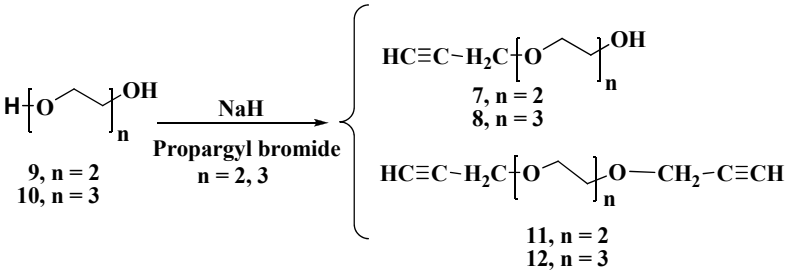

Scheme 5

The main product in the reaction of polyethyleneglycols with propargyl bromide is the monoalkyne, but the formation of dipropargyl derivatives **11** and **12** cannot be avoided. Diterminal diynes **11** and **12** were isolated but the yields in this case are poor. These diynes are interesting compounds and their good yields synthesis and structural investigations were reported in the literature [11].

Diyne **1** was reported by Wegner [12], but diyne 2 is a new compound.

The structural investigations on **3**-**6** were performed using NMR and LR ESI MS experiments.

The key signals in ^{1}H NMR spectra are those corresponding to the protons belonging to the CH_2 groups connected directly to the diene system (allylic positions). If the rotation of the 1,3-diene around the central simple bond is free the chirality of the system has no influence (an achiral average structure has to be considered) on the NMR signals and the ^{1}H NMR spectrum should show for the designed protons a singlet. If the rotation of the diene unit is hindered, the axial chirality of the molecule determines the diastereotopicity of the protons of the prochiral centers (CH_2 groups). In this situation the spectrum should exhibit two doublets (AB system) for the protons of the allyl CH_2 groups. The spectra for the investigated dienes (**3**-**6**) exhibit two doublets for the protons of the considered CH_2 groups (Figure 1, Table 1) proving the hindrance of the rotation in the diene unit.

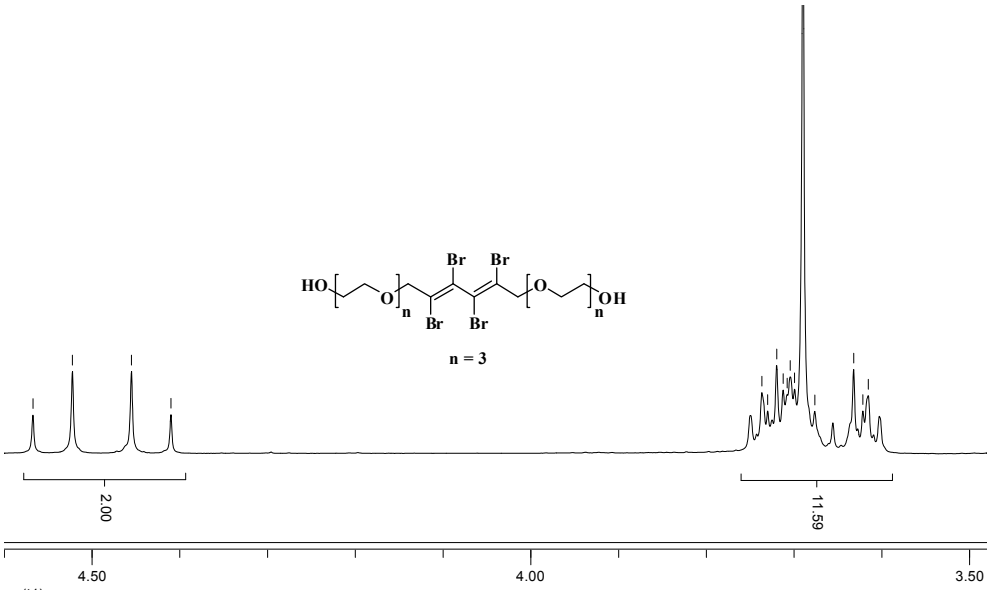

Figure 1. ^{1}H NMR spectrum ($CDCl_3$ rt,, fragment) of compound **4**

Table 1. Relevant NMR data for **3**-**6**

Compd.	δ (ppm)		Δδ (ppm)	*J* (Hz)
	-CX=CX-C*H*(H)-	-CX=CX-CH(*H*)-		
3	4.44	4.55	0.10	13.5
4	4.43	4.54	0.09	13.5
5	4.30	4.40	0.10	13.5
6	4.28	4.38	0.10	13.5

The spectrum of **4** run at *rt* (Figure 1) shows the two reference doublets at δ = 4.43; 4.53 ppm (J = 13.5 Hz), while the signals for the other protons of the CH_2 groups could not be assigned and they are all overlapped in the range 3.6-3.75 ppm. In the spectrum run at 60 °C no modification could be observed. This result is in agreement with the reported barriers for the racemization of other chiral tetrabromo $\Delta G^{\#}$ = 69.57±0.627 kJ/mol [5a] and tetraiodo $\Delta G^{\#}$ = 143 ± 1 kJ/mol [4] chiral dienes and reveals the high stability of the atropenantiomers of these compounds (the rotation in the diene unit is hindered at high temperatures, too).

CONCLUSIONS

Four new tetrahalogeno dienes with axial chirality were obtained in good yields and were investigated by NMR and ESI MS. The hindrance of the rotation in the diene unit and the high stability of the atropenantiomers of the compounds were also revealed. The high stability of the chiral unit located between two polyethylene glycol substituents recommend these compounds as useful building blocks for the obtaining of chiral host molecules.

EXPERIMENTAL SECTION

^{1}H NMR (300 MHz) and ^{13}C NMR (75 MHz) spectra were recorded in $CDCl_3$. LR ESI MS were recorded on ion trap spectrometer in positive mode. Melting points are uncorrected. Thin layer chromatography (TLC) was carried out on aluminium sheets coated with silica gel 60 F_{254} using UV and $KMnO_4$ visualization.

General procedure for the acetylenic coupling:

CuI (60 mmol) was added to a solution of alkynes **7** or **8** (3 mmol) in dry dichloromethane (200 mL) containing dry TMEDA (120 mmol). The reaction mixture was stirred for 1 hour under a stream of dry air. The mixture was then diluted with dichloromethane (100 ml) transferred into a separating funnel and washed with a solution of HCl 2M (2 x 30 ml) and then several times with water till the aqueous layer remains colourless. The organic layer was then separated, dried over Na_2SO_4 and evaporated. The final product was then purified by column chromatography (silica gel, diisopropylether/acetone 1/1).

3,6,13,16-tetraoxaoctadeca-8,10-diyne-1,18-diol (**1**) Colorless liquid, yield: 35% (300 mg); Calculated for $C_{14}H_{22}O_6$; C, 58.73; H, 7.74. Found: C, 58.89; H, 7.51. ^{1}H-NMR (300 MHz, $CDCl_3$) δ = 2.03 (2H, OH), 3.55-3.75 (m, 16H, 1-H, 2-H, 4-H, 5-H, 14-H, 15-H, 17-H, 18-H), 4.27 ppm (s, 4H, 7-H, 12-H); ^{13}C-NMR (75 MHz, $CDCl_3$) δ = 58.91 (7-C, 12-C), 61.70 (1-C, 18-C), 69.37, 70.13 (2-C, 4-C, 15-C, 17-C), 70.53 (9-C, 10-C), 72.47 (5-C, 14-C), 75.22 ppm (8-C, 11-C).

ESI-MS; m/z = 287.1 $[M+H]^+$, 309.1 $[M+Na]^+$.

3,6,9,16,19,22-hexaoxatetracosa-11,13-diyne-1,24-diol (**2**) Colorless liquid, yield: 33% (400 mg); Calculated for $C_{18}H_{30}O_8$; C, 57.74; H, 8.08. Found: C, 57.63; H, 8.28.^{1}H-NMR (300 MHz, $CDCl_3$) δ = 2.13 (2H, OH), 3.59-3.74 (m, 24H, 1-H, 2-H, 4-H, 5-H, 7-H, 8-H, 17-H, 18-H, 20-H, 21-H, 23-H, 24-H), 4.27 ppm (s, 4H, 10-H, 15-H); ^{13}C-NMR (75 MHz, $CDCl_3$) δ = 58.89 (10-C, 15-C), 61.69 (1-C, 24-C), 69.28, 70.24, 70.27, 70.60 (2-C, 4-C, 5-C, 7-C, 18-C, 20-C, 21-C, 23-C), 70.50 (12-C, 13-C), 72.51 (8-C, 17-C), 75.25 ppm (11-C, 14-C).
ESI-MS; m/z = 375.2 $[M+H]^+$, 397.2 $[M+Na]^+$.

General bromination procedure

To a solution of compounds **1** or **2** (0.26 mmol) in dichloromethane (20 ml), bromine (0.82 mmol, 130 mg solved in 1 ml dichloromethane) was added dropwise. The mixture was stirred at room temperature overnight, and at the end the organic phase was washed with a solution of sodium sulfite and then with water. After drying over sodium sulfate, the solvent was removed and the crude product was purified by column chromatography (silica gel, diisopropylether/acetone 1/1).

(8E,10E)-8,9,10,11-tetrabromo-3,6,13,16-tetraoxaoctadeca-8,10-diene-1,18-diol (**3**) Yellow liquid, yield: 47% (74 mg); Calculated for $C_{14}H_{22}Br_4O_6$; C, 27.75; H, 3.66; Br, 52.75. Found: C, 27.49; H, 3.78; Br, 52.91. ^{1}H-NMR (300 MHz, $CDCl_3$) δ = 1.88 (2H, OH), 3.61-3.76 (m, 16H, 1-H, 2-H, 4-H, 5-H, 14-H, 15-H, 17-H, 18-H), 4.44, (d, 2H, *J* = 13.5, 7-H, 12-H), 4.55 ppm (2d 2H, *J* = 13.5, 7'-H, 12'-H); ^{13}C-NMR (75 MHz, $CDCl_3$) δ = 61.79 (1-C, 18-C), 69.35, 70.18 (2-C, 4-C, 15-C, 17-C), 72.42 (5-C, 14-C), 73.06 (7-C, 12-C), 117.53 (8-C, 11-C), 124.79 ppm (9-C, 10-C).
ESI-MS; m/z (%) = 602.8 (21), 604.8 (79), 606.7 (100), 608.8 (66), 610.7 (16) $[M+H]^+$.

(11E,13E)-11,12,13,14-tetrabromo-3,6,9,16,19,22-hexaoxatetracosa-11,13-diene-1,24-diol (**4**) Yellow liquid, yield: 46% (85 mg); Calculated for $C_{18}H_{30}Br_4O_8$; C, 31.15; H, 4.36; Br, 46.05. Found: C, 31.44; H, 4.09; Br, 46.33. ^{1}H-NMR (300 MHz, $CDCl_3$) δ = 2.07 (2H, OH), 3.61-3.73 (m, 24H, 1-H, 2-H, 4-H, 5-H, 7-H, 8-H, 17-H, 18-H, 20-H, 21-H, 23-H, 24-H), 4.43, (d, 2H, *J* = 13.5, 10-H, 15-H), 4.54 ppm (d, 2H, *J* = 13.5, 10'-H, 15'-H); ^{13}C-NMR (75 MHz, $CDCl_3$) δ =61.75 (1-C, 24-C), 69.35, 70.29, 70.33, 70.67 (2-C, 4-C, 5-C, 7-C, 18-C, 20-C, 21-C, 23-C), 72.50 (8-C, 17-C), 73.09 (10-C, 15-C), 117.44 (11-C, 14-C), 124.85 (12-C, 13-C).
ESI-MS; m/z (%) = 690.9 (15), 692.9 (67), 694.9 (100), 696.8 (67), 698.8 (15) $[M+H]^+$.

General iodination procedure:

To a solution of compounds **1** or **2** (0.26 mmol) in methanol (10 ml), iodine (0.82 mmol) was added. The mixture was stirred at room temperature overnight, and at the end solvent was removed by low pressure evaporation.

Extraction was made with dichloromethane and was washed with water. After drying over sodium sulfate, the solvent was removed and the crude product was purified by column chromatography (silica gel, diisopropylether/ acetone 1/1).

(8E,10E)-8,9,10,11-tetraiodo-3,6,13,16-tetraoxaoctadeca-8,10-diene-1,18-diol (**5**) Red-brown liquid, yield: 40% (83 mg); Calculated for $C_{14}H_{22}I_4O_6$; C, 21.18; H, 2.79; I, 63.94. Found: C, 20.95; H, 2.93; I, 64.07. ^{1}H-NMR (300 MHz, $CDCl_3$) δ = 2.09 (2H, OH), 3.63-3.78 (m, 16H, 1-H, 2-H, 4-H, 5-H, 14-H, 15-H, 17-H, 18-H), 4.30, (d, 2H, *J* = 13.5, 7-H, 12-H), 4.40 ppm (d, 2H, *J* = 13.5, 7'-H, 12'-H); ^{13}C-NMR (75 MHz, $CDCl_3$) δ = 61.81 (1-C, 18-C), 69.27, 70.25 (2-C, 4-C, 15-C, 17-C), 72.40 (5-C, 14-C), 80.84 (7-C, 12-C), 97.08 (8-C, 11-C), 105.90 ppm (9-C, 10-C).

ESI-MS; m/z = 794.7 $[M+H]^+$, 816.7 $[M+Na]^+$.

(11E,13E)-11,12,13,14-tetraiodo-3,6,9,16,19,22-hexaoxatetracosa-11,13-diene-1,24-diol (**6**) Red-brown liquid, yield: 51% (120 mg); Calculated for $C_{18}H_{30}I_4O_8$; C, 24.51; H, 3.43; I, 57.55. Found: C, 24.44; H, 3.56; I, 57.74. ^{1}H-NMR (300 MHz, $CDCl_3$) δ = 1.86 (2H, OH), 3.61-3.74 (m, 24H, 1-H, 2-H, 4-H, 5-H, 7-H, 8-H, 17-H, 18-H, 20-H, 21-H, 23-H, 24-H), 4.28, (d, 2H, *J* = 13.5, 10-H, 15-H), 4.38 ppm (d, 2H, *J* = 13.5, 10'-H, 15'-H); ^{13}C-NMR (75 MHz, $CDCl_3$) δ =61.79 (1-C, 24-C), 69.30, 70.38, 70.73 (2-C, 4-C, 5-C, 7-C, 18-C, 20-C, 21-C, 23-C), 72.50 (8-C, 17-C), 80.87 (10-C, 15-C), 104.27 (11-C, 14-C), 106.02 (12-C, 13-C).

ESI-MS; m/z = 882.7 $[M+H]^+$, 903.7 $[M+Na]^+$.

ACKNOWLEDGMENTS

We acknowledge the financial support of this work by PNCDI II program (UEFISCSU; projects IDEAS 515, 570, 2358).

REFERENCES

1. a. Y. J. Zhang, H. Wei, W. B. Zhang, *Tetrahedron*, **2009**, *65*, 1281.; b. Y. Alpagut, B. Goldfuss, J. M. Neudoerfl, *Beilstein J. Org. Chem.*, **2008**, *4*, 25.; c. M. Kitamura, S. Shirakawa, Y. Arimura, X. Wang, K. Maruoka, *Chem. Asian. J.*, **2008**, *3*, 1702; d. Y. Sudo, D. Shirasaki, S. Harada, A. Nishida, *J. Am. Chem. Soc.*, **2008**, *130*, 12588.
2. Y.Q. Fang, M. Lautens, *Org. Lett.,* **2005**, *7*, 3549.
3. I. Grosu, G. Plé, S. Mager, E. Mesaros, A. Dulau, C. Gego, *Tetrahedron*, **1998**, *54*, 2905.
4. F. Piron, N. Vanthuyne, B. Joulin, J.-V. Naubron, C. Cismaş, A. Terec, R. A. Varga, C. Roussel, J. Roncali, I. Grosu, *J. Org. Chem*., 2009, Doi: 10.1021/jo901762j

5. a. G. Köbrich, A. Mannschreck, R. A. Misra, G. Rissmann, M. Rösner, W. Zündorf, *Chem. Ber.,* **1972**, *105*, 3794; b. G. Köbrich, B. Kolb, A. Mannschreck, R. A. Misra, *Chem. Ber.*, **1973**, *106*, 1601; c. H. L. Elbe, G. Köbrich, *Chem. Ber.*, **1974**, *107*, 1654; d. M. Rösner, G. Köbrich, *Angew. Chem. Int. Ed.,* **1974**, *13*, 741; e. H. O. Bödecker, V. Jonas, B. Kolb, A. Mannschreck, G. Köbrich, *Chem. Ber.,* **1975**, *108*, 3497; f. M. Rösner, G. Köbrich, *Angew. Chem.* **1975**, *87*, 715.
6. a. A. J. P. Devaquet, R. E. Townshend, W. J. Hehre, *J. Am. Chem. Soc.*, **1976**, *98*, 4068; b. S. M. Bachrach, M. Liu, *J. Am. Chem. Soc*., **1991**, *113*, 7929; c. M. E. Squillacote, F. Liang, *J. Org. Chem*., **2005**, *70*, 6564; d. A. E. Hansen, K. L. Bak, *J. Phys. Chem. A*, **2000**, *104*, 11362.
7. a. A. Mannschreck, M. Mintas, G. Becher, G. Stühler, *Angew. Chem*., **1980**, *92*, 490; b. G. Becher, A. Mannschreck, *Chem. Ber*., **1981**, *114*, 2365.
8. a. U. Berg, T. Liljefors, C. Roussel, J. Sandström, *Acc. Chem. Res*., **1985**, *18*, 80; b. R. Gallo, C. Roussel, U. Berg, *Adv. Heterocycl. Chem*., **1988**, *43*, 173.
9. a. b. G. Lu, S. Lam, K. Burgess, *Chem. Commun.*, **2006**, *15*, 1652.
10. S. Auricchio, S. Bruchner, L. Malpezzi, O. Vrajna de Pava, *J. Chem. Research (Miniprint)*, **1983**, 1201.
11. a. Z. J. Yao, H. P. Wu, Y. L. Yu, *J. Med. Chem.*, **2000**, *43*, 2484; b. M. M. McPhee, S. M. Kerwin, *Bioorg. Med. Chem.*, **2001**, *9*, 2809.
12. G.Wegner, *Makromolekulare Chemie* **1970**, *134*, 219.

STUDIA UNIVERSITATIS BABEŞ-BOLYAI, CHEMIA, LIV, 4, 2009

ELECTROCHEMICAL TREATMENT OF ACID WASTEWATERS CONTAINING METHYLORANGE

ADRIANA SAMIDE[1], MĂDĂLINA DUMITRU[a], ADINA CIUCIU[a], BOGDAN TUTUNARU[a], MIRCEA PREDA[a]

ABSTRACT. The degradation process of solutions containing Methylorange using electrochemical measurements, on Ti electrode was studied. In order to estimate the contribution of pure adsorption, behavior of Methylorange in open circuit was investigated. The color removal (CR) due to adsorption was estimated at 8.86%. From the anodic polarization, Ti electrode in the blank solution of 0.1 M HCl containing 0.035 M NaCl (ASB) or dye solution of 0.1 M HCl containing 0.035 M NaCl and Methylorange (ASC) a different behaviour was observed. In cathodic polarisation case, the ASC behavior being completely different towards ASB. It can be concluded that the polarisation curve for ASC in the potential range of-426mV to -900mV can be attributed to the dye reduction; thus the color removal was estimated at value of 23.6%. Galvanostatic method to evaluate the effect of current density on solution discoloration process was applied. The color removal at 250min increases of the value of 68.4% calculated at current density of 5mA/cm^2 until the value of 73.4% at current density equal to 15 mA/cm^2. Degradation process of Methylorange follows a first order kinetics reaction. Rate constants increase with the increase of current densities and their values are: 0.0047min^{-1}, in the case of degradation at a current density of 5 mA/cm^2, and 0.006min^{-1}, in the case of degradation at a current density of 15mA/cm^2.

Keywords: Methylorange, electrochemical degradation, titanium electrode, kinetics process

INTRODUCTION

Wastewaters contain a range of organic pollutants (about 10.000 different dyes) such as acids, alkalies, solid particles, toxic compounds and dyes which even in low concentrations must be removed. Synthetic dyes are used in textile industry (60%), paper industry (10%), plastic manufacture (10%) and it is estimated that 10-15% of the dyes is lost during fabrication processes. It is reported that approximately 5 tonnes of dyes discharge from coloration industries every year. Furthermore, some azo dyes, their precursors and a number of their reaction products are carcinogenic.

Due to environmental requirements in recent years, different techniques have been used for removal of such waste as adsorption, oxidation, reduction and electrochemical reactions. To eliminate dyes from aqueous coloured

[1] *Universitatea din Craiova, Facultatea de Chimie, Str. Calea Bucureşti, Nr. 107I, RO-200285, Craiova, Romania, samide_adriana@yahoo.com*

effluents and reduce their ecological impact, several biological, physical and chemical methods have been proposed: biological treatment [1-4], physical or chemical flocculation, electrofilteration, membrane filtration, electrokinetic coagulation [5-8], adsorption and precipitation [9-11] and other oxidative/ reductive chemical and photochemical processes [12-17].These methods have individual advantages, but also have some constrains when they are applied individually. Development of the appropriate techniques for treatment of dye wastewater is important for the natural waters protection. Other techniques including radiation and discoloration with ozone in combination with H_2O_2 are also employed [18].

Electrochemical treatments have certain advantages by comparison with other methods, namely: wide application, simple equipment, easy operation, lower temperature requirements and no sludge formation. It is important to select the proper electrode material, because the reaction products strongly depend on those materials as well as the experimental conditions. Selection of a proper electrode material is vital for an efficient and enduring operation of an electrode. Several researchers have tested the feasibility of electrochemical degradation using various electrode materials:glassy carbon, Pt, Pt+Ir, Ti, Al, Co+Pd, Fe, IrO_2, PbO_2, SnO_2, diamond paste doped with boron [19-33].

The objective of this research was to evaluate the electrochemical discoloration process of solutions with Methylorange content by direct electrochemical degradation, with an electrode made of Ti using a synthetic solution with Methylorange disolved in 0.1 M HCl aditivate with 0.035 M NaCl.

RESULTS AND DISCUSSION

The Methylorange was the organic compound studied, whose structure and spectrum are shown in Figure 1. This azo dye was purchased from Fluka and used as received. All others chemical compounds used were of analytical type. As it can be seen from Figure 1, the maximum absorption for dye in the visible region was at 502 nm. Beside the main peak, other two characteristic absorption peaks at the wavelength of 273 and 321 nm in the ultraviolet region, were identified.

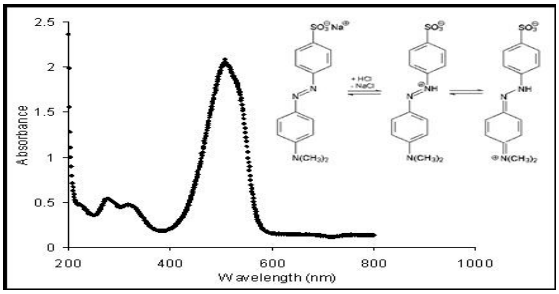

Figure 1. UV-Vis spectrum of initial Methylorange solution and molecular structure of Methylorange in acid medium aditivate with NaCl.

Study of Methylorange adsorption process

In order to estimate the contribution of pure adsorption, behaviour of Methylorange in open circuit was studied. In the open circuit, in ASB solution, the potential is stabilized after approximately 10 min, being of -306 mV at the end of the experiment (Figure 2 as an example). In the dye presence (ASC), within the first 25 minutes, the potential changes are major and can be attributed to a tendency of adsorption-desorbtion of dye on the titanium surface with the formation of a non-adherent and ruggedness film, which is interposed at the metal / solution interface. After 40 min the potential is stabilized, reaching the value of -266mV, at the end of the experiment. The potential shift to less negative values can be associated with the formation of a relative, uniform film, which is due to Methylorange adsorption on the titanium surface. This adsorption has a weak effect on the discoloration and it results from the fact that the titanium surface texture shows affinity for Methylorange, which can be adsorbed on the substrate through free electrons from azot atoms.

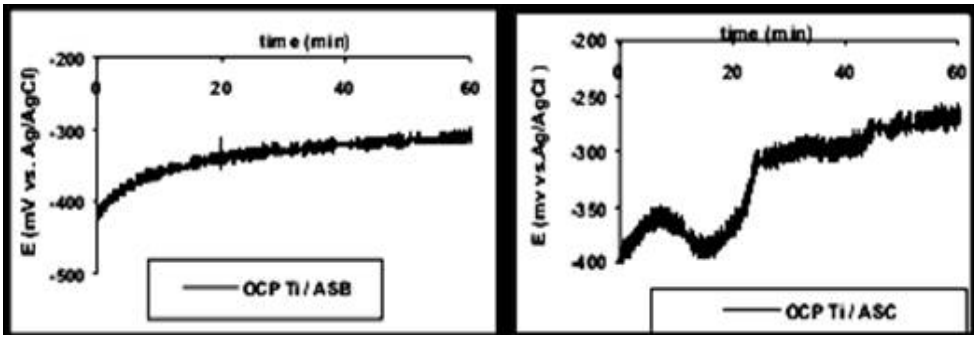

Figure 2. The potential dependence of time registered in open circuit in the absence and in the presence of Methylorange in 0.1 M HCl / 0.035 M NaCl solution.

UV-Vis spectra registered in open circuit, at the initial time and after 60 minutes are shown in Figure 3. A decrease of absorbance value from 2.03 to 1.85 which is attributed of Methylorange adsorption on the titanium surface was observed. Color removal (CR) due to the pure adsorption was determined using the following equation:

$$CR = (1 - A / A_0) \cdot 100 \quad (1)$$

where: A_0 and A represents the initial absorbance and absorbance at a moment “t”, 60 min in this case, respectively.

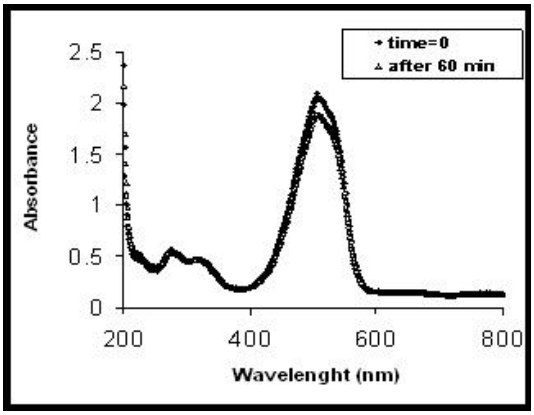

Figure 3. UV-Vis spectrum of Methylorange solution registered in open circuit.

The colour removal was 8.86% at an initial Methylorange concentration of 0.15 M.

Study of anodic and cathodic processes

The polarization curves of ASB and ASC on Ti electrode are shown in Figures 4 and 5. From the anodic polarization (Figure 4), it can be observed that Ti has a different behaviour in the blank solution and dye solution, respectively.

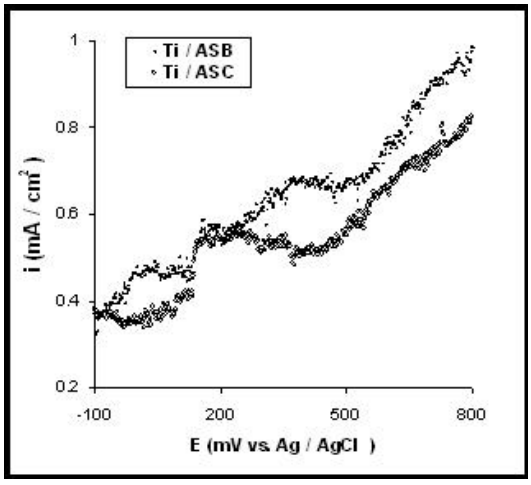

Figure 4. Anodic polarization curves of ASB and ASC on Ti electrode.

For the titanium electrode ASC has a major effect on the reaction in the range of positive potential; thus the potentials were shifted to less negative values, and current densities decreased. These changes may be associated with the formation of a film on the titanium surface, which modified the electronic change at metal / electrolyte interface. The anodic peak which appears at 200 mV is not attributed to an electro-oxidation, but to a tendency of titanium passivation. In spectrum UV-Vis the absorbance level was maintained on the initial value of 2.03. From cathodic polarization curve, a different behaviour of titanium electrode in ASC solution, by comparison with the ASB solution was observed. In the presence of Methylorange the current densities increased from a value of potential equal to -430 mV to -556 mV. This evolution could be attributed to the fact that the cathodic process is too slow to be controlled, therefore no characteristic peaks are obtained. Literature data [33] mentioned on glassy electrode the existence of two reduction peaks of azo group, first bielectronic at ε = - 425 mV / Ag, AgCl, with the formation of hydrazoderivate (according to Scheme 1), and the second tetraelectronic, at more negative potentials, up to -875 mV / Ag, AgCl leading to adequate amines according to Scheme 2:

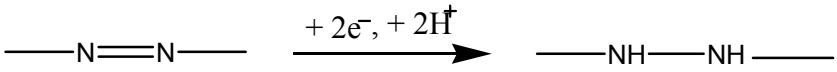

Scheme 1

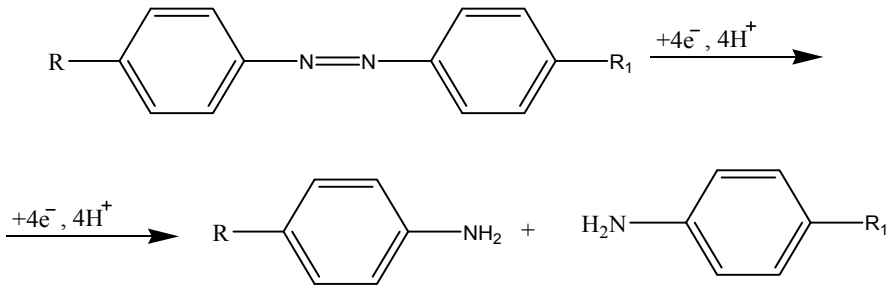

Scheme 2

Therefore, the ASC behaviour being completely different towards ASB, it can be concluded that the polarisation curve carriage for ASC in the potential range of -426 mV to -900 mV can be attributed to dye reduction.

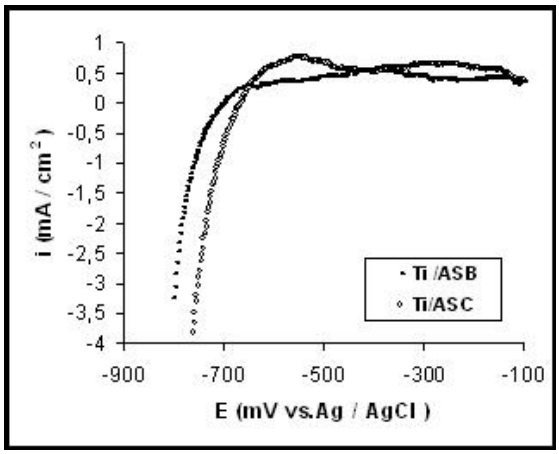

Figure 5. Cathodic polarization curves of ASB and ASC on Ti electrode.

UV-Vis spectrum of Methylorange solution registered at the end of the cathodic process is shown in Figure 6. A decrease of the absorbance from the 2.03 to 1.55 was observed, therefore the color removal calculated using the equation (1) has been calculated 23.6%.

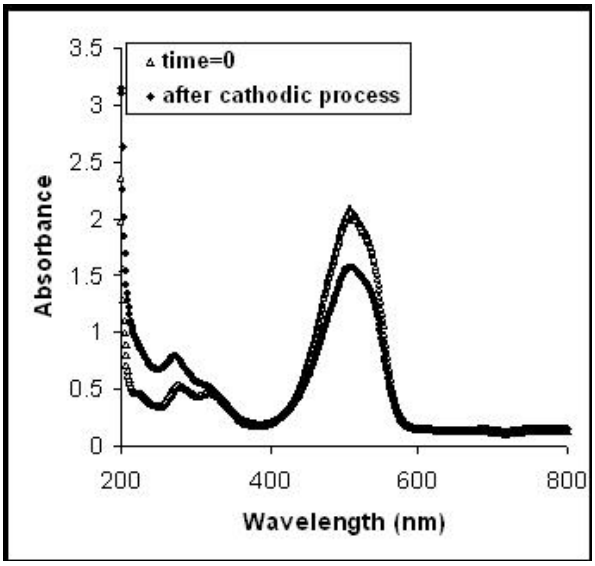

Figure 6. UV-Vis spectrum of Methylorange solution registered after cathodic process.

Study of discoloration process at different current densities

Galvanostatic technique was applied to evaluate the current density effect on discoloration process of dye solution. Electrochemical measurements, for two different current densities 5 mA/cm^2 and 15 mA/cm^2, respectively, were carried out. Each experiment ran for a time of 250 min, samples being analysed at certain time intervals, namely: 20 min, 40 min, 60 min, 80 min, 100 min, 150 min, 200 min, 250min. At specified time intervals absorbances values were evaluated. The degradation process of dye was followed by means of color removal (CR) values, which were calculated using equation (1). UV-Vis spectra of discolorated Methylorange at different current densities, 5 mA/cm^2 and 15 mA/cm^2 respectively, applied for 250 min, at room temperature are shown in Figures 7 and 8.

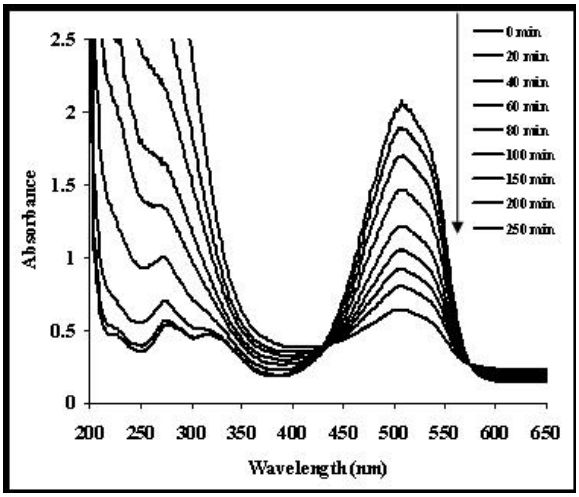

Figure 7. UV-Vis spectrum of Methylorange solution registered for current density of 5 mA/cm^2, for 250 min.

Figures 7 and 8 show that absorbance decreases in time, on the same current density, which demonstrates Methylorange degradation and discoloration. Absorbance values, at the same reaction time, present a significant decrease, hence a greater rate of degradation, with the current density increase. This may be shown by determining the colour removal (CR) using the equation 1, at time values when the spectral recordings were performed. Dependence of colour removal of time, at different current densities, is shown in Figure 9. Thus, the color removal at 250 min increases from 68.4% calculated at current density of 5 mA/cm^2 to the value of 73.4% at a current density equal to 15 mA/cm^2.

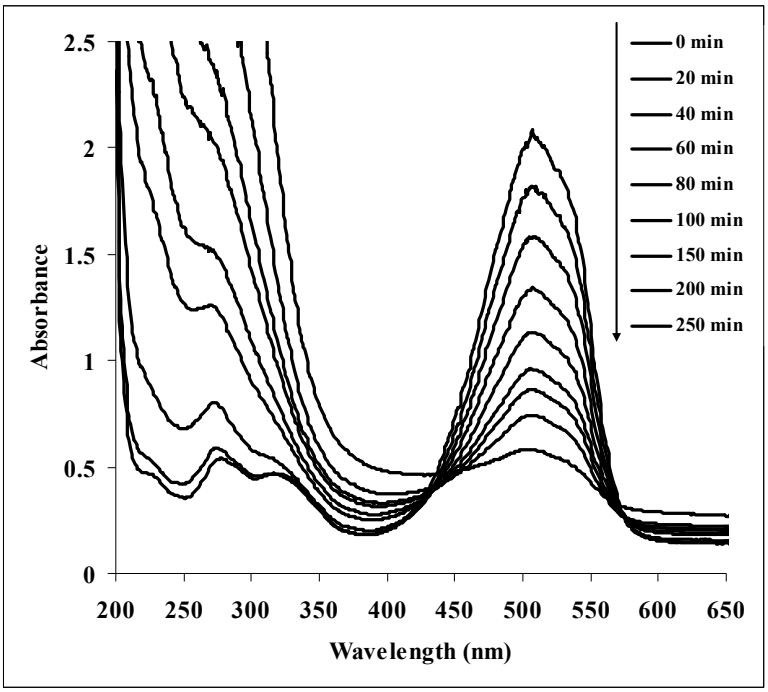

Figure 8. UV-Vis spectrum of Methylorange solution registered for current density of 15 mA/cm^2, for 250 min.

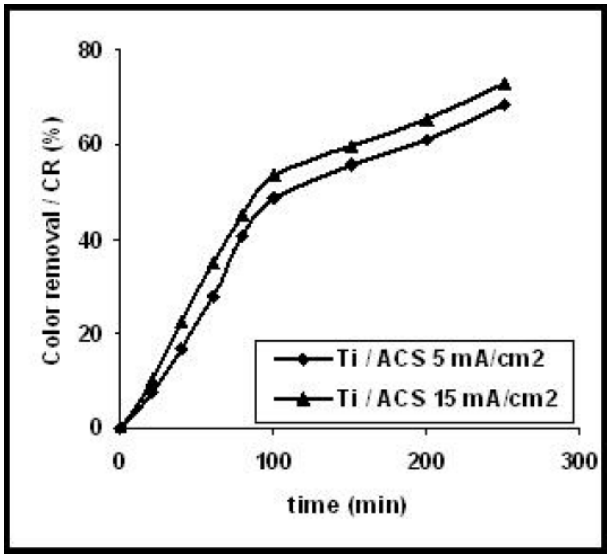

Figure 9. Dependence of color removal on time at different current densities.

Kinetics of Methylorange degradation

1). Determination of apparent rate constant

In general, degradation curves of dyes follow a first order kinetics reaction. The first order kinetic can written as follows:

$$-d[dye] / dt = k_{ap}[dye] \quad (2)$$

where: k_{ap} is apparent rate constant.

Integrating the equation (2), a first order kinetics equation was obtained:

$$\ln [dye]_0 / [dye]_t = k_{ap} \times t \quad (3)$$

Straight line plots $\ln [dye]_0 / [dye]_t = f(t)$ allow us to obtain the apparent rate constants for Methylorange, at both current densities. The absorbance is directly proportional with the concentration of Methylorange degraded; equation (3) can be written as:

$$\ln A_0 / A_t = k_{ap} \times t \quad (4)$$

where: A_0 and A represent the initial absorbance and absorbance at a given "t" time, respectively.

2) Verification of first order kinetics

a) Absorbance variation in time

The variation of absorbances resulted in the given experimental conditions were be evaluated, in time and as a function of the current densities whereat the degradation process of Methylorange had been studied. Absorbance versus time evolutions are shown in Figure 10.

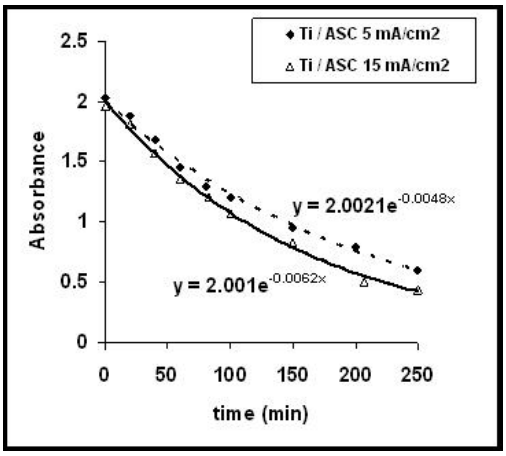

Figure 10. Absorbances variation during Methylorange degradation at different current densities applied.

It was noticed that, for the same current density, absorbance decreases exponentially with time, according to a relation $A = A_0 \exp(-kt)$, which corresponds to a first order kinetics, related to Methylorange degradation. From Figure 10, it can be seen that apparent rate constants values are: 0.0048 min^{-1}, in the case of degradation at a current density of 5 mA/cm^2, and 0.0062 min^{-1}, in the case of degradation at a current density of 15 mA/cm^2.

b) Integrated equation constant rate verification.
Rate constants determination

The curves $\ln A_0 / A = f$ (time) obtained from experimental data during the degradation process of Methylorange are shown in Figure 11. From Figure 11, it can be noticed that straight lines were obtained, passing through the origin and whose slope is $dy / dx = k_{ap}$;it can be observed that the value of R^2 is approximately equal 1;this proves that the degradation of ASC respects the first order kinetic. Rate constants (k_{ap}) increase with the increasing of current densities and have values ranging of 0.0047min^{-1}, in case of degradation at a current density of 5 mA/cm^2 and 0.006 min^{-1}, in case of degradation at a current density of 15 mA/cm^2, respectively.

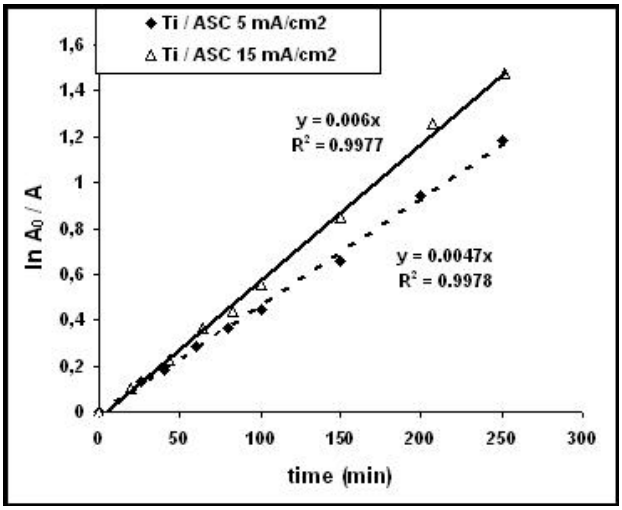

Figure 11. Diagrame corresponding with the first order kinetics in case of Methylorange degradation at different current densities.

From Figures 10 and 11, it can be observed that are obtained values of apparent rate constants approximately equal, for the same values of current densities; so it can be concluded that in the case of ASC degradation on Ti, it is respected the first order kinetics.

CONCLUSIONS

Electrochemical degradation process of a synthetic solution with Methylorange disolved in 0.1 M HCl solution aditivate with 0.035 M NaCl was studied.

In order to estimate the contribution of pure adsorption, behaviour of Methylorange in open circuit was studied. UV-Vis spectra registered in open circuit, at the initial moment and after 60 min had shown a decrease of the absorbance from t2.03 to 1.55, which was atributed to Methylorange adsorption on the titanium surface. The color removal (CR) due to adsorption was calculated to be 8.86% for a concentration of 0.08 mM Methylorange in ASB.

For the anodic polarization, observed that Ti in the blank and dye solution has a different behaviour. The anodic peak that appeared at 200 mV was not attributed to an electro-oxidation, but to a tendency passivation of titanium. In spectrum UV-Vis the absorbance level was maintained at the initial value of 2.03.

In cathodic polarisation case, the ASC behavior being totaly different towards ASB, it can be concluded that the polarisation curve carriage for ASC in the potential range of -426mV to -900mV can be atributted to the dye reduction. UV-Vis spectrum of Methylorange solution registered at the end of cathodic process had shown a decrease of the absorbance from 2.03 to 1.85; thus, the color removal was calculated to be 23.6%.

Galvanostatic technique was applied to evaluate the current density effect on discoloration process of dye solution. Thus, the color removal at 250 min increases from 68.4% calculated at current density of 5 mA/cm^2 to the value of 73.4% at a current density equal to 15 mA/cm^2.

The degradation process of Methylorange in ASB at studied current densities, 5 mA/cm^2 and 15 mA/cm^2, respectively, follows the first order kinetic reaction. Rate constants (k_{ap}) increase with the increase of current densities and their values are: 0.0047 min^{-1}, in the case of degradation at a current density of 5 mA/cm^2, and 0.006 min^{-1}, in the case of degradation at a current density of 15 mA/cm^2.

EXPERIMENTAL SECTION

Electrochemical measurements were carried out using a standard cell, with a working electrode made of Ti (the surface area of 2 cm^2), an auxiliary electrode in the form of glossy platinum plate (the surface area of 1 cm^2) and an Ag/AgCl electrode was used as a reference electrode. The electrode made of titanium was polished with very fine metallographic paper, washed with distilled water, degreased with acetone and dried. By electrochemical measurements azo dye Methylorange was degraded using a titanium electrode. The electrochemical behaviour of Methylorange was

evaluated by potentiostatic method using computerized electrochemical equipment VoltaLab 40 with software. The electrochemical degradation process was examined at positive and negative polarization, respectively, including open circuit condition, in a range of potential between -200mV and 800mV for the anodic process, and between -200 mV and -1000mV for the cathodic process, applying a scan rate of 10 mV/s. Galvanostatic technique was applied to evaluate the effect of current density on dyeing solution discoloration process. A SourceMeter 2420 3A potentiostat / galvanostat was used to controll the current density. The experiments were performed for two different current densities, 5 mA/cm^2 and 15 mA/cm^2, respectively. Each experiment ran for 250 min, samples being collected at certain time intervals. At specified time intervals absorbance values were assessed using an UV-Vis spectrophotometer, Varian Cary 50 with software.Temperature was maintained at 20ºC. Electrochemical solutions tested contained: acid blank solution composed of 0.035M NaCl, 0.1M HCl (ASB) and dye solution, which had the following components: 0.08mM Methylorange, 0.035M NaCl, 0.1M HCl (ASC).

REFERENCES

1. C.B. Shaw, C.M. Carliell, A. D. Wheately, *Water Research*, **2002**, *36*, 1193.
2. A.A. Oxpring, G. McMullan, W. F. Smyth and R. Merchant, *Biotechnology Letters*, **1996**, *18,* 527.
3. C.T. Matos, S. Velizarov, J.G. Crespo and M. A. M. Reis, *Water Research,* **2006**, *40*, 231.
4. H. Zilouei, B. Guieysse and B. Mattiasson, *Process Biochemistry*, **2006**, *41*, 1083.
5. J.I. Garrote, M. Bao, P. Castro, M.J. Bao, *Water Research*, **1995**, *29*, 26.
6. S.J. Judd and P. Hillis, *Water Research*, **2001**, *35*, 2895.
7. A.A. Chan, *Environmental Progress.*, **2006**, *25*, 152.
8. J. Bandara, J.A. Mielczarski and J. Kiwi, *Applied Catalysis B: Environmental*, **2001**, *34*, 321.
9. K.R. Ramakrishna and T. Viraraghavan, *American Dyestuff Reporter*, **1996**, *81*, 15.
10. S. Rio, L. Le Coq, C. Faur and P. Le Cloirec, *Water Science Technology*, **2006**, *53*, 237.
11. G. Crini, *Bioresource Technology*, **2006**, *97*, 1061.
12. J. Tokuda, R. Ohura, T. Iwasaki, Y. Takeuchi, A. Kawashida *Textiles Research J*ournal, **1999**, *69*, 956.
13. M. Dumitru, A. Samide, M. Preda, A. Moanta, *Revista de Chimie*, **2009**, *60*, 957.
14. H.Kusic, N.Koprivanac, L.Srsan, *Journal of Photochemistry and Photobiology A: Chemistry*, **2006**, *181*, 195.
15. B. Nasr and G. Abdellatif, *Journal of Electrochemical Society*, **2005**, *152*, D113.

16. M. Panizza, P.A. Michaud, G. Cerisola and Ch. Comninellis, *Electrochemistry Communications*, **2001**, *3*, 336.
17. N.H. Ince, *Water Research*, **1999**, *33*, 1080.
18. H.Y. Shu, *Journal of Hazardous Materials*, **2006**, *133*, 92.
19. J. Feng and D.C. Johnson, *Journal of Electrochemical Society*, **1991**, *138*, 3329.
20. R. Kotz, S. Stucki and B. Carcer, *Journal of Applied Electrochemistry*, **1991**, *21*, 1420.
21. J.M. Kesselman, O. Weres, N. SLewis and M.R. Hoffmann, *Journal of Physical Chemistry*, 1997, *101*, 2637.
22. C. Comninellis, C. Pulgarin, *Journal of Applied Electrochemistry*, **1993**, *23***,** 108.
23. S. Stucki, R. Kotz, B. Carcer, W. Suter, *Journal of Applied Electrochemistry*, **1991**, *21***,** 99.
24. A.M. Polcaro, S. Palmas, F. Renoldi, M. Mascia, *Journal of Applied Electrochemistry*, **1999**, *29*, 147.
25. J. Feng, L. Houk, D.C.Johnson, S. Lowery, J. Carey, *Journal of Electrochemical Society*, **1995**, *142*, 3626.
26. N.B. Tahar, A. Savall, *Journal of Applied Electrochemistry*, **1999**, *29*, 277.
27. X.M. Chen, G.H. Chen and P.L. Yue, *Journal of Physical Chemistry B*, **2001**, *105*, 4623.
28. B. Correa-Lozano, C. Comninellis, A.D. Battisti, *Journal of Applied Electrochemistry*, **1997**, *27*, 970.
29. R. Kotz, S. Stucki and B. Carcer, *Journal of Applied Electrochemistry*, **1991**, *21*, 14.
30. C. A.Martínez-Huitle, E.Brillas*, Applied Catalysis B: Environmental*, **2009**, *86*, 105.
31. N. Daneshvar, S. Aber, V. Vatanpour, M. Hossein Rasoulifard*, Journal of Electroanalytical Chemistry*, **2008**, *615*, 165.
32. Kai-sung Wang, Hsueh-Yu Chen, Long-Chiu Huang, Yu-Chun Su, Shih-Hsien Chang, *Chemosphere*, **2008**, *72*, 299.
33. M. Jitaru, A. Scorțeanu, C. Moldovan, *Revista de Chimie*, **2002**, 53, 35.